ISBN 978-82-326-4022-5 (printed version)
ISBN 978-82-326-4023-2 (electronic version)
ISSN 1503-8181

Daniel Rohde

Doctoral Thesis

Doctoral theses at NTNU, 2019:213

Daniel Rohde

Dynamic simulation of future integrated energy systems

NTNU
Norwegian University of
Science and Technology
Faculty of Engineering
Department of Energy and Process Engineering

NTNU
Norwegian University of
Science and Technology

Doctoral theses at NTNU, 2019:213

NTNU

NTNU
Norwegian University of
Science and Technology

Daniel Rohde

Dynamic simulation of future integrated energy systems

Thesis for the degree of Philosophiae Doctor

Trondheim, September 2019

Norwegian University of Science and Technology
Faculty of Engineering
Department of Energy and Process Engineering

NTNU
Norwegian University of
Science and Technology

NTNU
Norwegian University of Science and Technology

Thesis for the degree of Philosophiae Doctor

Faculty of Engineering
Department of Energy and Process Engineering

ISBN 978-82-326-4022-5 (printed version)
ISBN 978-82-326-4023-2 (electronic version)
ISSN 1503-8181

Doctoral theses at NTNU, 2019:213

Printed by Skipnes Kommunikasjon as

Acknowledgments

First of all, I would like to sincerely thank my supervisors Natasa Nord and Trond Andresen for their valuable support and guidance during the last five years. You both contributed to the fulfillment of this thesis in very different ways and I certainly benefited from the advantages of both.

Thank you also to all the co-authors of my papers, especially Hanne Kauko and Brage Rugstad Knudsen, for the fruitful collaboration. To all other colleagues/friends who know who they are: I very much appreciated the brain center talks, sports activities, countless cakes and coffees, and the almost philosophical discussions about modeling, simulation, and optimization with you.

I would also like to acknowledge the Norwegian Research Council and the staff at NTNU for providing the funding and the resources that made this work possible.

Last but not least, special thanks to Mareike and our daughters for always reminding me of the important things in life as well as to everyone who helped us during the stressful days before my final deadline.

Summary

The building sector is responsible for a large part of the world's total energy use. More than half of building energy use is needed for space heating, domestic hot water heating, and space cooling. Thermal energy supply systems are used to cover these thermal energy demands and are an integral part of new buildings and neighborhoods. These systems are becoming increasingly more complex due to the inclusion of renewable energy sources and thermal storages. Advanced simulations are required to analyze the design and the operation of these complex systems in detail and are thus an important part of the transition to new and improved building energy systems.

In this work, component and system models for thermal energy supply systems were developed in the modeling language Modelica. Numerical efficiency was an important part of the development process because the aim was to analyze long periods of time. In addition, the different requirements for simulation and optimization had to be considered during model development. Detailed description of all the developed Modelica models are given in this thesis. The models were used for dynamic simulations with Dymola as well as dynamic optimizations with JModelica.org, of which the latter proved to be more challenging. The optimization approach is therefore also described in detail in this thesis.

The design and the operation of two case study systems were analyzed in this work: 1) an existing integrated heating and cooling system at Vulkan, Oslo and 2) a planned local district heating grid at Brøset, Trondheim. The main components of the integrated heating and cooling system at Vulkan were heat pumps, plate heat exchangers, flat plate solar collectors, water storage tanks, ice thermal energy

storage, and borehole thermal energy storage. The system supplied a total floor area of 38 500 m^2 and is described in detail in this thesis. The main components of the local district heating grid at Brøset were a heat central, distribution pipes, and customer substations. The system was assumed to supply a total floor area of 178 000 m^2 and the different system design concepts that were analyzed are described in this thesis.

The main focus of this work was the case study system at Vulkan. The simulation results showed that the current operation of this system might be unsustainable due to an unbalanced long-term storage. Sustainable operation was possible in the simulations by increasing the number of solar collectors or the amount of imported heat from the district heating grid. The optimization results showed that variable setpoints for the heating and cooling supply temperatures could reduce the electricity use of the system. However, this would require the implementation of an advanced control system. The installation of larger storage tanks combined with optimal control was also investigated. It was shown that this combination could reduce the electricity costs of the system. However, the savings were not large enough to make an installation seem profitable with the current pricing scheme. Higher peak load tariffs and/or an increased variability of the electricity price might change this conclusion in the near future.

The analyses of the different system design concepts for the local district heating grid at Brøset showed that low-temperature grids were more environmentally-friendly than high-temperature-grids. This was mainly due to lower heat losses in the grid and the ability to include waste heat sources. The diameters of the district heating distribution pipes were shown to be important for the heat losses of the pipes and the required pumping power.

Several Modelica libraries with similar component models as the ones presented in this thesis are available. However, the system model development and the dynamic optimizations proved to be the most challenging tasks in this work. These tasks require a rather high level of user experience, but are expected to be increasingly important in the near future. This prediction is supported by the coordinated efforts that are currently going on in the IBPSA Project 1, which has a scope similar to the one of this thesis.

Table of contents

List of figures

List of tables

Nomenclature

Abbreviations

BAU	Business as usual
BTES	Borehole thermal energy storage
COP(s)	Coefficient(s) of performance
DAES	Differential algebraic equation system
DH	District heating
DHW	Domestic hot water
DS	Dymola screenshot
GHG	Greenhouse gas
GSHP(s)	Ground source heat pump(s)
HP(s)	Heat pump(s)
HVAC	Heating, ventilation, and air conditioning
HX	Heat exchanger
IHCS	Integrated heating and cooling system
ITES	Ice thermal energy storage
LMTD	Logarithmic mean temperature difference
LTDH	Low-temperature district heating
MPC	Model predictive control
MSL	Modelica standard library
NLP	Nonlinear programming
NTU	Number of transfer units
PRBC	Predictive rule-based control
TES	Thermal energy storage

Symbols

a_1	Linear heat loss coefficient $\left(\mathrm{W}/(\mathrm{m}^2 \cdot \mathrm{K})\right)$
a_2	Quadratic heat loss coefficient $\left(\mathrm{W}/(\mathrm{m}^2 \cdot \mathrm{K}^2)\right)$
A	Area (m^2)
c_p	Specific heat capacity at constant pressure $\left(\mathrm{J}/(\mathrm{kg} \cdot \mathrm{K})\right)$
c_v	Specific heat capacity at constant volume $\left(\mathrm{J}/(\mathrm{kg} \cdot \mathrm{K})\right)$
C	Heat capacity flow rate (W/K)
Δp	Pressure difference (Pa)
ΔT	Temperature difference (K)
δ	Slack parameter $(-)$
ε	Heat exchanger effectiveness $(-)$
η	Efficiency $(-)$
e	Electricity price (NOK/MWh)
E	Electricity use (kWh)
FtP	Flow-to-power coefficient ($\mathrm{MW} \cdot \mathrm{s}^2/\mathrm{m}^6$)
$\dot{m}$	Mass flow rate (kg/s)
Nu	Nusselt Number $(-)$
NTU	Number of transfer units $(-)$
P	Power (W)
q	Exponent for calculation of the heat transfer coefficient $(-)$
Q	Heat (kWh)
$\dot{Q}$	Heat flow rate (W)
ρ	Density (kg/m^3)
R	Solar radiation per square meter (W/m^2)
t	Time (s)
T	Temperature (K)
U	Heat transfer coefficient $\left(\mathrm{W}/(\mathrm{m}^2 \cdot \mathrm{K})\right)$
v	Variability $(-)$
V	Volume (m^3)
$\dot{V}$	Volume flow rate (m^3/s)

Subscripts

amb	Ambient
ann	Annual

avg	Average
col	Solar collector
cold	Cold side
cond	Condenser
const	Constant
cool	Cooling
del	Delivered
dem	Demanded
evap	Evaporator
heat	Heating
hot	Hot side
HP(s)	Heat pump(s)
HX	Heat exchanger
in	Inlet
L	Lorentz
LM	Logarithmic mean
max	Maximum
meas	Measured
min	Minimum
nom	Nominal
opt	Optical
out	Outlet
pump(s)	Circulation pump(s)
r	Ratio
ret	Return
SC	Space cooling
sec	Secondary
SH	Space heating
sim	Simulated
SM	Snow melting
sup	Supply
sys	System
sys+BTES	System and BTES
tot	Total

1 Introduction

1.1 Motivation

The building sector is responsible for a large part of the world's total energy use, with a share of around 40 % in the European Union [1] and the United States [2]. This energy use is responsible for significant greenhouse gas (GHG) emissions, which contribute to global warming. Emission reduction of building energy systems is therefore a goal of many research and development initiatives.

More than half of building energy use is needed for space heating, domestic hot water (DHW) heating, and space cooling. These thermal energy demands *"represent the single largest opportunity to reduce buildings energy consumption in most regions of the world"* according to the International Energy Agency [3]. In non-residential buildings, other thermal energy demands can also occur, e.g. heating of water in swimming halls, cooling of food products in supermarkets, cooling of medical products in hospitals, or cooling of IT equipment in data centers. In Norway, heating is sometimes also applied to highly frequented walking areas or stairs to melt snow and ice to ensure a safe environment for pedestrians during the winter.

Thermal energy supply systems are used to cover the thermal energy demands described above and are an integral part of new buildings and neighborhoods. Many different system solutions exist throughout the world due to the abundance of building types and climatic conditions, which influence the heating and cooling demands significantly. In addition, various solutions exist for different system scales, reaching from small private installations to large city-wide systems.

In Norway, electric heating and wood burning have long been the dominant choices for space heating and DHW heating due to the availability of cheap electricity and firewood. However, due to higher electricity prices and stricter legislation, more efficient solutions like heat pumps (HPs) [4] and district heating (DH) [5] have become more popular in recent decades. The development of low-temperature district heating (LTDH) grids [6], low- or zero-energy buildings [7], and even zero emission neighborhoods [8] has gained much attention recently. Future thermal energy supply systems are thus significantly different from traditional systems. To meet the strict targets for energy efficiency, system integration and "smart" control are prerequisites. System integration means the coupling of thermal systems for efficient interaction of heating and cooling demands as well as thermal energy storage (TES) and renewable energy sources. "Smart" control means using predictive control strategies and thermal energy storages to reduce energy use and/or operating costs. This development is heavily driven by coming dynamic tariff structures for electricity and district heating in Norway. Future thermal energy supply systems are thus more complex and flexible than traditional single-purpose systems and require a holistic design and control approach to make use of their flexibility in an optimal way.

Computer simulations are required to analyze the design and the operation of these complex systems in detail [9]. The simulation capability has increased significantly during the last decades due to the increase in available computational power. Many different software solutions exist, both for dedicated applications as well as sophisticated multi-purpose tools [10]. Using advanced computational methods for the design and analysis of future integrated energy systems is thus an important part of the transition to new and improved building energy systems.

1.2 Aim of study

The main aim of this work was the analysis of both the design and the operation of thermal energy supply systems on neighborhood scale to make these systems more energy- and/or cost efficient. Due to the importance of storages for such systems, focus was on both long- and short-term thermal energy storage. Dynamic simulations were chosen as computational method due to the inherent dynamics of thermal energy storages and flexible systems. The high level of com-

plexity and individuality of future integrated energy systems makes it difficult to draw general conclusions from case studies. The goal was therefore to develop simulation models, which can be reused easily and to apply them to selected case studies. Although closely related, building performance simulation, i.e. the calculation of the energy demands of buildings, was outside the scope of this work. To achieve the aim of this study, the following objectives were defined:

- Development of component models for dynamic simulation, which enable the analysis of future integrated energy systems. All the component models should have a similar level of detail and be accurate enough to include relevant component characteristics, but also fast enough to enable long-term simulations in reasonably short time.
- Development of system models for dynamic simulation, representing case study systems. This includes data acquisition for the heating and cooling demands, the coupling of component models, and the implementation of a control system.
- Development of component and system models for dynamic optimization. This should enable the detailed analysis of system control for one of the case study systems.
- Recommendations for the design and the operation of the case study systems. In particular, design suggestions for the planned system and retrofitting options as well as operating suggestions for the existing system.

1.3 Thesis content

This thesis is structured as follows: Chapter 2 gives information about thermal energy supply systems, modeling and simulation, as well as optimization. The case study systems that were analyzed are introduced and explained in Chapter 3. Afterwards, the simulation model development is described in detail in Chapter 4, which was the main task of this work. The optimization model development is described in Chapter 5 followed by results from the two case studies in Chapter 6 and Chapter 7. Concluding remarks and suggestions for further work are given in Chapter 8.

1.4 List of publications

The author of this thesis contributed to six scientific papers during his thesis work. The relation between the content of the thesis and the papers will be explained where necessary. All the papers are attached in the appendix and author contributions for each paper based on the CRediT taxonomy [11] are given below.

Paper I

D. Rohde, M. Bantle, T. Andresen, and N. Nord (2015). "Documentation of an Integrated Thermal Energy System for a Building Complex." In: *Proceedings of the 24th International Congress of Refrigeration, Yokohama, Japan.* DOI: 10.18462/iir.icr.2015.0445.

Author contributions: Conceptualization: D.R., N.N., Investigation: D.R., T.A., N.N., Resources: M.B., Writing – Original Draft: D.R., Writing – Review & Editing: D.R., T.A., N.N., Visualization: D.R., Supervision: T.A., N.N., Funding acquisition: N.N.

Paper II

D. Rohde, T. Andresen, and N. Nord (2016). "Interaction Between a Building Complex with an Integrated Thermal Energy System and a District Heating System." In: *Proceedings of the 12th REHVA World Congress, Aalborg, Denmark.*

Author contributions: Conceptualization: D.R., N.N., Methodology: D.R., T.A., Investigation: D.R., Resources: D.R., Writing – Original Draft: D.R., Writing – Review & Editing: D.R., T.A., N.N., Visualization: D.R., Supervision: T.A., N.N., Funding acquisition: N.N.

Paper III

H. Kauko, K. H. Kvalsvik, D. Rohde, A. Hafner, and N. Nord (2017). "Dynamic modelling of local low-temperature heating grids: A case study for Norway." *Energy* 139, pp. 289–297. DOI: 10.1016/j.energy.2017.07.086.

Author contributions: Conceptualization: H.K., A.H., N.N., Methodology: H.K., K.H.K., D.R., Investigation: H.K., K.H.K., D.R., Resources: H.K., Writing – Original Draft: H.K., K.H.K., Writing – Review & Editing: H.K., K.H.K., D.R.,

N.N., Visualization: H.K., Supervision: H.K., A.H., Project Administration: H.K., Funding acquisition: H.K., A.H.

Paper IV

H. Kauko, K. H. Kvalsvik, D. Rohde, N. Nord, and Å. Utne (2018). "Dynamic modeling of local district heating grids with prosumers: A case study for Norway." *Energy* 151, pp. 261–271. DOI: 10.1016/j.energy.2018.03.033.

Author contributions: Conceptualization: H.K., N.N., Å.U., Methodology: H.K., K.H.K., D.R., Investigation: H.K., K.H.K., D.R., Resources: H.K., Å.U., Writing – Original Draft: H.K., Writing – Review & Editing: H.K., K.H.K., D.R., N.N., Å.U., Visualization: H.K., Supervision: H.K., N.N., Project Administration: H.K., Funding acquisition: H.K.

Paper V

D. Rohde, T. Andresen, and N. Nord (2018). "Analysis of an integrated heating and cooling system for a building complex with focus on long–term thermal storage." *Applied Thermal Engineering* 145 (7), pp. 791–803. DOI: 10.1016/j.applthermaleng.2018.09.044.

Author contributions: Conceptualization: D.R., T.A., N.N., Methodology: D.R., T.A., Investigation: D.R., Resources: D.R., Writing – Original Draft: D.R., Writing – Review & Editing: D.R., T.A., N.N., Visualization: D.R., Supervision: T.A., N.N., Funding acquisition: N.N.

Paper VI

D. Rohde, B. R. Knudsen, T. Andresen, and N. Nord (2019). "Dynamic optimization of control setpoints for an integrated heating and cooling system with thermal energy storages." *Submitted to Energy (Status 08/2019: Revision under review).*

Author contributions: Conceptualization: D.R., B.R.K., N.N., Methodology: D.R., B.R.K., Software: D.R., B.R.K., Investigation: D.R., Resources: D.R., B.R.K., Writing – Original Draft: D.R., Writing – Review & Editing: D.R., B.R.K., T.A., N.N., Visualization: D.R., Supervision: T.A., N.N., Funding acquisition: N.N.

2 Background

The aim of this work was to study thermal energy supply systems by means of computational system analysis. Therefore, background information on these topics is given in the following sections.

2.1 Thermal energy supply systems for neighborhoods

2.1.1 Definition and system scale considerations

In order to cover the heating and cooling demands of large buildings, building complexes, or neighborhoods, the required thermal energy has to be delivered to the buildings and then be distributed to several areas and rooms within each building. In this work, only the supply system side was analyzed, the distribution system side was excluded. As mentioned in the introduction, different system solutions exist for different scales. The scale can roughly be divided into detached houses with individual systems, building complexes or neighborhoods with integrated thermal energy supply systems, and small cities or districts with district heating and cooling systems. The scale relevant for this work was the neighborhood scale, i.e. building complexes or small districts with a designated thermal energy supply system.

Such systems can show a high degree of individuality, especially when different heating and cooling demands at various temperature levels are present and when fluctuating renewable energy sources and storages are included. Such systems are therefore not standardized and need to be adapted to the neighborhood at hand. Other terms used for this kind of system are “smart thermal grid”, “ther-

mal network", "thermal micro-grid", "integrated energy system", "hybrid energy system", and "large-scale heating and cooling system" with definitions varying from source to source. In this thesis, the terms "integrated heating and cooling system" and "local district heating grid" are used for the two case study systems.

2.1.2 Key components for thermal systems

The key components for the thermal energy supply systems that were analyzed in this work are described in this chapter. Key components means that they are important for system performance, but not all of them are required for each system. The component choice is part of the system design phase and depends on the neighborhood at hand.

Heat exchanger A heat exchanger is used to transfer heat from a warmer fluid (liquid or gas) to a colder fluid. Heat exchangers are used in many different engineering applications and several different types have been developed. Heat exchangers are usually customized for their designated operating conditions so that a good trade off between heat transfer, pressure drop, and cost can be found. A very common type for heating, ventilation, and air conditioning (HVAC) systems is the counterflow plate heat exchanger, which is compact, cost effective, and readily available. This type of heat exchanger was the only type used for the case study systems in this work.

Heat pump A heat pump transfers heat from a colder environment to a warmer environment via a closed thermodynamic cycle by using work. The heat pump process includes evaporation and condensation of the working fluid. Depending on the application, the heat released during condensation of the working fluid is used for heating purposes, or the heat taken up during evaporation of the working fluid is used for cooling purposes. The coefficient of performance (COP) of a heat pump is an efficiency measure and depends significantly on the heat pump's temperature lift, i.e. the temperature difference between the evaporation temperature and the condensation temperature. High temperature lifts require more compressor power and lead to lower COPs. The COP of air source heat pumps thus depends highly on the outdoor temperature and is lowest on cold days when the most heating energy is needed. Ground source heat pumps

(GSHP) have therefore become increasingly popular in cold regions due to their higher COPs during the winter. However, the installation costs for GSHPs are high due to expensive drilling and can thus be critical for small residential applications. For larger installations, GSHPs are a promising choice and are often combined with seasonal thermal energy storage as described in one of the case study systems in this thesis.

Solar collectors Solar collectors are used to heat a fluid by radiation from the sun. Different types of solar collectors for different temperature levels exist. The most common type for building applications is the flat plate solar collector, which was the only type used for the case study systems in this work. The number of collectors to be installed depends on the available area and the expected heating demands. There is often a mismatch between the availability of solar heat and the heating demands, which is why the collectors are usually coupled to a storage tank. Seasonal storage of solar heat is also a common solution [12].

Thermal energy storage Thermal energy storage allows, to a certain extent, to decouple thermal demand and supply. This decoupling can be used to integrate fluctuating energy sources, e.g. solar heat, or to reduce expensive peak demands [13]. A classification of storage types is shown in Figure 2.1. Common storage components of thermal energy supply systems are water tanks for short-term storage and borehole thermal energy storage (BTES) for long-term (seasonal) storage. These were the only types used for the case study systems in this work. Phase change materials and thermochemical storage are emerging technologies which are not widely implemented yet [14]. An important aspect for the inclusion of thermal storages is the control strategy, i.e. when the storages should be charged or discharged and which temperature levels should be obtained. Different strategies are presented in Section 2.1.3.

Pipes The importance of pipes for thermal energy supply systems depends on the distance between the location of the heat source and the heating demand, i.e. the customer (for cooling demands, the distance between the heat sink and the cooling demand). They are thus less relevant for dense building complexes compared to larger neighborhoods. For district heating and cooling systems with

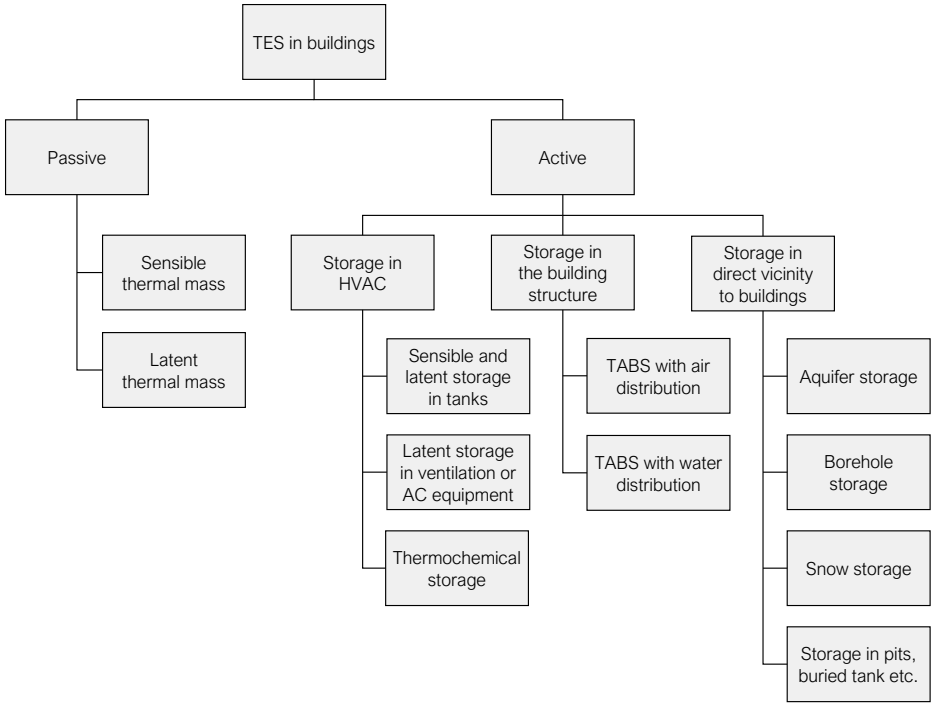

Figure 2.1: Classification of TES techniques [14].

several kilometers of buried pipes, the pipe selection is a crucial aspect. Especially the diameter of the pipes has to be chosen carefully to find a good trade-off between heat losses, required pump power, and cost in each branch. Different pipe materials and insulation thicknesses are available. Common for new grids are twin pipes, where both supply and return pipe are enclosed in the same insulation layer to reduce the grid's heat losses [15]. Both single and twin pipes were studied in this work.

2.1.3 The importance of system control

The operating performance of a thermal energy supply system does not only depend on the installed components, but also on the implemented control system. A classification of control methods is shown in Figure 2.2.

Classical control, see Figure 2.2, is the simplest and by far the most commonly used control method. With on/off control, a component is switched on and off depending on a measured variable that is to be kept between a lower and an

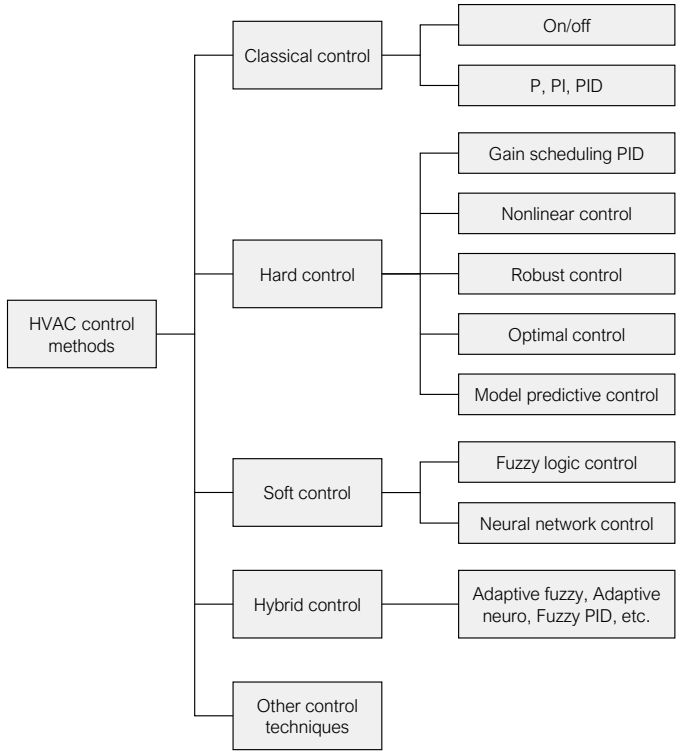

Figure 2.2: Classification of HVAC control methods [16].

upper threshold. This approach is very simple because only the two thresholds need to be defined. However, this control method is unsuitable for processes with large time delays because time delays can lead to large deviations between desired setpoint and measured variable. The aim of P, PI, or PID control is to keep a measured variable at a certain setpoint. The output of the controller is continuously adjusted based on the controller parameters and the control error, i.e. the difference between the measured value and the setpoint value. The parameters for the proportional (P), integral (I), and derivative (D) term have to be tuned for each application to achieve good results. This can be difficult in practice, especially when the operating conditions of the process change and thus differ from the tuning conditions. The other control methods shown in Figure 2.2 are more advanced. They may therefore lead to better results, but also require more implementation effort.

Apart from the control method, a control strategy also has to be defined, i.e.

how the thresholds and/or setpoints for the controllers are chosen and potentially changed during operation. This is especially important for systems with storages because it has to be determined when the storages should be charged or discharged. A good control strategy is crucial for efficient storage operation and different strategies exist. A classification of control strategies is shown in Figure 2.3.

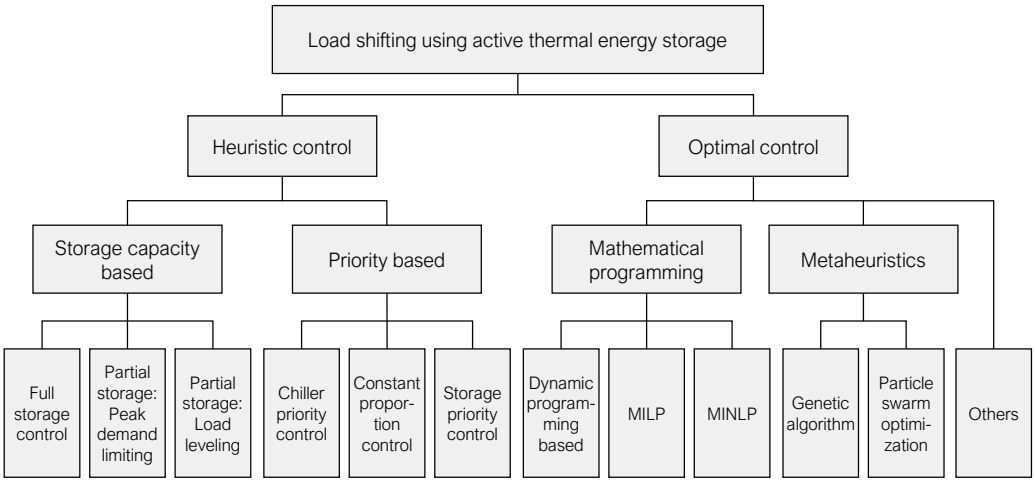

Figure 2.3: Classification of active TES control strategies [17] (MILP = Mixed integer linear programming, MINLP = Mixed integer nonlinear programming).

Recently, predictive control has received much attention because the implementation of forecasts for weather, demands, and prices can lead to improved operation. Two common approaches are predictive rule-based control (PRBC) and model predictive control (MPC). With PRBC, the setpoints for the local controllers are adjusted based on a set of heuristic "if-then-else" rules. PRBC is relatively easy to implement, but the performance depends highly on the rules, which can be difficult to define for complex systems or changing operating conditions [18]. With MPC, a system model is used to repeatedly solve an optimal control problem over a receding horizon, with the first control action of the optimal solution being implemented before re-optimization. MPC is more difficult to implement than PRBC and the performance is very dependent on the optimization model of the system [19]. Note that both MPC and optimal control are also listed as control methods in Figure 2.2. However, the control strategy is defined in the objective function of the optimal control problem, which is why they are

also treated as control strategies here. Typical objectives for optimal control are the minimization of energy use or operating costs. Optimal control is treated in this thesis and is explained in Section 2.2.3 and Chapter 5.

2.2 Methods for computational system analysis

Significant advances have been made in microprocessor performance during the last decades, see Figure 2.4.

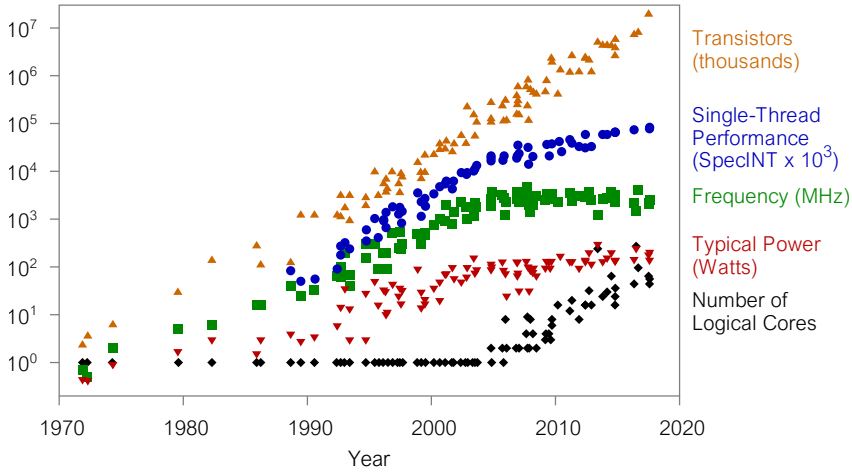

Figure 2.4: 42 years of microprocessor trend data [20].

The performance advances shown in Figure 2.4 have enabled the development of sophisticated computer simulation tools. However, computational performance is still a limiting factor for these tools and can restrict their simulation capability. Keeping computation times within reasonable limits is important and should be kept in mind during simulation model development. As G. Augenbroe stated in a book about building performance simulation [21]:

> "The art of modeling and simulation is leaving things out that don't affect the answer" – G. Augenbroe

Computation time obviously depends on the type of hardware used. Apart from that, the level of detail, the number of components, and the simulated time influence the computation time as shown in Figure 2.5.

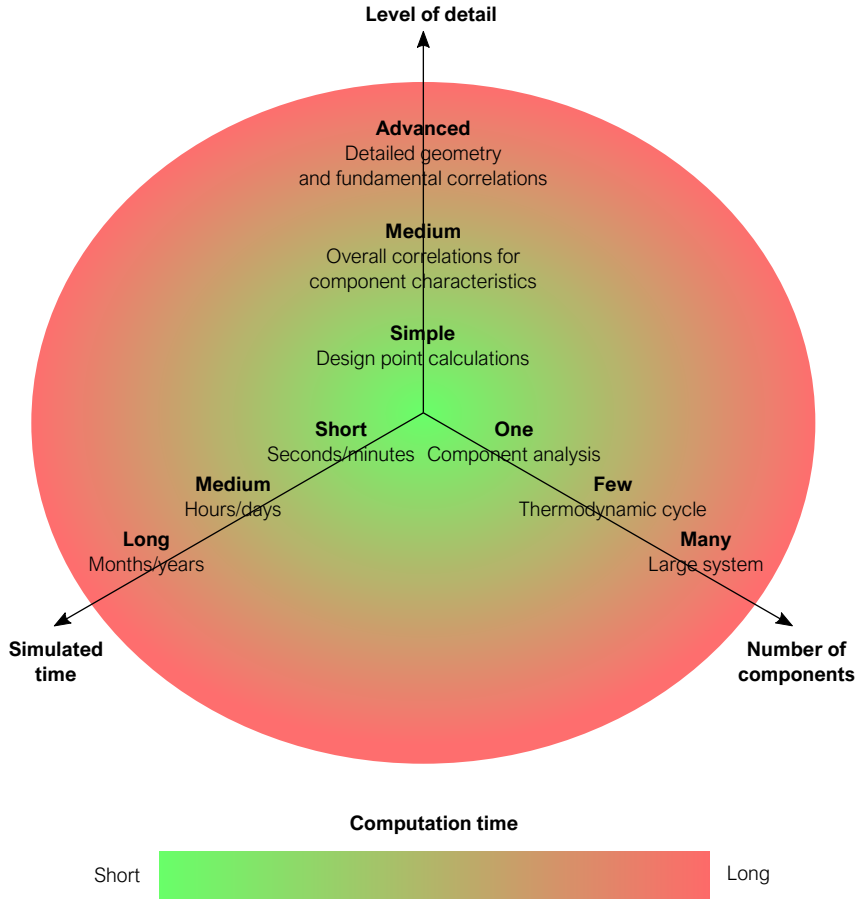

Figure 2.5: Computation times for system analysis.

Figure 2.5 is a very general representation. Other factors can also influence the computation time, e.g. the complexity of the system, i.e. the number of interactions between components, or the efficiency of the software used.

The number of components of a system and the simulated time for the specific analysis are usually known beforehand. The level of detail and the simulation software can also be predefined, but are often more free. The right choice depends first of all on the aim of the analysis, but in practice also to a high degree on the available resources and the experience of the user. The scope of work was to analyze the annual performance of systems with many components. Therefore, the level of detail of the component models was chosen to be "medium", see Figure 2.5. A higher level of detail could lead to unacceptably long computation

times and would also require much more user input data. Unless these inputs are available and can be specified at a sufficiently high level of certainty, the results would not necessarily be more correct with more detailed component models as shown in Figure 2.6.

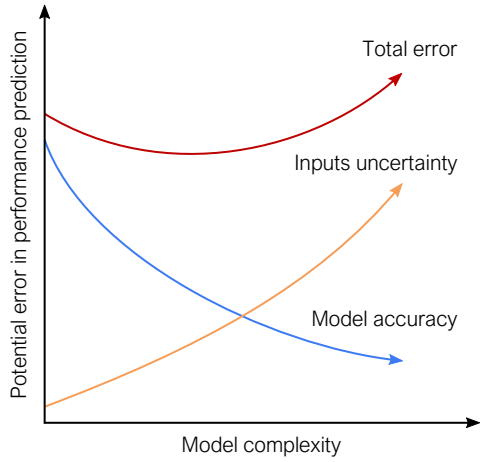

Figure 2.6: Potential error vs. model complexity [22].

2.2.1 Modeling with Modelica

Modeling is a broad term. In this thesis, modeling refers to the mathematical description of a component or a system. This mathematical description can be used in a computer simulation to study the behavior of the modeled component or system.

Originally, modeling and simulation were closely linked because programming languages were used for both modeling and simulation. Modeling was thus mainly writing code that a computer could execute. However, this approach suffered from several disadvantages. For one, the required explicit formulation of equations made it cumbersome to describe the component's or system's behavior in an intuitive way. In addition, small changes in the system to be modeled could lead to large changes in the computer code. Reusing the same model for different use cases was therefore limited.

A different approach are equation-based languages, which separate the modeling from the numerical solution. This allows to write implicit model equations,

i.e. relations between variables, and apply advanced computer algebra to create efficient simulation code from those equations afterwards [23]. Modelica is an equation-based, object-oriented modeling language, which has been developed because the 1990s and is widely used today. It is open-source and is under continuous development by the non-profit organization The Modelica Association. Modelica was chosen for this work and is therefore described below. For a full documentation of the Modelica language, the reader is referred to [24].

Models A model is the most generic type of definition in the Modelica language. It defines the name of the model as well as its variables, parameters, equations, and connectors. These elements are described below. Modelica uses the basic data types "Real" for floating point numbers, "Integer" for integer values, "Boolean" for true/false expressions, and "String" for text.

Variables Variables are usually time-varying and are calculated during a simulation based on the model equations. They are generally continuous, but may also contain discontinuities. Variables of type Real are used for physical variables, e.g. the mass flow rate of a fluid or the temperature of a thermal capacity. Attributes can be assigned to variables to define their usage. Two commonly-used attributes for variables of type Real are "unit", used to assign a physical unit to that variable and enable unit checking in the equations, and "start", used to set initial conditions for state variables. Variables of type Integer can be used for control purposes, e.g. the number of active parallel components. However, it is more common to use the type Boolean for control purposes, e.g. to define the mode of operation or to activate/deactivate components. Variables in Modelica are scalars by default but can also be defined as vectors or matrices/arrays.

Parameters Variables can be defined as parameters when they do not change during a simulation. Parameters need to be defined beforehand and are typically user input data, which define a specific model instance. Parameters of type Real can be used for component specifications, e.g. the length of a pipe or the volume of a tank. Parameters of type Integer can be used for discretization or to define a number of components, e.g. the number of fluid layers in a tank model or the number of series/parallel collectors in a solar collector model. Parameters of type Boolean can be used to activate/deactivate certain model parts, e.g. choosing

between a constant and a variable heat transfer coefficient or deciding if an input signal or a parameter should be used in the model.

Equations Modelica supports algebraic, differential, and discrete equations. Partial differential equations are not supported, i.e. Modelica is not suitable for finite element methods or computational fluid dynamics. Equations define the actual behavior of the model and are simply written as "left hand side" = "right hand side". Equations can be written implicitly due to the acausal structure and will be rearranged by the simulation tool afterwards. Therefore, the models have no input-output structure and can be simulated as long as the number of equations and unknown variables are equal. Special types of equations are initial equations, used for initialization of differential equations, conditional equations, i.e. if-then-else equations, and connect-equations, which are used to define connections between models.

Connectors Models can be connected in Modelica using connectors. Connectors can have a predefined input-output direction, e.g. for control signals or input data which need to be passed to component models. However, connectors can also be acausal to represent a physical connection, e.g. the junction of two pipes or the thermal connection of two fluid streams. In such a connection, the direction of flow is not defined beforehand, but instead calculated during the simulation. Flow reversal during a simulation is also possible. These physical connectors can contain "potential variables", "flow variables", and "stream variables", which trigger the automatic generation of balance equations when two or more connectors are connected. Potential variables are equal in connected connectors, e.g. pressure or temperature. The sum of all the flow variables in connected connectors is zero, e.g. the sum of all mass flow rates or heat flow rates. Stream variables are calculated based on the flow direction and the product of the flow variable and the stream variable, such that the sum of these products is zero. An example is the energy balance with mass flow rate as flow variable and enthalpy as stream variable.

The object-orientation of Modelica has several advantages. It ensures that models can contain other models and makes models extensible, i.e. one model can inherit the structure and behavior from another model. This is very useful

for hierarchical library structures, where a so-called "base class" can be used as basis for many other models. A model with four fluid ports can for example be used for a heat pump model and a heat exchanger model via the extends-clause. Such a base class can be a "partial model", i.e. it can have an unbalanced number of equations and variables and thus be unsuitable for simulation. The required additional equations can then be added in the model derived from the base class. This approach also allows to build models with different levels of detail from the same base class and ensures that these models can easily be exchanged in e.g. a system model. This inheritance structure and easy model exchange lead to a high degree of reusability, which is especially important for the development of comprehensible model libraries. Such libraries usually have a hierarchical model structure organized in packages. Many Modelica libraries are available, both commercial and open-source [25].

2.2.2 Dynamic simulation with Dymola

Simulation means using a mathematical model of a system to predict the system's behavior. Simulations can thus be used to compare different scenarios and thus help both during system design and during system operation. There are three different approaches to represent the dynamics of a system dynamics, i.e. how the system's state changes over time. The simplest is "steady-state", i.e. all variables are assumed constant over time. This approach is only suitable for rough calculations. In "quasi-steady-state" simulations, the simulated time (see Figure 2.5) is divided into a certain number of intervals or time steps. The states/variables are assumed constant in each time step, but can change from one time step to the next. The accuracy of this approach depends highly on the chosen time step. In "dynamic" simulations, differential equations can be used to describe how variables change over time. Thus, a numerical integration algorithm (often called "solver") is required to run a simulation. The scope of this work was dynamic simulation due to the increased flexibility and inherent dynamics of future thermal energy systems as mentioned in Section 1.2.

Different tools for dynamic simulations exist, which have individual strengths and weaknesses. The most common tools for dynamic simulation of energy systems are TRNSYS, IDA ICE, MATLAB/Simulink, and Modelica/Dymola. These are briefly described here. TRNSYS (Transient System Simulation Tool) is a

graphically based software environment for the simulation of transient systems with focus on thermal and electrical energy systems. It is widely used, but was not chosen for this work due to its causal modeling approach, which requires that the in- and outputs of models are predefined. IDA ICE (IDA Indoor Climate and Energy) is a simulation tool for building performance simulation. It employs acausal equation-based modeling of buildings and building energy systems. It also has many preconfigured subsystems available, but focus is more on single buildings rather than neighborhoods [26]. Since it is not open-source, the model equations in IDA ICE cannot be edited by the user easily, which is why it was not chosen for this work. MATLAB (MATrix LABoratory) has its origin in control engineering and strong support for optimization. Graphical energy system modeling is possible with Simulink, but as for TRNSYS, the modeling approach is causal, making MATLAB unsuitable for this work.

Models written in Modelica can be simulated by different simulation environments and both commercial and open-source tools are available [27]. To simulate a model, the Modelica model descriptions have to be translated into executable code and be linked with numerical solvers. To do so, the Modelica code is first flattened, which means that the hierarchical structure is broken up. All the required model equations are inserted during flattening, e.g. inherited equations from extends-clauses or equations resulting from connections. This leads to an unstructured set of differential, algebraic, and discrete equations. This set can then be sorted, simplified, and optimized by the application of advanced mathematical techniques. Afterwards, the optimized set of equations is used to generate executable code [23]. Dymola is a commercial Modelica-based tool developed by Dassault Systèmes. It is widely used for modeling and simulation due to its superior performance and efficient solvers. Dymola was chosen for this work and some aspects regarding its numerical performance are discussed in Section 4.2.

2.2.3 Dynamic optimization with JModelica.org

Simulations can be used to study system performance by comparing different system design concepts or control strategies. However, the best possible solution might not be among the ones that were selected for the study. To find the best possible solution, optimization has to be applied. The general concept of optimization is finding a vector of variables ($\mathbf{x}$) that minimizes a defined objective

function $f(\mathbf{x})$ subject to certain constraints $c(\mathbf{x})$

$$\begin{aligned} &\underset{\mathbf{x} \in \mathbb{R}^n}{\text{minimize}} && f(\mathbf{x}) \\ &\text{subject to} && c_i(\mathbf{x}) = 0, \quad i \in \mathcal{E} \\ &&& c_i(\mathbf{x}) \geq 0, \quad i \in \mathcal{I} \end{aligned}$$

with $\mathcal{E}$ and $\mathcal{I}$ being the sets of indices for equality and inequality constraints, respectively. This concept is applied in many different fields and a variety of optimization problem types and solution algorithms exist. A classification of optimization problems is shown in Figure 2.7.

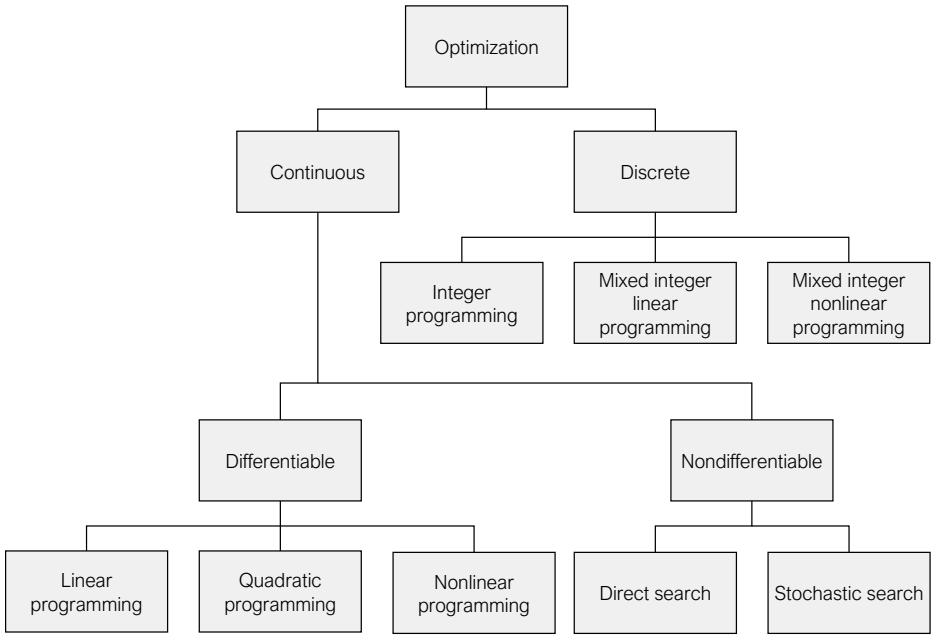

Figure 2.7: Classification of optimization problems [28].

Optimization algorithms are used to find the solution of an optimization problem. They are iterative, i.e. they need a starting point and stopping criteria. Different methods of how to move from one iterate to the next have been developed and an algorithm is usually only suitable for a certain problem type. This is known as the "No Free Lunch" theorem, which states that *"for any algorithm, any elevated performance over one class of problems is offset by performance over*

another class" [29]. A distinct difference can be made between algorithms that use gradient information during the iteration (gradient-based) and those that do not use it (derivative-free). Obtaining the first or second order derivatives of the objective function and the constraint functions can be difficult to obtain. However, algorithms using this information are usually much more efficient. In addition, the gradient information allows the definition of optimality conditions, which can confirm that the optimal solution has been found.

Optimization is a vital part of optimal control and MPC, see Figure 2.2. Optimal control is also called "trajectory optimization" and is used to find the best possible control sequence for a process over a given time horizon. This is very useful when different system design concepts are to be compared, i.e. different component sizes or different component combinations, because a fair comparison can only be made when the control strategy is equally well adapted for each of the design concepts. The more dynamic a system behaves, the more challenging it is to ensure equally good control with constant or rule-based setpoints for different system design concepts. Thus, optimal control is required for a fair comparison.

The optimization of a dynamic system, i.e. a system whose state changes over time, requires dynamic optimization techniques. Dynamic optimization problems, e.g. optimal control, are infinite-dimensional and can therefore not be solved directly. They can be transformed into a finite-dimensional problem by means of collocation on finite elements [30]. The continuous time horizon is then discretized into a finite number of elements in which the state profiles, i.e. the dynamic model variables, are approximated by polynomials. This yields a finite-dimensional nonlinear programming (NLP) problem, which can be solved. The size of this NLP depends on the equations of the system model to be optimized, the length of the time horizon, the number of finite elements, and the number of collocation points in each finite element, i.e. the degree of the polynomial approximation.

JModelica.org is an open-source platform for simulation and optimization of complex dynamic systems [31]. It is based on Modelica and the Functional Mock-up Interface standard, enabling coupling to different software packages. Two vital packages that are implemented are CasADi, which is used for the computation of derivatives using algorithmic differentiation [32], and IPOPT, which is used to solve the NLP. IPOPT stands for "Interior Point OPTimizer" and is an open-

source state-of-the-art solver for large scale sparse optimization problems [33]. JModelica.org also uses the language extension Optimica, which enables high-level formulation of optimization problems [34]. JModelica.org has recently been used for several optimization studies [35–40] and is also a key part of several compound tools [41–44]. JModelica.org was chosen for this work due to the Modelica-based approach. The optimization procedure used in this work is described in more detail in Section 5.1.

3 Description of the two case study systems

Two case study systems from Norway were analyzed for this thesis: an existing integrated heating and cooling system in Oslo and a planned local DH grid in Trondheim. The Oslo case study was part of the research project "Efficient interaction between energy demand, surplus heat/cool and thermal storage in building complexes" (INTERACT), which was the main funding source of this work. The Trondheim case study was part of the research project "Development of Smart Thermal Grids" (DSTG), to which the author of this thesis contributed due to the similar modeling and simulation requirements. However, the focus of this work was the Oslo case study, which is therefore described in more detail.

3.1 Integrated heating and cooling system at Vulkan, Oslo

The thermal energy supply system at Vulkan is called "integrated heating and cooling system" (IHCS) in this thesis due to its high level of integration with the buildings and the fact that it delivered both heating and cooling energy. The main aim of this case study was to analyze the design and the operation of the IHCS, especially the performance of the long- and short-term thermal energy storages.

3.1.1 Vulkan area and building stock

An area of about 100 by 200 meters in the Norwegian capital Oslo was renewed with several buildings and the IHCS. Construction was completed in 2014 and the

IHCS supplied a total floor area of 38 500 m^2. The area and the supplied buildings are shown in Figure 3.1. The total floor areas of the different building types are listed in Table 3.1.

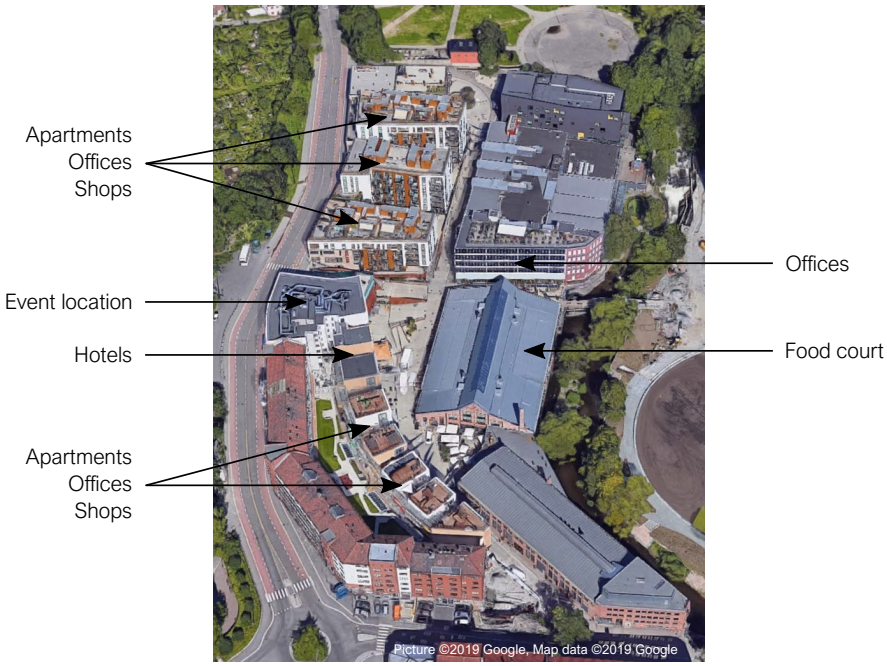

Figure 3.1: Overview of the Vulkan area and the existing buildings (arrows show the buildings that are connected to the IHCS).

Table 3.1: Building types and total floor areas at Vulkan.

Building type	Total floor area m^2
Offices	15 000
Shops	6 650
Hotels	7 600
Apartments	3 900
Food court	3 500
Event location	1 850
Total	38 500

3.1.2 The integrated heating and cooling system

The demands covered by the IHCS were space heating, DHW heating, snow melting, space cooling, and product cooling. Snow melting was applied to the walkways between the buildings and product cooling was delivered to the food court. The IHCS had separate heat exchangers for each building and demand type, which were connected to the heating and cooling loops of the IHCS in parallel. These parallel heat exchangers are shown as one heat exchanger with the corresponding total area of the parallel heat exchangers in Figure 3.2, which shows a schematic of the IHCS.

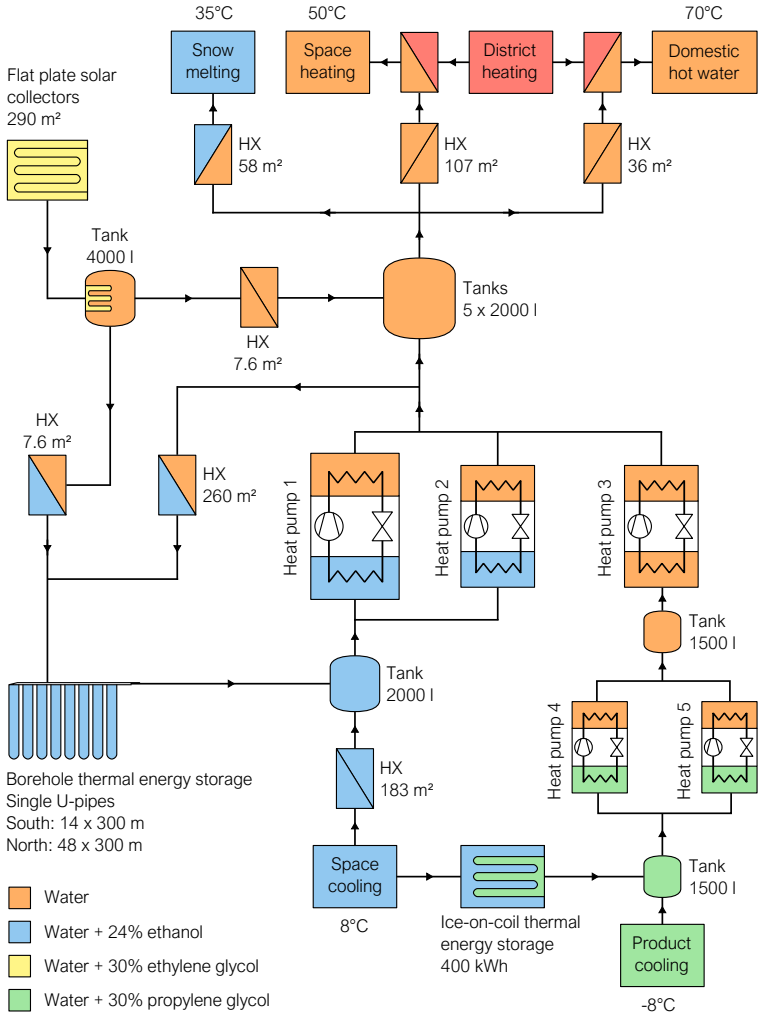

Figure 3.2: Schematic of the IHCS with main specifications.

The main components of the IHCS shown in Figure 3.2 were heat pumps, plate heat exchangers, flat plate solar collectors, storage tanks, ice thermal energy storage (ITES), and borehole thermal energy storage. The heat pump specifications are listed in Table 3.2.

Table 3.2: Heat pump specifications.

	HP 1	HP 2	HP 3	HP 4 & 5
Type	WSA2802X	WSA1602X	WSA0701X	NXW0600X
Working fluid	R134a	R134a	R134a	R410a
Compressor	Screw (2)	Screw (2)	Screw	Scroll
Design data cooling (evap/cond)				
Temperatures (°C)	4.5/48	4.5/48	20/55	-8/25
Capacities (kW)	595/772	334/436	224/283	87/110
COP (-)	4.36	4.27	4.8	4.78
Design data heating (evap/cond)				
Temperatures (°C)	0/50	0/50		
Capacities (kW)	473/652	264/365		
COP (-)	3.64	3.61		

The heat pumps were designed to deliver heat at a temperature of around 50 °C, see Table 3.2, so they could only cover parts of the DHW heating demand by preheating the DHW up to around 50 °C. Heat from Oslo's DH grid was then used to lift the DHW temperature to the required 70 °C. The space heating loops were also connected to the DH grid as backup system in case of very high space heating demands or heat pump failure.

During heating season, the BTES and the surplus heat from space cooling and product cooling were used as heat sources on the evaporator side of the heat pumps. The condenser heat from the heat pumps was sent to space heating, DHW preheating, and snow melting. During cooling season, a lot of surplus heat was available from the cooling systems, which needed to be released on the condenser side of the heat pumps, and the solar collectors. Only a part of this heat was needed for space heating and DHW preheating. Therefore, heat was injected into the BTES during cooling season. The ITES was used to reduce space cooling

peak demands during the summer. The ITES was charged during the night and discharged during the day.

3.1.3 Input data for the case study Vulkan

A simulation model of the IHCS described in the previous section was developed, see Section 4.5.1. The different heating and cooling demands as well as outdoor temperature and solar radiation were required as input data for the simulation model. An input file was created with hourly values of these variables, which were retrieved as explained below.

The IHCS was equipped with a control and monitoring platform. Energy meters were installed to measure the delivered energy for heating and cooling in each connected building. Aggregated daily demand data for 2015 and 2017 are shown in the figures 3.3 and 3.4, respectively. Data for 2016 were excluded from the analyses because long periods of data are missing from that year due to a server change.

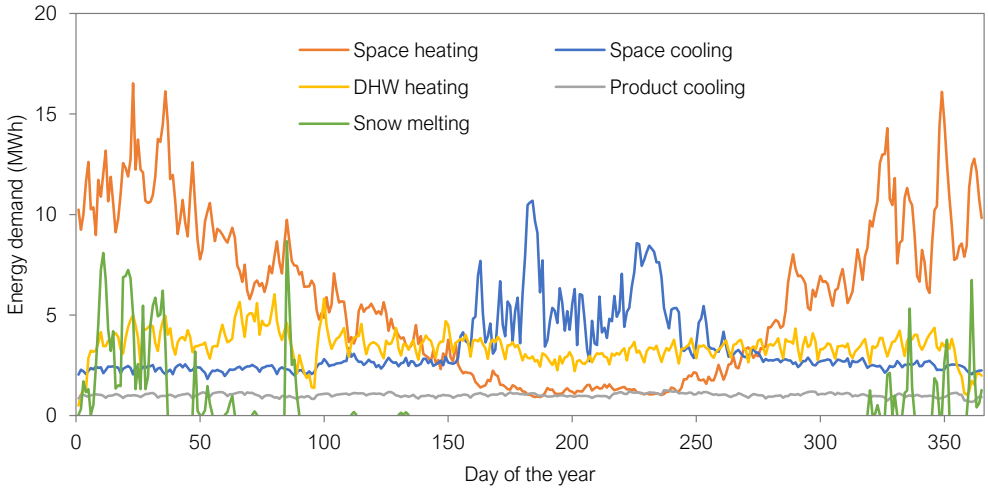

Figure 3.3: Measured daily heating and cooling demands in 2015 (hourly values were used as input data, daily values are shown for better readability).

The figures 3.3 and 3.4 show typical seasonal variations of the space heating, space cooling, and snow melting demands. The product cooling and DHW heating demands were relatively constant throughout the year.

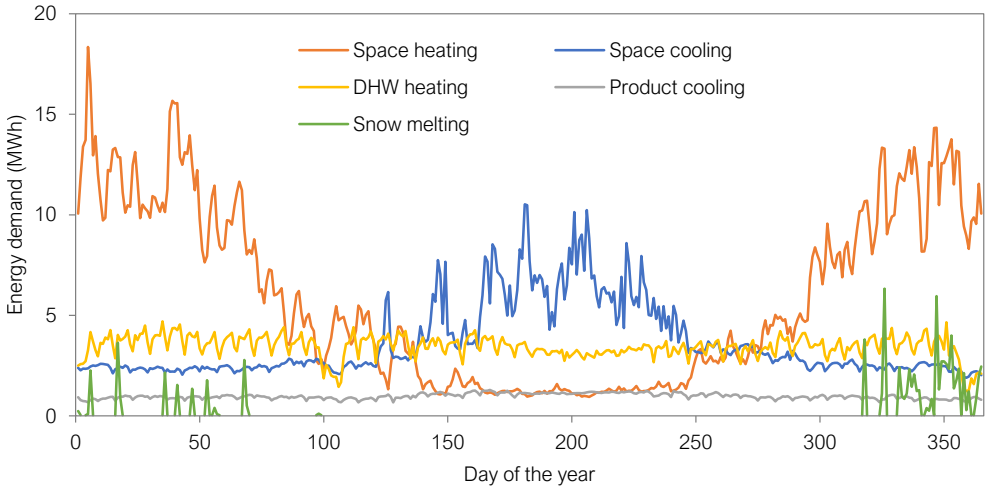

Figure 3.4: Measured daily heating and cooling demands in 2017 (hourly values were used as input data, daily values are shown for better readability).

Daily demand profiles for the different seasons are shown in the figures 3.5, 3.6, and 3.7, which show an average winter day, an average spring/fall day, and an average summer day, respectively (the same y-axis range was chosen for all three figures for better comparability).

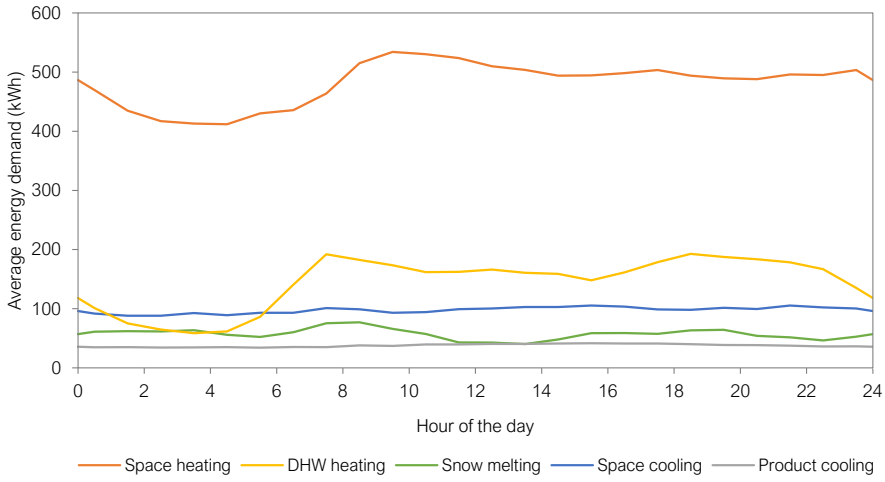

Figure 3.5: Average heating and cooling demands for a winter day.

The figures 3.5, 3.6, and 3.7 show that the product cooling and DHW heating demand did not change significantly during the year. The DHW heating demand

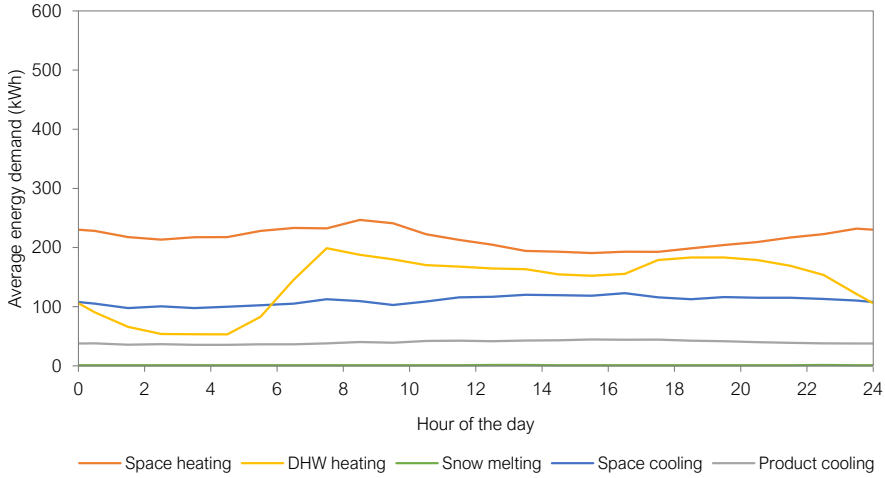

Figure 3.6: Average heating and cooling demands for a spring/fall day.

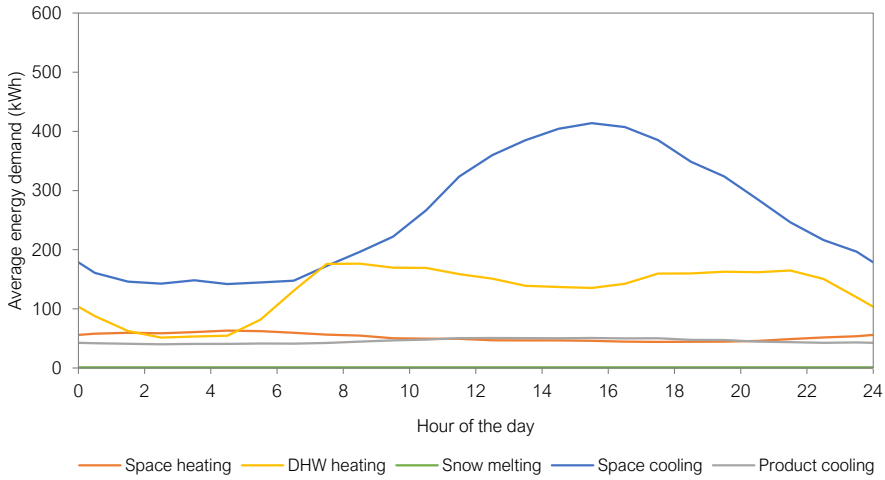

Figure 3.7: Average heating and cooling demands for a summer day.

showed a peak in the morning due to people taking showers and was the lowest during the night. Product cooling and snow melting did not show typical hourly variations. On the contrary, the space heating and space cooling demands showed large differences between the seasons. Especially the space cooling demand depended highly on the outdoor temperature during the summer, see Figure 3.7.

Unfortunately, no energy meters were installed to measure the energy exchange with the BTES or the performance of the solar collectors. In addition, only the total electricity use of the system was measured, the electricity use of single

components was not available. The amount of DH import was measured for each building. Daily total values for DH import and electricity use for the two years are shown in Figure 3.8.

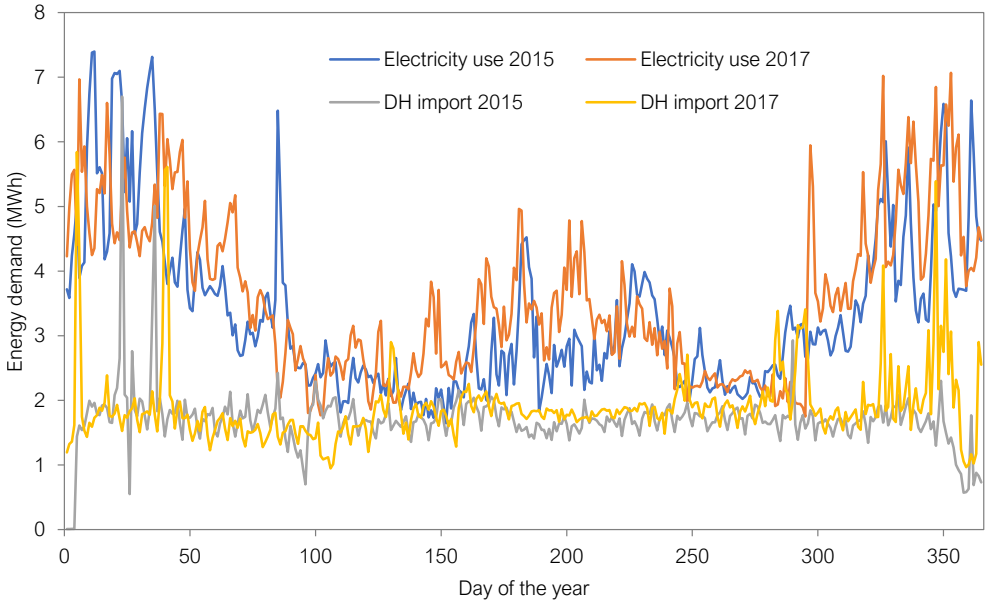

Figure 3.8: Measured daily electricity use and DH import in 2015 and 2017.

Figure 3.8 shows that the electricity use was the highest during winter and the lowest during spring and fall. The DH import was relatively constant during the years because it was mainly used for DHW heating. The peaks in DH import were caused by high space heating demands. In total, there was no significant difference between the measured energy amounts of the two years, see Figure 3.9.

The on-site temperature was only measured by one sensor and solar radiation was not measured at all. Therefore, outdoor temperature and solar radiation data from nearby weather stations were retrieved from [45]. The on-site temperature measurement was found to be around 5 K higher than nearby measurements, see Paper I. This might be due to the location of the sensor or an offset error. Therefore, 5 K were subtracted from the on-site temperature measurement values when they were used as input data. These corrected temperature values are shown in Figure 3.10.

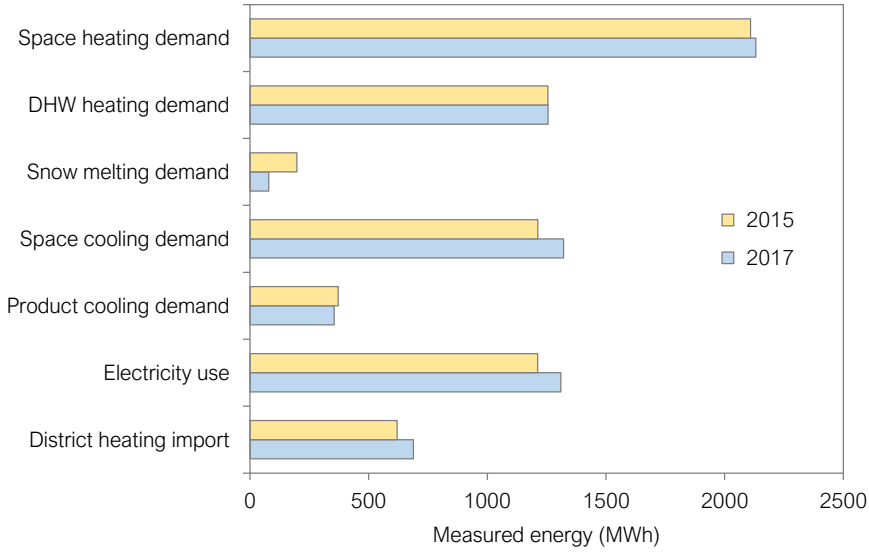

Figure 3.9: Total measured energy amounts in 2015 and 2017.

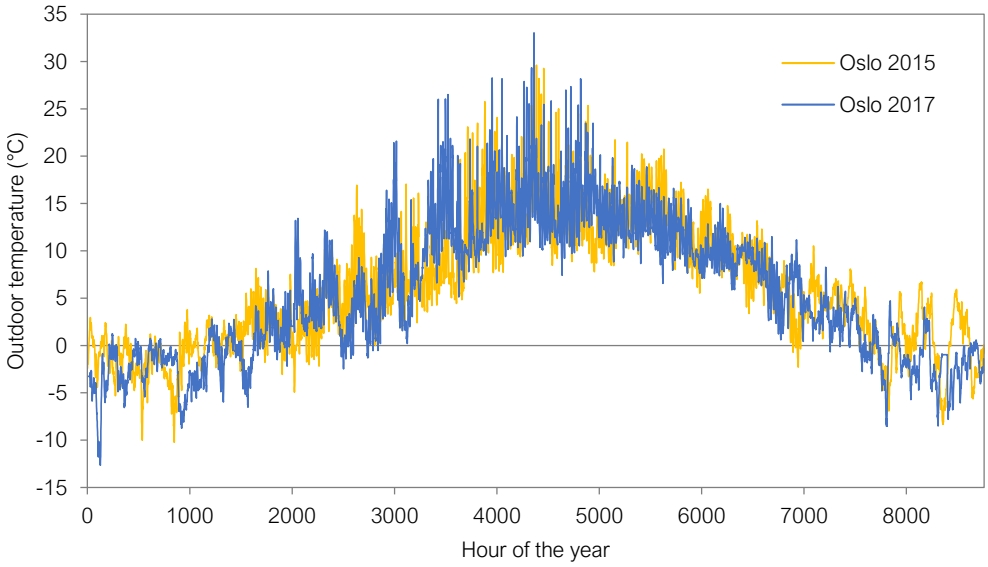

Figure 3.10: Input data for the case study Vulkan: Outdoor temperature.

Figure 3.11 shows the measured solar radiation from the nearest weather station for the years 2015 and 2017.

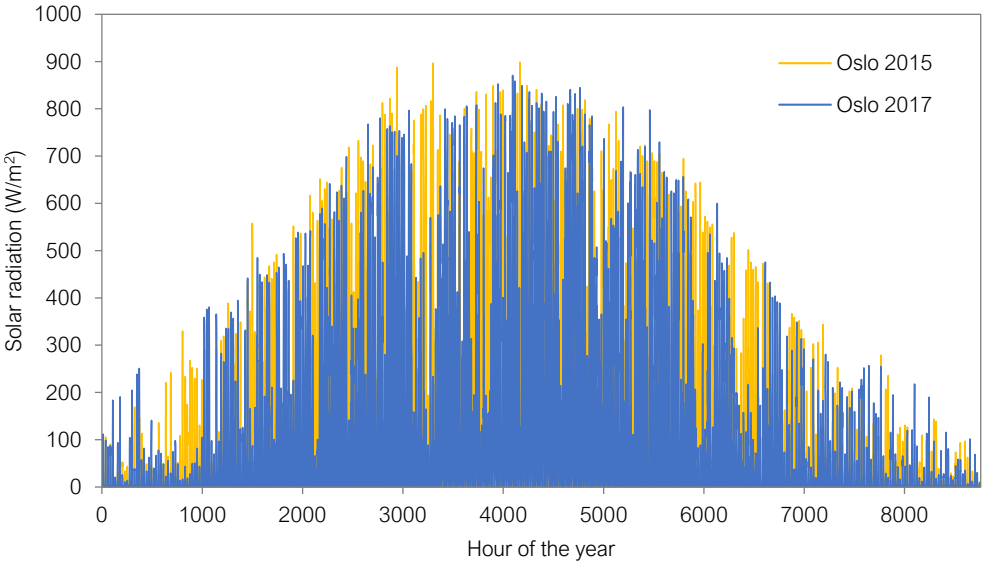

Figure 3.11: Input data for the case study Vulkan: Solar radiation.

3.2 Local district heating grid at Brøset, Trondheim

The main aim of this case study was to increase knowledge about the design of local DH grids and to investigate different solutions for the given area. As mentioned above, the author of this thesis contributed mostly to the modeling and simulation part of this case study, see also the author contributions listed in Section 1.4.

3.2.1 Brøset area and building stock

In 2013, Trondheim Municipality made plans to develop a new neighborhood at Brøset, which is a part of the city of Trondheim. The size of the available area was about 344 000 m^2 and the aim was to develop a low-emission neighborhood. The area and a development plan are shown in Figure 3.12.

Based on the existing buildings and the development plan shown in Figure 3.12, the building stock listed in Table 3.3 was assumed for this case study. This building stock was used as basis for the calculation of the heating demand profiles.

Figure 3.12: Overview of the Brøset area (left) and the planned buildings (right [46]).

Table 3.3: Building types and floor area at Brøset.

Building type	Number of buildings	Total floor area (m^2)
Apartment block (type A)	4	31 000
Apartment block (type B)	6	41 000
Apartment block (type C)	8	59 000
Kindergarten	3	4 400
Nursing home (old)	2	4 000
Nursing home (new)	1	12 600
Sports hall	1	10 000
School	1	6 000
Library	1	5 850
Office	1	4 000
Total	28	177 850

3.2.2 The local district heating grid

Trondheim Municipality wanted the CO_2 footprint of the new neighborhood to be considerably lower than the Norwegian average [47]. An efficient thermal energy supply system for the neighborhood was therefore sought. This system is called "local district heating grid" in this thesis due the fact that it delivered only heating energy and that the supplied area was relatively small. The total pipe

length was estimated to be around 7 km.

The existing DH grid in Trondheim delivers heat at supply temperatures between 75 °C and 115 °C as explained in Paper IV. LTDH with supply temperatures below 70 °C has recently received much attention [5, 48]. There are a number of benefits and some drawbacks related to LTDH. The main advantages are that the heat losses from the grid are reduced and that more renewable and waste heat sources can be included, leading to higher energy efficiency and lower emissions. The main disadvantages are that measures have to be taken to avoid the risk of Legionella bacteria in DHW systems and that existing buildings/substations might not be suitable for heat supply at such low temperatures [49]. Therefore, LTDH is especially relevant for new building areas.

Several design concepts for local DH grids with different temperature levels have been compared for this case study with focus on LTDH. The main heat supply was assumed to come from Trondheim's existing DH grid. The inclusion of prosumers, i.e. customers that can also deliver heat, was also analyzed. Several other solutions for increased energy efficiency of the neighborhood were originally discussed, e.g. heat recovery from waste water, solar collectors combined with thermal energy storage, heat pumps, and the use of geothermal energy [47]. These additional design concepts were not analyzed in this work due to time limitations.

3.2.3 Input data for the case study Brøset

Simulation models of the local DH grids described in the previous section were developed, see Section 3.2.2. Hourly values for space heating and DHW heating demand of the different building types were required as input data for the simulation models. An input file was created for each of the building types listed in Table 3.3. The DH demand data in each input file were based on DH use data from existing buildings of similar type and building code. These use data were retrieved from the local DH company and Trondheim Municipality. The DH use data only showed the total DH demand, i.e. both space heating and DHW heating. Therefore, generic DHW profiles were created and used to split the total DH demand data into space heating demand and DHW heating demand. Apartment blocks represented by far the largest share of floor area, see Table 3.3. Therefore, three different input files, based on DH use data from three

different buildings, were created. Daily values for the heating demands of the entire building stock (excluding prosumers) are shown in Figure 3.13.

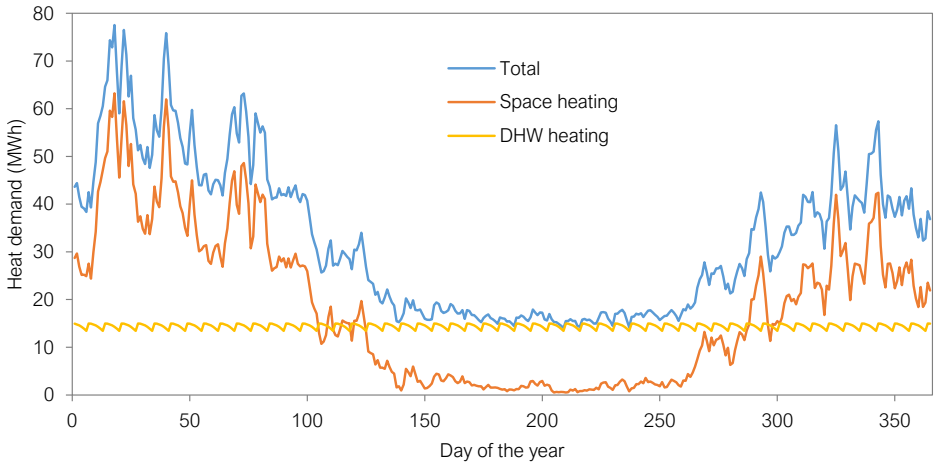

Figure 3.13: Input data for the case study Brøset: Daily heat demands (hourly values were used as input data, daily values are shown for better readability).

The total calculated heating demand shown in Figure 3.13 was 11 940 MWh, with 6 680 MWh required for space heating and 5 260 MWh required for DHW heating. The DH use data included the outdoor temperature for the year 2013, which was also used as input and is shown in Figure 3.14.

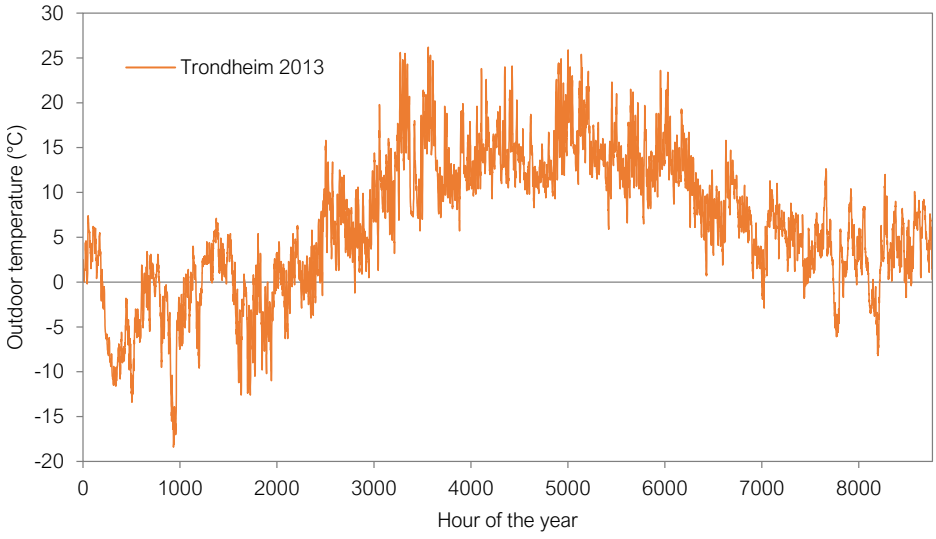

Figure 3.14: Input data for the case study Brøset: Outdoor temperature.

Two different prosumer heat profiles were created, which represented different types of prosumers and were used to study the effect of prosumers in the DH grid. These types were a data center and a supermarket. Their capacities were chosen based on values found in the literature and their heat profiles depended on the outdoor temperature, see Paper IV. The resulting heat profiles for the prosumers, which were based on the outdoor temperature shown in Figure 3.14, are shown in Figure 3.15.

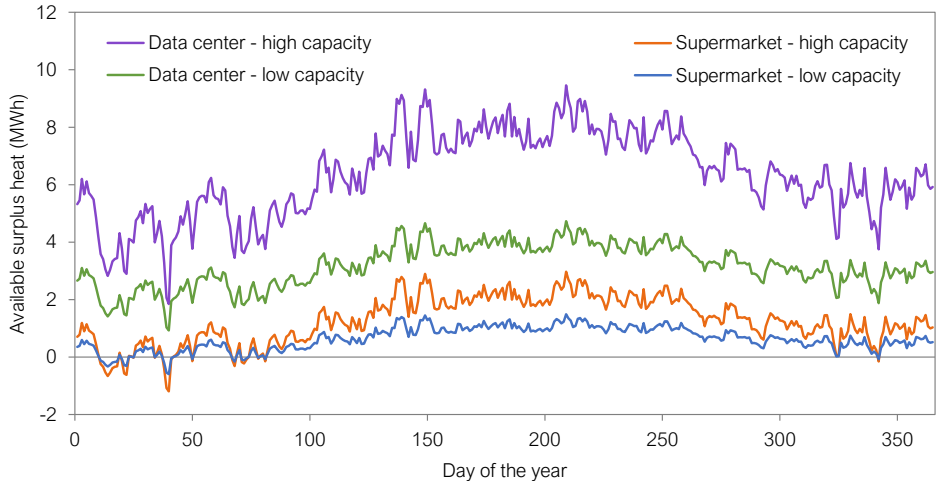

Figure 3.15: Input data for the case study Brøset: Prosumer heat profiles (hourly values were used as input data, daily values are shown for better readability).

It can be seen from the heat profile in Figure 3.15 that the supermarket was a customer, i.e. it required heat from the DH grid, on the coldest days of the year. However, for most part of the year it was a producer, i.e. it delivered heat to the DH grid. The data center was actually not a prosumer because it always delivered heat to the DH grid and could therefore be seen as decentralized renewable heat source.

4 Simulation models for future integrated energy systems

The simulation model development is explained in detail in this chapter. Simple models were used as starting point and were continuously extended and improved. This evolution of the simulation models over the course of this work will be explained where appropriate.

The term "model" has various meanings and it is therefore important to clarify the usage in this thesis. As described in Section 2.2.1, a model is the most generic type of definition in the Modelica language. It defines the name, input parameters, connections, variables, and equations of the specific model. In the following chapters, the term model refers to a Modelica model. Since Modelica is object-oriented, models can contain other models, e.g. a system model usually contains several component models.

4.1 Choice of Modelica library for simulation model development

To recall, sufficiently accurate but also fast models were sought as the scope of this work was the analysis of systems with several components and long simulated times. Therefore, the level of detail had to be limited to ensure reasonable computation time. However, the important characteristics of the components had to be represented by the models. At an early stage of this work, the use of component models from existing Modelica libraries was evaluated. The commercial library TIL from TLK-Thermo GmbH [50] and the open-source library Buildings

from Lawrence Berkeley National Laboratory [51] were selected as potential candidates. Both libraries seemed to be targeted at a higher level of detail than required for this work and were thus deemed unsuitable. Modifying the existing models in the libraries or building own models from the libraries' base classes was considered. However, the libraries are under constant development and modifications could lead to compatibility issues when library updates are released. The library Thermal from the Modelica Standard library (MSL) provides simple components for one-dimensional incompressible thermo-fluid flow models. It is also called library, but is very basic compared to TIL or Buildings and does not contain components like heat pumps or heat exchangers. It can be seen as a base class library and it has not been further developed since 2010. This library was chosen as basis for model development because the level of detail was suitable and no compatibility issues were expected to arise.

4.2 Numerical performance with the DASSL solver in Dymola

As described in Section 2.2.1, modeling and simulation are separate tasks. However, the numerical performance of the simulation depends highly on the simulation models, i.e. the modeling part. Thus, simulation-friendly modeling is desirable to achieve good numerical performance. This means that the simulation terminates successfully, i.e. the solver does not fail, and that the computation time is sufficiently low. Several reasons can cause the solver to fail, e.g. a division by zero, or lead to unacceptably long computation times, e.g. algebraic loops or chattering, which are explained below. Many different Modelica-based simulation tools and solvers exist, making it impossible to ensure good numerical performance for all simulation possibilities. Dymola was used for this work with the solver DASSL. Some aspects regarding the numerical performance of this choice are given below.

Numerical integration algorithms in Dymola Several different solvers, i.e. algorithms for numerical integration, are included in Dymola. Most solvers in Dymola are variable step size algorithms. These algorithms calculate the local error at each trial step and proceed if the error is lower than the defined tolerance.

At an early development stage, test runs were performed to compare the solvers in Dymola. The standard solver DASSL showed by far the best performance in terms of robustness and computation time. It was therefore chosen for all simulations in this work. DASSL is a multi-step solver, which means that it uses information from more than one previous step to calculate the solution of the next step. The way this is done cannot be changed in Dymola, the only allowed user input for the solver is the integration tolerance. The integration tolerance was set to 10^{-4} during model development and to 10^{-5} for result production. A diagnostics file of the solver's integration error can be obtained in Dymola. This file contains all state variables and lists the number of times that each variable

- Limits the solvers step size
- Dominates the integration error
- Exceeds 10% of the integration error

thus providing useful information for debugging slow or unstable simulations.

Algebraic loops As briefly explained in Section 2.2.2, Dymola processes the Modelica code to generate a differential-algebraic equation system (DAES). This DAES is then further processed to generate an efficient executable file. The statistics of this translation are available in Dymola's message window and contain important information about the size and structure of the DAES. Dymola lists the sizes of linear systems of equations before and after manipulation as well as the sizes of nonlinear systems of equations before and after manipulation. These sizes have significant influence on the computation time, especially the sizes after manipulation. If they are not zero, then Dymola could not break all algebraic loops, which means that the equation systems are still coupled. Solving these coupled systems of equations is more challenging, especially with nonlinear equations. It is sometimes possible to take measures in the Modelica models that reduce these algebraic loops [52]. These measures can affect the model behavior so an implementation should be carefully evaluated.

Time and state events Events are used to handle discontinuities in Dymola and can play an important role for the numerical performance. Discontinuities are defined by conditional expressions and can lead to abrupt changes in

the behavior of a system. If the conditional expression is related to time, e.g. `if time > 10 s`, then the event is called "time event". If the expression is based on a system variable, e.g. `if temperature > 50 °C`, then the event is called "state event". Due to the possibility of abrupt changes in system behavior, variable step size solvers take an iteration step up to the time of the event and restart the integration with new starting conditions afterwards. This slows down the simulation for several reasons: 1) events limit the step size of the solver by enforcing a step to be taken at the time of the event, 2) finding consistent restart conditions can be challenging, depending on the changes triggered by the event, and 3) for state events, the time of the event must be detected. The time at which a time event occurs is obviously known beforehand, but costly iterations can be necessary to detect the exact time of a state event, e.g. the time at which a temperature crosses a certain threshold. For good numerical performance, unnecessary events should be avoided and continuous behavior at events should be ensured. This is especially relevant for control structures, where conditional expressions often are used to activate/deactivate components or to adjust setpoints. A well-known effect that can occur in such situations is "chattering". Chattering describes a situation in which the numerical performance is degraded due to the generation of many state events. This can occur if the change introduced by a conditional expression leads to a change in the expression itself, leading to a loop of true/false solutions for that expression and thus the generation of many state events. The noEvent() operator can be used to suppress state events, allowing the solver to step past the event instead of determining its exact time of occurrence. This can avoid chattering and lead to improved numerical performance in some cases. However, events are also valuable for a solver because they inform about discontinuities. Without knowing about the event, the solver might struggle to find appropriate time steps, due to the discontinuity and its impact on system behavior. This can lead to simulation performance issues.

4.3 Handling of input data and results

The type and the amount of required input data depends on the type of simulation and the modeled system at hand. Input parameters, e.g. for system and component specification, are often manual user input unless automated parame-

ter studies are run. Time-varying input variables, e.g. outdoor temperature or energy demands, need to be specified by data containing the value of the variable at certain simulation times. In this work, the system boundary was set at the customer substation level, i.e. distribution systems and buildings were not modeled. Thus, all heating and cooling demands were required input data for the system models. The outdoor temperature and solar radiation were also required for the solar collector model. Hourly data points for the demands and weather data were stored in a file and read by the model `CombiTimeTable` from the MSL. The model offers several interpolation methods for the data points, e.g. linear segments and spline interpolation. Spline interpolation led to lower computation times compared to linear interpolation and was therefore chosen in this work. However, at the beginning of this work, the only spline interpolation method was `ContinuousDerivative`, which led to over- and undershoots as shown in Figure 4.1.

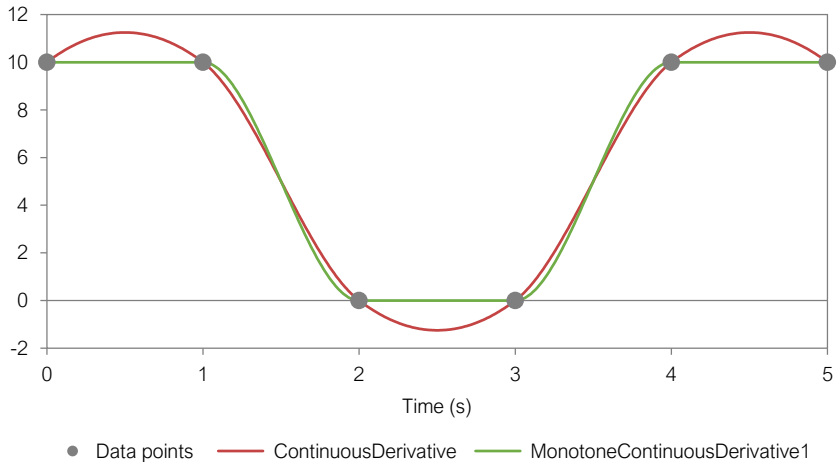

Figure 4.1: Different spline interpolations in Modelica.

As can be seen in Figure 4.1, negative energy demands could occur with this interpolation method, which led to numerical instabilities. Therefore, max() operators were used to avoid negative demands. In a later version of the model `CombiTimeTable`, new spline interpolation methods were available which did not overshoot. The method `MonotoneContinuousDerivative1`, see Figure 4.1, was therefore used in the final system models.

Another aspect that deserves attention for dynamic simulations is the plotting and saving of the results. Values for the variable trajectories are stored at certain

simulation times called “result points”, which can easily be plotted in Dymola. The user can specify the number of result points and also chose if variables should additionally be stored at events or not. Storing result points comes at a computational cost, but this is often insignificant. However, for models with many variables, storing many result points can lead to large result files and a noticeable increase in computation time. This can be avoided by only storing selected variables or by decreasing the number of result points. However, large output intervals can be misleading as shown in Figure 4.2.

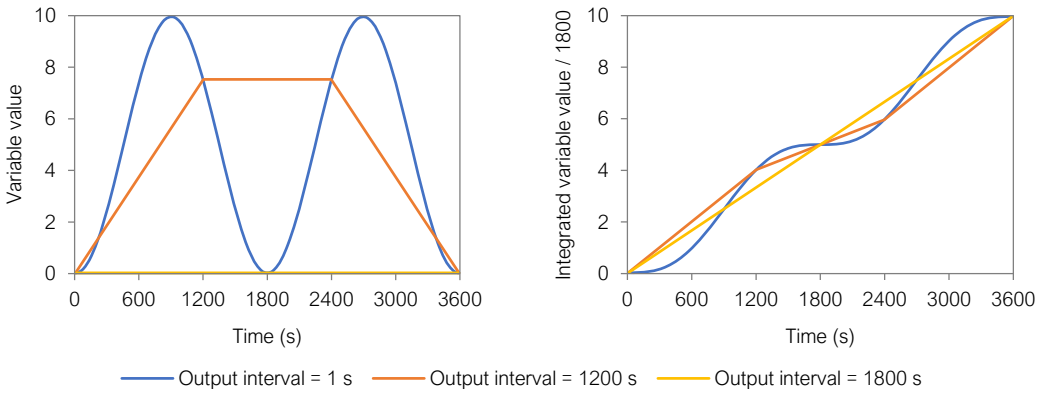

Figure 4.2: Same simulation with different output intervals.

Figure 4.2 shows that small time steps should be chosen for the investigation of fast dynamics, e.g. when tuning the output of a controller. Figure 4.2 also shows that the result points should not be used as average value when large output intervals are chosen. Instead, the variable of interest should be sent to an integrator model so that the average can be calculated precisely from the stored result points. In this work, the output interval was set to one hour for result production and all result variables were integrated.

4.4 Component models

The component models developed during this work are explained in this section. Reusability and a common level of detail were important aspects to enable the analysis of different case study systems. As explained in Section 4.1, the library Thermal from the MSL was used as basis for component model development. Icons of frequently used models and connectors in this work are shown in

Figure 4.3.

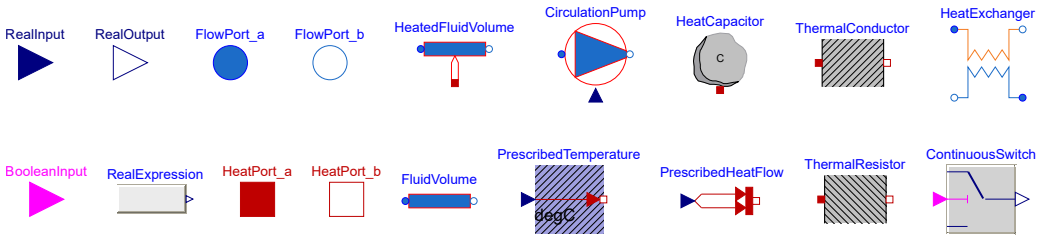

Figure 4.3: Icon legend for simulation model screenshots from Dymola.

The base class of this library is called `TwoPort` and contains two fluid flow connectors, which enable the connection to other models. The energy balance equation included in the model is shown in Equation (4.1).

$$\dot{m} \cdot c_p \cdot (T_{\text{in}} - T_{\text{out}}) + \dot{Q} = V \cdot \rho \cdot c_v \cdot \frac{dT_{\text{out}}}{dt} \tag{4.1}$$

The volume (V) and the type of fluid were input parameters of the `TwoPort` model. The fluid's density (ρ) and specific heat capacities (c_p and c_v) were assumed constant. Their values were calculated with Excel using the add-in CoolProp [53] and were stored in the Modelica class "Record". Since these properties are temperature-dependent, they were calculated for different temperature levels for each fluid. In the system models, the Record with the temperature closest to the expected average temperature in that loop was selected. Minimum and maximum allowed temperatures were also stored in the Records and were used to print warning messages when the fluid temperature was outside these limits.

The `TwoPort` model was used as basis for the models `FluidVolume` and `HeatedFluidVolume`, which were needed in all the component models described below. The models `FluidVolume` and `HeatedFluidVolume` were extensions of the `TwoPort` model and additionally contained equations to define the pressure drop in the fluid volume. The heat flow rate ($\dot{Q}$) in Equation (4.1) was set to zero for the model `FluidVolume`. The model `HeatedFluidVolume` had a thermal connector called `HeatPort`, which enabled heat transfer to and from the fluid.

4.4.1 Circulation pump model

The model `CirculationPump` was an extensions of the `TwoPort` model with a `RealInput` connector. This connector defined the mass flow rate in the `CirculationPump` model and typically originated from PI-controllers in the system model. The required power (P_{pump}) was calculated based on Equation (4.2) assuming a constant wire-to-fluid efficiency (η), which was an input parameter of the `CirculationPump` model.

$$P_{\text{pump}} = \frac{\dot{V} \cdot \Delta p}{\eta} \tag{4.2}$$

Defining the mass flow rate as input signal and the power as output variable avoided numerically expensive iterations that would otherwise be needed to find the interdependent variables $\dot{V}$ and Δp at a given power input. This enabled stable control of the system and kept computation times low. However, this could also lead to nonphysical solutions such as negative pressures, especially at high mass flow rates. The choice of a reasonable mass flow rate limit was therefore required and resulting pressure levels had to be checked for plausibility.

4.4.2 Continuous switch model

As explained in Section 4.2, discontinuities can lead to problems for the solver during simulation. The model `Switch` from the MSL switches discontinuously. Therefore, the model `ContinuousSwitch` was developed, which switches continuously between two inputs over a certain time interval. This interval was an input parameter called transitionTime. Setting this parameter to zero gives a discontinuous signal as in the `Switch` model from the MSL. Example graphs for the model output for three different cases are shown in Figure 4.4.

Different transition times can be defined for switching from Input 1 to Input 2 and vice versa for better usability. A `ContinuousSwitch` model with continuously differentiable output was also tested, but did not lead to better performance and was therefore not used.

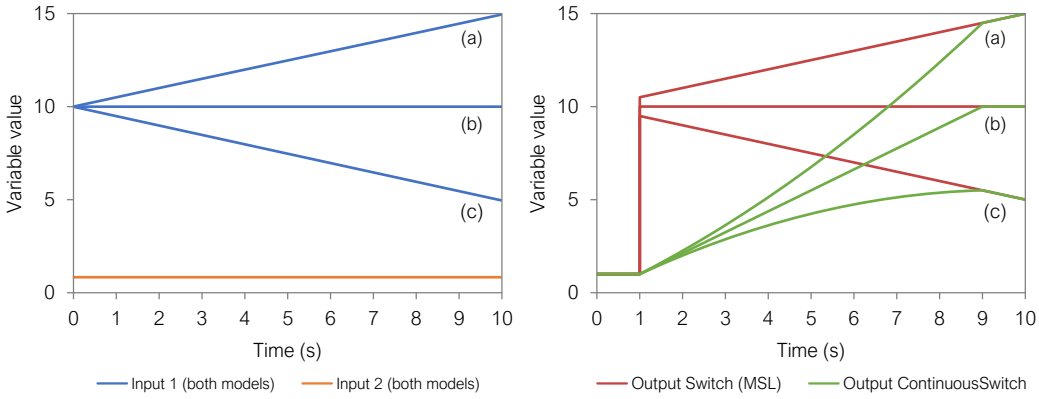

Figure 4.4: Switch model comparison (switch from Input 2 to Input 1 at t = 1 with transitionTime = 8 s).

4.4.3 Controller model

The model `Controller` was developed and included the PID-controller model `LimPID` from the MSL. However, several features for better usability and numerical performance were added over the course of this work. The derivative part of the `LimPID` model was not used in this work, i.e. all controllers were PI-controllers. A Dymola screenshot (DS) of the `Controller` model's parameter window is shown in Figure 4.5 and the parameters "use_activation_input" and "delay_measurement" are described below because they were important for the simulation performance.

Parameter use_activation_input, see Figure 4.5: setting this parameter to false deactivated the activation input connector. The measurement and setpoint signals were then always sent to the included `LimPID` model and its output was always used as output from the model `Controller`. Setting this parameter to true allowed to deactivate the use of the `LimPID` model via a Boolean signal. When deactivated, the value of the parameter output_inactive was used as output from the `Controller` model, which was typically set to zero. In addition, the input signals for the measurement and the setpoint value of the included `LimPID` model were set to zero to avoid unnecessary calculations. The integrator of the `LimPID` model thus received zero as input leading to a constant output value. When the controller was activated, this constant value affected the response of the `Controller` model. This was undesired, so the integrator input of the `LimPID` model was modified to reset the output to zero when the controller was deacti-

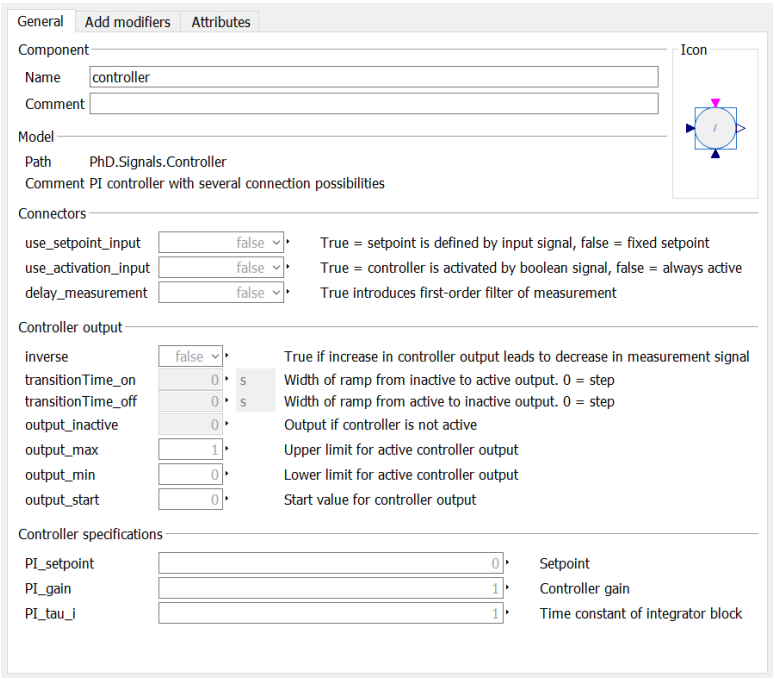

Figure 4.5: Parameter window of the `Controller` model (DS).

vated. When the activation signal became true, the `LimPID` model was used. A `ContinuousSwitch` model was used to switch between the output of the `LimPID` model and the value of the parameter output_inactive to define the output of the `Controller` model. This required the definition of the two input parameters transitionTime_on and transitionTime_off.

Parameter delay_measurement, see Figure 4.5: setting this parameter to true could break algebraic loops resulting from feedback control by delaying the measurement signal with a `FirstOrder` model from the MSL. This introduced an additional state but could still lead to more stable simulations and significantly lower computation times.

4.4.4 Heat pump model

Four heat pump models were developed in this work. Since calculating the heat pump's thermodynamic cycle was outside the scope of this work, all developed heat pump models consisted of two `HeatedFluidVolume` models, which represented the secondary fluid in the condenser and the evaporator of the heat

pump.

In the first heat pump model, `HeatPump1`, an input signal of type Real defined the heat pump power P_{HP}. The COP of the heat pump was an input parameter of the model and the heat flow rates in the condenser and the evaporator were calculated with the equations (4.3) and (4.4).

$$P_{\mathrm{HP}} \cdot \mathrm{COP}_{\mathrm{HP}} = \dot{Q}_{\mathrm{evap}} \tag{4.3}$$

$$P_{\mathrm{HP}} + \dot{Q}_{\mathrm{evap}} = \dot{Q}_{\mathrm{cond}} \tag{4.4}$$

The second heat pump model, `HeatPump2`, was based on a variable COP. Nominal operating conditions were required as input parameters and the COP depended on the actual operating conditions during the simulations. An advanced circuit simulation and optimization tool was used to generate polynomial coefficients for the COP calculation. These coefficients were included in the model `HeatPump2`, details can be found in Paper II. This model required the calculation of the polynomial coefficients for each heat pump based on detailed manufacturer specifications, which might not always be available. It was therefore decided to develop a more generic heat pump model with less user input requirements.

In the third heat pump model, `HeatPump3`, the COP of the heat pump was calculated based on the Lorentz efficiency (η_{L}) of the heat pump, which was an input parameter of the model. The Lorentz cycle is similar to the well-known Carnot cycle, but does not assume the heat source and sink to be isothermal. Instead, they have a finite heat capacity and thus change temperature during heat addition/extraction [54]. Therefore, the COP of the heat pump depended on both inlet and outlet temperatures of the `HeatedFluidVolume` models as shown in the equations (4.5) to (4.7).

$$T_{\mathrm{L,cond/evap}} = \frac{T_{\mathrm{in,sec,cond/evap}} - T_{\mathrm{out,sec,cond/evap}}}{\ln\left(\dfrac{T_{\mathrm{in,sec,cond/evap}}}{T_{\mathrm{out,sec,cond/evap}}}\right)} \tag{4.5}$$

$$\mathrm{COP}_{\mathrm{L}} = \frac{T_{\mathrm{L,evap}}}{T_{\mathrm{L,cond}} - T_{\mathrm{L,evap}}} \tag{4.6}$$

$$\mathrm{COP}_{\mathrm{HP}} = \mathrm{COP}_{\mathrm{L}} \cdot \eta_{\mathrm{L}} \tag{4.7}$$

An additional change was made for the fourth and final heat pump model, `HeatPumpFinal`. In the first three heat pump models, the power was used as input signal. This signal typically came from a `Controller` model, which controlled the outlet temperature on either condenser or evaporator side. This controller was difficult to tune due to the variations in operating conditions, see Section 2.1.3. In addition, the diagnostics file, see Section 4.2, showed that this controller output was computationally expensive. Therefore, a desired outlet temperature was used as input signal in the model `HeatPumpFinal` and the resulting power was calculated by the model. A Boolean input signal was used to define whether the condenser or evaporator outlet temperature should be set. The model `ContinuousSwitch`, explained in Section 4.4.2, was used to avoid instabilities during switching. A diagram of the model `HeatPumpFinal` and its parameter window in Dymola are shown in Figure 4.6 and Figure 4.7, respectively.

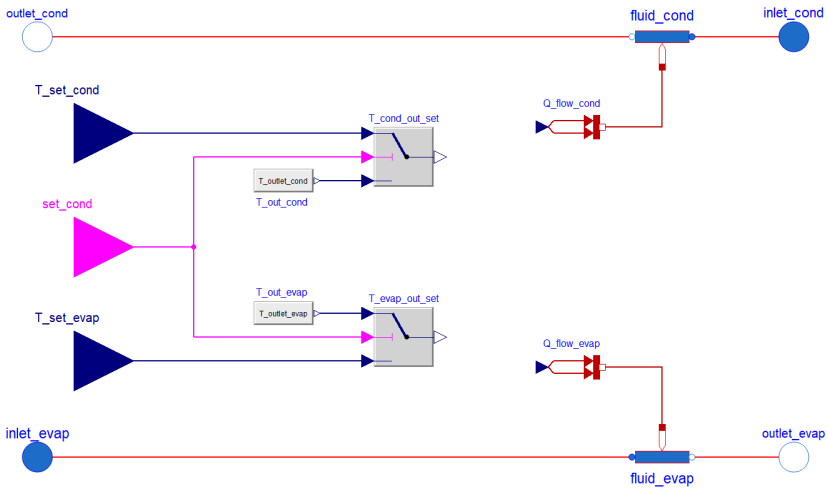

Figure 4.6: Diagram of the model `HeatPumpFinal` (DS).

The model `HeatPumpFinal` was not a physical representation of a real heat pump because of the unrealistic external definition of one of the outlet temperatures explained above. However, this modeling approach only affected the short-term response of the heat pump model. The results from one-year simulations with the third `HeatPump` model were almost identical to simulations with the

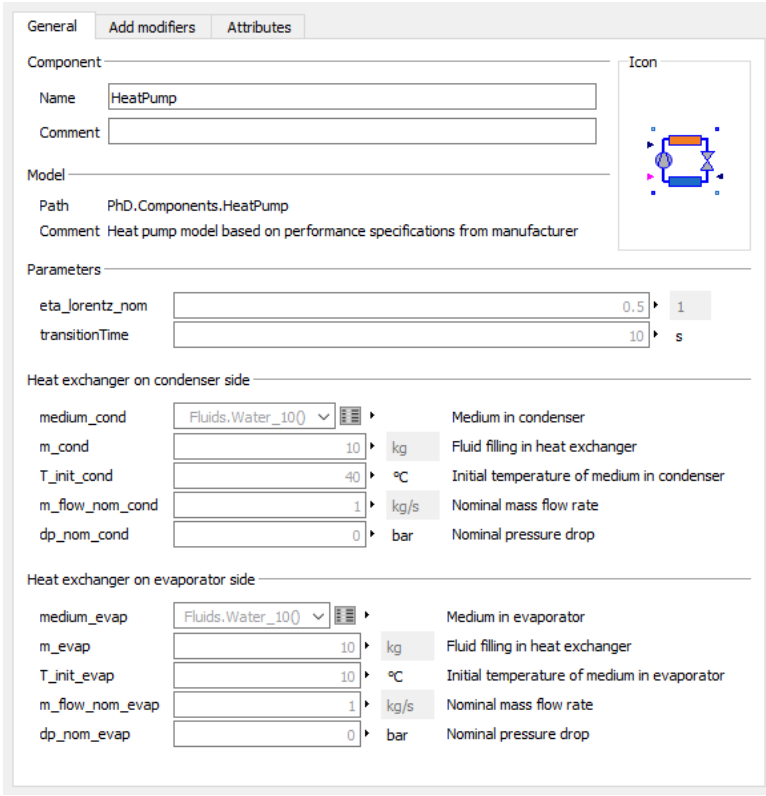

Figure 4.7: Parameter window of the model `HeatPumpFinal` (DS).

model `HeatPumpFinal`. The main difference was that the simulations with the fourth `HeatPump` model were significantly faster and more stable. The only disadvantage of the model `HeatPumpFinal` was that unrealistically high values for P_{HP} could be obtained. In the first three `HeatPump` models, P_{HP} could easily be limited by specifying a maximum output in the `Controller` model, which was used to control P_{HP}. In the model `HeatPumpFinal`, this was not possible and thus the results had to be checked for plausibility.

4.4.5 Heat exchanger models

Three heat exchanger models were developed in this work. All represented plate heat exchangers in counterflow direction. Headers and heat transfer to the ambient were neglected. Nominal values for mass flow rate and pressure drop for both fluid streams were input parameters of the models. Based on these nominal

values, the pressure drop from inlet to outlet could be chosen to be constant or a function of the mass flow rate.

The first heat exchanger model, `HeatExchanger1`, consisted of an array of `HeatedFluidVolume` models, which were connected via an array of `ThermalConductor` models, see Figure 4.8.

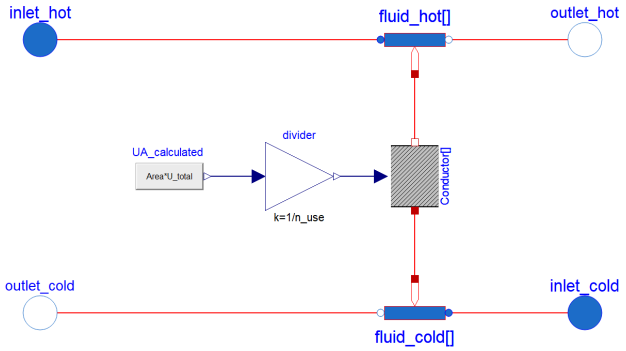

Figure 4.8: Diagram of the model `HeatExchanger1` (DS).

The heat exchange area (A_{HX}), the overall heat transfer coefficient (U_{tot}), and the number of `ThermalConductor` models (n) were input parameters of the model `HeatExchanger1`. This model was used for the simulations for Paper II with $n = 8$. This discretization value was found to give good agreement with logarithmic mean temperature (LMTD) calculations at reasonable computation times.

The discretization approach chosen for the model `HeatExchanger1` led to many state variables in the system models, which increased the computation time. To reduce the number of state variables, the model `HeatExchanger2` was developed, which was based on the widely-used LMTD approach shown in the equations (4.8) and (4.9).

$$\Delta T_{\mathrm{LM}} = \frac{(T_{\mathrm{hot,in}} - T_{\mathrm{cold,out}}) - (T_{\mathrm{hot,out}} - T_{\mathrm{cold,in}})}{\ln\left(\dfrac{T_{\mathrm{hot,in}} - T_{\mathrm{cold,out}}}{T_{\mathrm{hot,out}} - T_{\mathrm{cold,in}}}\right)} \tag{4.8}$$

$$\dot{Q}_{\mathrm{HX}} = U_{\mathrm{tot}} \cdot A_{\mathrm{HX}} \cdot \Delta T_{\mathrm{LM}} \tag{4.9}$$

This approach allowed using only one `HeatedFluidVolume` model for each

fluid stream and led to reduced computation time. However, Equation (4.8) is numerically challenging because the solver can easily take steps into undefined areas of the function during iteration. This led to unstable simulations. Therefore, the model LMTD was developed, which contained a lookup-table from which ΔT_{LM} could be obtained with the input signals dT1 $= T_{\mathrm{hot,in}} - T_{\mathrm{cold,out}}$ and dT2 $= T_{\mathrm{hot,out}} - T_{\mathrm{cold,in}}$ as shown in Figure 4.9.

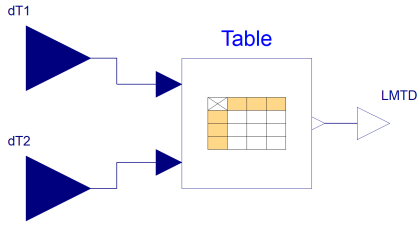

Figure 4.9: Diagram of the model LMTD (DS).

The parameter values for the lookup-table were calculated in Excel and spline-interpolation was used to interpolate between these values in Dymola. The model LMTD was included in the model HeatExchanger2 and led to increased stability of the simulations. However, the LMTD method requires both inlet and outlet temperatures of the fluid streams to calculate the heat flow rate in the heat exchanger, which in turn influences the outlet temperatures of the fluid streams. This interdependence led to long computation times.

The "effectiveness-NTU" method is based on the same theory and assumptions as the LMTD method. However, it only requires the inlet temperatures of the fluid streams to calculate the heat flow rate in the heat exchanger. The effectiveness-NTU method was therefore used in the model HeatExchangerFinal. The NTU-relation for the effectiveness of a counterflow heat exchanger from [55] was implemented in the model HeatExchangerFinal and is shown in the equations (4.10) to (4.15).

$$C_{\mathrm{hot/cold}} = \dot{m}_{\mathrm{hot/cold}} \cdot c_p \tag{4.10}$$

$$C_{\mathrm{min/max}} = \min/\max(C_{\mathrm{hot}}, C_{\mathrm{cold}}) \tag{4.11}$$

$$C_{\mathrm{r}} = \frac{C_{\mathrm{min}}}{C_{\mathrm{max}}} \tag{4.12}$$

$$\mathrm{NTU} = \frac{U_{\mathrm{tot}} \cdot A_{\mathrm{HX}}}{C_{\mathrm{min}}} \tag{4.13}$$

$$\varepsilon = \frac{1 - \exp[-\mathrm{NTU} \cdot (1 - C_{\mathrm{r}})]}{1 - C_{\mathrm{r}} \cdot \exp[-\mathrm{NTU} \cdot (1 - C_{\mathrm{r}})]} \tag{4.14}$$

$$\dot{Q}_{\mathrm{HX}} = \varepsilon \cdot C_{\mathrm{min}} \cdot (T_{\mathrm{hot,in}} - T_{\mathrm{cold,in}}) \tag{4.15}$$

Measures were taken to avoid numerical instabilities for $\dot{m}_{\mathrm{hot/cold}} = 0$ and $C_r = 1$. After the implementation of these measures, the model `HeatExchanger-Final` showed significant improvements in the simulation performance compared to the model `HeatExchanger2`. In addition, the overall heat transfer coefficient U_{tot} could be chosen to be a function of the mass flow rate in the model `Heat-ExchangerFinal`. Nominal conditions for the mass flow rate and the heat transfer coefficient were then required as input parameters and U_{tot} was calculated with Equation (4.16) and q set to 0.63 based on [56].

$$U_{\mathrm{tot}} = U_{\mathrm{nom}} \cdot \frac{(\dot{m}_{\mathrm{hot,nom}})^{-q} + (\dot{m}_{\mathrm{cold,nom}})^{-q}}{(\dot{m}_{\mathrm{hot}})^{-q} + (\dot{m}_{\mathrm{cold}})^{-q}} \tag{4.16}$$

A diagram of the model `HeatExchangerFinal` and its parameter window in Dymola are shown in Figure 4.10 and Figure 4.11, respectively.

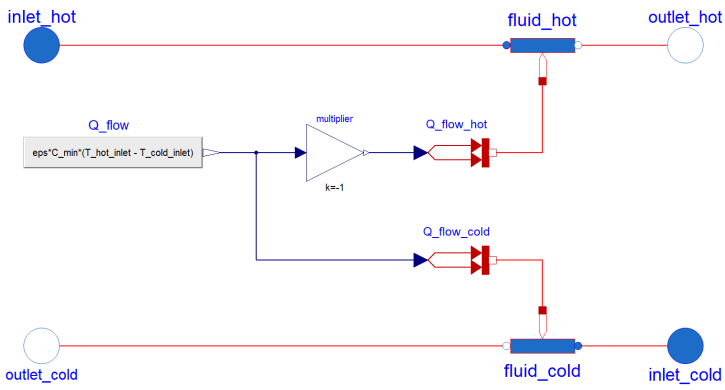

Figure 4.10: Diagram of the model `HeatExchangerFinal` (DS).

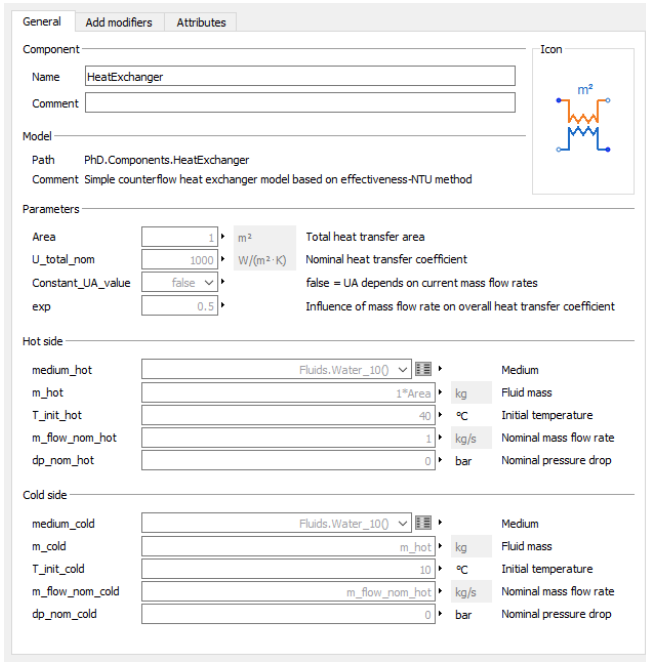

Figure 4.11: Parameter window of the model `HeatExchangerFinal` (DS).

4.4.6 Borehole thermal energy storage model

The model `BTES` represented a BTES with single U-tube pipes. Although a BTES is used as long-term storage, its short-term response can be important for system performance [57]. Therefore, an approach was chosen which included both long- and short-term dynamics in the model. The model `BTESCrossSection` was developed and several of these `BTESCrossSection` models were connected in series in the model `BTES`. The number of `BTESCrossSection` models was an input parameter of the model `BTES`, which is shown in Figure 4.12.

All input values were equal in the `BTESCrossSection` models, e.g. the fluid volume in the pipes or the thermal capacity of the ground. Therefore, the values were calculated in the model `BTES` and defined as "inner" parameters/variables. This way, they could be imported as "outer" parameters/variables in the `BTES-CrossSection` model and did not need to be calculated in each `BTESCrossSection` model. This inner/outer approach avoids duplicate code and should therefore be used when possible. The parameter window of the model `BTES` is shown in Figure 4.13.

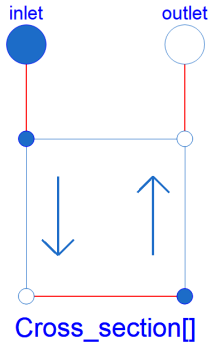

Figure 4.12: Diagram of the model BTES (DS).

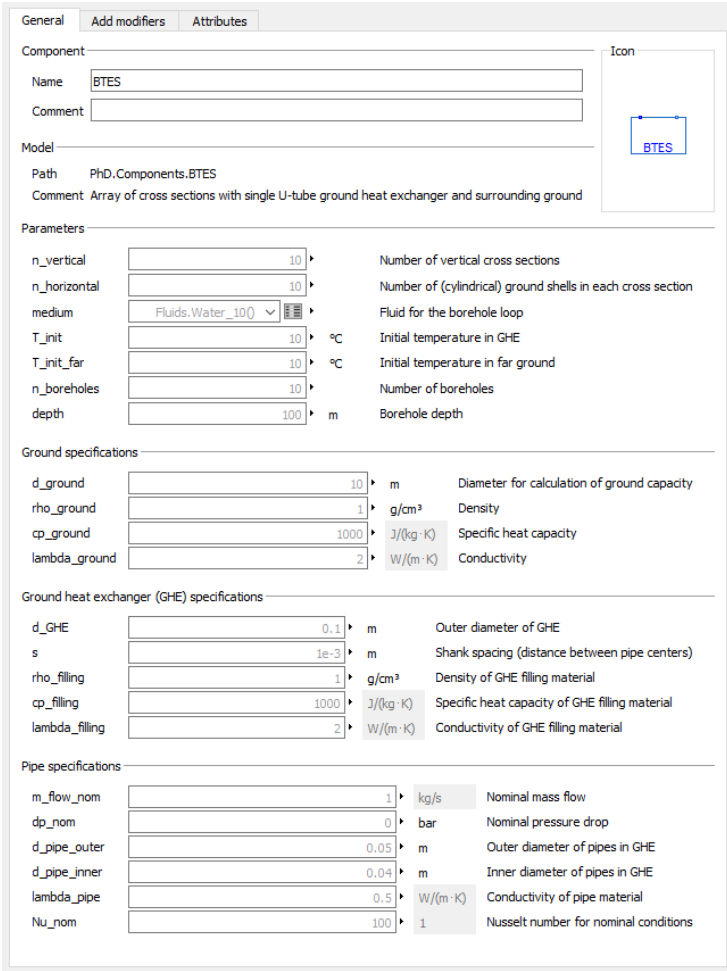

Figure 4.13: Parameter window of the model BTES (DS).

The three main parts of a BTES were included in the BTESCrossSection model: a single U-tube pipe, the borehole with filling material, and the surrounding ground. A schematic of the model and the diagram of the simulation model are shown in the figures 4.14 and 4.15, respectively.

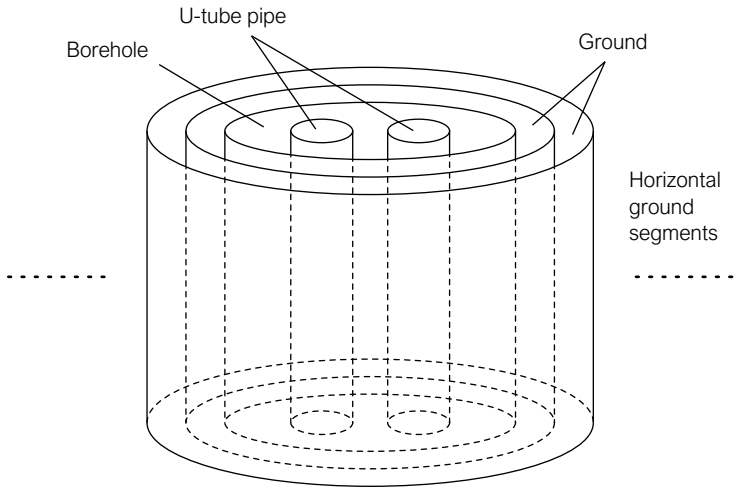

Figure 4.14: Schematic of the model BTESCrossSection.

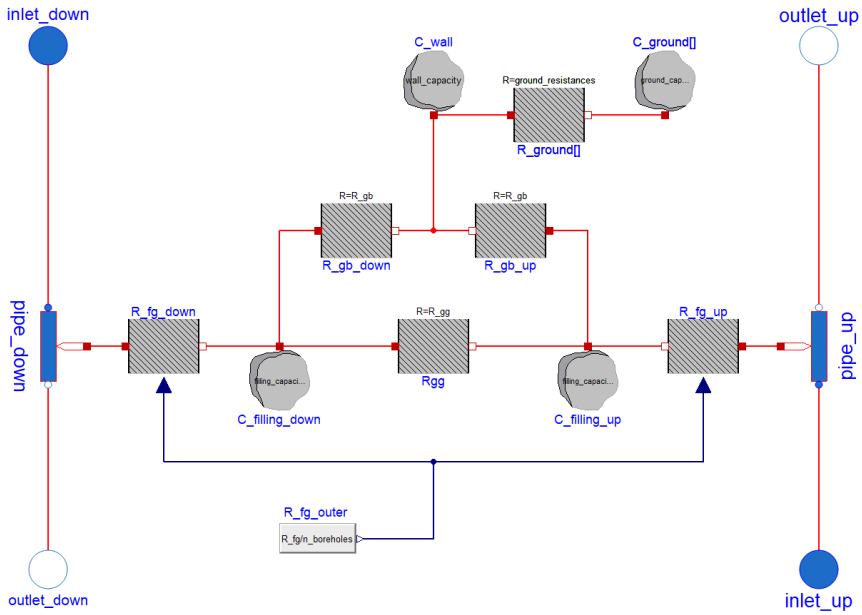

Figure 4.15: Diagram of the model BTESCrossSection (DS).

HeatedFluidVolume models were used to represent the U-tube pipe segments in each BTESCrossSection. The borehole filling and the surrounding ground were modeled with HeatCapacitor models. ThermalResistor models were added to model two-dimensional heat transfer between the fluid in the pipe and the borehole wall according to the methodology published by Bauer et al. [58]. The only variable thermal resistance was between fluid and filling material and depended on the fluid mass flow rate in the pipe due to the convective resistance R_fg, see Figure 4.15. One-dimensional, radial, heat transfer was modeled in the cylindrical ground shells. The capacities and heat transfer coefficients corresponded to the geometry of each shell element according to [59]. The number of ground shells and the ground diameter were input parameters of the model BTES, see the parameter window in Figure 4.13.

Arranging boreholes in a pattern and connecting them in series can increase the performance of a BTES, as described for example in [60]. In this work, it was assumed that all boreholes were connected in parallel with resulting equal mass flow rates. In addition, the thermal properties of the ground were assumed isotropic. These assumptions led to identical temperatures for the outermost ground shell of all boreholes. Thus, no heat was transferred between boreholes in this model and all boreholes showed identical behavior. Thus, they were lumped to one single borehole model with the input parameter n_boreholes, which defined the number of modeled boreholes, see Figure 4.13. All thermal capacities in the model BTES were multiplied by n_boreholes and all thermal resistances were divided by n_boreholes. This lumping reduced the computation time significantly without introducing an additional error. Simulations were performed to validate that the behavior of the lumped model BTES was identical to several individual BTES models.

Beier et al. published experimental data for a 52-hour charging period of a grouted single U-tube borehole heat exchanger surrounded by wet sand [61]. The short-term response of the model BTES developed in this work was validated against this experimental data set. The experimental setup was imitated by setting all input parameters of the model BTES to the respective values of the experimental setup and using the measured inlet temperature and mass flow rate as simulation input. The simulated outlet temperature, the average wall temperature, and three average ground temperatures at different distances from the

borehole were compared to the measured values from [61]. The developed BTES model showed very good agreement with the measurement data as shown in Figure 4.16.

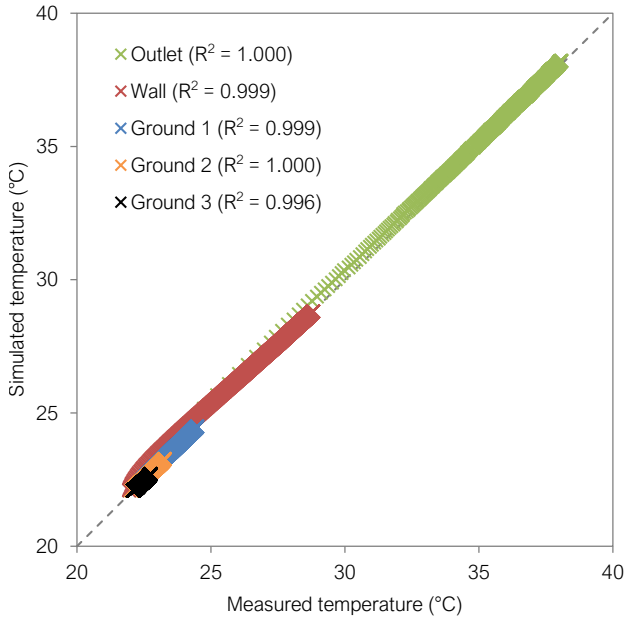

Figure 4.16: Validation of the model BTES with experimental data (data from [61]).

4.4.7 Solar collector models

Three solar collector models were developed in this work. All of them represented flat plate solar collectors and required the ambient temperature and solar radiation as input signal. The outdoor temperature was used as ambient temperature for all simulations. HeatedFluidVolume models were used to represent the fluid in the collectors. The number of serial and parallel collectors, as well as the effective collector area and the optical efficiency were input parameters of the models.

In the model SolarCollectors1, all collectors were lumped into one HeatedFluidVolume. An incoming heat flow was calculated based on the solar radiation, the total area, and the optical efficiency. To account for heat transfer from the fluid to the ambient air, a ThermalConductor model was implemented. The thermal conductance was an input parameter of the model SolarCollectors1.

In the model SolarCollectors2, an array of HeatedFluidVolume models was used. The interaction of parallel collectors was still neglected and parallel collectors were lumped to reduce computation time. However, collectors in series were modeled individually with respective flow connections. This led to a more realistic calculation of the collector outlet temperature compared to the model SolarCollectors1, which was based on only one perfectly mixed HeatedFluid-Volume model.

In the third and final solar collector model, the total heat flow rate $\dot{Q}_{\text{col}}$ in each collector was calculated based on the widely used European Standard EN 12975 1:2006

$$\dot{Q}_{\text{col}} = A_{\text{col}} \cdot \left[R \cdot \eta_{\text{opt}} - a_1 \cdot (T_{\text{col}} - T_{\text{amb}}) - a_2 \cdot (T_{\text{col}} - T_{\text{amb}})^2\right] \tag{4.17}$$

with R being the solar radiation and T_{col} being the average fluid temperature in the respective collector. The linear and the quadratic heat loss coefficient, a_1 and a_2, respectively, were input parameters of the model SolarCollectorsFinal. A diagram of the model SolarCollectorsFinal and its parameter window in Dymola are shown in Figure 4.17 and Figure 4.18, respectively.

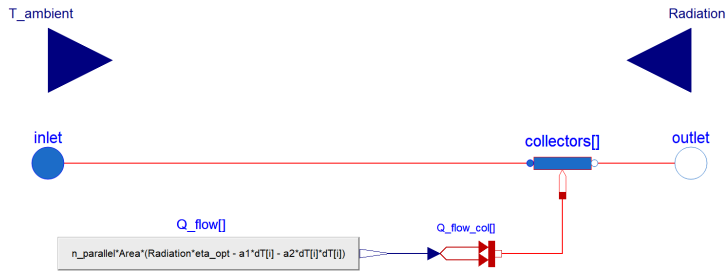

Figure 4.17: Diagram of the model SolarCollectorsFinal (DS).

T_max was an input parameter, which was used to print warning messages when a collector outlet temperature exceeded the maximum temperature. It was also used for the control of the circulation pumps in the solar collector loop.

4.4.8 Storage tank models

Two storage tank models were developed in this work. One-dimensional flow was assumed inside the tank and the tank's volume was an input parameter. Heat

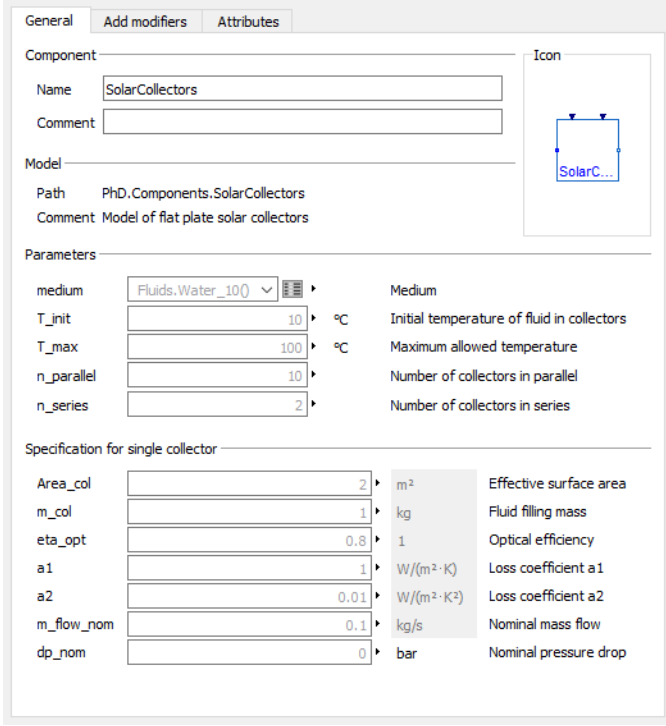

Figure 4.18: Parameter window of the model `SolarCollectorsFinal` (DS).

transfer to the ambient was modeled with a `ThermalConductor` model and the ambient temperature as input signal. Note that this ambient temperature could be different from the ambient temperature of the solar collectors, depending on the location of the storage tank.

In the model `StorageTank1`, only one `HeatedFluidVolume` was used to model the fluid in the tank, i.e. the tank was assumed to be perfectly mixed. In the model `StorageTankFinal`, an array of `HeatedFluidVolume` models was used to represent different fluid layers in the tank. This gave a more realistic temperature profile. However, thermal stratification and heat exchange between the different layers was deemed too detailed and therefore not modeled. The number of `HeatedFluidVolume` models was an input parameter of the model `StorageTankFinal`.

In the model `StorageTankFinal`, an internal heat exchanger could also be added to the tank. This was required for the storage tank in the solar collector loop. An array of `HeatedFluidVolume` models and `ThermalConductor` models

was used to represent the internal heat exchanger, with the array size equal to the number of fluid layers. The fluid in the internal heat exchanger was thermally connected to the fluid in the tank with a constant conductivity in each layer. The conductivity value was an input parameter of the model `StorageTankFinal`, which is shown in Figure 4.19.

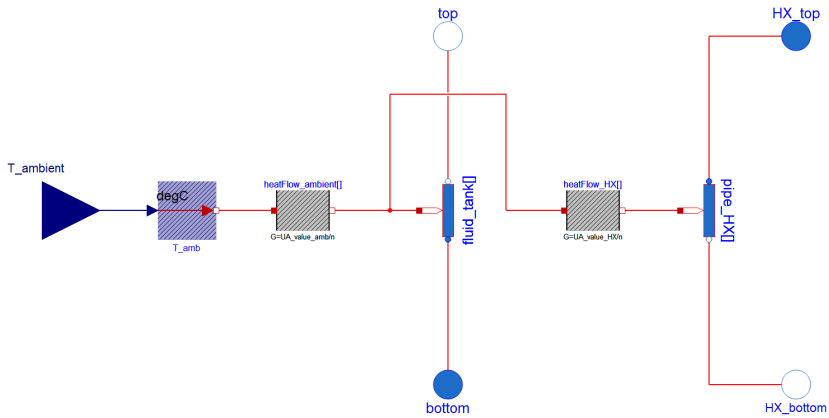

Figure 4.19: Diagram of the model `StorageTankFinal` with internal heat exchanger (DS).

4.4.9 Insulated pipe models

A single pipe model and a twin pipe model were developed in this work. Both consisted of an array of `HeatedFluidVolume` models to represent the fluid inside the pipes. The number of `HeatedFluidVolume` models as well as the pipe dimensions and the insulation properties were input parameters of the models.

The model `SinglePipe` was developed to represent insulated distribution pipes over ground. The ambient temperature was an input signal and was connected to the pipe fluid via an array of `ThermalResistor` models, see Figure 4.20.

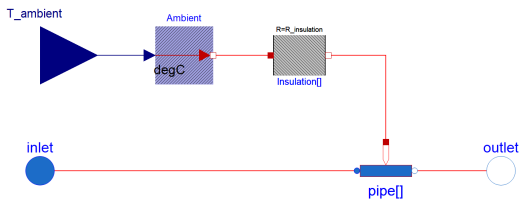

Figure 4.20: Diagram of the model `SinglePipe` (DS).

The model TwinPipe was developed to represent insulated distribution pipes underground because twin pipes are common for new grids, see Section 2.1.2. Correlations for heat losses from twin pipes were implemented in the model TwinPipe, details can be found in Paper IV. Ground specifications were input parameters of the model and the surface temperature of the ground was an input signal. The model TwinPipe is shown in Figure 4.21.

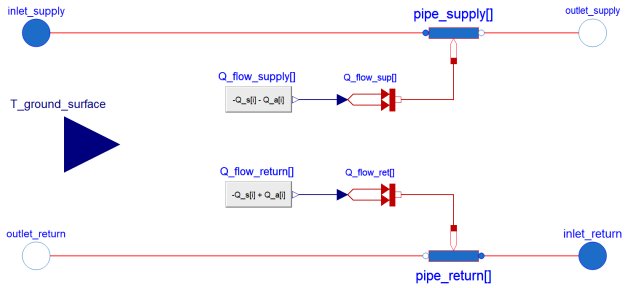

Figure 4.21: Diagram of the model TwinPipe (DS).

4.4.10 Customer substation models

Different customer substation models were developed in this work based on the substation types of the two case study systems, see Chapter 3. The customer substation models were used to model the transfer of heat between a thermal energy supply system and a customer, i.e. the HVAC system of one or several buildings. To recall, these HVAC systems of the buildings were not modeled, i.e. the customer substations were the modeled system boundary. Thus, the heating and cooling demands of the customers were required as input data.

The highly simplified model CustomerSubstation1 was developed first. It consisted of a CirculationPump model and a HeatedFluidVolume model and is shown in Figure 4.22.

The heat flow rate specified in the input data was added to or removed from the fluid and the mass flow rate was controlled by the circulation pump to yield a fixed temperature difference between inlet and outlet of the substation. This temperature difference was an input parameter of the model. The model CustomerSubstation1 was only used for testing purposes and for the very first steps of the system model development.

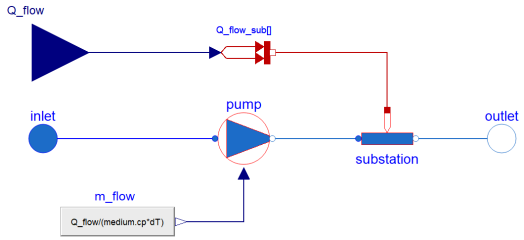

Figure 4.22: Diagram of the model `CustomerSubstation1` (DS).

The model `CustomerSubstationVulkan` was developed for the case study Vulkan and could be used as heating or cooling substation. The inlet temperature on the secondary side, i.e. the return temperature (T_{ret}) from the buildings, was an input parameter of the model. The model `CustomerSubstationVulkan` as used for cooling is shown in Figure 4.23.

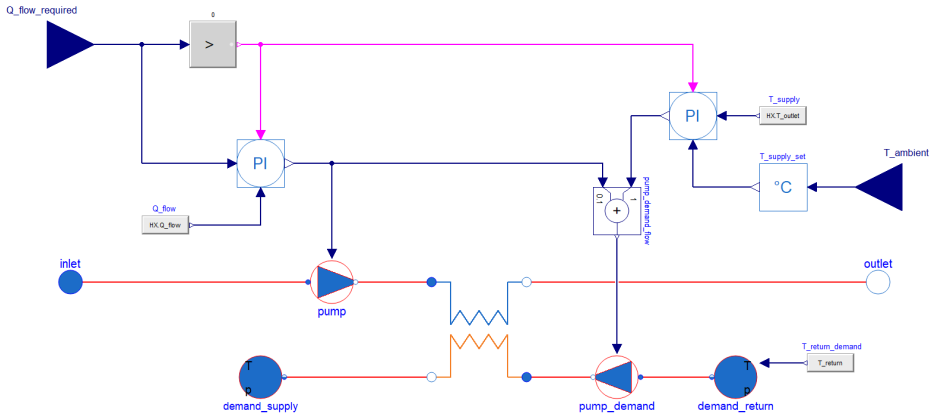

Figure 4.23: Diagram of the model `CustomerSubstationVulkan` (DS).

The model `CustomerSubstationVulkan` contained a heat exchanger and two circulation pumps as can be seen in Figure 4.23. The primary circulation pump, i.e. the one on the thermal energy supply system side, was controlled to deliver the specified heat flow rate. The secondary circulation pump, i.e. the one on the customer side, was controlled to deliver a certain supply temperature to the customer. This temperature could either be constant or outdoor temperature compensated. This supply temperature control could also be deactivated so that both circulation pumps received the same mass flow rate signal. As for the model `HeatPumpFinal`, the model `CustomerSubstationVulkan` was not a physi-

cal representation of a real customer substation because of the unrealistic control approach. However, the model led to fast and stable simulations and the obtained results were reasonable.

A customer substation and a prosumer substation model were developed for the case study Brøset. These are explained in detail in Paper IV and are therefore only briefly introduced here. The model `CustomerSubstationBroeset` had two heat exchangers: one for space heating and one for DHW heating as shown in Figure 4.24.

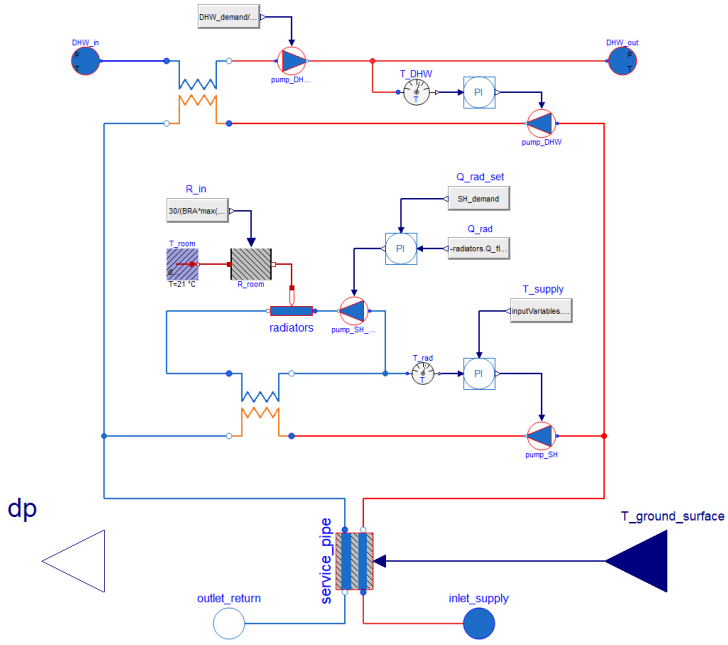

Figure 4.24: Diagram of the model `CustomerSubstationBroeset` (DS).

The model `ProsumerSubstationBroeset` was modeled as return/supply connection for prosumers, i.e. customers that can also deliver heat to the grid. The model is shown in Figure 4.25.

4.5 System models

Several system models were developed for the two case study systems described in Chapter 3. As mentioned before, focus was on the Vulkan case study. The

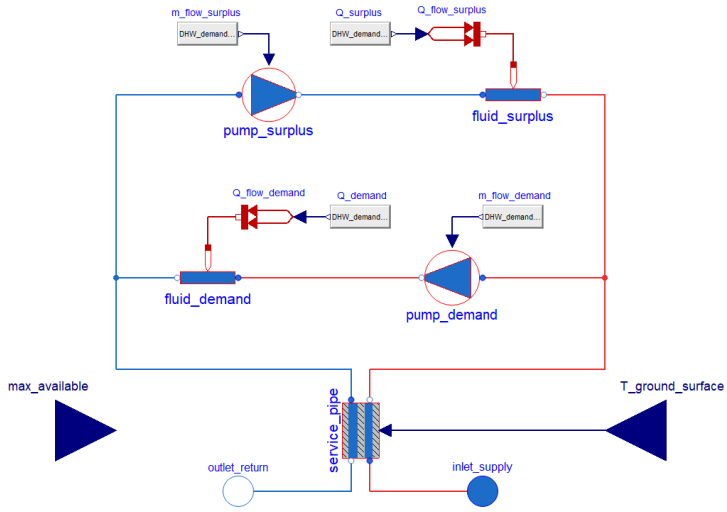

Figure 4.25: Diagram of the model `ProsumerSubstationBroeset` (DS).

author contributed to the Brøset system models by giving general modeling advice, supporting component and system model development, and providing component models for the system model used in Paper IV.

Connecting component models in Modelica is very simple. In Dymola, the graphical user interface allows connecting ports by click and drag. This will automatically create connect-equations in the model. However, implementing a control system can be challenging due to the physical modeling approach, especially for systems with many interconnected components. For such systems, it is advisable to build system models successively, i.e. modeling a part of the system first and adding more components when the control of the modeled part is working satisfactory. However, component models and system models were developed in parallel in this work. Therefore, the system model development was an iterative process and required many adjustments of the control structure.

4.5.1 Integrated heating and cooling system at Vulkan

The system model development for the Vulkan case study was one of the main tasks of this work. The system model has undergone many small and large modifications during the course of this work, but only the two versions that were used for publications, namely Paper II and Paper V, are presented here.

The first system model for Vulkan

The first system model for Vulkan was used for the analysis of heat export to the local DH grid as described in Paper II. The model is shown in Figure 4.26.

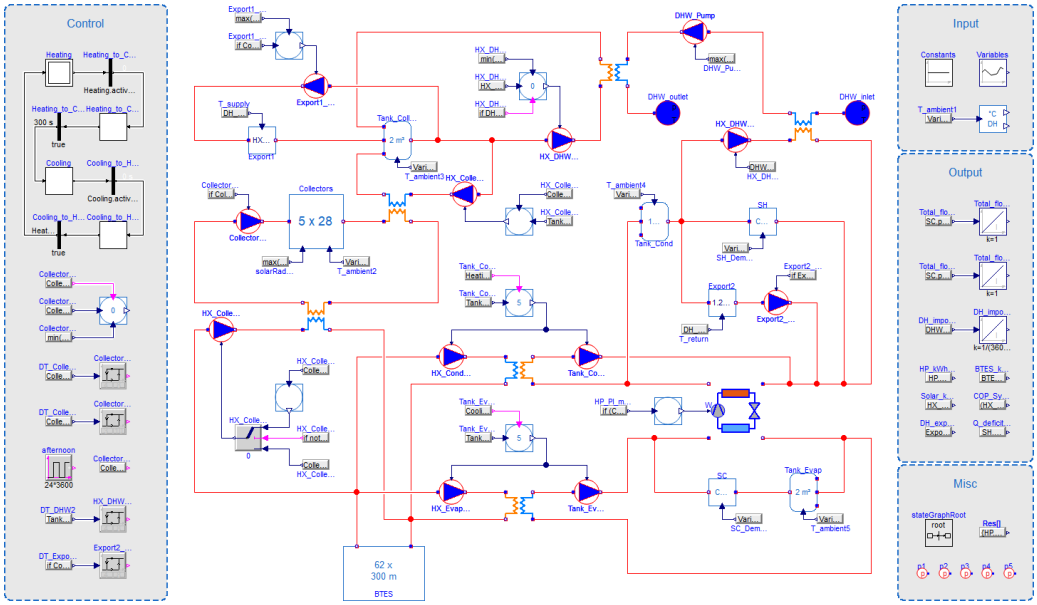

Figure 4.26: Diagram of the first system model for Vulkan as used for Paper II (DS).

The system model shown in Figure 4.26 contained some issues, which are listed below.

- The following non-final component models were used: `StorageTank1`, `HeatExchanger1`, `SolarCollectors1`, and `HeatPump2`, see Section 4.4.
- Only one heat pump was included in the system model. This simplification was made because the condenser heat from all heat pumps was sent to the same secondary fluid loop of the IHCS. The product cooling demand was therefore added to the space cooling demand.
- The snow melting demand and the ITES were neglected.
- The included model `StorageTank1` did not have an internal heat exchanger, so an own loop was modeled to transfer heat from the solar collectors to the tank. Two loops were modeled to transfer heat from the collector tank to the DH grid or to DHW heating.

- A constant initial temperature of the ground was assumed in the model BTES (instead of a linear profile) and the ground radius was set to 5 m (instead of 8 m).
- A heat exchanger was falsely included in the BTES discharging loop on the evaporator side of the heat pump.
- The input data for radiation were retrieved from the software Meteonorm and thus represented a typical year (instead of data for the analyzed year from the nearest weather station).

Due to these issues, the control of this system version is not described in detail here. A short description can be found in Paper II.

The final system model for Vulkan

The issues listed above were fixed in the final system model, in which the final versions of all component models were used. This system model was used for Paper V. A Dymola screenshot of the model and a modified version with selected specifications are shown in Figure 4.27 and Figure 4.28, respectively.

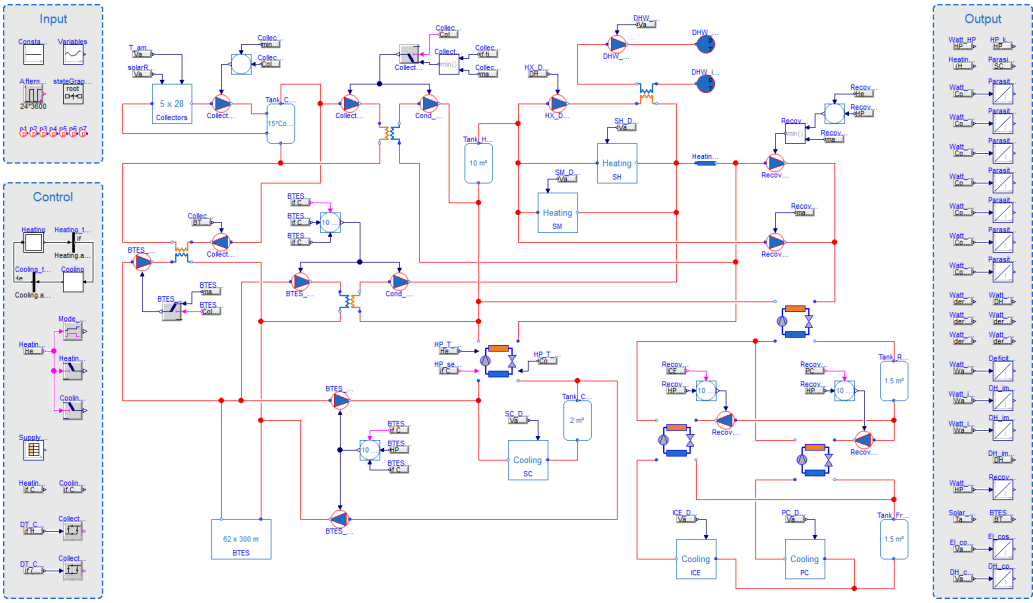

Figure 4.27: Diagram of the final system model for Vulkan as used for Paper V (DS).

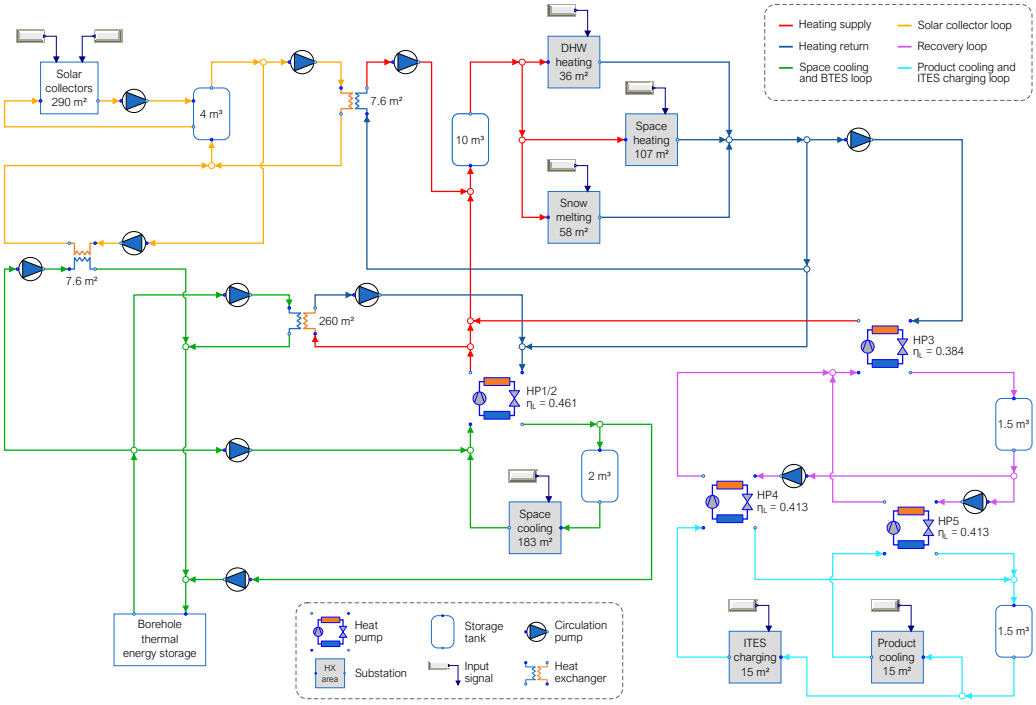

Figure 4.28: Schematic of the final system model for Vulkan with legend and selected specifications.

The main component specifications used for system simulations can be seen in Figure 4.28. Additional specifications are listed in the tables 4.1, 4.2, and 4.3.

The existing IHCS was equipped with a simple control system. The heat pumps received stepwise control signals to activate/deactivate their parallel circuits and compressor stages. These step signals were based on the storage tank temperatures. The circulation pumps were controlled based on pressure difference setpoints or temperature setpoints. The storage tanks were only used as buffers. In the system model, the heat pumps were controlled continuously because the individual compressor stages were not included in the heat developed pump models. The circulation pumps were controlled with PI-controllers based on temperature setpoints. The PI-controller outputs were limited to avoid unrealistically high mass flow rates.

The IHCS had two operation modes: 1) “heating mode” and 2) “cooling mode”. A free cooling mode was originally planned but was not implemented as

Table 4.1: Heat exchanger model specifications used in the final system model.

	Heat transfer area m^2	Nominal heat transfer coefficient $W/(m^2 \cdot K)$	Nominal mass flow rate kg/s
Space heating	107.0	4 400	8.0
Snow melting	58.0	3 300	5.0
DHW heating	36.0	2 700	1.0
Space cooling	183.0	3 300	20.0
Product cooling	15.0	3 500	3.0
ITES loading	15.0	3 500	6.0
Solar to heating	7.6	3 500	0.8
Solar to BTES	7.6	3 500	0.8
HP to BTES	260.0	3 500	10.0

Table 4.2: Solar collector model specifications used in the final system model.

Parameter	Value	Unit
Number of serial collectors	5	-
Number of parallel collectors	28	-
Effective surface area	1.9	m^2
Optical efficiency	0.773	-
Linear heat loss coefficient	3.676	$W/(m^2 \cdot K)$
Quadratic heat loss coefficient	0.0143	$W/(m^2 \cdot K^2)$
Fluid filling	1.2	kg

explained in Paper I. Models from the library StateGraph, which is included in the MSL, were used in the system model to switch between the two operation modes. This operation mode switching was triggered based on the average temperatures in the storage tanks for heating and space cooling as shown in Figure 4.29.

An operation mode switch triggered the activation/deactivation of the BTES circulation pumps, a change in heating supply temperature setpoint, and different control strategies for the solar collectors and the ITES. Details are given in the following paragraphs. The real system required some downtime for an operation

Table 4.3: BTES model specifications used in the final system model.

Parameter	Value	Unit
Number of boreholes	62	-
Vertical discretization	4	-
Horizontal discretization	30	-
Borehole depth	300	m
Borehole diameter	0.14	m
Ground diameter	9	m
Ground density	2 600	kg/m^3
Ground heat capacity	850	$J/(kg \cdot K)$
Ground conductivity	2.75	$W/(m \cdot K)$
U-tube diameter	0.04	m
U-tube conductivity	0.42	$W/(m \cdot K)$
Nusselt number inside borehole	5	-

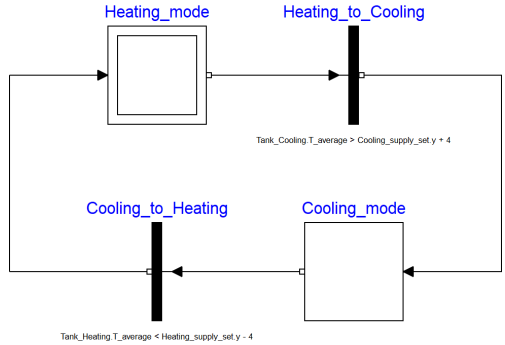

Figure 4.29: StateGraph logic applied for switching between operating modes (DS).

mode switch due to manual valve adjustments. Therefore, only one operation mode switch was performed between heating and cooling season. In the system model, this downtime was neglected and several operation mode switches were allowed.

In heating mode, the outlet temperature of HP 1/2 on the condenser side was set to equal the heating supply temperature of 55 °C. The outlet temperature on the evaporator side of HP 1/2 was controlled by the BTES pump with the space cooling supply temperature of 6 °C as setpoint. When the space cooling demand

increased, less heat had to be extracted from the BTES. At some point, the BTES was not needed as heat source and the temperature in the cooling tank increased. When the average temperature in the cooling tank was higher than 10 °C, an operation mode switch was triggered to ensure that the space cooling demand could be covered. The ITES was not used in heating mode.

In cooling mode, the outlet temperature of HP 1/2 on the evaporator side was set to equal the space cooling supply temperature of 6 °C. The outlet temperature on the condenser side of HP 1/2 was controlled by the BTES pump with a reduced heating supply temperature of 51 °C as setpoint. When the heating demands increased, less heat was available to be injected into the BTES. At some point, the BTES was not needed as heat sink and the temperature in the heating tank decreased due to the increasing heating demands. When the average temperature in the heating tank was lower than 47 °C, an operation mode switch was triggered to ensure that the heating demands could be covered. The ITES was used to reduce space cooling peak demands and was charged by HP 4 during the night.

The heat from the solar collectors was accumulated in a storage tank. The circulation pump was controlled with a floating collector outlet temperature, which was set to 10 °C above the temperature at the top of the solar storage tank, similar to [62]. The accumulated heat could be sent to the heating supply line or to the BTES loop via separate heat exchangers, see Figure 4.28. Rule-based control was applied to decide when the heat should be sent to which heat exchanger. The chosen strategy is described below and shown in Figure 4.30. Boolean signals and hysteresis models were used to implement the strategy in the system model.

In cooling mode, the solar heat was used to charge the BTES because enough condenser heat from the heat pumps was available to cover the heating demands. In cooling mode, sending solar heat to the heating supply line was prioritized. Therefore, the collector tank was charged until the temperature at the top was higher than the heating supply temperature setpoint. The solar radiation peaks around noon, so the temperature in the storage tank was not expected to rise significantly after 1 p.m. The heat was then used to charge the BTES. Most heat was accumulated during the summer when the system was operating in cooling mode. Therefore, around 90% of the heat was used to charge the BTES throughout the year.

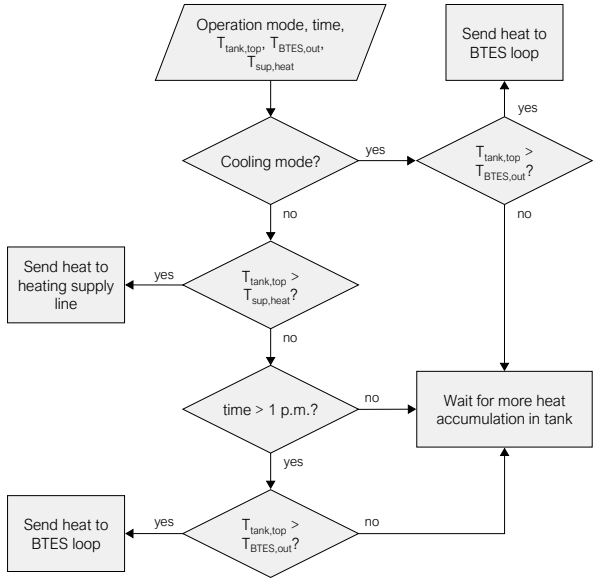

Figure 4.30: Rule-based controller logic for use of the solar heat.

The Dymola statistics of the final system model are shown in Figure 4.31. It can be seen from Figure 4.31 that there were no remaining algebraic loops in the DAES (Sizes after manipulation of the linear systems: $\{0, 0, 0, 0, 0, 0, 0, 0, 0\}$). The computation time for a one-year simulation was about 70 seconds with an Intel© Core™ i7 6700K processor (4 GHz) and 64 GB RAM. Setting the parameter delay_measurement in all `Controller` models to false (see Section 4.4.3) led to remaining nonlinear loops (Sizes after manipulation of the nonlinear systems: $\{9, 4, 10\}$). In this case, the computation time was increased by about 60%. This shows how even small changes in a model can have a large effect on the final DAES and the numerical performance.

The main simplifications and assumptions behind the final system model are summarized below.

- Pipes between components were neglected because no detailed information was available. Distribution heat losses from the IHCS were thus not calculated. However, the losses from the distribution systems of the buildings were included in the measured heating demands. The distances were short compared to the pipe lengths of DH grids due to the small area of the building complex.

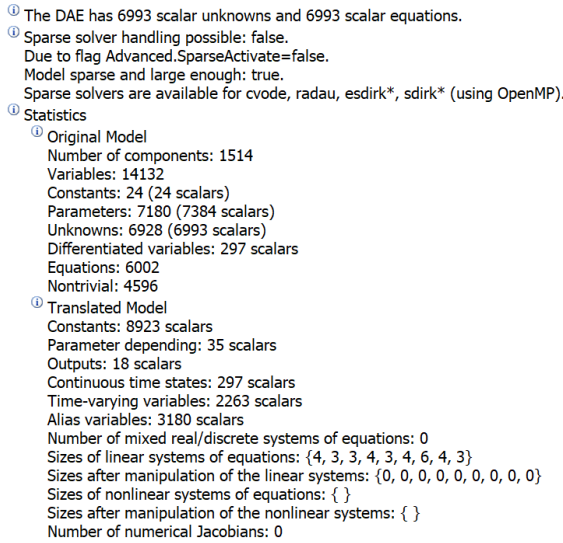

Figure 4.31: Dymola statistics for the final system model for Vulkan (DS).

- Each building substation contained five separate heat exchangers. These were used for space heating from the IHCS and the DH grid, DHW heating from the IHCS and the DH grid, and space cooling from the IHCS. Heat exchangers for the same purpose were lumped in the system model and one substation model for each demand type was used.

- The heat exchangers for heat import from the DH grid were not modeled. Instead, the required heat import was calculated based on the remaining heating demand after the heat exchanger connection to the IHCS.

- The real system required some downtime for an operation mode switch due to manual valve adjustments. Therefore, only one operation mode switch was performed between heating and cooling season. In the system model, this downtime was neglected and several operation mode switches were allowed.

- The return temperature from the buildings was assumed constant because modeling of the building was outside the scope of this work.

- The ITES was not modeled physically. Instead, load profiles were created to represent charging/discharging as explained in Paper V.

- HP 1/2 in Figure 4.28 represented two parallel heat pumps of the same type. These were modeled as one unit because their efficiencies were very similar. Continuous rule-based control was used in the system model although the heat pumps were controlled with stepwise on/off control
- Heat losses from the storage tanks were neglected due to missing temperature measurements at the tank's locations.

4.5.2 Local district heating grid at Brøset

Several system models have also been developed for the case study Brøset, but only the two versions that were used for publications, namely Paper III and Paper IV, are presented here. As mentioned before, the author contributed to the modeling part of these studies, especially Paper IV, but much modeling work has also been done by others.

First system model for Brøset

The commercial library TIL from TLK-Thermo GmbH was initially used for this case study. The first system model for Brøset was therefore developed using this library and was used for the analyses in Paper III. The model is shown in Figure 4.32.

As for the Vulkan case study, the first system model for Brøset was much less mature than the final model. The main issues of the first system model are summarized below.

- The customer substation models (with different building icons in Figure 4.32) were similar to the one shown in Figure 4.22, i.e. extremely simplified.
- Single pipe models were used (similar to the one shown in Figure 4.20) instead of twin pipe models for the DH distribution pipes.
- Only the pipes of the main grid were modeled, the supply pipes to and from the buildings were neglected. The total pipe length was therefore only 3.5 km (compared to 6.8 km in the final system model).

Due to these issues, this system version is not described in more detail here. A description can be found in Paper III. The computation time for a one-year

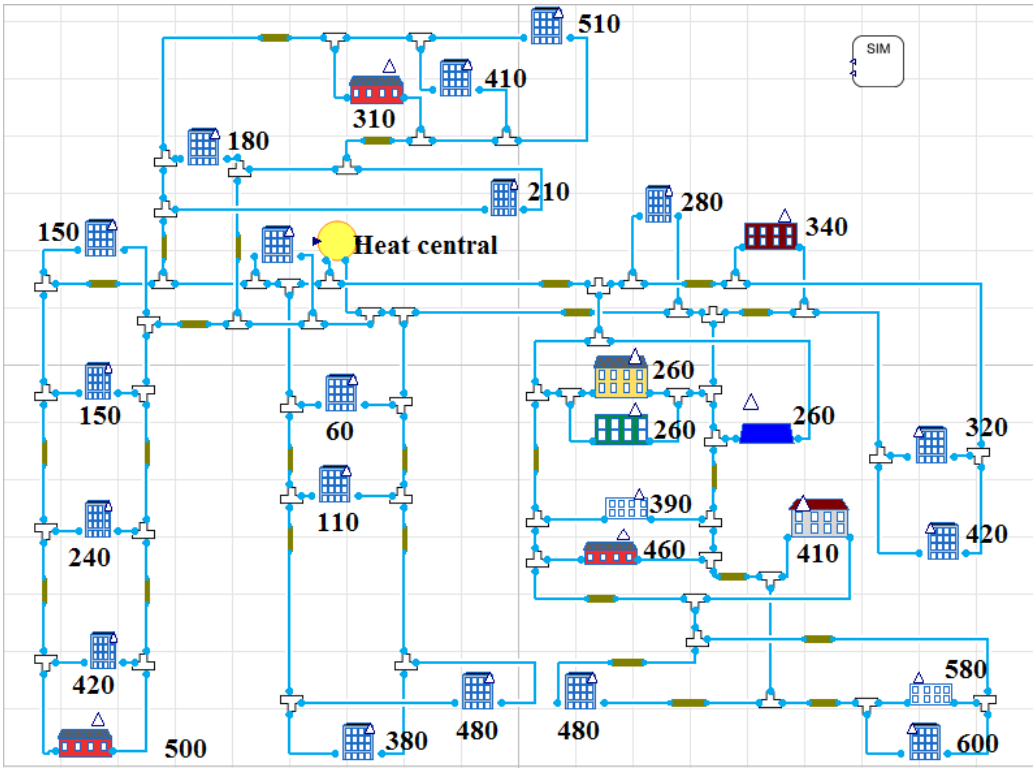

Figure 4.32: Diagram of the first system model for Brøset (taken from Paper III).

simulation with this system model was several hours. The reasons for this were not analyzed in detail. The implementation of a heat exchanger model in the customer substation model was tested, but led to significantly longer computation times and was thus deemed impracticable. It was therefore decided to build a new system model with the simulation models described in this thesis.

Final system model for Brøset

The system model used for Paper IV is shown in Figure 4.33. In this version, the model `CustomerSubstationBroeset`, see Figure 4.24, was used, which had separate heat exchanger models for space heating and DHW heating and a supply pipe. These supply pipes as well as all other pipes in the grid were `TwinPipe` models as shown in Figure 4.21. In addition, several `ProsumerSubstationBroeset` models, see Figure 4.25, were added to the system model.

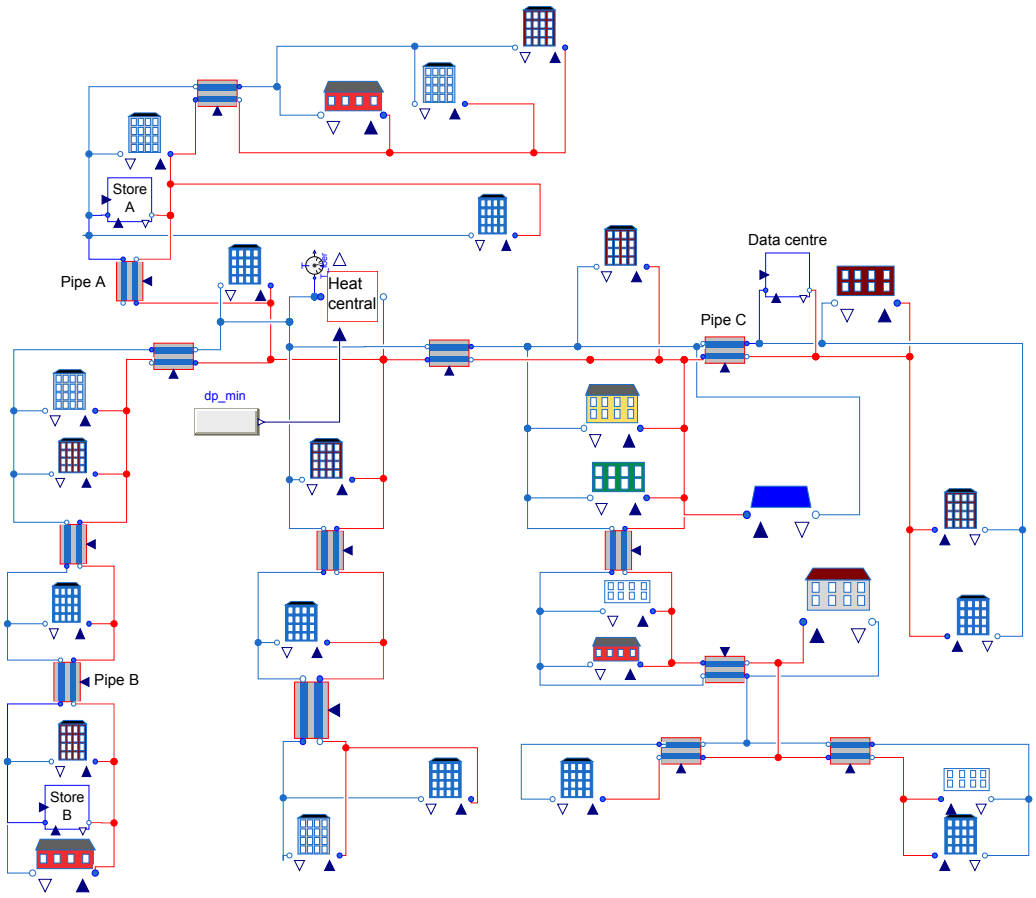

Figure 4.33: The final system model for Brøset (taken from Paper IV).

As explained in Section 3.2.2, the main heat supply was assumed to come from Trondheim's existing DH grid. This connection was not modeled in detail. Instead, the heat central in the system model contained a heat source, which delivered the heat flow rate required to reach the supply temperature setpoint. The pressure lift in the heat central was controlled to ensure a minimum pressure difference of 70 kPa in all the customer substations. The pressure drop in the furthest substation was therefore measured in each branch and the minimum value of these was an input signal of the heat central model, see Paper IV for details.

The Dymola statistics of the final system model are shown in Figure 4.34. It can be seen from Figure 4.34 that there were no remaining algebraic loops in the

DAES of the system model. However, the DAES was much larger compared to the Vulkan system model, see Figure 4.31, which is why computation times were still about two hours for a one-year simulation.

```
ⓘ The DAE has 21977 scalar unknowns and 21977 scalar equations.
ⓘ Sparse solver handling possible: false.
  Due to flag Advanced.SparseActivate=false.
  Model sparse and large enough: true.
  Sparse solvers are available for cvode, radau, esdirk*, sdirk* (using OpenMP).
ⓘ Statistics
    ⓘ Original Model
      Number of components: 5674
      Variables: 46608
      Constants: 115 (115 scalars)
      Parameters: 24760 (24899 scalars)
      Unknowns: 21733 (21977 scalars)
      Differentiated variables: 558 scalars
      Equations: 19046
      Nontrivial: 15715
    ⓘ Translated Model
      Constants: 27028 scalars
      Parameter depending: 313 scalars
      Outputs: 2 scalars
      Continuous time states: 558 scalars
      Time-varying variables: 8466 scalars
      Alias variables: 11184 scalars
      Number of mixed real/discrete systems of equations: 0
      Sizes of linear systems of equations: {3, 3, 4, 4, 7, 6, 3, 3, 3, 3, 5, 3, 4, 3, 3, 4, 3, 3, 3, 3, 5, 3, 5, 3, 3, 3, 3, 4, 8, 3, 5, 3, 3, 5, 3, 3, 4, 3, 3, 3, 3, 5, 3, 3, 3, 3, 3, 3, 3}
      Sizes after manipulation of the linear systems: {0, 0, 0, 0, 0, 0, 0, 0, 0, 0, 0, 0, 0, 0, 0, 0, 0, 0, 0, 0, 0, 0, 0, 0, 0, 0, 0, 0, 0, 0, 0, 0, 0, 0, 0, 0, 0, 0, 0, 0, 0, 0, 0, 0, 0, 0, 0, 0, 0}
      Sizes of nonlinear systems of equations: { }
      Sizes after manipulation of the nonlinear systems: { }
      Number of numerical Jacobians: 0
```

Figure 4.34: Dymola statistics for the final system model for Brøset (DS).

5 Approach for optimization-based control of thermal energy systems with storages

The importance of system control has briefly been described in Section 2.1.3. Especially systems with storages require a suitable control strategy to operate efficiently. In this chapter, which is based on Paper VI, an approach for optimization-based control is presented. The main idea of this approach was to find optimized setpoint trajectories for the system's PI-controllers.

The methodology was applied to analyze the case study system at Vulkan, see Section 3.1. The currently used setpoints described in Section 4.5.1 were called "business as usual" (BAU). Optimizations were performed to obtain setpoints for minimized electricity use and minimized electricity costs. Afterwards, these were implemented into the final system model and the simulation results with optimized setpoints were compared to the results with BAU setpoints. This workflow is shown in Figure 5.1.

All elements of the optimization procedure (Part 2 in Figure 5.1) are explained in detail in the next sections.

5.1 Optimization procedure

JModelica.org is an open-source platform for simulation and optimization of complex dynamic systems and is explained in Section 2.2.3. All the optimizations in this work were performed with JModelica.org version 2.2 via 64-bit Python

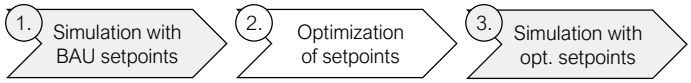

Model	Final system model	Seasonal models	Final system model
Environment	Dymola	JModelica.org	Dymola
Task	Simulation	Optimization	Simulation
Result	Electricity use/costs for the BAU case	Optimized setpoints	Electricity use/costs with improved control

Figure 5.1: Interaction of simulation and optimization.

scripting. It is worth noting that JModelica.org version 2.0 was used initially, which only supported 32-bit Python. The memory usage of a 32-bit Python process is limited to about 2 GB. This was insufficient for the optimizations in this work and led to frequent memory allocation errors. JModelica.org version 2.2 was released in March 2018 and was the first version to support 64-bit Python. The upgrade to version 2.2 was therefore crucial for this work. The main steps of the optimization procedure used to obtain the optimized setpoints are shown in Figure 5.2 and are described below.

Step 1: An initial simulation was required to obtain variable trajectory data for initialization and scaling of the NLP variables in Step 5, see Figure 5.2. To this end, the Modelica model for initialization was compiled into a Functional Mock-Up Unit and simulated using the CVode solver from the SUNDIALS suite [63], which is included in JModelica.org.

Step 2: The Modelica model for optimization and the problem formulation (Optimica code) were compiled and transferred to the CasADi interface of JModelica.org. CasADi was used for the computation of derivatives using algorithmic differentiation [32].

Step 3: Routines for symbolic elimination based on block-triangular ordering are included in JModelica.org and can be applied to reduce the number of algebraic variables as explained in [64]. Symbolic elimination was implemented in this work and was found to be crucial for successful converge as it significantly reduced the size of the resulting NLP.

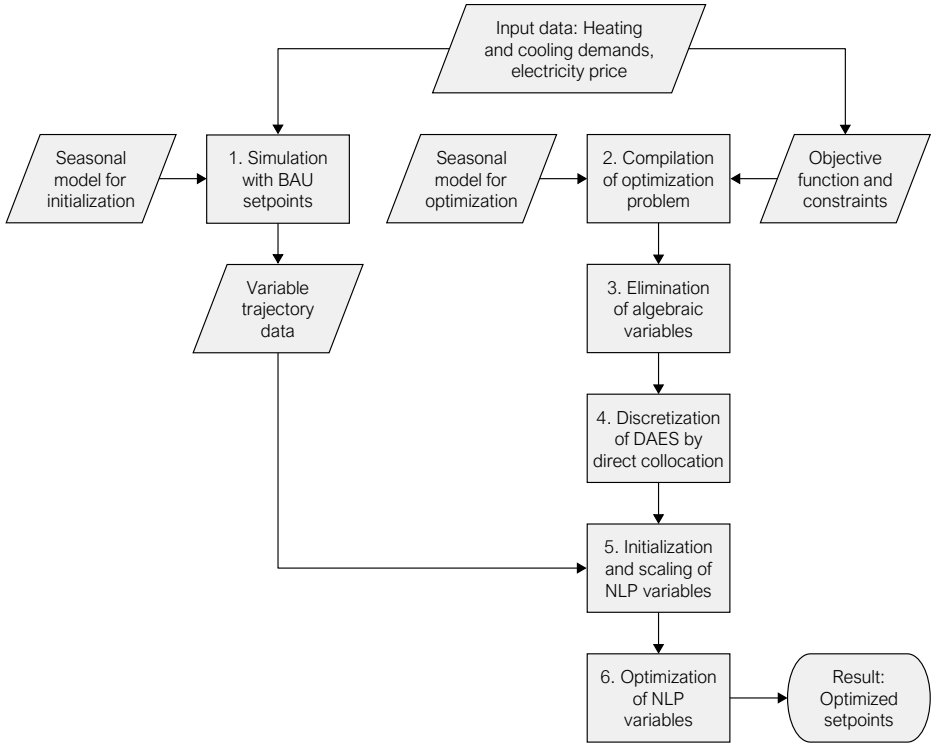

Figure 5.2: Flowchart for main steps of the optimization with JModelica.org.

Step 4: Code for orthogonal collocation on finite elements is included in JModelica.org and was used to transform the infinite-dimensional dynamic optimization problem into a finite-dimensional NLP. The number of collocation elements and the number of collocation points in each element has a strong influence on the size of the resulting NLP. See Paper VI for details.

Step 5: Variable trajectory data obtained during the initial simulation (Step 1) were used for automatic initialization and scaling of the NLP variables.

Step 6: The resulting NLP was solved using version 3.12.4 of the primal-dual interior-point solver IPOPT [33] with linear solver MA57 from HSL [65].

5.2 Adaption of simulation models for optimization

JModelica.org is Modelica-based, which means that simulation models created in Dymola can be used as optimization models in JModelica.org. However, the

different numerical use of the model equations during simulation and optimization often makes it impossible to use simulation models for optimization directly. The adaptions that were required to make the simulation models suitable for dynamic optimization are explained in this section.

5.2.1 Reduction of the final system model

Initial testing showed that the final system model for Vulkan, see Section 4.5.1, could not be used for dynamic optimization due to the large number of components and their interconnections. Therefore, certain parts of the system were removed to reduce the complexity and the size of the resulting NLP. The final system model and the removed parts (covered with gray) are shown in Figure 5.3.

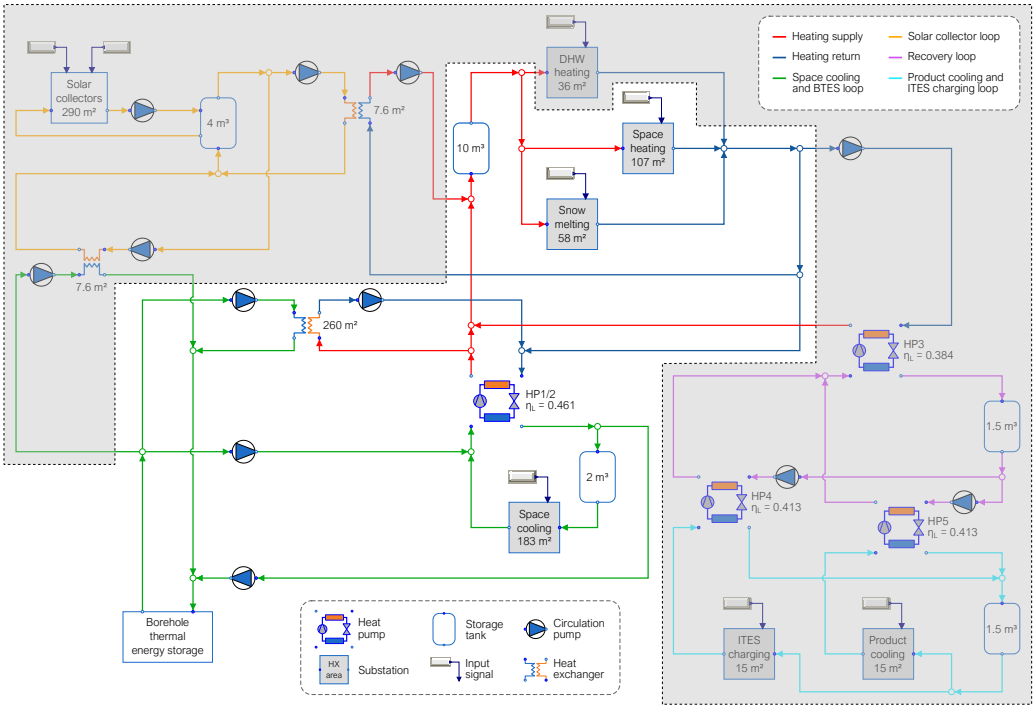

Figure 5.3: Reduction of the final system model (gray part excluded in optimizations).

It can be seen in Figure 5.3 that the solar collector loop, the DHW heating substation, the product cooling and ITES charging loop, and the recovery loop were removed from the final system model. These decisions were based on simulation results, which are presented in Chapter 6. These results showed that the

solar collector loop played a minor role for system performance due to the small total collector area. The DHW heating substation, the product cooling, and the ITES charging loop were removed because the recovered heat from HP 3 was similar to the delivered heat in the DHW heating substation. Removing these parts therefore caused insignificant mismatch in the total heat balance. The simulated electricity use of the removed parts accounted for 18 % of the total electricity use for the BAU case, which showed that the key components of the system were kept. For clarity, a schematic of the reduced system model is shown in Figure 5.4.

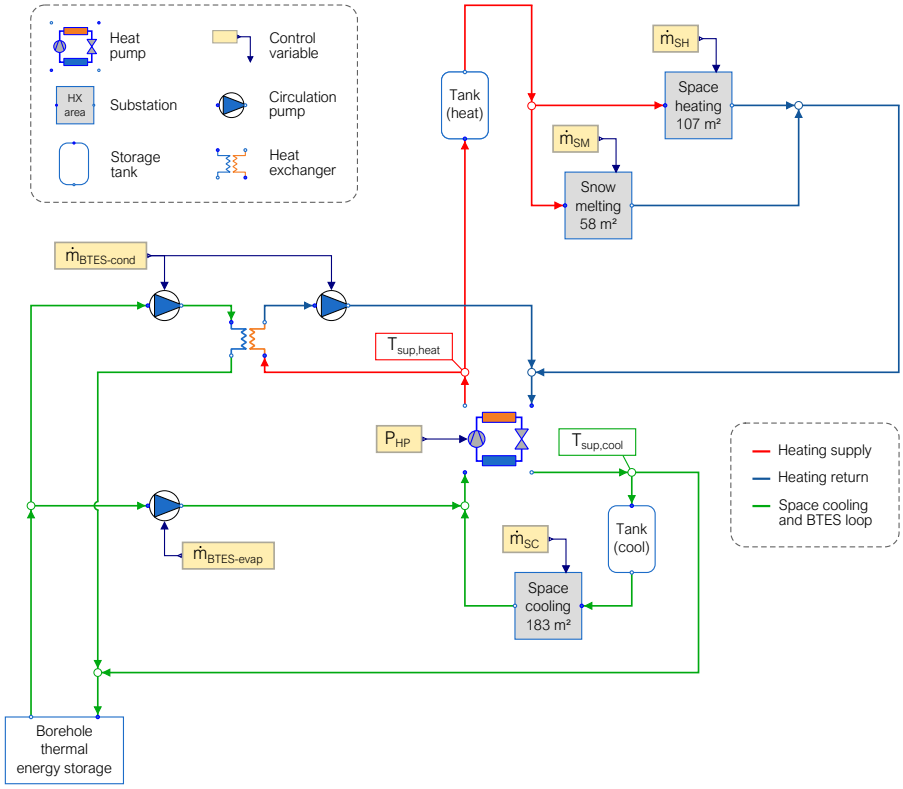

Figure 5.4: Schematic of the reduced system model for optimization.

5.2.2 Modifications of component models

The component models described in Section 4.4 were developed for stable and fast dynamic simulations. However, as mentioned above, some modifications were required to make all the component models suitable for dynamic optimization. These modifications are described below.

The model CustomerSubstationVulkan, see Figure 4.23, received a demanded heat flow rate as input signal, which was sent to the included Controller model. Initial testing showed that this Controller model led to convergence issues. Therefore, the model CustomerSubstationVulkanOpt was developed in which the mass flow rate of the circulation pumps was used as input signal, see the yellow boxes in Figure 5.4. The required heat flow rate in the substation was formulated as a constraint in the optimization problem, see Section 5.3.2. A diagram of the model CustomerSubstationVulkanOpt is shown in Figure 5.5.

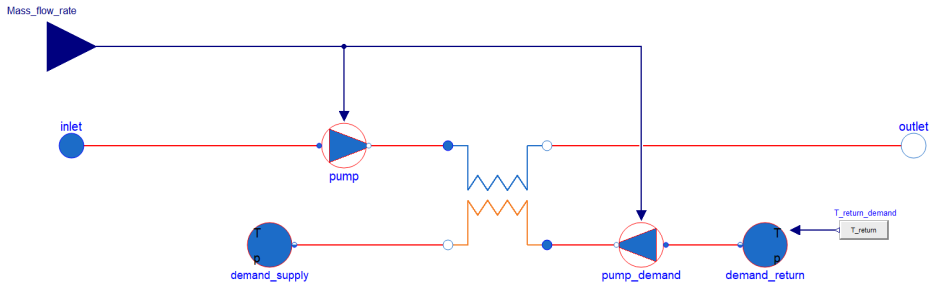

Figure 5.5: Diagram of the model CustomerSubstationVulkanOpt (DS).

The model HeatPumpFinal, see Figure 4.6, contained Boolean signals, which are not suitable for dynamic optimization. In addition, initial testing showed that the calculation of the Lorentz temperature, see Equation (4.5), led to convergence issues. Therefore, the model HeatPumpOpt was developed, which received the heat pump power as input signal and contained an approximation of the Lorentz temperature shown in Equation (5.1). The difference in Lorentz temperature due to this modification was less than 0.1 K for all relevant operating conditions, which was regarded as insignificant.

$$T_{\mathrm{L,cond/evap}} = \frac{T_{\mathrm{in,sec,cond/evap}} + T_{\mathrm{out,sec,cond/evap}}}{2} \tag{5.1}$$

The numerical discretization of the BTES model and the StorageTank model, see Figure 4.12 and Figure 4.19, respectively, had a strong influence on the number of NLP variables. A one-week test optimization was performed to compare the resulting setpoint temperatures with high and low discretization values. The horizontal and vertical discretization of the BTES model was set to 30 and 4 for the high discretization case (as used during simulation) and 10 and 2 for the low

discretization case, respectively. The discretization of the StorageTank models for the heating and cooling tanks was set to 15 and 5 for the high discretization case (as used during simulation) and 5 and 2 for the low discretization case, respectively. The low discretization reduced the number of NLP variables and the solution time of IPOPT by a factor of three and ten, respectively. However, the average absolute difference between the optimized setpoints for the high and low discretization case was less than 0.1 K, which was regarded as insignificant. Therefore, the low discretization values were used for all the optimizations in this work.

5.2.3 Splitting into seasonal models

As mentioned before, the BTES was charged during the summer and discharged during the winter. Thus, the heat exchanger and circulation pumps for BTES charging were not required during the winter and the circulation pump for BTES discharging was not required during the summer. Therefore, the reduced system model for optimization, see Figure 5.4, was split into seasonal models, in which the unused part of the season could be removed. This reduced the optimization problem size significantly. The three seasonal models that were created are listed in Table 5.1 together with the removed parts.

Table 5.1: Seasonal models used for optimization.

Seasonal model	Parts that were removed from the reduced system model
WinterOpt	BTES charging heat exchanger
	BTES charging circulation pumps
SpringFallOpt	Snow melting substation
SummerOpt	Snow melting substation
	BTES discharging circulation pump

An addition, Two versions of each seasonal model were required: one for the initial simulation and one for the optimization, see Figure 5.2. In the initialization models, the component models developed for simulation were used. The component models adapted for optimization were used in the seasonal models for optimization.

5.3 Optimal control problem formulation

To recall, the seasonal models described in the previous section were used to find optimal heating and cooling supply temperature setpoints for simulations with the final system model, see Figure 5.1. The optimization problems for the different seasons were formulated as continuous-time optimal control problems. The control variables, constraints, and objective functions of the optimization problems are explained in the following subsections.

5.3.1 Control variables

The control variables in the optimal-control problems were the heat pump power, P_{HP}, and the mass flow rates for the circulation pumps. These are marked yellow in Figure 5.4 and are written as a vector:

$$\mathbf{u}(t) \coloneqq \left[P_{\mathrm{HP}}(t),\, \dot{m}_i(t)\right]^{\top}, \qquad i \in \mathcal{P} \tag{5.2}$$

with the definition $\mathcal{P} \coloneqq \{\mathrm{SH},\, \mathrm{SM},\, \mathrm{SC},\, \mathrm{BTES\text{-}cond},\, \mathrm{BTES\text{-}evap}\}$. The temperatures $T_{\mathrm{sup,heat}}$ and $T_{\mathrm{sup,cool}}$ were not included in the vector $\mathbf{u}(t)$. This was due to the fact that the optimization models did not contain `Controller` models, as explained in Section 5.2.2, so setpoint temperatures were not needed. Instead, the temperatures $T_{\mathrm{sup,heat}}$ and $T_{\mathrm{sup,cool}}$ depended on the control variables and were calculated during the optimizations. The resulting values were then used as input for the new simulations (see Part 3 in Figure 5.1).

5.3.2 Operating constraints

Lower and upper bounds were defined for the control variables based on their operating limits, yielding the following linear inequality constraints:

$$0 \leq P_{\mathrm{HP}}(t) \leq 300\,\mathrm{kW} \tag{5.3}$$

$$0 \leq \dot{m}_i(t) \leq \dot{m}_{i,\max}\,, \qquad i \in \mathcal{P} \tag{5.4}$$

To ensure practically feasible operation, the supply temperatures for heating

and cooling were constrained by:

$$T_{\text{sup,heat}}(t) \leq 65\,^{\circ}\text{C} \tag{5.5}$$

$$T_{\text{sup,cool}}(t) \geq -5\,^{\circ}\text{C} \tag{5.6}$$

Constraints were also added to ensure that the correct amount of energy was delivered by the IHCS to the connected buildings. Enforcing this demand satisfaction as an equality constraint led to convergence issues. Therefore, the following upper and lower bounds were defined for the heat flow rates in the substations, with Qi,dem being the measured values for heating and cooling demands (input data):

$$\dot{Q}_{i,\text{del}}(t) \geq \quad \dot{Q}_{i,\text{dem}}(t), \qquad i \in \mathcal{D} \tag{5.7}$$

$$\dot{Q}_{i,\text{del}}(t) \leq \varepsilon \cdot \dot{Q}_{i,\text{dem}}(t), \qquad i \in \mathcal{D} \tag{5.8}$$

with the definition $\mathcal{D} \coloneqq \{\text{SH, SM, SC}\}$ and $\varepsilon = 1.005$. This formulation improved the numerical performance significantly. A validation was performed to confirm that the energy demand constraints were not violated during the optimizations. This validation can be found in Paper VI.

5.3.3 Objective function for reduction of electricity use

The simulated electricity use of the IHCS consisted of three parts: the electricity use of the heat pumps, the electricity use of the circulation pumps, and the electricity use of the auxiliary systems. This is explained in more detail in Section 6.2.1. Reducing this total electricity use was defined as the first objective for optimization. Therefore, the following objective function was defined in order to minimize total electricity use

$$\underset{\mathbf{u}(t)}{\text{minimize}} \quad \int_{t_{\text{start}}}^{t_{\text{end}}} \Big(P_{\text{HP}}(t) + P_{\text{pumps}}(t) \Big) dt \tag{5.9}$$

with P_{HP} and P_{pumps} being the heat pump power and total circulation pump power, respectively. The power of auxiliary systems was assumed constant and

thus had no influence on the optimal solution. It was therefore removed from the objective function.

5.3.4 Objective function for reduction of electricity costs

The reduction of electricity costs was defined as the second objective for optimization. Therefore, the following objective function was defined in order to minimize total electricity costs

$$\underset{\mathbf{u}(t)}{\text{minimize}} \quad \int_{t_{\text{start}}}^{t_{\text{end}}} \Big[e(t) \cdot \Big(P_{\text{HP}}(t) + P_{\text{pumps}}(t) \Big) \Big] dt \tag{5.10}$$

with $e(t)$ being the time-varying electricity price.

6 Analysis of the case study system Vulkan

The main aim of this case study was to analyze the design and the operation of the IHCS at Vulkan, see Section 3.1. To this end, the simulation models described in Chapter 4 and the optimization approach described in Chapter 5 were used for several analyses. The main results from these analyses are described and discussed in this chapter.

Focus was on the performance of the long- and short-term thermal energy storages. The BTES of the IHCS was used as seasonal thermal energy storage, i.e. heat was injected during the summer and extracted during the winter. The annual heat balance of the BTES (heat injected minus heat extracted) was an important result of the simulations because it affected the average temperature of the surrounding ground. If the ground temperature became too high, the heat injection rate decreased and could lead to operating difficulties during the summer. Similarly, a too low ground temperature could lead to inefficient heat extraction during the winter.

6.1 Heat export to district heating grid

The analysis described in this section was performed when the first system model for Vulkan, see Section 4.5.1, had been developed. The simulation results showed a positive heat balance of the BTES of around 200 MWh for the year 2015. Therefore, the possibility of exporting heat to the local DH grid was analyzed. Two heat export cases were defined and compared to the BAU case, see Table 6.1.

Table 6.1: Defined cases for the analysis of heat export.

Case	Heat export	Number of solar collectors	Solar collector area (m^2)	BTES
BAU	No export	140	290	Unbalanced
Export 1	To DH return line	140	290	Balanced
Export 2	To DH supply and return line	500	1 036	Balanced

For the case Export 1, heat export from the heating tank to the DH return line was simulated. For the case Export 2, heat export from the collector tank to the DH supply line was simulated additionally, see Paper II for details. The amount of exported heat was controlled to yield a balanced BTES at the end of the year for both export cases.

The installed solar collectors at Vulkan are integrated into the facade of one of the buildings. This corresponds to a small fraction of the total roof area. A map showing the solar potential of the roof areas at Vulkan is shown in Figure 6.1, which also shows the location of the installed collectors (blue mark).

Installing more solar collectors was therefore considered as realistic retrofitting option and the number of collectors was increased from 140 to 500 for the case Export 2. In addition, the volume of the collector tank was increased from 2 m^3 to 10 m^3.

To compare the total operating costs of the three cases, relative cost factors were defined for electricity, DH import, DH export to the supply line, and DH export to the return line. Electricity was assumed most expensive and was set to 1. The chosen cost factors for DH import and export are listed in Table 6.2.

All three cases listed in Table 6.1 were simulated with input data for the year 2015. Detailed results can be found in Paper II. The resulting operating costs relative to the BAU case are listed in Table 6.3.

The results showed that the operating costs could be reduced by 5.4 % for the case Export 1 and 8.2 % for the case Export 2. However, these numbers should only be taken as rough indications due to two reasons: 1) the system model used

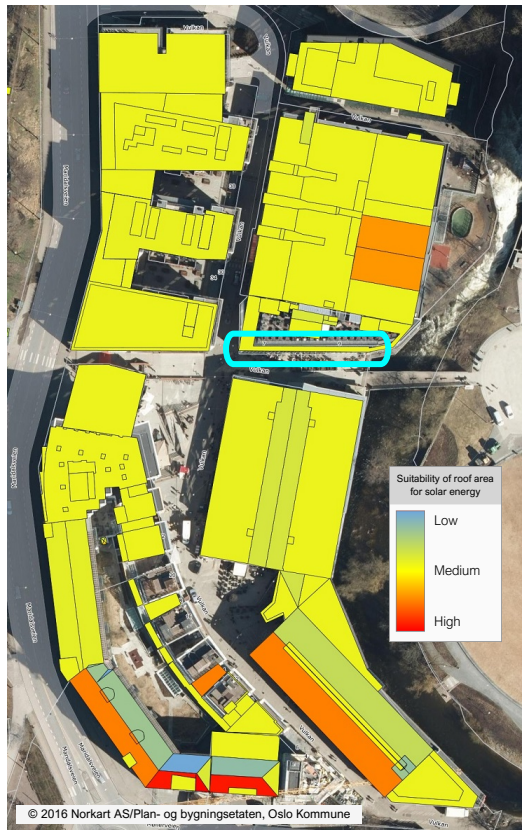

Figure 6.1: Solar potential of the roof area at Vulkan [66].

Table 6.2: Relative cost factors for the different energy types.

Energy type	Cost factor
Electricity	1.00
DH import	0.95
DH export to supply line	0.80
DH export to return line	0.40

for the simulations had several issues, which are explained in Section 4.5.1, and 2) the prices for electricity and DH were assumed constant in this study although they can show large variations over time.

Further development of the component models and the system model led to the final system model for Vulkan, see Section 4.5.1. To increase the reliability of the

Table 6.3: Total operating costs compared to the BAU case.

Case	Relative operating costs (%)
BAU	100.0
Export 1	94.6
Export 2	91.8

results, a calibration of the simulated electricity use was performed. In addition, a sensitivity analysis was performed to study the impact of input parameters on the simulated system performance. The calibration and the sensitivity analysis are described in the next section.

6.2 Calibration and sensitivity analysis

6.2.1 Calibration of the system's electricity use

As explained in Section 3.1.3, only the total electricity use of the system was measured, i.e. the electricity use of components was unknown. The total simulated electricity use of the system ($E_{\text{sim,tot}}$) consisted of three parts: the electricity use of all the heat pumps (E_{HPs}), the electricity use of all the circulation pumps (E_{pumps}), and the electricity use of all auxiliary systems (E_{aux}), see Equation (6.1).

$$E_{\text{sim,tot}} = \underbrace{\int \big(P_{\text{HPs}}(t)\big)dt}_{E_{\text{HPs}}} + \underbrace{\int \big(P_{\text{pumps}}(t)\big)dt}_{E_{\text{pumps}}} + \underbrace{\int \big(P_{\text{aux}}\big)dt}_{E_{\text{aux}}} \tag{6.1}$$

E_{HPs} was calculated by integrating the simulated power of all heat pump models (P_{HPs}) as shown in Equation (6.1). The circulation pump model calculated the required power (P_{pump}) of each circulation pump based on the volume flow rate and the pressure difference, see Equation (4.2). However, the pressure difference was not calculated correctly in the final system model because connecting pipes were neglected and the heat exchangers, solar collectors, and BTES were lumped models. Therefore, P_{pump} was assumed proportional to the squared volume flow rate of the circulation pump in the final system model. This assumption corresponds to a linear relation between pressure drop and volume flow rate in

Equation (4.2). The squared volume flow rate was multiplied with the constant flow-to-power coefficient FtP to calculate P_{pump}, see Equation (6.2).

$$P_{\text{pump}} = 10^{-6} \cdot \text{FtP} \cdot \dot{V}^2 \tag{6.2}$$

The power of the auxiliary systems (P_{aux}) was assumed constant and E_{aux} was calculated by integrating P_{aux}, see Equation (6.1). A system-level approach was chosen to calibrate the values for FtP and P_{aux}. To this end, the monthly difference between the measured electricity use and the simulated electricity use was minimized, see Equation (6.3).

$$\min \sum_{i=1}^{12} \left(E_{\text{tot,meas}} - E_{\text{sim,tot}}\right)^2, \quad i = \text{month of the year} \tag{6.3}$$

The calibration was performed with input data for the year 2015 and yielded values of 70.65 $\text{MW} \cdot \text{s}^2/\text{m}^6$ and 30.5 kW for FtP and P_{aux}, respectively. These values were implemented in the final system model. Monthly values for $E_{\text{meas,tot}}$ and $E_{\text{sim,tot}}$ for the two simulated years are shown in Figure 6.2.

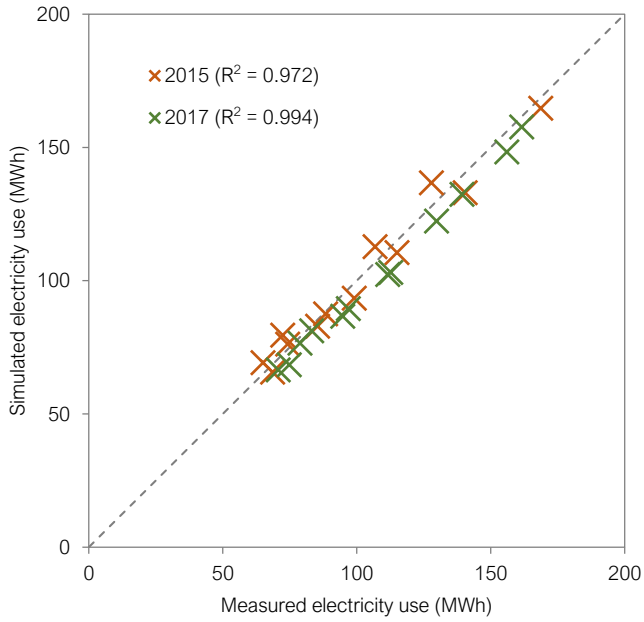

Figure 6.2: Measured and simulated electricity use after the calibration.

It can be seen from Figure 6.2 that the calibration led to good agreement between the measured values and the simulated values.

6.2.2 Sensitivity analysis

A sensitivity analysis was performed to evaluate the influence of selected input parameters on the simulated system performance. Two COPs were defined to measure the system performance: $\mathrm{COP_{sys}}$ and $\mathrm{COP_{sys+BTES}}$. These were evaluated at the end of a simulated year. $\mathrm{COP_{sys}}$ was defined as the ratio of the heating and cooling energy delivered by the IHCS to the electricity use of the IHCS as shown in Equation (6.4). Note that the amount of imported heat from the DH grid was not included in $Q_{\mathrm{heat,tot}}$.

$$\mathrm{COP_{sys}} = \frac{Q_{\mathrm{heat,tot}} + Q_{\mathrm{cool,tot}}}{E_{\mathrm{sim,tot}}} \tag{6.4}$$

$\mathrm{COP_{sys+BTES}}$ was similar to $\mathrm{COP_{sys}}$ but included the annual heat balance of the BTES ($Q_{\mathrm{BTES,ann}}$) in the numerator as shown in Equation (6.5). The heat balance was included because it affected long-term operation as explained above. $\mathrm{COP_{sys+BTES}}$ thus gave a more holistic indication of system performance by penalizing unsustainable operation.

$$\mathrm{COP_{sys+BTES}} = \frac{Q_{\mathrm{heat,tot}} + Q_{\mathrm{cool,tot}} + Q_{\mathrm{BTES,ann}}}{E_{\mathrm{sim,tot}}} \tag{6.5}$$

Parameters were changed one at a time during the sensitivity analysis and the difference in COP compared to the BAU case was calculated. A 20 % change was chosen as the default value. However, some parameters were varied by a different percentage as can be seen in Table 6.4 and explained in the notes below:

1. According to [67].
2. ΔT of 3 K chosen instead of default percentage.
3. According to [68].
4. According to manufacturer specifications. All efficiency values were changed at once, see Equation (4.7).
5. See Equation (4.16).

Table 6.4: Parameter values used for the sensitivity analysis (notes on pages 92 & 94).

Parameter	Unit	Lower value	Base value	Upper value	Change %	Note
Numerical discretization						
Factor storage tanks	-	0.8	1.0	1.2	20	
Factor BTES	-	0.8	1.0	1.2	20	
Uncertain inputs						
BTES: Nusselt number	-	3.5	5.0	6.5	30	1
BTES: Initial temp. (near)	°C	22	25	28	12	2
BTES: Initial temp. (far)	°C	7	10	13	30	2
BTES: Ground conductivity	$\mathrm{W/(m \cdot K)}$	2.10	2.75	3.40	24	3
Lorentz efficiency HP 1/2	%	41.0	46.1	51.2	11	4
Lorentz efficiency HP 3	%	34.6	38.4	42.2	10	4
Lorentz efficiency HP 4 & 5	%	33.9	41.3	48.7	18	4
Exponent q in HX model	-	0.50	0.63	0.76	20	5
Coefficient FtP	$\mathrm{MW \cdot s^2/m^6}$	56.6	70.7	84.8	20	6
Assumed return temperatures						
Space heating	°C	37	40	43	8	7
Snow melting	°C	13	20	27	35	7
Space cooling	°C	13.2	15.0	16.8	12	7
Product cooling	°C	-5.2	-4.0	-2.8	30	7
Heating/cooling demands						
Demand factor all	-	0.8	1.0	1.2	20	8
Demand factor heating	-	0.8	1.0	1.2	20	9
Demand factor cooling	-	0.8	1.0	1.2	20	10
Control setpoints						
Mode switch ΔT	K	3.2	4.0	4.8	20	11
Heating supply	°C	52	55	58	5	12
Space cooling supply	°C	4.2	6.0	7.8	30	12
System design						
Factor HX area	-	0.8	1.0	1.2	20	13
Number of solar collectors	-	110	140	170	21	14
Number of boreholes	-	50	62	74	19	15

6. See Equation (6.2).
7. Secondary side changed to give 20 % change in ΔT.
8. All demand values changed.
9. Only heating demand values changed.
10. Only cooling demand values changed.
11. Used to switch between heating and cooling mode, see Section 4.5.1.
12. Primary side changed to give 20 % change in ΔT.
13. All area values listed in Table 4.1 were changed at once.
14. The storage tank volume and the heat exchanger areas in the solar collector loop were scaled accordingly.
15. The maximum mass flow rates of the BTES circulation pumps were scaled accordingly.

The sensitivity analysis was performed with input data for the year 2015. The results are shown in Figure 6.3.

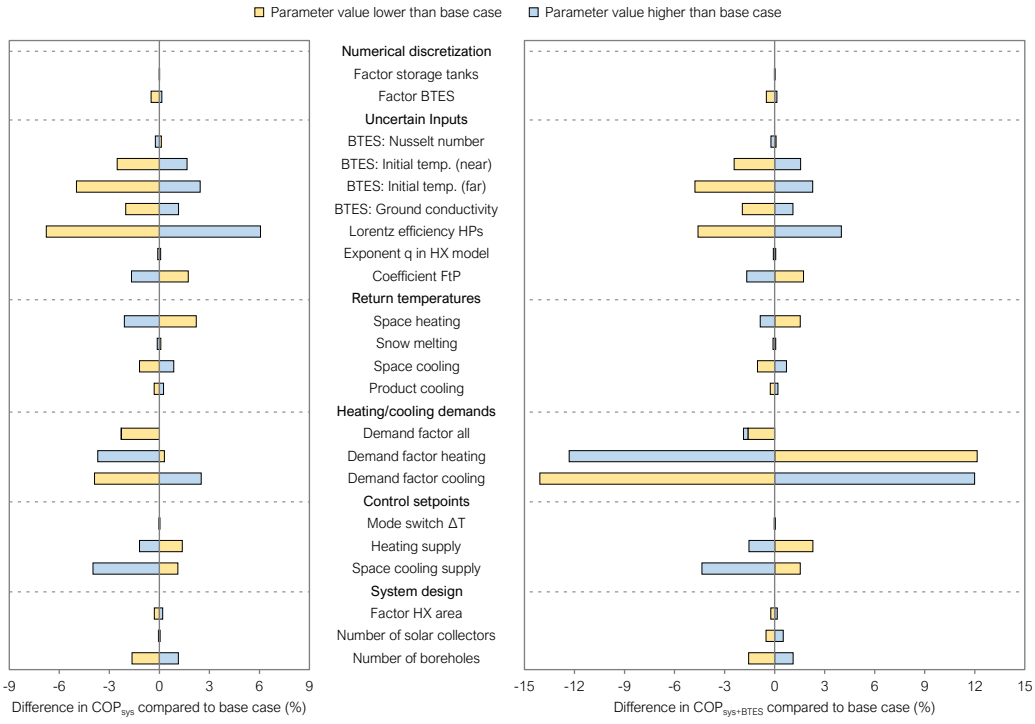

Figure 6.3: Results from the sensitivity analysis.

Increasing the numerical discretization had a negligible effect on the COPs. A reduction in discretization of the BTES led to a decrease of 0.5 %, showing that the chosen values were reasonable.

Some of the uncertain inputs influenced the COPs significantly. The heat pumps were the main electricity users, which is why their efficiency had a strong influence, especially on $\mathrm{COP}_{\mathrm{sys}}$, see Figure 6.3 (left). The initial temperature profile and the conductivity of the ground also showed strong influence on the COPs, while the Nusselt number for natural convection inside the borehole and the heat exchanger exponent q used in Equation (4.16) were less important.

The return temperatures from the buildings' heating and cooling systems (T_{ret}) were assumed constant in this study. The influence of these temperatures on system performance varied. It depended on the total amount of delivered energy for each demand type. Space heating was the largest demand, which is why $T_{\mathrm{ret,SH}}$ had the strongest influence on the COPs.

The heating and cooling demands were based on the available measurements. The cooling demands were heat sources for the IHCS and the heating demands were heat sinks. Therefore, the difference between the total heating demand and the total cooling demand highly influenced the annual heat balance of the BTES. Changing all demands simultaneously thus altered the BTES balance less than changing only heating or cooling demands. This is why changing all demands showed less effect than changing only heating or cooling demands, especially for $\mathrm{COP}_{\mathrm{sys+BTES}}$.

The control setpoint for a mode switch had insignificant influence on the system performance due to the small number of mode switches during a year. The supply temperature setpoints $T_{\mathrm{sup,heat}}$ and $T_{\mathrm{sup,cool}}$ changed the heat pump outlet temperatures and thus affected both the temperature lift of the heat pumps and the mass flow rates of the circulation pumps. Especially an increase of $T_{\mathrm{sup,cool}}$ showed strong influence on the COPs.

The system design parameters showed little effect on the COPs. Only a change in the number of boreholes changed the COPs by more than 1 %. This change in COP was mainly due to the difference in required circulation pump power. The BTES outlet temperature changed slightly when the number of boreholes was

changed, leading to a small change in the heat pump's COP. However, the annual heat balance of the BTES did not change significantly because almost the same amounts of energy had to be injected/extracted each day.

6.3 Ensuring sustainable long-term operation

The analysis described in this section was performed after the calibration of the final system model for Vulkan, which is explained in the previous section. The aim of this analysis was to ensure sustainable long-term operation, i.e. to avoid deterioration of system performance over time. As explained in Section 3.1.3, measurement data from the years 2015 and 2017 were used as input for the analysis. The simulation results with the final system model showed a negative heat balance of the BTES of -469 MWh and -263 MWh for the years 2015 and 2017, respectively as shown in the figures 6.4 and 6.5.

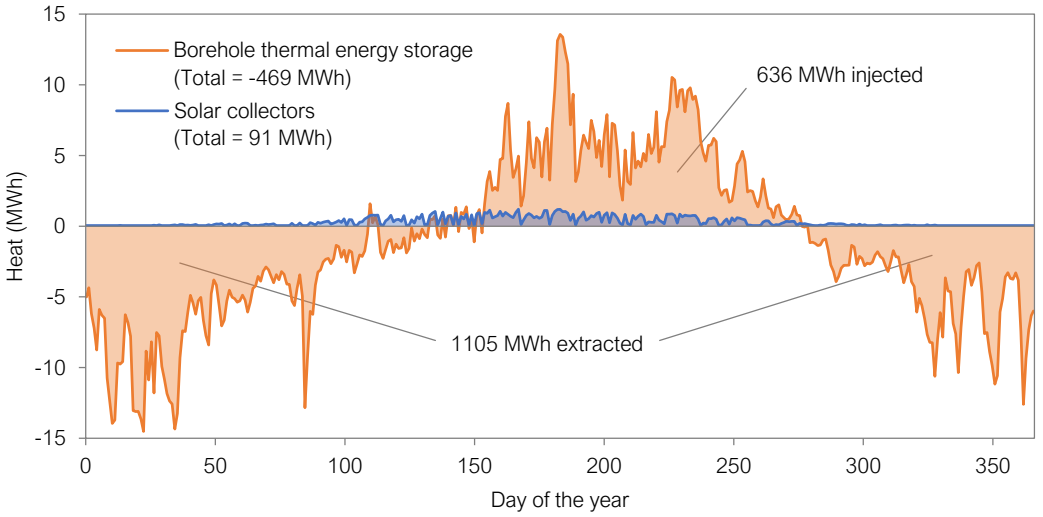

Figure 6.4: Simulated daily heat balance for BTES and solar collectors for 2015.

This is a large difference in the simulated heat balance compared to the results presented in Section 6.1. This difference is due to the issues of the first system model, which are described in Section 4.5.1, especially the neglection of the snow melting demand.

As mentioned in Section 6.1, an unbalanced BTES can lead to decreased long-

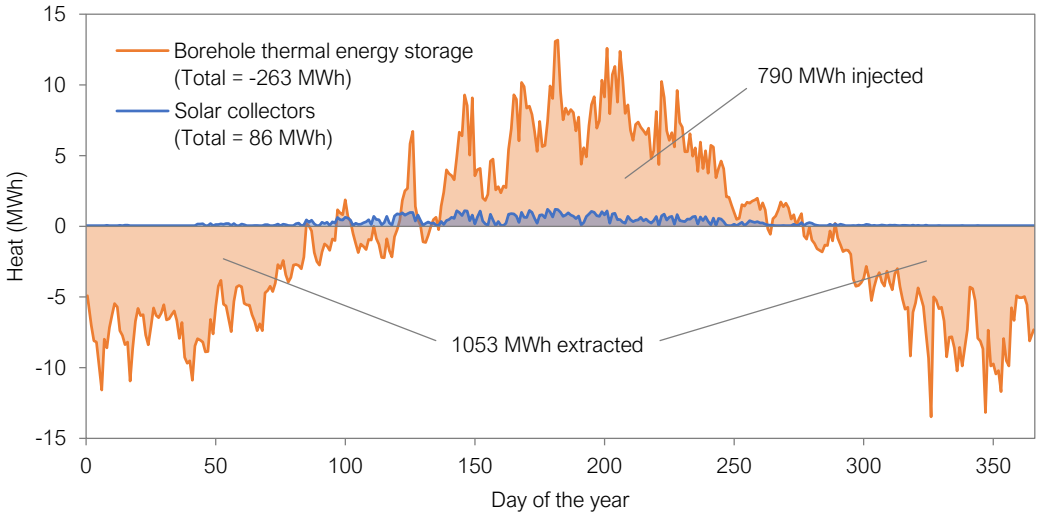

Figure 6.5: Simulated daily heat balance for BTES and solar collectors for 2017.

term performance. The figures 6.4 and 6.5 showed that the charging of the BTES during the summer was insufficient and that the solar collectors only accounted for a small fraction of the charging capacity. Therefore, two solutions to avoid a negative heat balance were analyzed: the installation of more solar collectors and the increase of DH import for DHW heating. These cases are listed in Table 6.5 and described below.

Table 6.5: Defined cases for the analysis of long-term operation.

Case	Number of collectors	Collector area (m^2)	DH import for DHW heating
BAU	140	290	Based on DHW demand
More solar collectors	830	1 719	Based on DHW demand
More DH import	140	290	Reduced by 55 % during cooling mode, zero during heating mode

More solar collectors For this case, the number of solar collectors was increased from 140 to 830 because this increase led to a balanced BTES for the year 2015 as explained in Paper V. There is a lot of roof area at Vulkan suitable for the installation of solar collectors, see Figure 6.1. However, installation possibilities and costs were not analyzed further.

More DH import For this case, the mass flow rate from the IHCS to the DHW heating substation was reduced. This mass flow rate reduction led to an increased amount of DH import for DHW heating. The mass flow rate was reduced by 55 % during cooling mode and by 100 % during heating mode compared to the BAU case. Heat for DHW heating was thus only delivered by the IHCS during cooling mode, when excess heat was available.

To analyze long-term operation, the input data for the years 2015 and 2017 were repeated three times so that a six-year simulation could be performed. The change in total electricity use compared to the first year is shown in Figure 6.6.

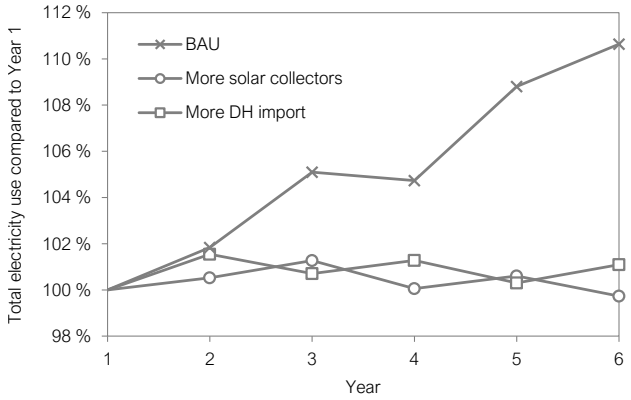

Figure 6.6: Change in total electricity use of the IHCS (input data for 2015 and 2017 repeated).

It can be seen from Figure 6.6, that the total electricity use increased by 10 % during the six simulated years for the BAU case. For the cases "More solar collectors" and "More DH import", the simulated electricity use stayed almost constant. The increase for the BAU case was due to a ground temperature decrease, which led to higher electricity use of the circulation pumps, especially the BTES circulation pump during heating mode as shown in Paper V. The electricity use of all the circulation pumps is shown in Figure 6.7 for the six simulated years.

The electricity use of HP 1/2, see Figure 4.28, also increased over the years for the BAU case due to the lower evaporator inlet temperature. This lower inlet temperature led to a decrease of the calculated COP during heating mode from an average of 3.5 in Year 1 to an average of 3.4 in Year 6.

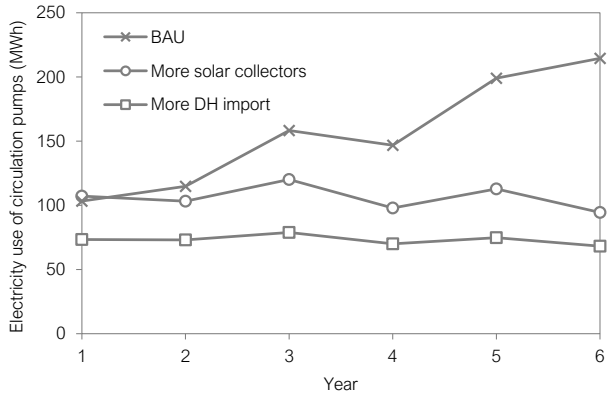

Figure 6.7: Electricity use of circulation pumps (input data for 2015 and 2017 repeated).

The results presented in this section depended highly on the BTES model. The short-term response of the BTES model was validated against experimental data and the heat transfer in the ground was calculated based on established heat transfer theory. However, the idealization of the ground in the BTES model could lead to wrong results, e.g. in the case of groundwater flow. Unfortunately, the simulation results could not be validated because the mass flow rate in the BTES was not measured.

The long-term analysis clearly showed that the simulated system performance decreased for the BAU case. Sustainable operation was achieved with the cases "More solar collectors" and "More DH import". However, the installation of solar collectors would cause installation costs and the import of heat would increase the operating costs. An economic evaluation should therefore be performed, which was outside the scope of this work. Instead, the reduction of electricity use by improving the control setpoints was analyzed. This is explained in the next section.

6.4 Reduction of electricity use

The sensitivity study in Section 6.2.2 showed that the setpoints for $T_{\mathrm{sup,heat}}$ and $T_{\mathrm{sup,cool}}$ influenced the simulated system performance. Therefore, the aim of this analysis was to analyze the control of the IHCS in detail with the objective to reduce the system's electricity use. To this end, the seasonal models for optimization, see Section 5.2.3, were used for dynamic optimizations with JModelica.org as explained in Chapter 5.

To recall, the final system model for Vulkan was not suitable for dynamic optimization. It was therefore reduced and split into seasonal models. The year 2015 was divided into seasonal periods and each period was optimized separately with the corresponding model. The length of each season and the resulting NLP problem size of the respective optimization are listed in Table 6.6.

Table 6.6: Optimization periods and problem sizes.

Days	Seasonal model	Number of finite elements	Number of NLP variables	Number of NLP constraints
1 – 95	`WinterOpt`	4562	$7.2 \cdot 10^5$	$7.8 \cdot 10^5$
96 – 155	`SpringFallOpt`	2883	$4.2 \cdot 10^5$	$4.6 \cdot 10^5$
156 – 260	`SummerOpt`	5043	$6.7 \cdot 10^5$	$7.3 \cdot 10^5$
261 – 290	`SpringFallOpt`	1443	$2.0 \cdot 10^5$	$2.2 \cdot 10^5$
291 – 365	`WinterOpt`	3602	$5.7 \cdot 10^5$	$6.2 \cdot 10^5$

The initial state of the BTES and storage tank models for each season were chosen based on the result of the previous season.

The optimized values for the control variables leading to minimized electricity use are presented in this section. The optimal heat pump power P_{HP} is shown in Figure 6.8, the optimal mass flow rates for the substation circulation pumps are shown in Figure 6.9, and the optimal mass flow rates for the BTES circulation pumps are shown in Figure 6.10.

The optimized values for $T_{\mathrm{sup,heat}}$ and $T_{\mathrm{sup,cool}}$ are shown in Figure 6.11 and Figure 6.12, respectively together with the simulated BAU setpoints. The optimized setpoints were implemented into the final system model for simulation, see Part 3 in Figure 5.1). The resulting energy amounts for the simulated year are shown in Figure 6.13.

It can be seen from Figure 6.13 that the electricity use for the heat pumps and the circulation pumps decreased by 5 % and 14 %, respectively, with the optimized setpoints compared to the BAU case. The amount of heat taken from the long-term storage decreased by 7 %. These reductions would decrease the operating

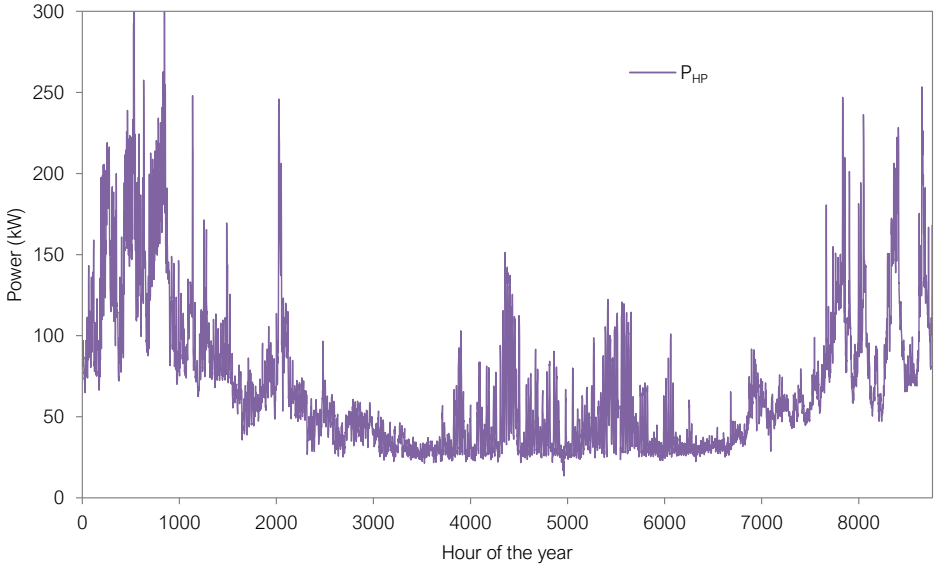

Figure 6.8: Optimized heat pump power.

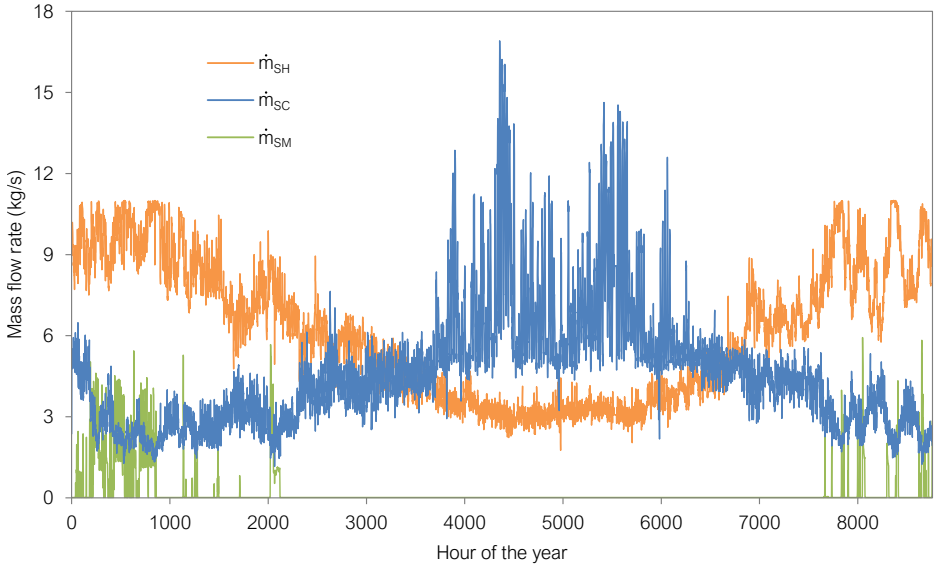

Figure 6.9: Optimized mass flow rates for the substation circulation pumps.

costs significantly. However, the amount of heat imported from DH increased by 12 % for the simulated year. Therefore, the net savings depend on the prices for electricity and DH import. An optimization of the electricity costs is described in the next section.

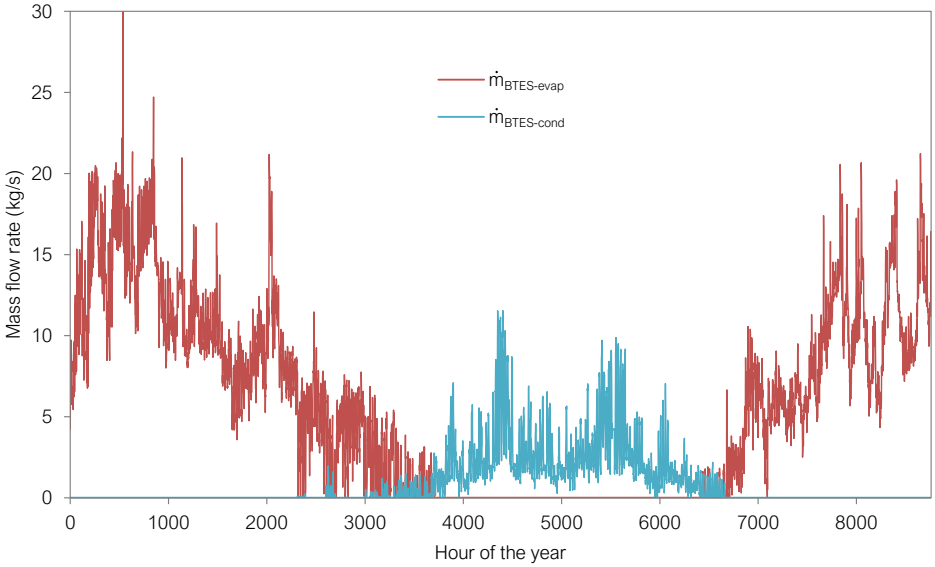

Figure 6.10: Optimized mass flow rates for the BTES circulation pumps.

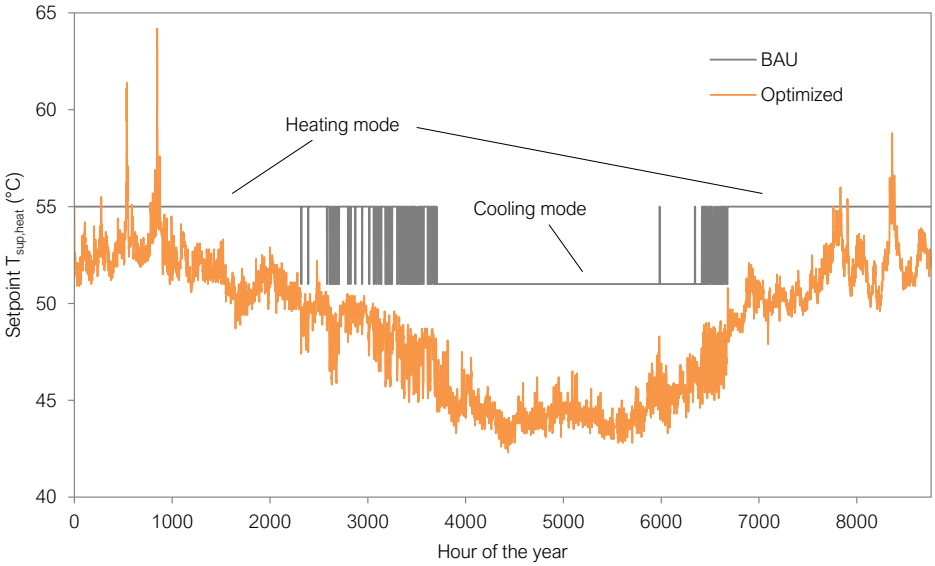

Figure 6.11: Heating supply temperature setpoint.

6.5 Reduction of electricity costs

The storage tanks of the IHCS were relatively small and only used as buffer to even out the supply temperatures of the heating and cooling loop. Storage tanks

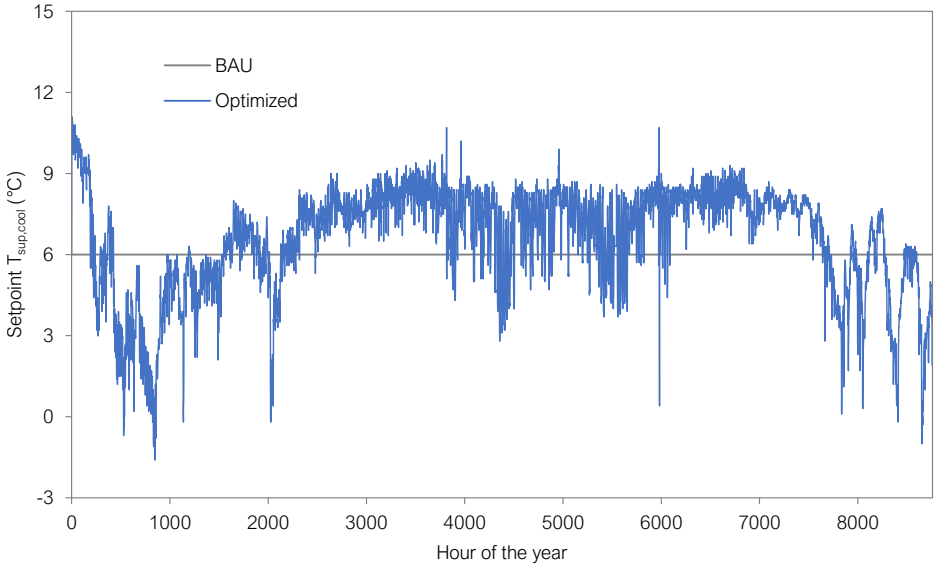

Figure 6.12: Space cooling supply temperature setpoint.

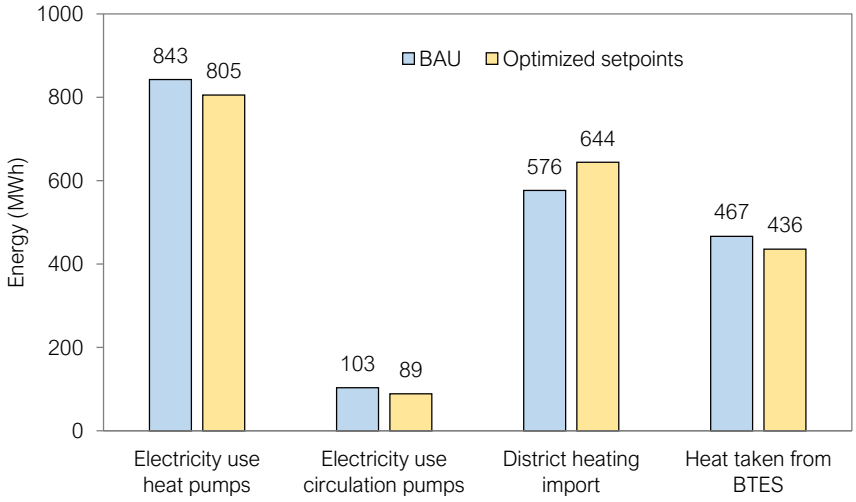

Figure 6.13: Total simulated energy amounts for 2015.

are a relatively cheap component, so the installation of larger tanks was considered as realistic retrofitting option. To investigate the effect of larger storage tanks and optimal control on the cost saving potential, three different tank size combinations were chosen: the installed 10 m^3 and 2 m^3 for the heating and cooling tank, respectively, as well as 100 m^3 and 500 m^3 for both tanks.

In Norway, electricity prices are typically higher during the winter than during the summer due to the market-based electricity price and the high amount of electricity used for space heating. Therefore, the first three months of the year 2015 were chosen for this analysis to limit the number of required optimizations. This way, all the optimizations could be performed with the seasonal model `WinterOpt`, see Section 5.2.3. The electricity spot prices for the location of the IHCS for the first three months of the years 2015 to 2019 are shown in Figure 6.14.

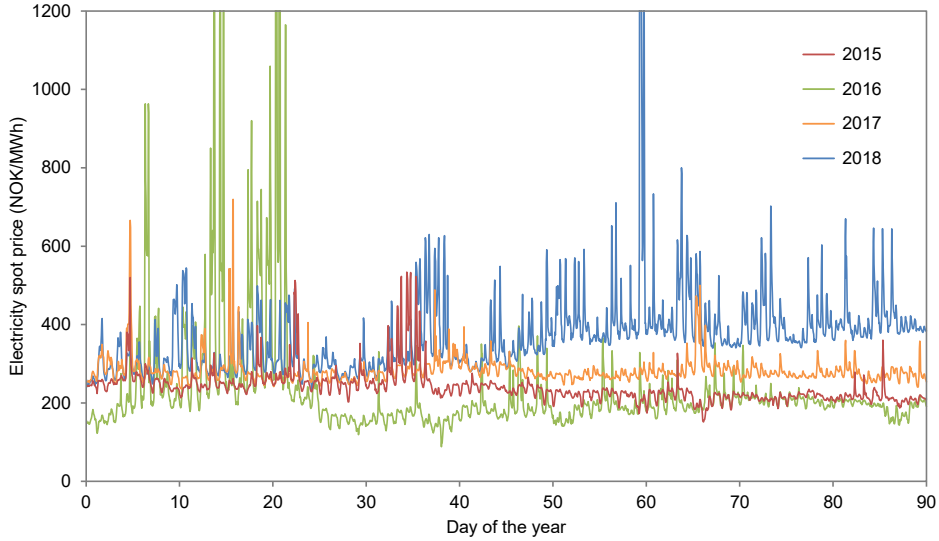

Figure 6.14: Hourly electricity spot prices for Oslo, Norway [69]. Peak values omitted for better readability (max value = 2454).

It can be seen from Figure 6.14 that the electricity price showed relatively little variation in 2015. Therefore, additional price signals were defined with different fluctuations to analyze the influence of the variability of the electricity price (v) on the cost saving potential. The price signals were based on the average price of the first three months of 2015 (239 NOK/MWh) and the original price signal ($e_{Oslo,2015}$). Values of 0, 1, 2, and 3 were chosen for v and the price signals were calculated as follows:

$$e_v(t) = 239 + v \cdot \left(e_{Oslo,2015}(t) - 239\right) \tag{6.6}$$

The four resulting price signals were used for the optimizations and are shown in Figure 6.15.

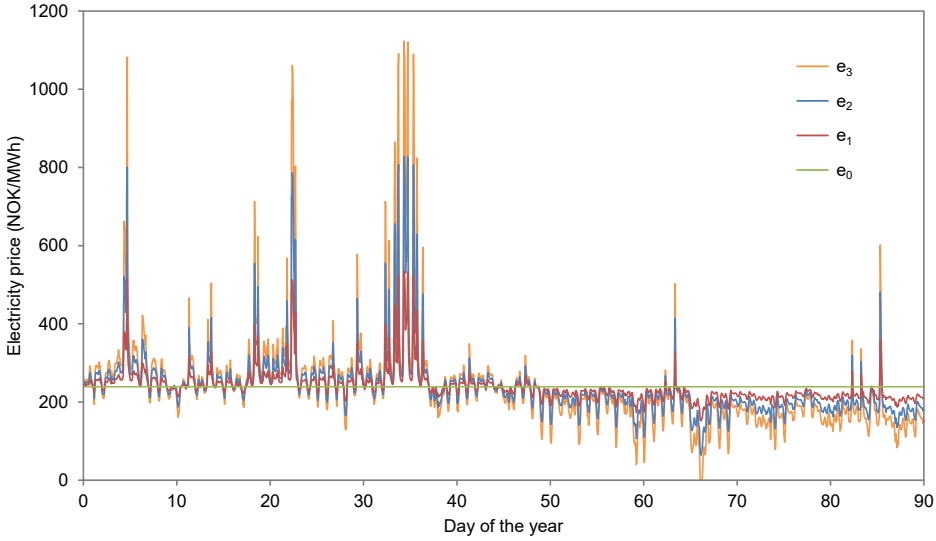

Figure 6.15: Electricity prices used for optimization ($e_1 = e_{Oslo,2015}$).

This approach, similar to the one presented in [70], was chosen instead of using electricity prices from other years to maintain the correlation between the electricity price and the climate conditions. Note that this correlation is not kept for $v = 0$, which corresponds to a constant and thus unrealistic electricity price.

The four different price signals and the three different tank size combinations led to the twelve optimization cases listed in Table 6.7.

Table 6.7: Defined cases for the analysis of electricity cost reduction.

Heating tank volume (m^3)	Cooling tank volume (m^3)	Electricity price signal			
		e_0	e_1	e_2	e_3
10	2	10-2_e_0	10-2_e_1	10-2_e_2	10-2_e_3
100	100	100-100_e_0	100-100_e_1	100-100_e_2	100-100_e_3
500	500	500-500_e_0	500-500_e_1	500-500_e_2	500-500_e_3

All the cases listed in Table 6.7 were optimized separately with the seasonal model `WinterOpt`, see Section 5.2.3. Optimal operation over this period would lead to emptied short-term storages at the end of the period, i.e. the average temperature (T_{avg}) in the hot storage tank would be as low as possible and the average temperature in the cold storage tank would be as high as possible. This

would lead to an unfair comparison, especially when different tank sizes were compared. Therefore, the constraints in Equation (6.7) and Equation (6.8) were added for these twelve optimizations to avoid this effect and thus ensure a fair comparison.

$$T_{\text{tank,heat,avg}}(t_{\text{end}}) \geq T_{\text{tank,heat,avg}}(t_{\text{start}}) \tag{6.7}$$

$$T_{\text{tank,cool,avg}}(t_{\text{end}}) \leq T_{\text{tank,cool,avg}}(t_{\text{start}}) \tag{6.8}$$

Selected result values from the optimizations leading to minimized electricity costs are shown in this section. February 14$^{\text{th}}$ and February 3$^{\text{rd}}$ were days with very different variations in electricity spot price. The price signals for these two days are shown in Figure 6.16 and Figure 6.17, respectively.

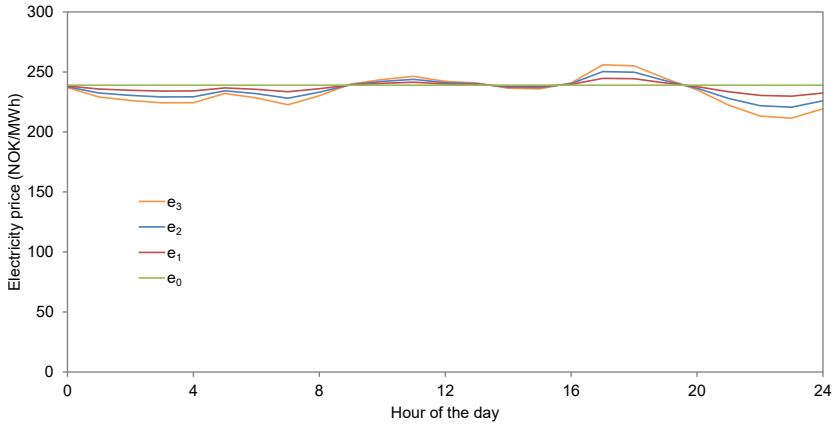

Figure 6.16: Electricity prices for February 14$^{\text{th}}$ ($e_1 = e_{\text{Oslo,2015}}$).

It can be seen from Figure 6.16 that the electricity price was almost constant on February 14$^{\text{th}}$. On the contrary, the electricity price varied significantly on February 3$^{\text{rd}}$ as shown in Figure 6.17 with peak hours in the morning and the afternoon. Detailed results for the optimal heat pump power and temperature setpoints are presented for these two days for selected cases from Table 6.7. The results for February 14$^{\text{th}}$ for the cases with the original electricity price and different tank size combinations are shown in Figure 6.18.

It can be seen from Figure 6.18 that the different tank size combinations

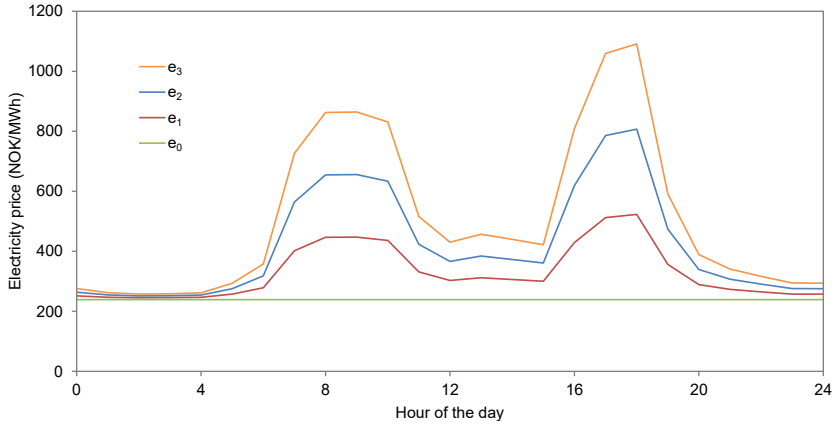

Figure 6.17: Electricity prices for February 3rd ($e_1 = e_{Oslo,2015}$).

yielded very similar results for February 14th. This was expected due to the relatively constant electricity price during that day. The results for February 3rd for the same cases are shown in Figure 6.19.

It can be seen from Figure 6.19 that the optimal control trajectories for February 3rd depended highly on the size of the storage tanks. Larger tanks led to larger variations, due to the possibility to shift electricity use from high-price hours to low-price hours and thus decrease the total electricity costs.

Figure 6.19 clearly shows that the installed tanks (case 10-2_e_1) were too small to take advantage of the electricity price variations. The heat pump power only varied between 150 kW and 270 kW for this case and the temperatures setpoints were relatively constant as well, expect for two short peaks of $T_{sup,heat}$. For the case 100-100_e_1, the heat pump power varied across nearly the entire allowed range from 0 to 300 kW. It was higher during low-price hours to charge the storage tanks, corresponding to high values for $T_{sup,heat}$ and low values for $T_{sup,cool}$. On the contrary, the heat pump power was low during high-price hours and the energy demands of the buildings were to a large extent covered by discharging the tanks. For the case 500-500_e_1, this effect was even more pronounced, leading to the largest variations in the optimal values for $T_{sup,heat}$ and $T_{sup,cool}$.

The results for February 3rd for the cases with the largest tanks and different variability of the electricity price are shown in Figure 6.20.

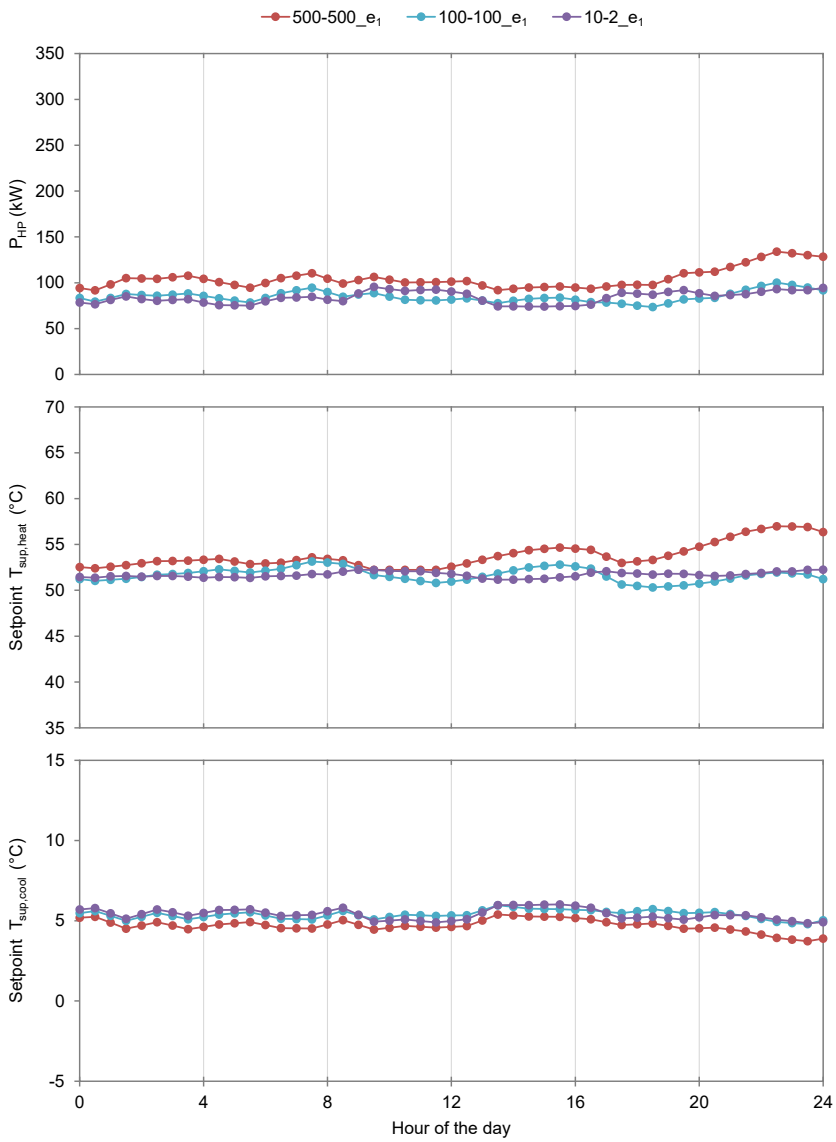

Figure 6.18: Optimization results for February 14$^{\text{th}}$ with different tank size combinations.

It can be seen from Figure 6.20 that there were large differences between the results with a constant electricity price (case 500-500_e_0) and the cases with price variations. Although the costs were optimized for all the cases, the constant price led to a minimization of the total electricity use for the case 500-500_e_0 (i.e. the objective functions Equation (5.9) and Equation (5.10) yielded equal

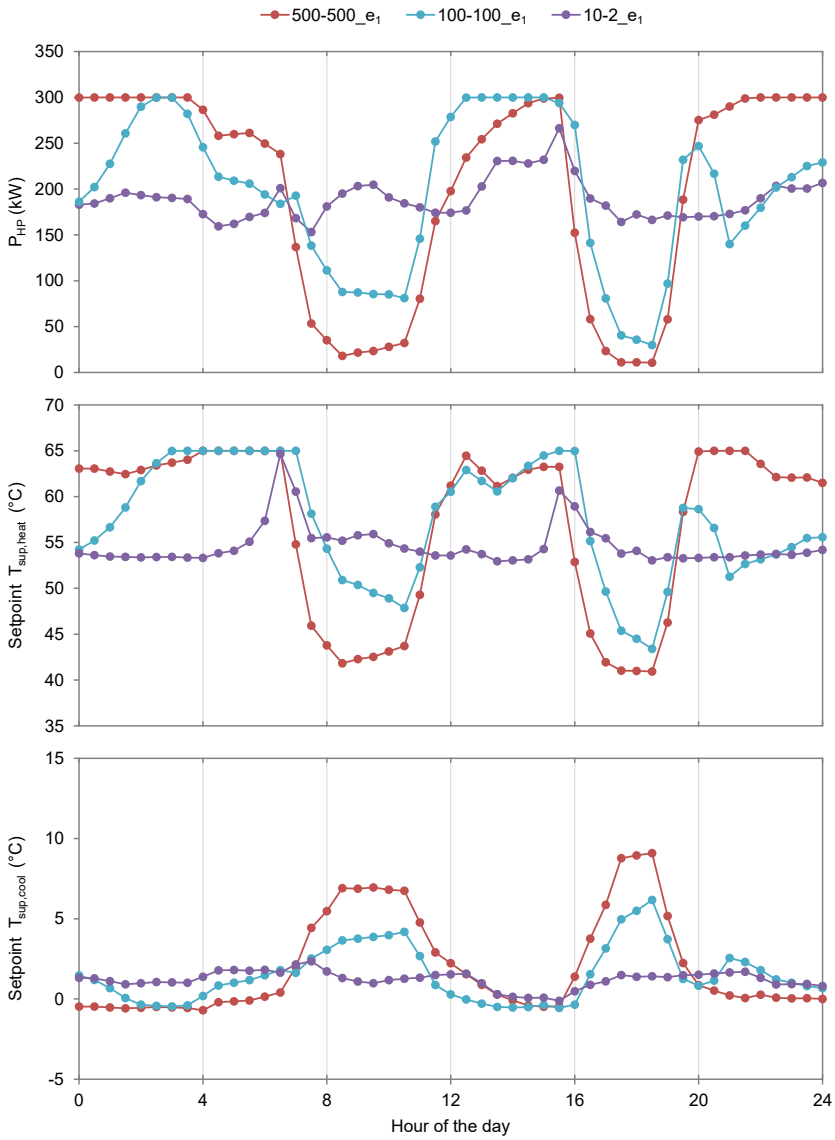

Figure 6.19: Optimization results for February 3rd with different tank size combinations.

results). The control of the heat pump and the circulation pumps were therefore optimized depending on the energy demands of the buildings. For the other three cases, the electricity use was significantly higher during low-price hours. The cases with different variability showed very similar results for February 3rd. The optimal control trajectories became slightly more pronounced for larger values

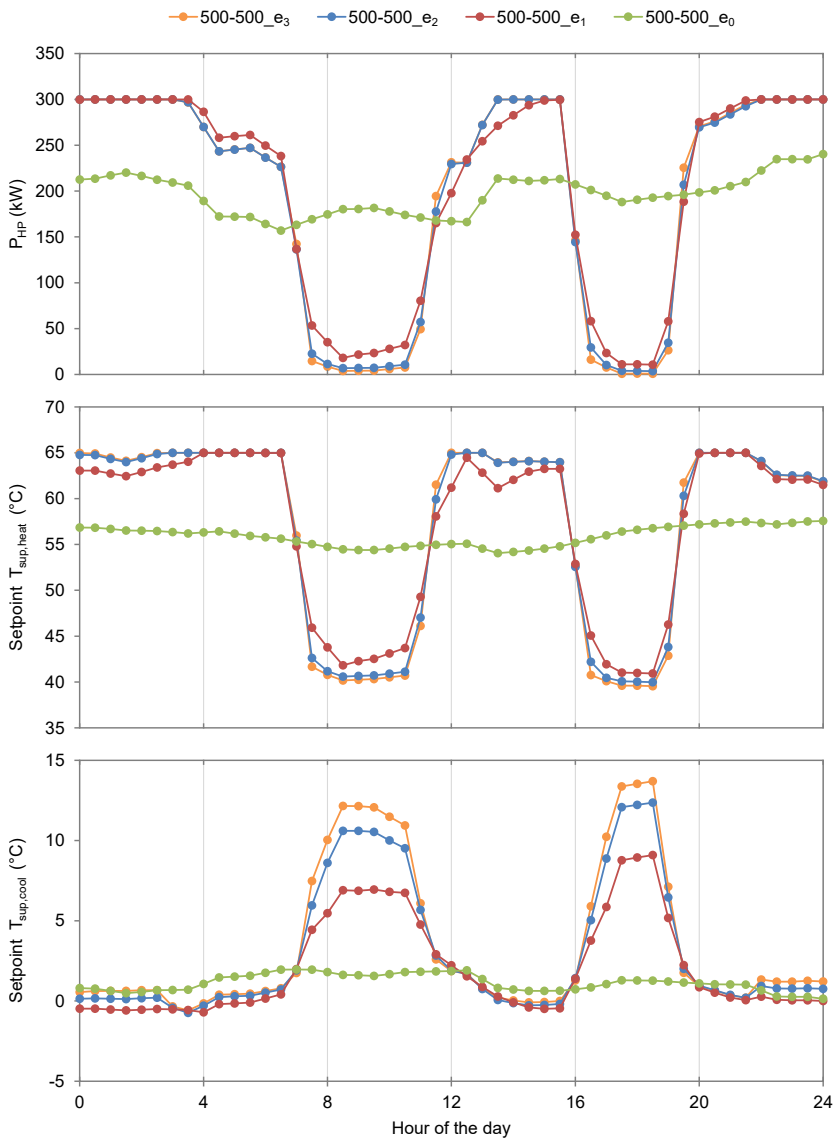

Figure 6.20: Optimization results for February 3rd with different electricity price variability ($e_1 = e_{Oslo,2015}$).

of variability, but only $T_{\text{sup,cool}}$ showed significant differences. This showed that even larger tanks would be required to take advantage of the variations during that day. However, other days showed larger differences between these cases.

The optimized setpoints were implemented into the final system model and a simulation for the first three months of 2015 was performed for all the cases

listed in Table 6.7. The simulated total electricity costs for this period are shown in Figure 6.21. The simulated costs with BAU control were included to show the potential savings. All the results are shown relative to the BAU case because the different price signals led to different costs for the BAU case.

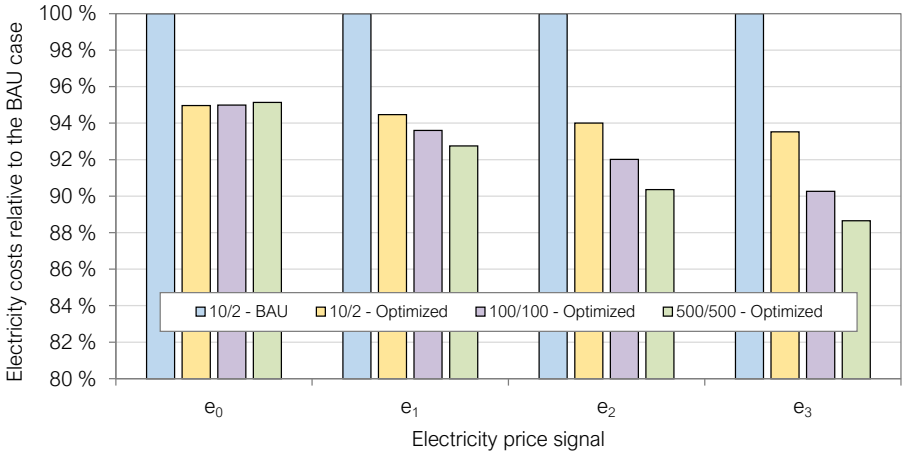

Figure 6.21: Simulated electricity costs for the first three months of 2015 relative to the BAU case ($e_1 = e_{Oslo,2015}$).

It can be seen from Figure 6.21 that all the optimized cases led to lower electricity costs compared to the BAU case. The relative savings were in the range of 5 to 11 %. The relative savings increased with larger variability of the electricity price signal. Larger tanks also led to increased relative savings, except for the cases with constant electricity price (e_0). However, the difference between the BAU case (10/2 - BAU) and the case with the currently installed tanks and optimized setpoints (10/2 - Optimized) was larger than the difference between the cases with different tank sizes and optimized setpoints (10/2 – Optimized vs. 500/500 - Optimized). This means that the optimized control led to higher relative savings than the installation of larger tanks. However, these savings only included the electricity costs and not the costs for DH import. Since the DH import increased for the cases with the optimized setpoints compared to the BAU case, an economic analysis including the calculation of the total operating costs is required to decide if larger storage tanks should be installed. The costs for the advanced control system should be taken into account in such an analysis because the installation of larger tanks would not lead to savings with the BAU control strategy.

It is also worth noting that the electricity costs shown in Figure 6.21 were calculated by multiplying the electricity use of the system by the electricity spot price. However, this is only a part of the actual costs that large customers have to pay in Norway. The electricity grid in Norway is stressed significantly more during the winter than during the rest of the year due to the high use of electricity for space heating. Therefore, the electricity grid prices include additional costs to consider the electricity grid stress. For business customers, this may induce peak-load tariffs and charging for their peak electricity use of each calendar month. This was not taken into account in this study as the measurement data showed that the peak use of the IHCS was almost the same for all the winter months. This cost was therefore assumed fixed and not included in the optimizations. The 25 % taxes that have to be paid were also neglected because they did not affect the relative savings.

7 Analysis of the case study system Brøset

In this chapter, the results of the case study Brøset are presented. The details about the case study are given in Chapter 3. Different local DH grids were investigated for the given area by means of dynamic simulation. Focus was on LTDH with the motivation to reduce the GHG emissions of the grid by reducing the grid's heat losses and utilizing waste heat sources. In Section 7.1, which is based on Paper III, the effect of different temperature levels on the pumping power and heat losses was analyzed. In Section 7.2, which is based on Paper IV, the inclusion of prosumers in the local LTDH grid was analyzed. As mentioned before, the author of this thesis contributed mostly to the modeling and simulation part of this case study.

7.1 Comparison of different local district heating grids

For this analysis, the first system model for Brøset was used, see Figure 4.32. This system model was built with components from the commercial Modelica library TIL as explained in Section 4.5.2. One-year simulations were performed and the data described in Section 3.2.3 were used as input for this analysis. The main aim of this analysis was to calculate the pumping power and heat losses for different DH system design concepts. The cases listed in Table 7.1 were defined and simulated.

Three different supply temperature levels were considered: 95 °C, 65 °C and 55 °C. 95 °C was chosen because it is the expected temperature at substations of

Table 7.1: Defined cases for the analysis of different local DH grids.

Case	Supply temperature °C	Return temperature °C	Comments
95	95-70	47.5-35.0	Current practice
65	65	32.5	Based on Norwegian legislation
55	55	27.5	Future scenario
55P	55	27.5	Case 55 with 50 % larger pipe diameters
LR	95-70	40.5-28.0	Case 95 with lower return temperature
PS	95-70	47.5-35.0	Case 95 with peak demands reduced by 20 %

the DH grid in Trondheim, 65 °C was considered as a potential future temperature level considering the Norwegian legislation, and 55 °C was included as ultimate goal for LTDH systems. For the 95 °C cases, the supply temperature was outdoor temperature compensated. A constant supply temperature was assumed for the low-temperature cases. Three additional cases were included: a low-temperature case with larger pipe diameters (55P), a high-temperature case with lower return temperature (LR), and a high-temperature case with peak shaving (PS). See Paper III for details.

The pipe diameter was an important input parameter of the pipe model because it affected both the pumping power and the heat losses. The diameter was chosen so that the maximum pressure drop in the grid did not exceed 150 Pa/m for the case 95. To this end, a one-year simulation of the case 95 with uniform pipe diameters was performed to find the maximum mass flow rates for each pipe. These maximum values were then used to set the diameter for each pipe based on the calculated pressure drop as explained in Paper III. All pipe diameters were increased by 50 % for the case 55P.

The main results from the simulations are shown in Figure 7.1 and Figure 7.2 (note that these figures are taken from Paper III and therefore do not follow the notation used in this thesis).

Compared to the case 95, the simulated heat losses were 16 and 31 % lower for

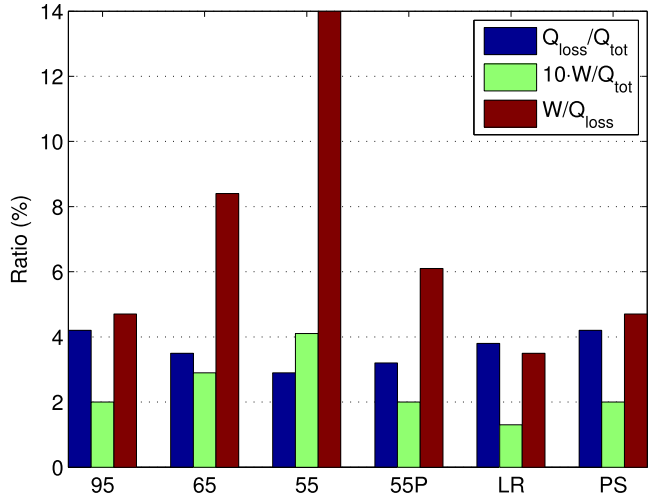

Figure 7.1: Ratios of total heat losses (Q_{loss}), pump energy (W), and delivered heat (Q_{tot}) for all the cases (taken from Paper III).

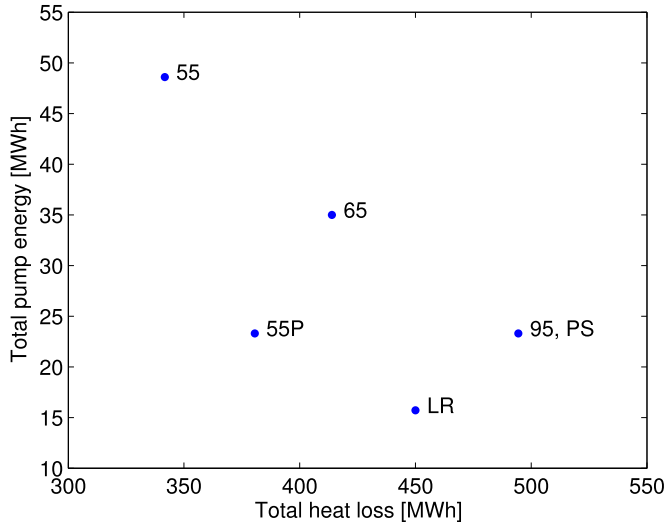

Figure 7.2: Total pump energy and heat losses for all the cases (taken from Paper III).

the cases 65 and 55, respectively as shown in the figures 7.1 and 7.2. The required pump energy increased significantly for the low-temperature cases compared to the case 95, but the total pump energy was an order of magnitude lower than the total heat losses. Therefore, a lower supply temperature had a positive overall environmental impact. The simulation results from the case 55P showed that the heat losses could be reduced without increasing pump energy by using pipes with

larger diameters. The case LR showed that a lower return temperature led to reduced heat losses and reduced pump energy. The case PS showed the same results as the case 95 in terms of heat losses and pump energy. However, the peak heating demand and the maximum pump power were reduced significantly.

Further results can be found in Paper III. These are not presented here due to the issues of the system model used for this study, see Section 4.5.2.

7.2 Including prosumers in local district heating grids

As explained in Section 4.5.2, further development of the first system model led to unacceptably long simulation times. Therefore, the final system model was built based on the simulation models explained in this thesis. One-year simulations were performed with the final system model and the data described in Section 3.2.3 were used as input. The main aim of this analysis was to investigate the effect of including prosumers into the local LTDH grid to reduce GHG emissions. The cases listed in Table 7.2 were defined and simulated.

Table 7.2: Defined cases for the analysis of prosumers in local DH grids.

Case	Supply temperature °C	Comments
HT	115-75	Current high-temperature practice
LT	65	Low-temperature based on Norwegian legislation
LTP1	65	Case LT with low-capacity prosumers
LTP2	65	Case LT with high-capacity prosumers

The supply temperature for the case HT was outdoor temperature compensated and represented the current practice of the main DH grid in Trondheim. For the other cases, a constant supply temperature of 65 °C was assumed as a potential future temperature level considering the Norwegian legislation. For the two cases with prosumers, three distributed prosumers (one data center and two food retail stores) were included in the system model, see Figure 4.33. The waste heat profiles of the prosumers are shown in Figure 3.15. The pipe diameters were different for the cases HT and LT. They were chosen to yield a maximum pressure

drop of 150 Pa/m for each case with the same approach as in the previous section. The diameters from the case LT were also used for the cases with prosumers.

To calculate the GHG emissions, the energy mix of the local DH provider was used as reference. The heat production was divided between the available heat sources, which had given operating limits. Waste incineration was the first priority because the operator gets paid for burning the waste. The remaining heat sources were prioritized based on their emission factors so that the least polluting sources were used first. All heat sources as well as their operating limits and associated emission factors in equivalent $COCO_2$ are listed in Table 7.3.

Table 7.3: Heat sources with operating limits and emission factors.

Heat source	Upper operating limit (kW)	Emission factor kg CO_2e/MWh
Surplus heat from prosumers	-	0
Waste incineration	1 330	11
Bio-oil	1 426	10
Biogas	1 444	11
Recycled wood	1 717	12
Wood chips	1 851	18
Electricity	3 086	110
Liquefied petroleum gas	-	274

The main results from the simulations are presented below (note that the figures are taken from Paper IV and therefore do not follow the notation used in this thesis).

Figure 7.3 shows that the prosumers accounted for a significant share of the total delivered heat, especially during the summer. The share was higher for the case LTP2 due to the higher capacity of the prosumers. To recall, the capacity of the prosumers was based on values from the literature, so the presented results can be considered realistic. However, it should be noted that the prosumers were assumed to be able to deliver heat to the supply line of the grid, i.e. at 65 °C. Due to this relatively high temperature level, a heat pump might be required in a real system to deliver heat to the supply line.

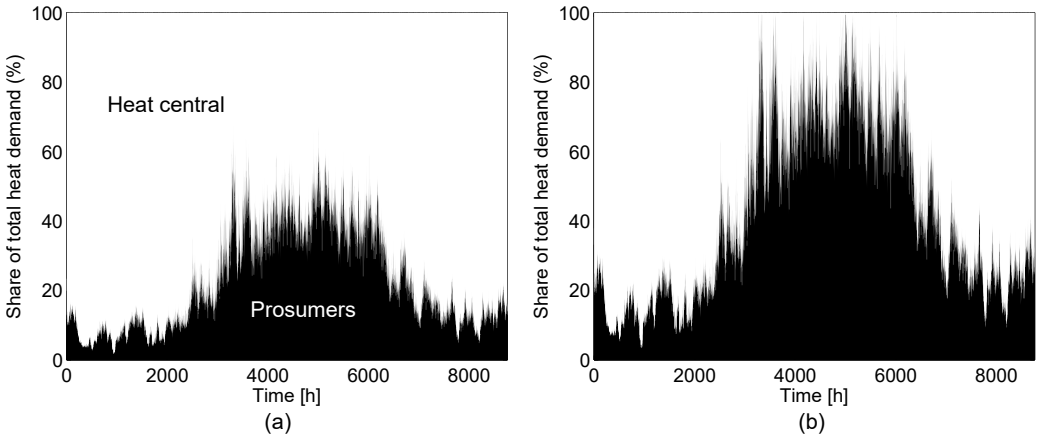

Figure 7.3: Share of heat delivered by the heat central and the prosumers. Cases: (a) LTP1, (b) LTP2 (taken from Paper IV).

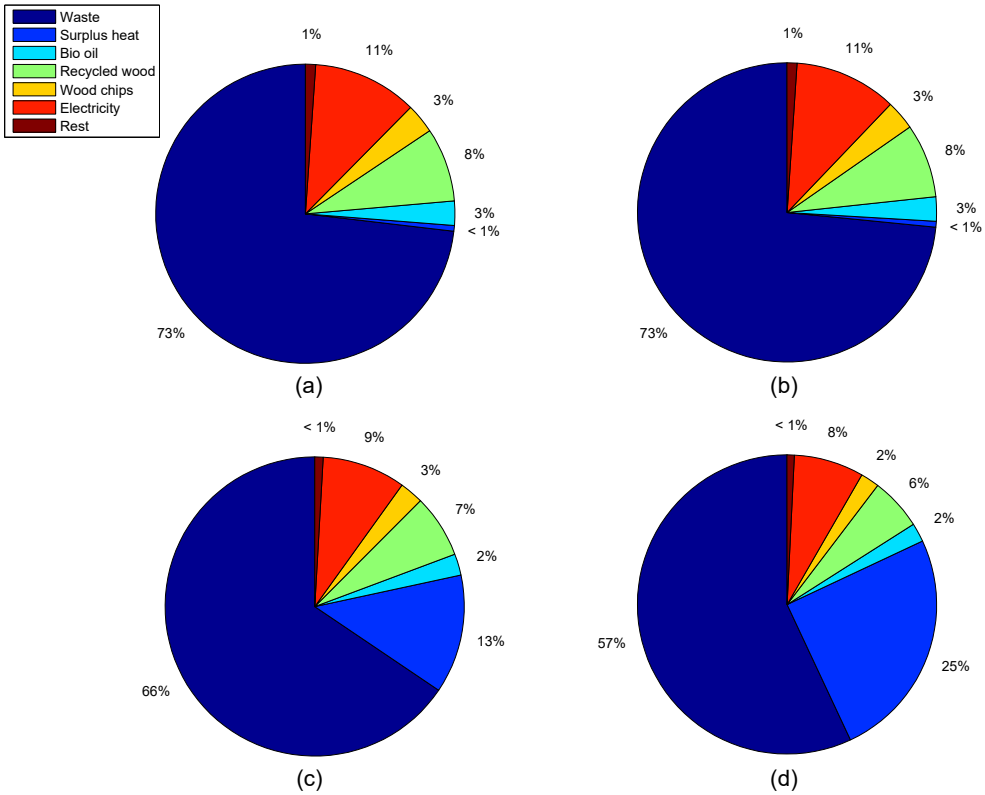

Figure 7.4: The share of heat received from the different heat sources (Rest = Gas). Cases: (a) HT, (b) LT, (c) LTP1, (d) LTP2 (taken from Paper IV).

The resulting share of the heat sources for the local LTDH grid are shown in Figure 7.4 for all simulated cases. The most polluting heat sources are colored in red. It can be seen from Figure 7.4 that the waste heat from the prosumers accounted for 13 % and 25 % for the cases LTP1 and LTP2, respectively. This clearly shows the potential for waste heat utilization in the LTDH grid. The calculated GHG emissions for all the cases are listed in Table 7.4.

Table 7.4: Calculated GHG emissions for all the cases.

Case	Average emissions kg CO_2e/MWh	Reduction compared to the case HT (%)
HT	23.8	0.0
LT	23.6	1.1
LTP1	19.9	16.4
LTP2	17.0	28.9

Table 7.4 shows that significant reductions in GHG emissions were obtained when the emission-free prosumers were included in the grid (16.4 % and 28.9 % for the cases LTP1 and LTP2, respectively). However, most of the waste heat was available during the summer, so the peak heating demand was not reduced significantly. In addition, the heat supply from the prosumers peaked around noon, while the heat demand peaked in the morning due to DHW heating. Reducing peak demands is important for emission reduction because peak heat sources are associated with high emissions. The use of thermal storages for peak shaving could therefore further reduce the GHG emissions of the grid.

Economic aspects were not considered in this study. The inclusion of prosumers was shown to be beneficial in terms of energetic and environmental performance. However, the profitability for the DH supplier depends highly on the applied pricing scheme for waste heat delivery and the investment costs related to prosumer substations.

8 Conclusions and suggestions for further work

8.1 Main conclusions

The main aim of this work was the analysis of both the design and the operation of thermal energy supply systems on neighborhood scale to make these systems more energy- and/or cost efficient. To this end, component and system models were developed in Modelica and used for several analyses. Dynamic simulations with Dymola as well as dynamic optimizations with JModelica.org were successfully performed. Several general conclusions can be drawn from this modeling, simulation, and optimization effort:

1) Modelica-based modeling and simulation are relatively mature and many Modelica libraries with sophisticated simulation models exist. However, an important aspect for system analysis is to ensure that the aim of the analysis and the level of modeling detail are well aligned. No suitable library was available for the planned tasks of this work, i.e. fast simulation of complex thermal energy systems over long time horizons. Therefore, the component models needed to be developed. This was a time-consuming task, but was necessary for successful analysis and can make this work a useful reference for others.

2) Even when suitable component models are available, dynamic simulations can still be a cumbersome task. Entering component model specifications and assembling component models into a system model are usually straightforward tasks. However, the modeling of the control system can be challenging, especially for complex systems with many interconnections. Several simulation performance

issues can arise due to control-related discontinuities, chattering, or algebraic loops. These can make the simulation unnecessary slow or even fail. Efficient system simulation models can therefore only be developed with a certain level of user-experience.

3) Due to the potentially high amount of time required for dynamic system simulation, its use should be carefully evaluated and should not be seen as "low-hanging fruit". However, energy systems are expected to become more complex in the near future - due to the inclusion of fluctuating energy sources, (thermal) energy storages, and more advanced pricing schemes for electricity and district heating – and the operation of such systems cannot be analyzed easily. Dynamic simulations are a suitable tool and are thus expected to be of increasing importance to meet stricter efficiency targets and/or ensure economic operation of future energy systems.

4) JModelica.org, a framework for Modelica-based dynamic optimization, has recently been developed at Lund University and was used in this work. No Modelica library with optimization-ready components for this type of system is available yet. The simulation models developed in this work were therefore used, but had to be adapted due to different handling of the model equations during simulation and optimization. While the required component model changes were minor, the system model complexity had to be reduced. The models were then suitable for dynamic optimization over long time horizons and can therefore be a useful reference for others. However, dynamic optimization is even more advanced than dynamic simulation and can thus be seen as an expert-tool, which is not expected to be widely used outside the research community.

The methodology chosen for this work was shown to be suitable for the analysis of complex thermal energy supply systems with varying load profiles and prices. Reuse of the developed component models was an important aspect and enabled the analysis of different case study systems. Several specific conclusions can be drawn from the analyses of the case study system at Vulkan, Oslo:

1) The annual heat balance of the long-term storage is important for system operation. The current operation might be unsustainable and lead to system performance degradation. Two solutions for sustainable operation were suggested: installing more solar collectors and increasing the heat import from the district

heating grid. These results depended heavily on the simulation model of the long-term storage. Although the short-term response of the model has been validated, a long-term validation could not be performed due to lacking mass flow rate measurements. The installation of flow meters for calibration of the simulation model should be considered to increase the reliability of the results.

2) Changing from constant heating and cooling supply temperature setpoints to variable setpoints could reduce the electricity use of the system. However, the setpoint optimization presented in this work cannot be implemented in a practical manner because the optimized setpoints are adjusted twice an hour. From a practical point of view, operation does not need to be optimal, rather good enough and simple to implement. The optimization approach presented in this work could therefore be used to find practical setpoint adjustments, e.g. outdoor temperature compensated setpoints or setpoints based on daily and/or seasonal schedules. These results depended on the part-load operation of the heat pump. The heat pump COP was only based on the temperature lift of the heat pump during the optimizations in this work. However, a more specific heat pump model considering part-load operation based on advanced circuit simulations was also developed. Using this model could be considered for practical system analyses.

3) Installing larger storage tanks is probably not profitable. Although larger storage tanks could be used for peak shaving and electricity cost reduction, the variability of the electricity price was too low to lead to significant savings for the analyzed period. In addition, savings could only be obtained with a more advanced control system than the one currently implemented. However, higher variability of the electricity price or higher peak load tariffs might lead to a different conclusion.

The simulations of the planned case study system at Brøset, Trondheim confirmed that low-temperature district heating grids are beneficial, especially for new development areas. The pipe diameters were shown to be important for the heat losses in the grid and the required pumping power. The inclusion of prosumers in low-temperature district heating grids was found to reduce greenhouse-gas emissions significantly.

8.2 Suggestions for further work

Recent advances in the development of computational tools for simulation and optimization, supported by increased computational power, have enabled the work presented in this thesis. Due to the high level of individuality of future integrated energy systems and the broadness of the topic, much work remains and some suggestions for further work are given below:

1) Several of the component and system models developed in this work were called "final". Still, many refinements and/or extensions are possible, e.g. the inclusion of pipe models in the system model for Vulkan, a more realistic calculation of the return temperature on the secondary side of the customer substation models, a physical model of the ice thermal energy storage, or a prosumer substation with heat exchangers for more realistic heat supply to the grid. New cases could also be defined and investigated, e.g. charging the borehole thermal energy storage at Vulkan with low-temperature heat from the district heating return line, optimizing the system at Vulkan with a more advanced pricing scheme including district heating prices, or the inclusion of storages and/or solar collectors in the system model for Brøset.

2) The Modelica models developed in this work were tailored to the analyzed case study systems and the aims of the analyses. Developing new models for different types of components would allow the analysis of a wider range of systems and should therefore be considered. Nevertheless, many new use cases for both simulation and optimization have already been defined in the ongoing research projects HighEFF, LTTG+, and LowEmission.

3) Comparing the models developed in this work to the models in the Modelica library IBPSA could give valuable insights. This library is a main part of IBPSA Project 1 (duration 2017 to 2022), which aims at developing a Modelica-based framework for building and community energy system design and operation. This is well within the scope of this work. Optimization with JModelica.org is also part of Project 1 but is, to the best of the author's knowledge, still in an early development phase because many of the simulation models cannot be used for optimization (as was the case in this work). Following the development of the IBPSA library, especially the optimization efforts, is therefore recommended.

4) All the simulation input data were also used as input for the optimizations, i.e. perfect prediction was assumed for the optimization approach presented in this work. Obviously, perfect prediction is not a realistic scenario because energy demands of buildings and the electricity price in Norway both depend on ambient conditions. In practice, the uncertainty of the weather forecast thus makes detailed optimizations over a long prediction horizon obsolete. Repeatedly optimizing a shorter period over a receding horizon, as in Model Predictive Control, is thus a more practical approach. It is therefore suggested to develop Python code for Model Predictive Control in addition to the developed open loop optimization code.

References

[1] European Union (2010). "Directive 2010/31/EU of the European Parliament and of the Council of 19 May 2010 on the energy performance of buildings." *Official Journal of the European Union* L 153, 13–35.

[2] X. Cao, X. Dai, and J. Liu (2016). "Building energy-consumption status worldwide and the state-of-the-art technologies for zero-energy buildings during the past decade." *Energy and Buildings* 128, pp. 198–213. DOI: 10.1016/j.enbuild.2016.06.089.

[3] International Energy Agency (2013). "Heating and Cooling Technologies." In: *Transition to Sustainable Buildings: Strategies and Opportunities to 2050*. Chap. 4. ISBN: 978-92-64-20241-2.

[4] P. Lundqvist (2015). "The role of heat pumps in the smart energy systems." In: *Proceedings of the 24th International Congress of Refrigeration, Yokohama, Japan*. DOI: 10.18462/iir.icr.2015.1009.

[5] D. Schmidt (2018). "Low Temperature District Heating for Future Energy Systems." *Energy Procedia* 149, pp. 595–604. DOI: 10.1016/j.egypro.2018.08.224.

[6] H. Lund et al. (2018). "Future district heating systems and technologies: On the role of smart energy systems and 4th generation district heating." *Energy* 165, pp. 614–619. DOI: 10.1016/j.energy.2018.09.115.

[7] L. Belussi et al. (2019). "A review of performance of zero energy buildings and energy efficiency solutions." *Journal of Building Engineering* 25, p. 100772. DOI: 10.1016/j.jobe.2019.100772.

[8] C. Lausselet, V. Borgnes, and H. Brattebø (2019). "LCA modelling for Zero Emission Neighbourhoods in early stage planning." *Building and Environment* 149, pp. 379–389. DOI: 10.1016/j.buildenv.2018.12.034.

[9] F. Jorissen et al. (2018). "Implementation and verification of the IDEAS building energy simulation library." *Journal of Building Performance Simulation* 11 (6), pp. 669–688. DOI: 10.1080/19401493.2018.1428361.

[10] G. Schweiger et al. (2018). "District energy systems: Modelling paradigms and general-purpose tools." *Energy* 164, pp. 1326–1340. DOI: 10.1016/j.energy.2018.08.193.

[11] A. Brand et al. (2015). "Beyond authorship: attribution, contribution, collaboration, and credit." *Learned Publishing* 28 (2), pp. 151–155. DOI: 10.1087/20150211.

[12] M. Lanahan and P. C. Tabares-Velasco (2017). "Seasonal Thermal-Energy Storage: A Critical Review on BTES Systems, Modeling, and System Design for Higher System Efficiency." *Energies* 10 (6). DOI: 10.3390/en10060743.

[13] G. Alva, Y. Lin, and G. Fang (2018). "An overview of thermal energy storage systems." *Energy* 144, pp. 341–378. DOI: 10.1016/j.energy.2017.12.037.

[14] J. Heier, C. Bales, and V. Martin (2015). "Combining thermal energy storage with buildings – a review." *Renewable and Sustainable Energy Reviews* 42, pp. 1305–1325. DOI: 10.1016/j.rser.2014.11.031.

[15] A. R. Mazhar, S. Liu, and A. Shukla (2018). "A state of art review on the district heating systems." *Renewable and Sustainable Energy Reviews* 96, pp. 420–439. DOI: 10.1016/j.rser.2018.08.005.

[16] A. Afram and F. Janabi-Sharifi (2014). "Theory and applications of HVAC control systems – A review of model predictive control (MPC)." *Building and Environment* 72, pp. 343–355. DOI: 10.1016/j.buildenv.2013.11.016.

[17] R. Ooka and S. Ikeda (2015). "A review on optimization techniques for active thermal energy storage control." *Energy and Buildings* 106, pp. 225–233. DOI: 10.1016/j.enbuild.2015.07.031.

[18] J. Clauß et al. (2019). "Predictive rule-based control to activate the energy flexibility of Norwegian residential buildings: Case of an air-source heat pump and direct electric heating." *Applied Energy* 237, pp. 500–518. DOI: 10.1016/j.apenergy.2018.12.074.

[19] P. Rockett and E. A. Hathway (2017). "Model-predictive control for non-domestic buildings: a critical review and prospects." *Building Research and Information* 45 (5), pp. 556–571. DOI: 10.1080/09613218.2016.1139885.

[20] K. Rupp (2018). *"42 Years of Microprocessor Trend Data"*. www.karlrupp.net/2018/02/42-years-of-microprocessor-trend-data. Accessed 05/2019.

[21] G. Augenbroe (2011). "The role of simulation in performance based building." In: *Building Performance Simulation for Design and Operation*. Spon Press. Chap. 2, pp. 15–36. ISBN: 978–0–415–47414–6.

[22] M. Trčka and J. L. M. Hensen (2010). "Overview of HVAC system simulation." *Automation in Construction* 19 (2), pp. 93–99. DOI: 10.1016/j.autcon.2009.11.019.

[23] M. Wetter, M. Bonvini, and T. S. Nouidui (2016). "Equation-based languages – A new paradigm for building energy modeling, simulation and optimization." *Energy and Buildings* 117, pp. 290–300. DOI: 10.1016/j.enbuild.2015.10.017.

[24] Modelica Association (2017). “Modelica - A Unified Object-Oriented Language for Systems Modeling.” *Language Specification Version 3.4*. URL: www.modelica.org/documents/ModelicaSpec34.pdf.

[25] Modelica Association. *“Modelica Libraries”*. www.modelica.org/libraries. Accessed 03/2019.

[26] J. Allegrini et al. (2015). “A review of modelling approaches and tools for the simulation of district-scale energy systems.” *Renewable and Sustainable Energy Reviews* 52, pp. 1391–1404. DOI: 10.1016/j.rser.2015.07.123.

[27] Modelica Association. *“Modelica Tools”*. www.modelica.org/tools. Accessed 03/2019.

[28] S. Dutta (2016). “A Brief Discussion on Optimization.” In: *Optimization in Chemical Engineering*. Cambridge University Press. Chap. 1, p. 7. ISBN: 978-1-107-09123-8.

[29] D. H. Wolpert and W. G. Macready (1997). “No Free Lunch Theorems for Optimization.” *IEEE Transactions on Evolutionary Computation* 1 (1), pp. 67–82. DOI: 10.1109/4235.585893.

[30] L. T. Biegler (2010). “Simultaneous Methods for Dynamic Optimization.” In: *Nonlinear Programming*. MOS-SIAM Series on Optimization. Chap. 10, pp. 287–324. ISBN: 978-0-89871-702-0.

[31] F. Magnusson and J. Åkesson (2015). “Dynamic Optimization in JModelica.org.” *Processes* 3 (2), p. 471. DOI: 10.3390/pr3020471.

[32] J. A. E. Andersson et al. (2019). “CasADi: a software framework for nonlinear optimization and optimal control.” *Mathematical Programming Computation* 11 (1), pp. 1–36. DOI: 10.1007/s12532-018-0139-4.

[33] A. Wächter and L. T. Biegler (2006). “On the implementation of an interior-point filter line-search algorithm for large-scale nonlinear programming.” *Mathematical Programming* 106 (1), pp. 25–57. DOI: 10.1007/s10107-004-0559-y.

[34] J. Åkesson (2008). “Optimica - An Extension of Modelica Supporting Dynamic Optimization.” In: *Proceedings of the 6th International Modelica Conference*.

[35] F. Belkhir et al. (2015). “Optimal Startup Control of a Steam Power Plant Using the JModelica Platform.” *IFAC-PapersOnLine* 48 (1), pp. 204–209. DOI: 10.1016/j.ifacol.2015.05.050.

[36] A. Holmqvist and F. Magnusson (2016). “Open-loop optimal control of batch chromatographic separation processes using direct collocation.” *Journal of Process Control* 46, pp. 55–74. DOI: 10.1016/j.jprocont.2016.08.002.

[37] S. Barsali et al. (2017). “Optimised operation of storage systems integrated with MV photovoltaic plants, considering the impact on the battery lifetime.” *Journal of Energy Storage* 12, pp. 178–185. DOI: 10.1016/j.est.2017.05.003.

[38] Y. Cao et al. (2017). "Real-time feasible multi-objective optimization based nonlinear model predictive control of particle size and shape in a batch crystallization process." *Control Engineering Practice* 69, pp. 1–8. DOI: 10.1016/j.conengprac.2017.08.008.

[39] A. Sellberg et al. (2018). "Multi-flowrate Optimization of the Loading Phase of a Preparative Chromatographic Separation." *Computer Aided Chemical Engineering* 43, pp. 1619 –1624. DOI: 10.1016/B978-0-444-64235-6.50282-5.

[40] F. Audino et al. (2019). "Systematic optimization approach for the efficient management of the photo-Fenton treatment process." *Science of The Total Environment* 646, pp. 902–913. DOI: 10.1016/j.scitotenv.2018.07.057.

[41] R. De Coninck et al. (2016). "Toolbox for development and validation of grey-box building models for forecasting and control." *Journal of Building Performance Simulation* 9 (3), pp. 288–303. DOI: 10.1080/19401493.2015.1046933.

[42] G. Schweiger et al. (2017). "District heating and cooling systems – Framework for Modelica-based simulation and dynamic optimization." *Energy* 137, pp. 566–578. DOI: 10.1016/j.energy.2017.05.115.

[43] F. Jorissen, W. Boydens, and L. Helsen (2019). "TACO, an automated toolchain for model predictive control of building systems: implementation and verification." *Journal of Building Performance Simulation* 12 (2), pp. 180–192. DOI: 10.1080/19401493.2018.1498537.

[44] B. Knudsen, H. Kauko, and T. Andresen (2019). "An optimal-control scheme for coordinated surplus-heat exchange in industry clusters." *Energies* 12 (10). DOI: 10.3390/en12101877.

[45] Norwegian Institute of Bioeconomy Research. *"Weather Data for Norway"*. https://lmt.nibio.no/agrometbase/getweatherdata_new.php. Accessed 03/2018.

[46] Trondheim Municipality (2013). *"Områdeplan for Brøset. Vedlegg 4 - illustrasjonsplan"*. www.trondheim.kommune.no/globalassets/10-bilder-og-filer/10-byutvikling/byplankontoret/temaplaner/omradeplan-for-broset/vedlegg-4---illustrasjonsplan-04.04.13.pdf. Accessed 04/2019.

[47] Trondheim Municipality (2011). *"Områdeplan for Brøset. Vedlegg 19 - energiløsninger" (in Norwegian)*. www.trondheim.kommune.no/globalassets/10-bilder-og-filer/10-byutvikling/byplankontoret/temaplaner/omradeplan-for-broset/vedlegg-19---energilosninger.pdf. Accessed 04/2019.

[48] H. Lund et al. (2014). "4th Generation District Heating (4GDH): Integrating smart thermal grids into future sustainable energy systems." *Energy* 68, pp. 1–11. DOI: 10.1016/j.energy.2014.02.089.

[49] T. Tereshchenko and N. Nord (2018). "Future Trends in District Heating Development." *Current Sustainable/Renewable Energy Reports* 5 (2), pp. 172–180. DOI: 10.1007/s40518-018-0111-y.

[50] TLK-Thermo GmbH. *"TIL Suite – Simulates thermal systems"*. https://www.tlk-thermo.com/index.php/en/software-products/til-suite. Accessed 06/2019.

[51] M. Wetter et al. (2014). "Modelica Buildings library." *Journal of Building Performance Simulation* 7 (4), pp. 253–270. DOI: 10.1080/19401493.2013.765506.

[52] F. Jorissen, M. Wetter, and L. Helsen (2015). "Simulation Speed Analysis and Improvements of Modelica Models for Building Energy Simulation." In: *Proceedings of the 11th International Modelica Conference*. DOI: 10.3384/ecp1511859.

[53] I. H. Bell et al. (2014). "Pure and Pseudo-pure Fluid Thermophysical Property Evaluation and the Open-Source Thermophysical Property Library CoolProp." *Industrial and Engineering Chemistry Research* 53 (6), pp. 2498–2508. DOI: 10.1021/ie4033999.

[54] H. Sofrata (1993). "Carnot and Lorenz cycles for dual absorption system." *Wärme - und Stoffübertragung* 28 (3), pp. 107–116. DOI: 10.1007/BF01541106.

[55] F. P. Incropera et al. (2007). "Heat Exchangers." In: *Fundamentals of Heat and Mass Transfer*. John Wiley & Sons. Chap. 11. ISBN: 978-0-471-45728-2.

[56] J. Yang, A. Jacobi, and W. Liu (2017). "Heat transfer correlations for single-phase flow in plate heat exchangers based on experimental data." *Applied Thermal Engineering* 113, pp. 1547–1557. DOI: 10.1016/j.applthermaleng.2016.10.147.

[57] F. Ruiz-Calvo et al. (2015). "Experimental validation of a short-term Borehole-to-Ground (B2G) dynamic model." *Applied Energy* 140, pp. 210–223. DOI: 10.1016/j.apenergy.2014.12.002.

[58] D. Bauer et al. (2011). "Thermal resistance and capacity models for borehole heat exchangers." *International Journal of Energy Research* 35 (4), pp. 312–320. DOI: 10.1002/er.1689.

[59] P. Stephan (2010). "Fundamentals of Heat Transfer." In: *VDI Heat Atlas*. Springer Berlin Heidelberg. Chap. B1, pp. 15–30. ISBN: 978-3-540-77876-9.

[60] B. Sibbitt et al. (2012). "The Performance of a High Solar Fraction Seasonal Storage District Heating System – Five Years of Operation." *Energy Procedia* 30, pp. 856–865. DOI: 10.1016/j.egypro.2012.11.097.

[61] R. A. Beier, M. D. Smith, and J. D. Spitler (2011). "Reference data sets for vertical borehole ground heat exchanger models and thermal response test analysis." *Geothermics* 40 (1), pp. 79–85. DOI: 10.1016/j.geothermics.2010.12.007.

[62] F. Mosallat et al. (2013). "Modeling, Simulation and Control of Flat Panel Solar Collectors with Thermal Storage for Heating and Cooling Applications." *Procedia Computer Science* 19, pp. 686–693. DOI: 10.1016/j.procs.2013.06.091.

[63] A. C. Hindmarsh et al. (2005). "SUNDIALS: Suite of nonlinear and differential/algebraic equation solvers." *ACM Transactions on Mathematical Software* 31 (3), pp. 363–396. DOI: 10.1145/1089014.1089020.

[64] F. Magnusson and J. Åkesson (2018). "Symbolic elimination in dynamic optimization based on block-triangular ordering." *Optimization Methods and Software* 33 (1), pp. 92–119. DOI: 10.1080/10556788.2016.1270944.

[65] HSL. *"A collection of Fortran codes for large scale scientific computation"*. www.hsl.rl.ac.uk. Accessed 03/2018.

[66] Sivilingeniør Carl Christian Strømberg AS. *"Solar potential of roof areas in Norway"*. https://solkart.no. Accessed 04/2019.

[67] H. Holmberg et al. (2016). "Numerical model for non-grouted borehole heat exchangers, Part 2 - Evaluation." *Geothermics* 59, pp. 134–144. DOI: 10.1016/j.geothermics.2014.11.002.

[68] R. K. Ramstad et al. (2015). "Thermal conductivity map of the Oslo region based on thermal diffusivity measurements of rock core samples." *Bulletin of Engineering Geology and the Environment* 74 (4), pp. 1275–1286. DOI: 10.1007/s10064-014-0701-x.

[69] Nord Pool AS. *"Historical Market Data"*. https://www.nordpoolgroup.com/historical-market-data/. Accessed 02/2019.

[70] D. Fischer et al. (2016). "Impact of PV and variable prices on optimal system sizing for heat pumps and thermal storage." *Energy and Buildings* 128, pp. 723–733. DOI: 10.1016/j.enbuild.2016.07.008.

Appendix

Paper I

D. Rohde, M. Bantle, T. Andresen, and N. Nord (2015). "Documentation of an Integrated Thermal Energy System for a Building Complex." In: *Proceedings of the 24th International Congress of Refrigeration, Yokohama, Japan.* DOI: 10.18462/iir.icr.2015.0445.

DOCUMENTATION OF AN INTEGRATED THERMAL ENERGY SYSTEM FOR A BUILDING COMPLEX

Daniel ROHDE[(*)], Michael BANTLE[(**)], Trond ANDRESEN[(**)], Natasa NORD[(*)]
[(*)]Norwegian University of Science and Technology, Kolbjørn Hejes vei 1A, Trondheim, 7491, Norway
daniel.rohde@ntnu.no
[(**)]SINTEF Energy Research, Sem Sælands vei 11, Trondheim, 7034, Norway

ABSTRACT

In large buildings and building complexes, energy use can be reduced by efficient interaction between heating and cooling demands and thermal storage (short and long term storage). This work describes an integrated energy system in Norway which supplied several commercial and residential buildings with heating and cooling. The integrated thermal energy system consisted of heat pumps (~1 MW total cooling capacity), solar thermal collectors (290 m^2), district heating connection as well as water tanks (15000 l) and boreholes (62 x 300 m) for thermal energy storage. The water tanks acted as buffer and balanced the mismatch of supply and demand during a day. The seasonal operation modes were chosen depending on the outdoor conditions. In summer, the condenser heat from the cooling systems and the solar collectors was sent to the boreholes. In winter, the heat pumps used the boreholes and the surplus heat from the cooling systems as heat source and delivered heat to the buildings for space heating and domestic hot water. In spring, certain cooling demands could be covered by free-cooling as long as the borehole temperature was low enough. District heating was utilized to lift the temperature for the domestic hot water and also served as backup system. In this work, the system is described in detail and operational data is presented. Improvement suggestions are made which could cut operational costs.

1. INTRODUCTION

There is an extensive focus on reducing the energy use of buildings as the buildings sector accounts for a large share of the world's energy use (around 40% in the European Union (European Union, 2010)). The main part of this energy is used for heating, ventilation, and air conditioning (HVAC), and domestic hot water (DHW) production (Pérez-Lombard et al., 2008). The DHW demand is relatively constant throughout the year, while the demand of the HVAC system highly depends on the outdoor temperature (Pedersen, 2007). Both heating and cooling load vary greatly between different buildings or building complexes as they are influenced by the building construction, type, use, size, and the climatic conditions (Guo, 2011). Thermal storage at high or low temperature can be used for heating and cooling, respectively. This allows, to a certain extent, to decouple the current thermal load of a building from the current energy demand which can reduce expensive peak demands. Common storage components of building energy systems are water tanks for short-term storage and underground thermal energy storage (UTES) for long-term (seasonal) storage. Examples of UTES are aquifer storage and borehole thermal energy storage (BTES). Both allow storing surplus heat during the summer period which can be used as heat source during the winter period (Heier et al., 2015). BTES is often combined with a heat pump system (Nord et al., 2012) and such combined systems are especially suited for colder climate countries (Hesaraki et al., 2015). The heat loss from a BTES depends significantly on the ground conditions, especially the amount and/or flow of ground water (Reuss, 2015).

An old industrial area (size roughly 100 x 200 m) in the Norwegian capital Oslo has recently been renewed with several buildings and an integrated thermal energy system (construction started in 2009). Various building types were built, namely apartments, shops, event locations, restaurants, food court, hotels, sport facilities, offices, and a university. Almost all of these were connected to the main integrated thermal energy system described in this paper. Each connected building had an individual distribution system which exchanged heat with the main system by a designated heat exchanger in the corresponding substation. The complete system has been in operation since the end of 2013 and was subject to efficiency improvement measures. The aim of this study was to document the system's operation during the year 2014 and give improvement suggestions.

2. INTEGRATED THERMAL ENERGY SYSTEM AND ITS CONTROL MODES

2.1. System and Component Description

A simplified scheme of the integrated thermal energy system can be seen in Figure 1. It also shows the fluids that were used for energy transport in the different closed circuits as well as the thermal energy users and their corresponding temperatures that were covered by the system. Product cooling was needed for the display cabinets in the food court.

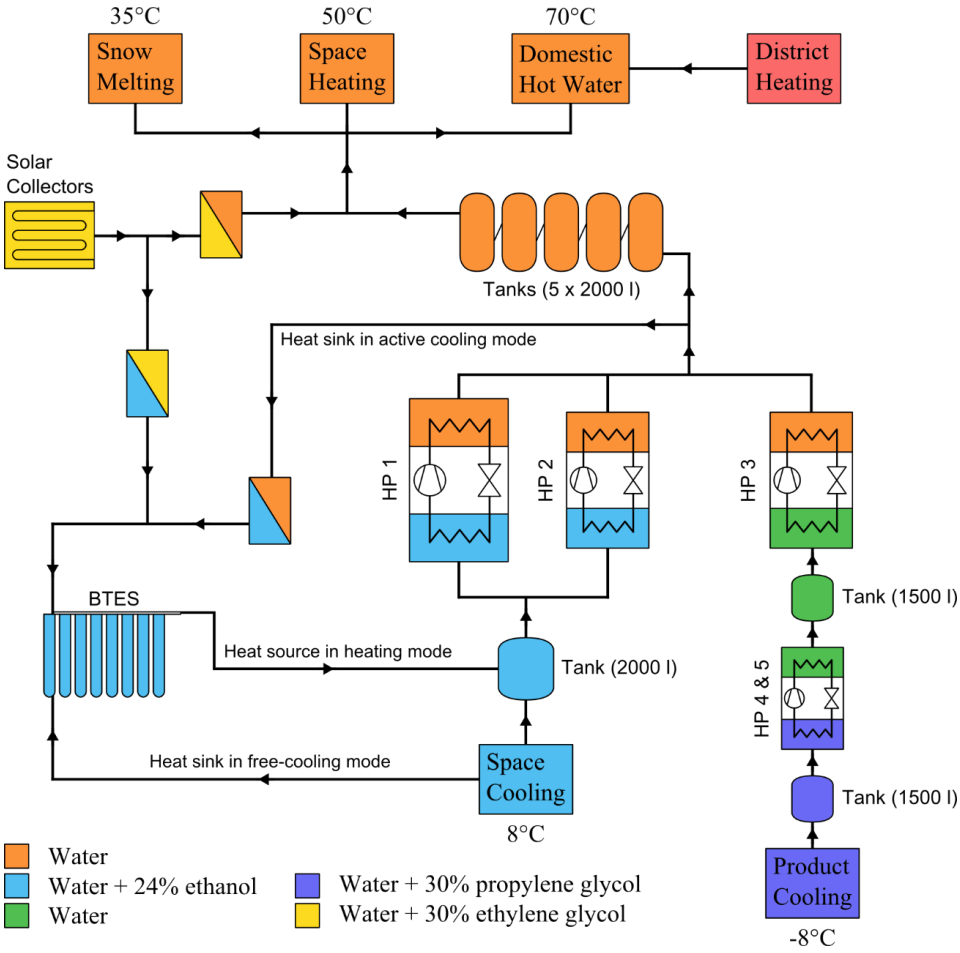

Figure 1. Simplified system overview.

The main parts of the integrated energy supply system were five heat pumps (HP), tanks and boreholes for thermal energy storage, and solar thermal collectors as shown in Figure 1. The specifications of the five heat pumps are listed in Table 1. The BTES consisted of U-pipes, 300 m deep, where the design flow rate was 0.81 l/s per pipe. 14 boreholes were drilled in the southern part of the area (hereafter called BTES South) and 48 boreholes were drilled in the northern part (hereafter called BTES North). However, they are shown as one unit in Figure 1 for simplicity. The solar thermal collectors consisted of 290 m² flat plate collector panels, integrated in the south-facing facade of an office building.

It can be seen from Table 1 that the heat pumps were designed to deliver heat at 50°C, so they could only cover parts of the DHW demand by preheating the DHW up to ~50°C. District heating was then employed to lift the temperature to the required 70°C. The space heating circuits were also connected to the district heating network (not shown in Figure 1) as backup system in case of very high space heating demands or heat pump failure.

Table 1: Heat pump specifications

	HP 1	HP 2	HP 3	HP 4 & 5
Type	WSA2802X	WSA1602X	WSA0701X	NXW0600X
Working fluid	R134a	R134a	R134a	R410a
Compressor	Screw (2)	Screw (2)	Screw	Scroll
Design data cooling (evap./cond.)				
Temperatures	4.5°C / 48°C	4.5°C / 48°C	20°C / 55°C	-8°C / 25°C
Capacities	595 / 772 kW	334 / 436 kW	224 / 283 kW	87 / 110 kW
COP	4.36	4.27	4.80	4.78
Design data heating (evap./cond.)				
Temperatures	0°C / 50°C	0°C / 50°C		
Capacities	473 / 652 kW	264 / 365 kW		
COP	3.64	3.61		

2.2. Control Modes

The system had several closed circuits for energy transfer and different operation modes were developed to cover the various energy demands throughout the year. Specifically, heating, free-cooling, and active cooling mode were developed and are described below. For all control modes, the tanks could be used to ensure even supply and return temperatures during operation.

Heating mode was developed for the winter period with typically high space heating demand. In this mode, the BTES as well as the surplus heat from space cooling and product cooling were used as heat sources for the heat pumps. The condenser heat from HP 1, 2, and 3 was then sent to the substations for space heating, DHW preheating, and snow melting when necessary. The solar collectors were not used during heating mode due to the very low solar irradiation in Oslo during winter. The ground temperature around the boreholes decreased during heating mode.

Free-cooling mode was implied during spring. In this mode, the ground temperature was at its minimum due to the heat extraction during winter. If the fluid's return temperature from the boreholes was lower than 8°C, it could directly be sent to the space cooling substation. This mode was called free-cooling because the surplus heat from space cooling did not need to be upgraded to a higher temperature level to be released (as usually done with the help of a heat pump). The ground temperature increased during heating mode. The surplus heat from product cooling was still used as heat source for the heating demands like in heating mode. The solar collectors and snow melting circuits were activated depending on the outdoor conditions.

Active cooling mode was used during summer. Due to the typically high space cooling demand, a lot of surplus heat needed to be released from HP 1 and 2. In addition, the solar collectors and HP 3 also delivered heat and only a part of this was needed for space heating and DHW preheating. Therefore, the main part was sent to the BTES and led to an increase in the ground temperature.

3. OPERATION EXPERIENCE

3.1. Data Acquisition and Quality

Measurement data for 2014 was received from the operator's server. Due to different logging intervals of the sensors, all data points were averaged for each hour of the year before being analyzed. Due to the slow thermal response of some of the components (especially the BTES), this could lead to errors in the hourly values during transient operation. The monthly values were less affected by this averaging. Short periods of missing data due to sensor problems and/or server errors were not long enough to influence the results significantly.

3.2. Performance of the Integrated Thermal Energy System

Monthly values for energy use and the system's coefficient of performance (COP) are shown in Figure 2.

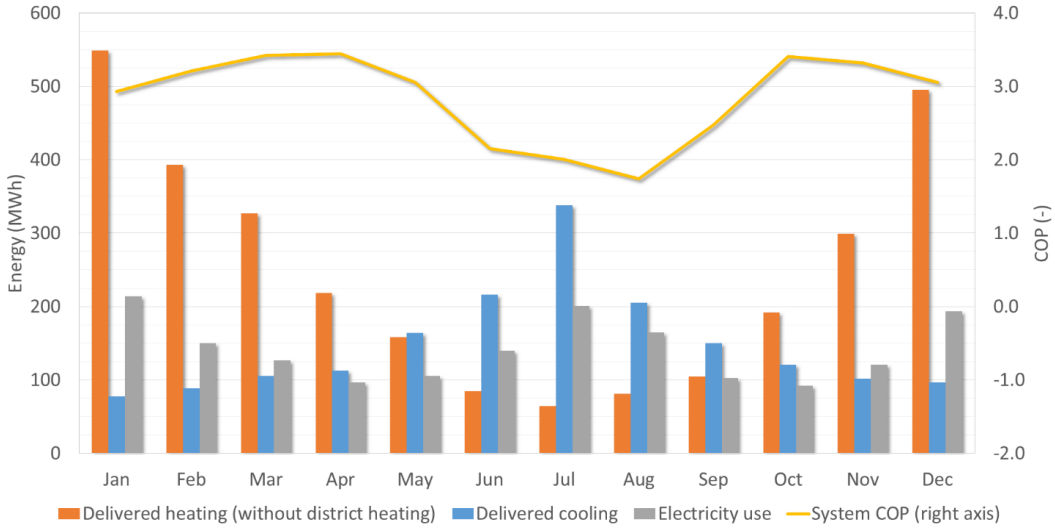

Figure 2. Monthly energy amounts and average system COP for 2014.

The variation of heating and cooling demand throughout the year can clearly be seen in Figure 2. This is mostly due to space heating and cooling. DHW preheating and product cooling were relatively constant demands. The electricity use in Figure 2 was the amount used by the whole system, including all pumps, control system, safety systems, etc. It also varied throughout the year and was highest during the peak load months in summer and winter. The COP of the system shown in Figure 2 was calculated as:

$$\text{COP} = \frac{\text{Delivered heating} + \text{Delivered cooling}}{\text{Electricity use}} \quad (1)$$

The system COP ranged from 1.7 to 3.4 in 2014. In total, 1 707 MWh of electricity were used to deliver 384 MWh for product cooling, 1 393 MWh for space cooling, 309 MWh for snow melting, and 2 658 MWh for space heating and DHW preheating.

District heating was not included in the COP calculation. The daily use of district heating compared to the delivered heat from the energy system is shown in Figure 3. The outdoor temperature is also shown, but the measured values were too high. This is explained afterwards and shown in Figure 4.

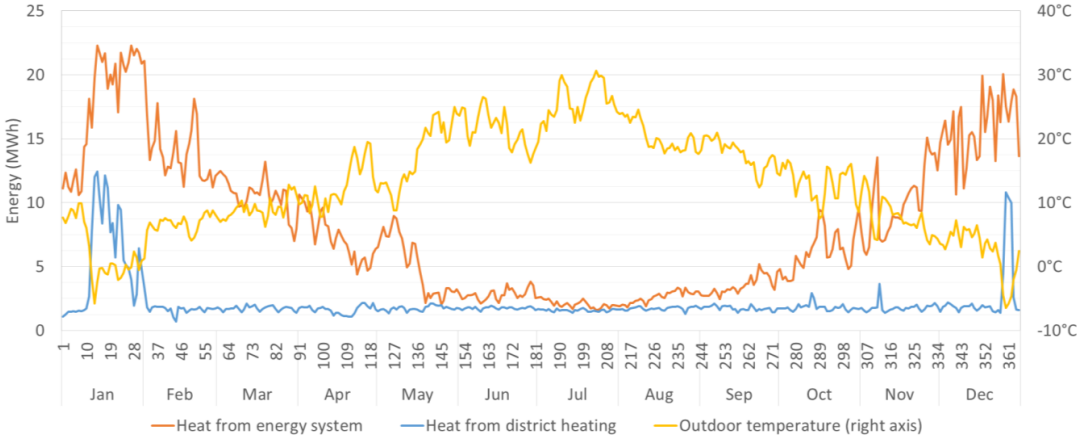

Figure 3. Daily heat amounts and average outdoor temperature for 2014.

It can be seen from Figure 3 that the district heating load was almost constant for most of the year. This was due to the typically low variation in DHW use which was the only recipient of district heating during normal operation. However, when the outdoor temperatures were very low in the middle of January and the end of December, a significant increase in district heating use could be observed. The district heating network then also delivered heat to the buildings for space heating.

The system's outdoor temperature measurements seemed high and were compared to data from a weather station 20 km away (Bioforsk, 2015). The comparison in Figure 4 shows that the suspected offset was about 6°C.

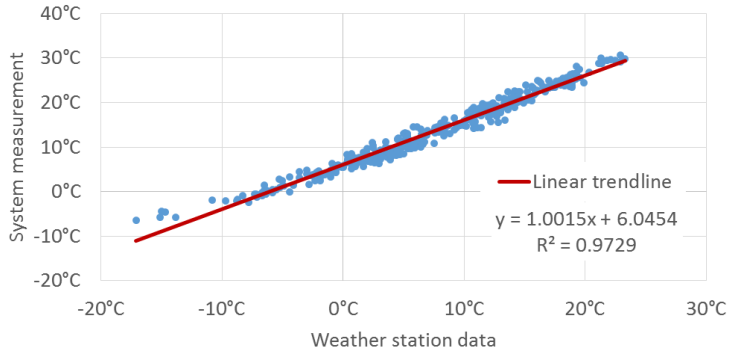

Figure 4: Comparison of daily average outdoor temperatures.

The monthly heat exchange with the boreholes is shown in Figure 5. It can be seen that the boreholes were loaded during summer and unloaded during winter, as intended. However, the amount of energy stored in summer (1 190 MWh) was a lot higher than the amount taken out during winter (734 MWh) in 2014. If this tendency continues over the next years, the ground around the boreholes will heat up making it increasingly difficult to use the BTES as heat sink in summer. However, 2014 was a very warm year with the average temperature in Oslo being almost 2°C higher in 2014 compared to the ten previous years (Bioforsk, 2015). This is a possible reason for the deviation as higher outdoor temperatures lead to decreased heating load during winter and increased cooling load during summer. Still, the energy balance should be analyzed each year to avoid operational difficulties in the future.

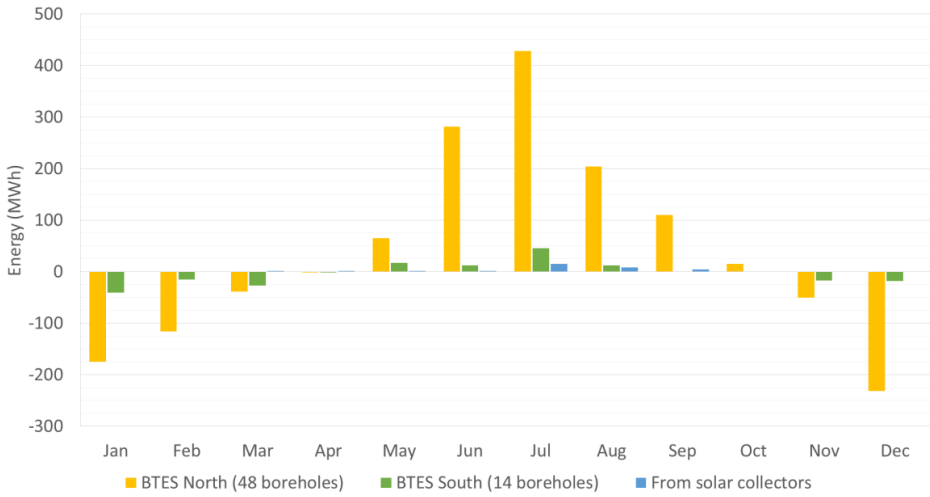

Figure 5. Monthly energy amounts for borehole storages for 2014.

The in- and outflow temperatures of the two borehole-arrays are shown in Figure 6. Gaps in the data indicate periods with no flow circulation.

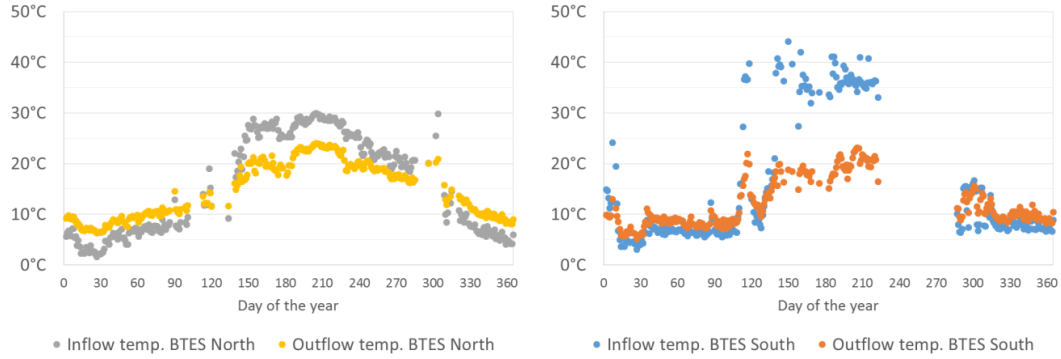

Figure 6. Daily average in- and outflow temperatures of the borehole-arrays for 2014 (gap = no flow).

The supply and return temperatures in Figure 6 confirm that the BTES were loaded during summer and unloaded during winter. However, it is difficult to identify periods of free-cooling mode. Such periods would be characterized by inflow temperatures of 10-15°C and outflow temperatures around 6°C which cannot be seen in Figure 6. This suggests that this operation mode is not used as planned.

4. IMPROVEMENT SUGGESTIONS

The integrated thermal energy system operated successfully in 2014. No failures occurred and the user demands could be satisfied by the system apart from short periods where the district heating backup was active. The system COP was acceptable but could be improved with the following measures. An economic evaluation of the different options has not been performed.

4.1. Heat Pump Performance

HP 4 & 5 (see Figure 1) were two identical heat pumps in parallel that could be operated independently (a third heat pump was originally planned as backup but has not been installed). They were used for product cooling which required constant operation of at least one of the heat pumps. They are each designed for a cooling load of 87 kW (see Table 1) which shows that the predicted product cooling load was around 1 500 MWh per year. However, the actual load for 2014 was 384 MWh which is only around 25% of the predicted load. HP 4 & 5 were therefore running in part load for most of 2014 with the associated decrease in efficiency. The same holds true for HP 3 which was also designed based on the predicted product cooling load.

4.2. Solar Collectors

The solar collectors were integrated in the facade of an office-building which they supplied with heating energy directly (not shown in Figure 1). The surplus heat was sent to the BTES, the monthly amounts can be seen in Figure 5. As the solar collectors can deliver higher temperatures than the heat pumps, they could be used to lift the temperature of the DHW after it has been preheated by the heat pumps. However, office buildings have relatively low DHW demands and the other buildings were not connected so a main part of the high temperature heat was not used optimally. The surplus heat sent to the BTES played a minor role in the system in 2014.

4.3. Different Fluid for Cold Circuit

The properties of the water/ethanol mixture are worse than those of pure water in terms of performance. The higher viscosity of ethanol increases pressure drops and the lower heat capacity requires larger mass flows both leading to increased pumping power for the same heat transfer. The ethanol was added to lower the freezing point as even local freezing of the working fluid could impede the system's functionality. However, the minimum temperature in the water/ethanol circuit was 1.5°C in 2014. This means that water or at least a lower ethanol concentration mixture could be used in the circuit instead. This would reduce the parasitic losses in this circuit and increase the overall system COP.

4.4. Buffer Tank on Cold Side

Figure 7 shows the buffer tank on the cold side of the system and the flows in heating mode.

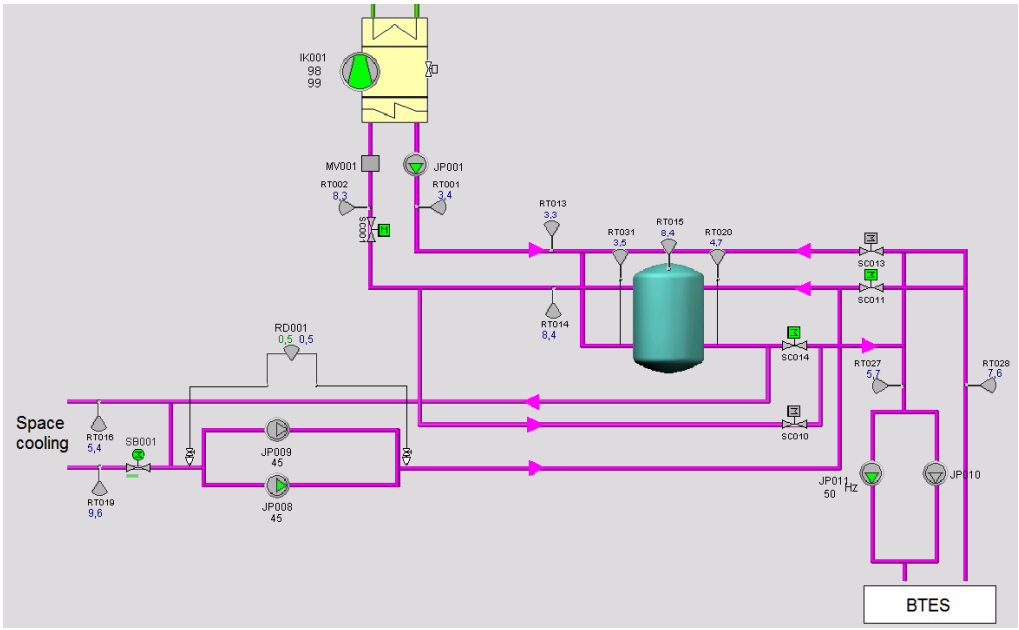

Figure 7. Detail of cold buffer tank in heating mode (green components are active).

The evaporator of HP 2 takes up heat from the water/ethanol mixture and cools it from 8.3°C to 3.4°C. It is then sent to the space cooling and BTES heat exchangers to be heated up again. On its way there, it passes through the lower (colder) end of the buffer tank where it is preheated from 3.5 to 4.7°C. This preheating reduces the amount of heat that the fluid will take up in the following heat exchangers and should thus be avoided. On the return side, after the flows from space cooling (9.6°C) and BTES (7.6°C) are joined, the fluid passes through the same tank again. It is not significantly cooled with the current flows in Figure 7, but mixing with the (usually lower) tank content is possible. This could easily be avoided by installing a separate buffer tank for supply and return flow and would reduce mixing losses.

5. CONCLUSIONS

An integrated thermal energy system was presented in this work. This energy system delivered heating and cooling energy to several buildings and employed boreholes as seasonal thermal energy storage. Operational data from 2014 showed that the BTES was successfully used to store heat during summer and recover it during winter. All heating and cooling demands could be covered, but district heating was needed as backup system during very cold periods. Also, the product cooling load was overestimated during the design phase which led to the installation of oversized heat pumps. Still, the system COP ranged from 1.7 to 3.4 which is satisfactory. However, it could be improved by replacement of the unsuitable heat pumps, better utilization of the high temperature heat from the solar collectors, installation of an extra buffer tank in the space cooling circuit, or using pure water instead of a water/ethanol mixture.

6. ACKNOWLEDGEMENTS

The authors gratefully acknowledge the support from the Research Council of Norway (INTERACT 228656 / E20) and the partners Aspelin Ramm Eiendom AS, Statkraft Varme AS, Rema 1000 Norge AS, COWI AS, Asplan Viak AS and SWECO.

7. REFERENCES

1. Bioforsk. 2015, Weather data downloaded from http://lmt.bioforsk.no, retrieved April 2015.
2. European Union. 2010, Directive 2010/31/EU of the European Parliament and of the Council of 19 May 2010 on the energy performance of buildings, *Official Journal of the European Union*, L 153: 13–35.
3. Guo, W. 2011, *Building systems' energy interaction studies*, Ph.D. Thesis, University of Arkansas, USA.
4. Heier J., Bales C., Martin V. 2015, Combining thermal energy storage with buildings – a review, *Renewable and Sustainable Energy Reviews* 42(0): 1305-1325.
5. Hesaraki A., Holmberg S., Haghighat F. 2015, Seasonal thermal energy storage with heat pumps and low temperatures in building projects—A comparative review, *Renewable and Sustainable Energy Reviews* 43(0): 1199-1213.
6. Nord N., Novakovic V., Frydenlund F. 2012, Performance estimation and documentation of an integrated energy supply solution. *Technoport Renewable Energy Research Conference*. Trondheim, Norway.
7. Pedersen L. 2007, *Load Modelling of Buildings in Mixed Energy Distribution Systems*, Ph.D. Thesis, Norwegian University of Science and Technology, Trondheim, Norway.
8. Pérez-Lombard L., Ortiz J., Pout C. 2008, A review on buildings energy consumption information, *Energy and Buildings* 40(3): 394-398.
9. Reuss M. 2015, The use of borehole thermal energy storage (BTES) systems, In: *Advances in Thermal Energy Storage Systems*, Woodhead Publishing: 117-147.

Paper II

D. Rohde, T. Andresen, and N. Nord (2016). "Interaction Between a Building Complex with an Integrated Thermal Energy System and a District Heating System." In: *Proceedings of the 12th REHVA World Congress, Aalborg, Denmark.*

Interaction Between a Building Complex with an Integrated Thermal Energy System and a District Heating System

Daniel Rohde[#1], Trond Andresen[*2], Natasa Nord[#3]

[#]*Department of Energy and Process Engineering*
Norwegian University of Science and Technology
Kolbjørn Hejes vei 1A, 7491 Trondheim, Norway

[1]daniel.rohde@ntnu.no

[3]natasa.nord@ntnu.no

[*]*SINTEF Energy Research*
Sem Sælands vei 11, 7034 Trondheim, Norway

[2]trond.andresen@sintef.no

Abstract
Integrated thermal energy systems provide heating and cooling for several commercial and residential buildings. These systems usually have both short-term and seasonal thermal energy storages. High cooling demands lead to a big amount of excess heat. This heat could be exported to a district heating system. Low temperature district heating can increase the integration of renewable and waste energy sources and may significantly contribute to the overall efficiency of future energy systems. In this study, the interaction of an integrated thermal energy system in Norway with district heating was investigated. The main parts of the energy system were heat pumps with 1 MW total cooling capacity, solar thermal collectors as well as water tanks and boreholes for thermal energy storage. It was assumed that heat from the solar collector tank could be exported to the district heating supply line, while the condenser heat from the heat pump was considered to be exported to the return line. Dynamic simulations were performed using a Modelica model of the energy system. An important result of the system simulations was the energy balance of the borehole thermal energy storage. Without heat export, the storage was charged more during summer than it was discharged during winter. This imbalance could lead to a ground temperature increase. To ensure feasible long-term operation of the energy system, the average annual ground temperature should remain constant. By exporting heat to the district heating system, borehole heat balance could be achieved and operating costs could be reduced.

Keywords - Integrated thermal energy system; District heating; Interaction; Dynamic simulation

1. Introduction

Integrated thermal energy systems provide heating and cooling for several commercial and residential buildings. In this study, the interaction of an integrated thermal energy system in Norway with a district heating (DH)

system was investigated. Due to high DH temperatures, the real system can only import heat. However, a technology shift towards low temperature DH systems is ongoing. This will lead to an increased integration of renewable and waste energy sources and may significantly contribute to the overall efficiency of future sustainable energy systems [1-3]. Therefore, a case study was defined with lower DH temperatures to investigate the possibility for export of excess heat from the building complex to the DH system.

2. Case Study

The basis for this case study was a thermal energy system that was integrated into a building complex of different building types with a total area of 38 000 m². The main parts of the energy system were heat pumps with 1 MW total cooling capacity, flat plate solar thermal collectors as well as water tanks and boreholes for thermal energy storage. The system is described in detail in [4] and a simplified version was modeled in Dymola/Modelica. The main system modifications and all investigated cases are explained in this chapter.

Hourly energy demand data from 2015 was used as input for the simulation model and the resulting monthly demands are shown in Figure 1. The demand for domestic hot water (DHW) varied significantly between 2014 and 2015 and so an average was used to give a representative demand profile for the building complex.

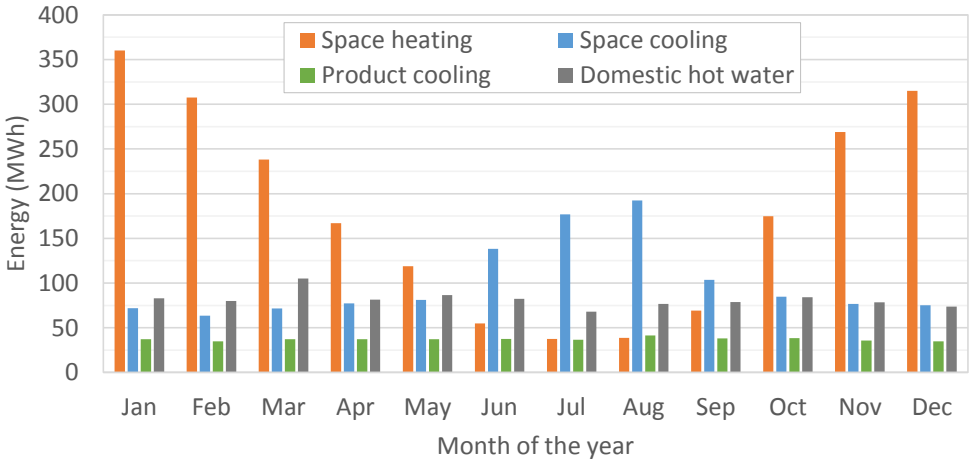

Figure 1: Monthly heating and cooling demands for the case study

To investigate the effects of changes in average annual temperatures, a warmer and a colder year were also simulated. For the warmer year, a temperature offset of +1°C, a radiation factor of 1.05, a space heating demand factor of 0.95 and a space cooling demand factor of 1.05 were used. Accordingly, a temperature offset of -1°C, a radiation factor of 0.95, a space heating demand factor of 1.05 and a space cooling demand factor of 0.95 were

implemented for the colder year. The average, warmer, and colder year simulations were respectively defined as Cases 1, 2, and 3, as shown in Table 1. The annual energy balance of the system's borehole thermal energy storage (BTES) was an important result for these cases.

Table 1: Case overview

Case	Year	Solar Collectors	Heat Export
1	Average	140	No export
2	Warmer	140	No export
3	Colder	140	No export
4	Average	140	To DH return line
5	Average	500	To DH supply and return line

The real system had five heat pumps connected in parallel and series. The condenser heat from all of them was led to the same secondary fluid loop. To simplify the control of the system, the heat pumps were modeled as one large heat pump. The system was connected to the local DH system to import heat for DHW heating and as backup for space heating. The outdoor temperature compensation curve is given in Figure 2.

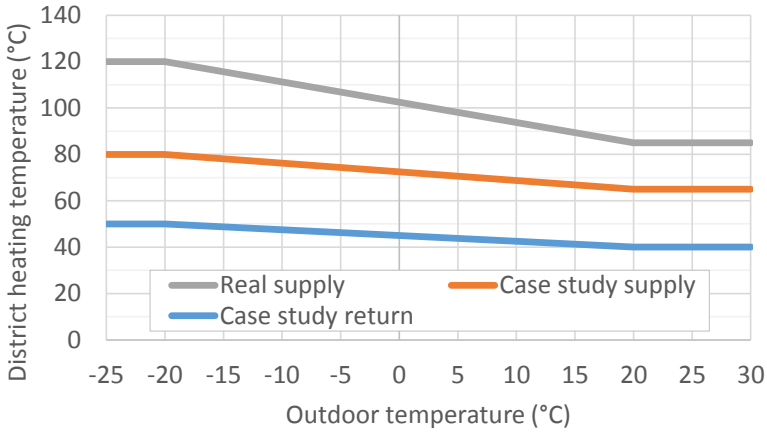

Figure 2: DH outdoor temperature compensation curves

The temperatures of the real DH system were too high to export heat economically even during summer. Therefore, a DH case was defined with lower supply and return temperature as shown in Figure 2. These temperatures represent a third generation system ("Scandinavian district heating technology" [2]) and were chosen because they satisfied the system's temperature requirement for DHW heating (>60°C), but also enabled export of excess heat from the building complex to the DH system.

To investigate export of excess heat, Cases 4 and 5 (see Table 1) were defined. For Case 4, heat export from the heat pump condenser tank to the DH

return line was enabled. For Case 5, heat export from the solar collector tank to the DH supply line was enabled. The amount of exported heat was controlled to yield a balanced BTES at the end of the year for both cases.

The real system had 140 solar collectors for space heating and DHW heating. However, this number was chosen based on the demand of only one single building and not the whole building complex. They were also only used within that building and thus showed little effect on the overall system performance. Therefore, the collector loop was connected to all buildings for Cases 4 and 5. Also, the number of solar collectors was increased to 500 and the volume of the collector tank was increased from 2 m^3 to 10 m^3 for Case 5.

3. Model Description

All simulation models were developed using the open modeling language Modelica with the *Thermal* library [5] as basis for component and system development. Dymola was used as simulation environment and the main component models and the control system are described here.

3.1. Component Models

The heat exchangers were modelled as an array of thermally connected pipes in counterflow configuration, where the local heat balance was solved in each element. A discretization of eight was found to give good agreement with logarithmic mean temperature calculations at reasonable simulation times. The heat transfer coefficient was chosen to be constant and equal in all array segments.

The BTES was modelled as an array of vertical segments. Each segment consisted of several thermal resistances and capacities. The resistances and capacities representing the ground heat exchanger were modelled according to [6]. The surrounding ground was modelled as an array of cylindrical shells with capacities and heat transfer coefficients corresponding to the geometry of each shell element according to [7].

The interaction between the boreholes and heat transfer to the ambient were neglected in the model. The horizontal ground discretization was found to be more important than the vertical discretization. Discretization values of sixteen (horizontal) and eight (vertical) were found to give good agreement with higher values at significantly reduced simulation times.

The heat pump was a key component and it was therefore desirable to include a model that realistically predicted performance and behavior under variable operating conditions. As an efficient means to introduce realistic off-design performance, the in-house circuit simulation and optimization tool *CSIM* [8] was used to generate a polynomial function to include in the Modelica model. *CSIM* has been developed by SINTEF and the Norwegian University of Science and Technology over the last decades.

The heat pump's coefficient of performance (COP) was defined as function of the scaled condenser heat load Q_s and the scaled temperature lift

ΔT_s. These parameters were considered key factors for heat pump performance and are defined in (1) and (2). The temperature lift ΔT was defined as the difference between average secondary fluid temperature in the condenser and average secondary fluid temperature in the evaporator. The nominal values used for scaling were parameters from the heat pumps design point.

$$Q\_s = Q\_actual/Q\_nominal \quad (1)$$

$$\Delta T\_s = \Delta T\_actual/\Delta T\_nominal \quad (2)$$

$$COP = COP\_nominal \cdot (a + b \cdot Q\_s + c \cdot \Delta T\_s + d \cdot Q\_s \cdot \Delta T\_s) \quad (3)$$

More than 50 detailed simulations were performed with *CSIM* to map COP for conditions in the targeted operating range. A regression analysis was performed to find the coefficients for the polynomial function (3) and the resulting coefficients can be seen in Table 2.

Table 2: Parameters for polynomial heat pump model

Coefficient	a	b	c	d
Value	2.2451	-0.5868	-0.9228	0.2647

The resulting expression was implemented in the Modelica model and predicted the COP to within ±5% compared to the detailed simulation results from *CSIM*.

The solar collectors were modelled as fluid pipes which were heated by solar radiation. To account for heat transfer with the ambient, a constant value for thermal conductance from fluid to ambient was included. This value was chosen based on manufacturer specifications. The average error for the collector efficiency under different operating conditions was 2% with the parameters shown in Table 3.

Table 3: Solar collector model parameters (single collector)

Parameter	**Value**	**Unit**
Effective surface area	1.9	m²
Optical efficiency	0.773	-
Fluid filling	1.2	kg
Thermal conductance (fluid to ambient)	8.6	W/K

The solar radiation was not measured on site, so data from the software Meteonorm was used as input for the simulations.

The thermal storage tanks were modeled to be perfectly mixed, i.e. without stratification. The thermal conductance from fluid to ambient was chosen to yield a capacity loss of 1% during a twelve hour period which is feasible according to [9].

3.2. Control System

A key part of the system modeling was the control system. Simple pump models were used to control the fluid flows between the components. The signals for activation of the pumps and the setpoints of their controllers were received from control blocks.

The system had two main modes of operation: Heating mode and cooling mode. The temperatures in the tanks after the heat pump's condenser and evaporator were used to define the mode of operation. In heating mode, the condenser tank was kept at a constant temperature (50°C) by the heat pump's PI controller and the evaporator tank and the BTES were used as heat sources. When the cooling load increased, the temperature in the evaporator tank also increased until the BTES was no longer needed as heat source. If the temperature in the tank reached a certain limit, the system switched to cooling mode, keeping the evaporator tank at a constant temperature (5°C). The condenser tank and the BTES were then used as heat sinks. Similarly, increasing heating loads led to a decreased temperature in the condenser tank and at a certain limit, the system switched to heating mode. The parameters for the heat pump's PI controller were chosen according to rules from [10] and blocks from the *StateGraph* library [11] were used to switch between modes.

The solar collector loop included two heat exchangers. The first one enabled heat transfer to the collector tank while the second one enabled heat transfer to the BTES. The control system was designed to transfer as much heat as possible to the collector tank at high temperature and only store low grade heat in the BTES. The fluid in the collector tank was then used for lifting the DHW temperature or heat export to the DH supply line, depending on the case. The DHW demand was prioritized to reduce the amount of imported heat. The control block settings had a significant influence on the total amount of accumulated solar heat and thus also on the energy balance of the system, especially for the case with increased number of collectors.

4. Results and Discussion

4.1. Energy Flows in the Integrated Thermal Energy System

For Case 1 (see Table 1), the BTES was charged with 799 MWh during summer and 602 MWh were discharged during winter. This imbalance of 197 MWh corresponds to an average ground temperature increase of almost 1°C. To ensure feasible long-term operation of the energy system, the average annual ground temperature should remain constant. For the simulated warmer year (Case 2), the imbalance was 350 MWh and 47 MWh for the colder year (Case 3). This clearly showed a potential for heat export.

Cases 1, 4 and 5 had the same weather and demand inputs and their total accumulated energies are shown in Figure 3. It can be seen that the heat pump is by far the most significant component, because it used the highest amount of energy.

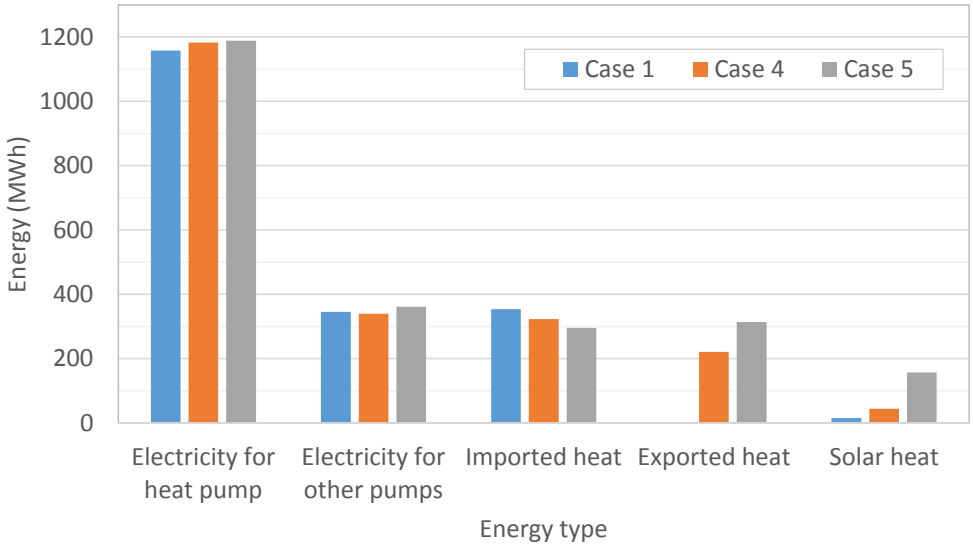

Figure 3: Total energy amounts for cases 1, 4, and 5

The electricity use of the system increased for the heat export Cases (4 and 5) compared to Case 1. At the same time, less heat needed to be imported due to better utilization of the solar collectors. As expected, more heat could be exported when the number of solar collectors was increased. Monthly values for the interaction with the DH system are shown in Figure 4.

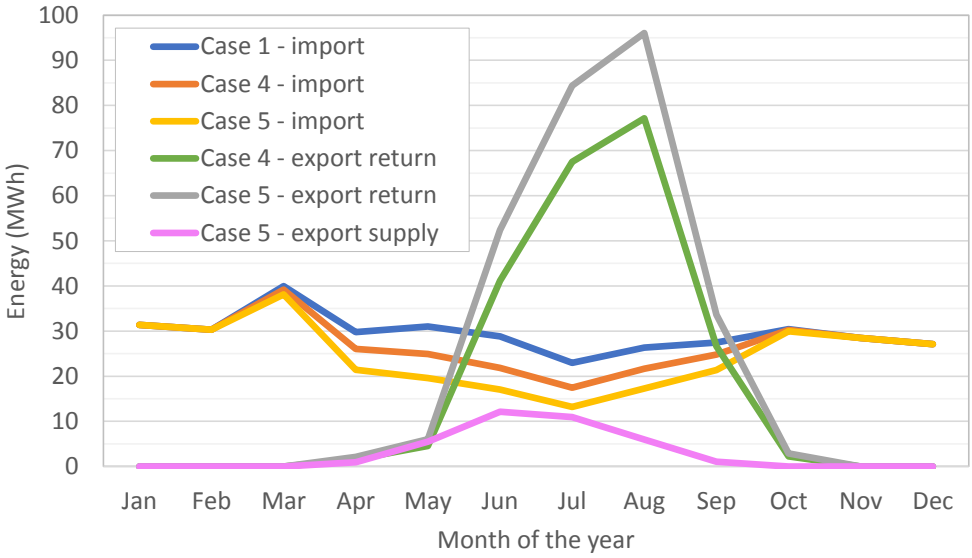

Figure 4: Monthly imported and exported heat for Cases 1, 4, and 5

It can be seen from Figure 4 that no heat was exported during winter because the system was in heating mode and did not have any excess heat

available. Heat import could not be avoided during summer even for Case 5. This was mainly due to the typical demand peak for DHW in the morning. This can be seen in Figure 5 which shows daily average profiles for a year.

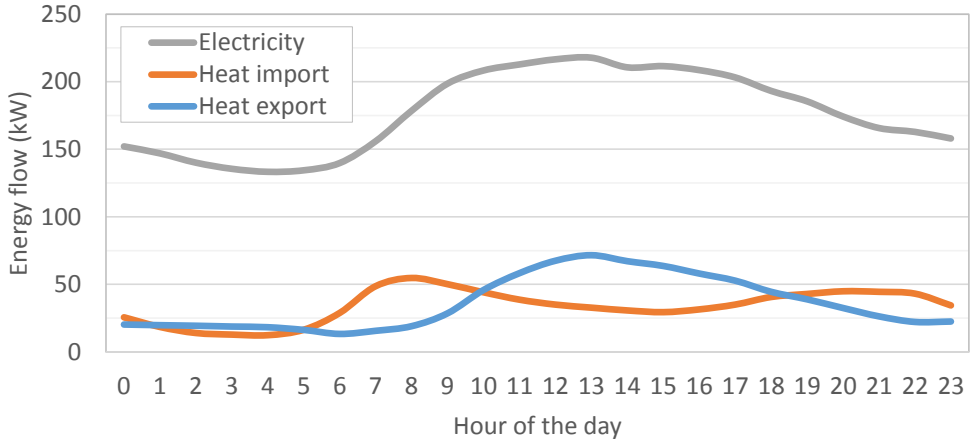

Figure 5: Daily average energy flows for different energy types over a year (Case 5)

It is not reasonable to reduce this import peak by storing high temperature solar heat during the night as this would lead to unnecessarily high losses. This can also be seen in Figure 6.

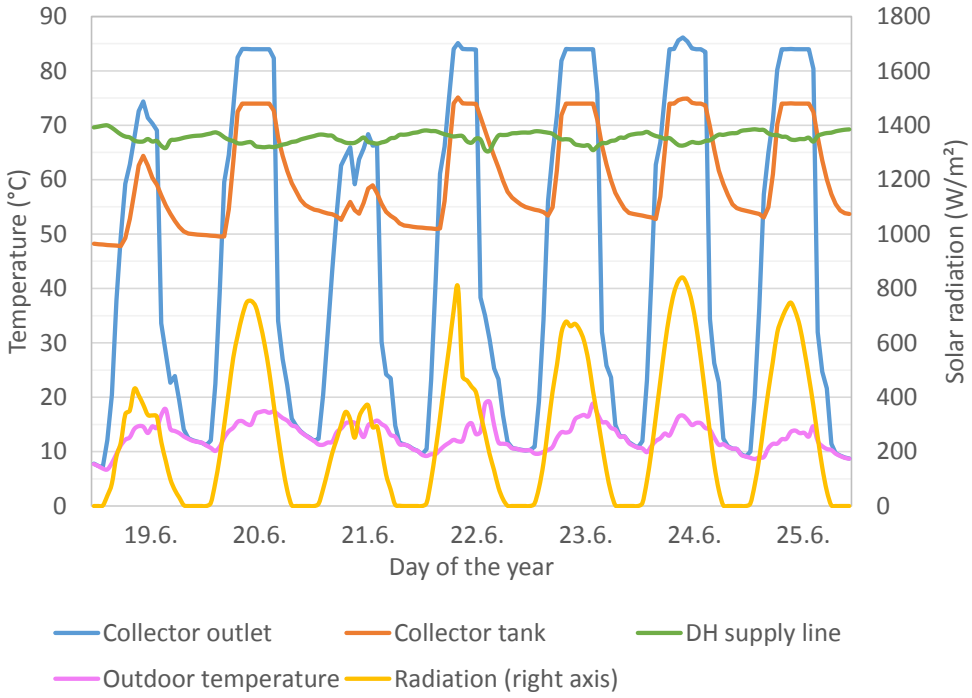

Figure 6: Solar collector loop details for one week (Case 5)

Figure 6 shows the temperatures of the collector tank loop for the period of one week. During the night, the collectors cool down to the outdoor temperature level and the temperature in the storage tank also decreases.

Heat export to the supply line was only possible when the temperature difference between collector tank and DH supply line exceeded the set threshold. Figure 6 shows that this was only the case during a few hours on clear summer days.

4.2. Cost Analysis

To compare the total operating costs of all the cases, price factors for the different energy types in Figure 3 were defined and are shown in Table 4.

Table 4: Price factors for different energy types

Energy Type	Electricity	DH import	DH export to supply	DH export to return
Price Factor	1.00	0.95	0.80	0.40

With these factors, the total operating costs compared to Case 1 were calculated and the results are shown in Table 5.

Table 5: Total operating costs compared to Case 1

Case	1	2	3	4	5
Operating costs	100 %	97.5 %	103 %	94.6 %	91.8 %

Energy prices for both electricity and DH vary significantly over time. However, this was not treated in the current study, due to the complexity of pricing mechanisms [12]. Therefore, the current results can only give an indication of the real costs and advantages of heat export. They showed that the influence of changed weather and demands (Cases 1 to 3) is rather small if the BTES is not balanced. However, depending on the heat losses from the storage (e.g. from ground water flow), this may not be feasible in the long run because the storage could overheat. Also, the operating costs for the heat export cases (4 and 5) were lower than for Case 1 so the only disadvantage are the higher installation costs. These are expected to be especially high for Case 5 which has the lowest operating costs. An economic analysis with more detailed pricing schemes is thus required to make recommendations for an improved system operation.

5. Conclusions

The interaction of a building complex with an integrated thermal energy system and a district heating system was analyzed. It was shown that the seasonal thermal energy storage could be balanced by exporting heat if the DH temperatures were lower than they are for the real system. Dynamic

simulations were performed and the results showed that the total operating costs decreased when heat was exported. A further decrease in operation cost could be achieved by increasing the number of solar collectors. Installation costs for heat export and increased collectors were not considered.

Acknowledgment

The authors gratefully acknowledge the support from the Research Council of Norway (INTERACT 228656 / E20) and the partners Aspelin Ramm Eiendom AS, Statkraft Varme AS, Rema 1000 Norge AS, COWI AS, Asplan Viak AS and SWECO.

References

[1] D. Connolly, H. Lund, B.V. Mathiesen, S. Werner, B. Möller, U. Persson, T. Boermans, D. Trier, P.A. Østergaard, and S. Nielsen. *Heat Roadmap Europe: Combining district heating with heat savings to decarbonise the EU energy system.* Energy Policy, 2014. 65: p. 475-489.

[2] H. Lund, S. Werner, R. Wiltshire, S. Svendsen, J.E. Thorsen, F. Hvelplund, and B.V. Mathiesen. *4th Generation District Heating (4GDH): Integrating smart thermal grids into future sustainable energy systems.* Energy, 2014. 68: p. 1-11.

[3] D. Schmidt, A. Kallert, M. Blesl, S. Svendsen, N. Nord, and K. Sipilä. *Low temperature district heating for future energy systems*. The 14th International Symposium on District Heating and Cooling, Stockholm, Sweden. September 7-9, 2014.

[4] D. Rohde, M. Bantle, T. Andresen, and N. Nord. *Documentation of an Integrated Thermal Energy System for a Building Complex*. 24th International Congress of Refrigeration, Yokohama, Japan. August 16-22, 2015.

[5] Modelica Association. *Modelica Libraries*. Available from: https://www.modelica.org/libraries, accessed January 2016.

[6] D. Bauer, W. Heidemann, H. Müller-Steinhagen, and H.J.G. Diersch. *Thermal resistance and capacity models for borehole heat exchangers.* International Journal of Energy Research, 2011. 35(4): p. 312-320.

[7] P. Stephan. *Chapter B1: Fundamentals of Heat Transfer*, in *VDI Heat Atlas*. Springer Berlin Heidelberg. 2010.

[8] T. Andresen. *Mathematical modeling of CO2 based heat pumping systems*. PhD Thesis, Norwegian University of Science and Technology, Trondheim, Norway. 2009.

[9] ASHRAE. *Chapter 37: Solar Energy Equipment*, in *ASHRAE Handbook - Heating, Ventilating, and Air-Conditioning Systems and Equipment (SI Edition)*. American Society of Heating, Refrigerating and Air-Conditioning Engineers, Inc. 2012.

[10] S. Skogestad and C. Grimholt. *Chapter 5: The SIMC Method for Smooth PID Controller Tuning*, in *PID Control in the Third Millennium*. Springer London. 2012.

[11] M. Otter, K.-E. Årzén, and I. Dressler. *StateGraph-A Modelica Library for Hierarchical State Machines*. 4th International Modelica Conference, Hamburg, Germany. March 7-8, 2005.

[12] H. Li, Q. Sun, Q. Zhang, and F. Wallin. *A review of the pricing mechanisms for district heating systems.* Renewable and Sustainable Energy Reviews, 2015. 42: p. 56-65.

Paper III

H. Kauko, K. H. Kvalsvik, D. Rohde, A. Hafner, and N. Nord (2017). "Dynamic modelling of local low-temperature heating grids: A case study for Norway." *Energy* 139, pp. 289–297. DOI: 10.1016/j.energy.2017.07.086.

Energy 139 (2017) 289–297

Contents lists available at ScienceDirect

Energy

journal homepage: www.elsevier.com/locate/energy

Dynamic modelling of local low-temperature heating grids: A case study for Norway

Hanne Kauko [a, *], Karoline Husevåg Kvalsvik [a], Daniel Rohde [b], Armin Hafner [b], Natasa Nord [b]

[a] SINTEF Energy Research, Kolbjørn Hejes vei 1B, Trondheim 7491, Norway
[b] Department of Energy and Process Engineering, Norwegian University of Science and Technology (NTNU), Kolbjørn Hejes vei 1B, Trondheim 7491, Norway

ARTICLE INFO

Article history:
Received 1 November 2016
Received in revised form
12 May 2017
Accepted 12 July 2017
Available online 29 July 2017

Keywords:
Low-temperature district heating
Thermal system modelling
Energy planning

ABSTRACT

Today's district heating (DH) networks in Norway are 2nd and 3rd generation systems, with supply temperatures ranging from 80 to 120 °C. In new developments, it is desirable to shift to 4th generation, low-temperature district heating (LTHD) in order to reduce the heat losses and enable better utilization of renewable and waste heat sources. A local LTDH grid for a new development planned in Trondheim, Norway, has been modelled in the dynamic simulation program Dymola in order to study the effect of lowered supply temperatures to heat losses and circulation pump energy use. Different scenarios with supply temperatures ranging from 55 to 95 °C, lowered return temperature as well as peak shaving were analyzed. Real DH use data for buildings in Trondheim were employed. The environmental impact in terms of the total produced CO_2 equivalent emissions was estimated for each scenario, assuming a heat production mix corresponding to that of the local DH provider. The results showed that by lowering the supply temperature to 55 °C, the heat losses could be reduced by one third. The total pump energy increased significantly with reduced supply temperature, however the pump energy was generally an order of magnitude lower than the heat losses.

1. Introduction

District heating (DH) will play an important role in the future fossil-free energy systems by allowing an increased utilization of renewable heat and waste heat sources, however, a prerequisite for this is a reduction in the distribution temperatures [1,2]. Through reduced supply temperature, DH production with renewable heat sources, such as solar thermal and heat pumps, becomes more efficient. Utilization of heat pumps in DH production becomes more beneficial with reduced supply temperatures as it enables improved coefficient of performance (COP) for the heat pumps, resulting into lower heat costs and primary energy use [3]. Reduced temperature level allows also improved utilization of low-temperature waste heat sources from buildings and industry [2]. Moreover, the distribution heat losses will be greatly reduced with lowered distribution temperatures [4,5], and shifting to cheaper piping materials is enabled [2].

Current DH networks in Norway are 2nd and 3rd generation systems, with supply temperatures ranging from 80 to 120 °C. The DH companies are nevertheless interested in lowering the temperature level to comply with the lower heat demand of modern building mass, as well as to reduce heat losses. In Denmark, low-temperature DH (LTDH) systems with supply temperatures down to 50–55 °C have already been introduced [6]. In Norway, however, the minimum temperature requirement is limited to 65 °C by legislation related to control of Legionella [7], whenever domestic hot water (DHW) preparation is required. This is still a considerable reduction considering today's temperature levels.

Due to the high investment costs related to DH systems, there is a great interest in simulation and planning software to find the most optimal solutions regarding production and distribution of heat [8]. There are many software tools available for simulation of DH systems; a comprehensive overview has been given in Ref. [9]. Optimization with respect to e.g. energy efficiency or exergy, costs and environmental impact is usually the main objective for such software [9]. For detailed physical modelling of DH systems, the dynamic simulation program Dymola using the object-oriented modelling language Modelica has been proven to be a flexible

* Corresponding author.
E-mail address: hanne.kauko@sintef.no (H. Kauko).

http://dx.doi.org/10.1016/j.energy.2017.07.086
0360-5442/

and efficient tool [5,8,10,11].

In the present study, the potential of LTDH for a green neighborhood, Brøset, planned in Trondheim, Norway, has been investigated using Dymola/Modelica. The total heat demand, heat losses and the energy demand of the circulation pump were analyzed for three different supply temperatures: 95 °C with outdoor temperature compensation, and constant supply temperatures of 65 and 55 °C. In addition, the effect of lowered return temperature and peak shaving were analyzed. In order to have realistic demand profiles, the DH demand of the building mass was modelled using real DH use data for buildings from the same region.

The objectives of this study were to perform a quantitative assessment of DH grid performance in terms of thermal and hydraulic losses in modern building areas; to demonstrate the potential savings in energy and greenhouse gas (GHG) emissions enabled through lowered distribution temperatures; as well as to validate the use of Dymola as a tool for modelling local heating grids. The central research questions are: (1) What is the impact of lowered supply temperatures on heat losses and pump energy use and (2) How do lowered distribution temperatures affect the DH-related GHG emissions for the case of Trondheim.

2. Methodology

The methodology consisted of three primary steps:

1. Collect data for DH demand profiles for modern buildings representing different building categories, located in Trondheim (results presented in a separate report [12]). Select suitable demand profiles to represent the building stock at Brøset.
2. Create a model in Dymola for the local heating network, including the buildings, piping network and a heat supply plant.
3. Simulate different scenarios with various supply temperature levels in order to study the feasibility of a LTDH network from an energetic and environmental perspective.

These steps are described in more detail in the following.

2.1. The building stock

The investigated building area was a new neighborhood, Brøset, which is planned to be built in Trondheim, Norway. The building types, number of buildings in each category and the total building area are given in Table 1. The area was of interested because the local DH company will have to provide a solution for heat supply for this area in the future. Furthermore, the area will include several types of buildings as shown in Table 1, and it was interesting to analyze the heat supply system for an area with such a heterogeneous building stock. Several protected historical buildings are present in the area as well (main building, psychiatric hospital and another smaller building, see Table 1). The total area of the neighborhood was 344 000 m^2.

Table 1
The modelled building stock.

Building type	Number	Area [m^2]	Share
Apartment block	18	140 898	75%
Nursery	3	4400	2%
School	1	6000	3%
Nursing home	1	12 600	7%
Culture building	1	4000	2%
Sports hall	1	10 000	5%
Main building	1	5850	3%
Psychiatric hospital	1	3700	2%
Other historical buildings	1	300	0.2%
Total	**28**	**185 748**	**100%**

The DH demand of the buildings was modelled using real DH use data from existing buildings, with the building type and standard matching with the buildings to be built as well as possible. For apartment blocks for instance, DH use data from apartment blocks built according to the Norwegian passive house standard were used [13], as this is the newest building standard and is on its way to become the national building code. The data included the total heating demand, i.e., both space heating and DHW preparation. The duration curves for each building type are shown in Fig. 1. The motivation to use existing data was to be able to model the simultaneity of heat demand peaks throughout a day and the year as realistically as possible.

Fig. 2 presents the total hourly DH demand for the buildings in Brøset together with the outdoor temperature for 2013. Year 2013 was chosen for the study, as this year had on average normal temperature levels, seen from a statistical perspective. This year was characterized by very low temperatures during the first months of the year, reflected in a high peak DH demand (4800 kW). The load characteristic of the area can be described by the coincidence factor S, defined as

$$S = \frac{P_{max,tot}}{\sum_i P_{max,i}} \quad (1)$$

where $P_{max,tot}$ is the maximum total load for all the buildings in the area, and $P_{max,i}$ is the maximum load for an individual building. The coincidence factor was 0.93 for the modelled building stock based on real DH use data. This indicates a very high simultaneity for the peak heating demands, resulting from a high share of apartment buildings with similar load profiles.

2.2. Modelling approach

The modelling was carried out using the dynamic simulation program Dymola, version 2017, utilizing a component oriented physical modelling approach supported by the Modelica modelling language [14] and the TIL thermal component library [15]. With this approach, all the created components, such as pipes and buildings, represent real physical parts in the system, and can be re-used in

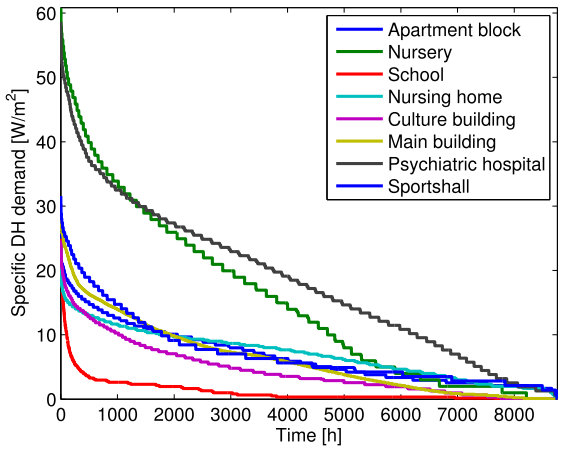

Fig. 1. Duration curves for DH demand for the different building types in the modelled neighborhood.

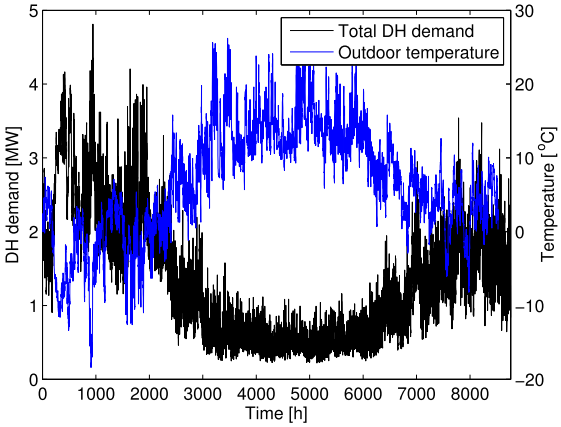

Fig. 2. The total hourly DH demand for the buildings in Brøset and ambient temperature in Trondheim in 2013.

different settings. Both text-based and graphical user interfaces are included in Dymola.

Being a dynamic simulation program implies that the simulated variables are obtained as a function of time for each component. Variables do not need to have explicit expressions; the Modelica code is transformed into efficient simulation code by Dymola using symbolic manipulation. Several numerical solvers are included in Dymola and the standard solver, DASSL, was used for this study.

The modelled network included the building stock, pipe network, and a heat supply plant delivering heat at the desired temperature level and the required pressure. These components are described in more detail below, and an outline of the network model in Dymola is shown in Fig. 3. The chosen modelling approach ensured that the time delay between the different grid elements, as well as the mixing of flow from different return lines with different temperatures was included in the system model. This allowed the thermal storage capacity of the network to be simulated realistically. It further allowed realistic regulation using PI-controller blocks, which led to the controlled variables to deviate slightly from the set-point values.

2.2.1. Building models

In the modelled network, the building models represent the customer substations. The model was simplified such that subareas consisting of several buildings of the same type were modelled as single large buildings. Each building model (substation) controls its mass flow rate and heat supply from the heat grid based on the DH demand taken as input and the DH supply temperature, which is continuously measured. The mass flow rate is controlled by a valve coupled to a PI-controller. The heat exchange takes place in a simple pipe model with a heat transfer rate based on the DH demand data. This approach was chosen because the objective was to study the effects of lower distribution temperatures on the primary side, that is, as seen from the perspective of the DH supplier. The effects on the secondary side were not of interest in this study, and were not modelled. This resulted in a more simple model and thereby faster simulations, and no assumptions considering the temperature levels or control of space heating and DHW preparation at the customers were needed. The approach did however make the return temperatures more equal for the different buildings than if heat exchangers had been used, and also made the return temperature a function of inlet temperature alone, i.e., independent of mass flow.

2.2.2. The network

The pipe models forming the network included hydraulic and heat losses. This section presents the approach taken for modelling these losses, as well as for dimensioning the pipes.

2.2.2.1. Pressure loss and dimensioning of the pipes. To model the hydraulic losses in the pipes, an approach similar to [16] was adopted. The pressure drop was calculated using the basic equation

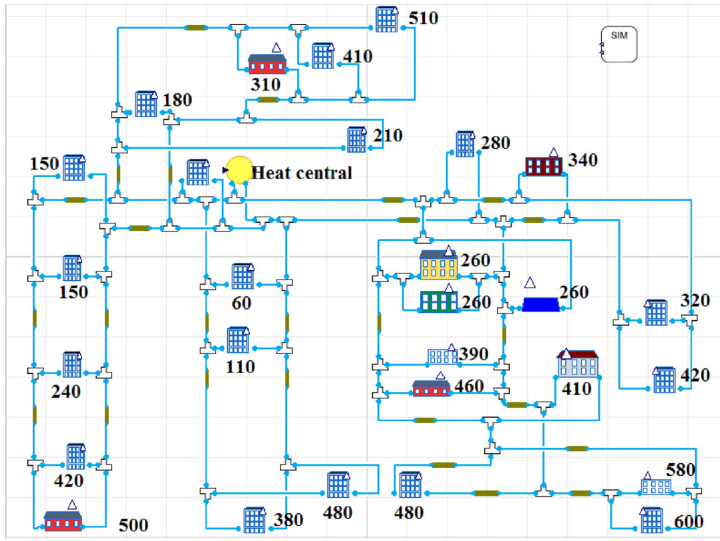

Fig. 3. The modelled building area in Dymola, including different building types and a heat supply plant. Approximate distances from the heat supply plant are given in meters. The building closest to the heat supply plant was co-located with the plant. The brown segments represent the pipe models. (For interpretation of the references to colour in this figure legend, the reader is referred to the web version of this article.)

for fluid inside a circular channel, i.e. the Darcy-Weisbach equation [17]:

$$\Delta p = f \cdot \frac{\rho v^2}{2D} L = f \cdot \frac{8\dot{m}^2}{\pi^2 D^5 \rho} L = R \cdot L \tag{2}$$

where D is the pipe diameter, L the length of the pipe segment, ρ the water density, v the flow velocity, and f is the friction factor. The piping distances were approximated using the building plan, as shown in Fig. 3. For the friction factor, the following expression was used, assuming smooth pipes [18]:

$$\frac{1}{\sqrt{f}} = -2.0 \log_{10}\left(\frac{2.51}{\sqrt{f}Re}\right) \tag{3}$$

The friction factor was assumed to be constant in the simulations, however Eq. (3) was needed for finding an expression for pipe diameter as a function of maximum mass flow (see below). The maximum pressure drop per unit length was set to $R = \Delta p/L = 150$ Pa/m.

The pipes in the heating grid were dimensioned based on the maximum mass flow for each segment. An expression for the diameter as a function of maximum mass flow was hence needed. This was done as follows:

1. Choose an arbitrary mass flow rate in relevant range
2. Assume maximum pressure drop, $\Delta p/L = 150$ Pa/m
3. Estimate the diameter such that Eqs. (2) and (3) are valid

Using this procedure, the pipe diameter was calculated for different values of mass flow rate. Thereafter, an empirical equation for the diameter as a function of maximum mass flow rate, $\dot{m}_{max}$, was obtained by least squares fitting, as shown in Fig. 4. The resulting equation was

$$D = 0.0379 \cdot \dot{m}_{max}^{0.37}. \tag{4}$$

Once the expression for diameter as a function of mass flow rate had been obtained, the pipe diameters for each segment could be easily calculated. The maximum mass flow is determined by the (maximum) heat demand and the corresponding supply and return temperatures, while the pipe diameter has a negligible effect on the mass flow. This was verified by simulations. The values for $\dot{m}_{max}$ could thus be found by running a simulation for one year assuming uniform pipe diameters. Based on the obtained values for $\dot{m}_{max}$, ideal diameters were calculated using Eq. (4). Realistic pipe diameters were then chosen based on values from Ref. [19], always rounding up such that $R \leq 150$ Pa/m was fulfilled for each pipe. The pipe model was discretizised in three pipe cells in the direction of the flow.

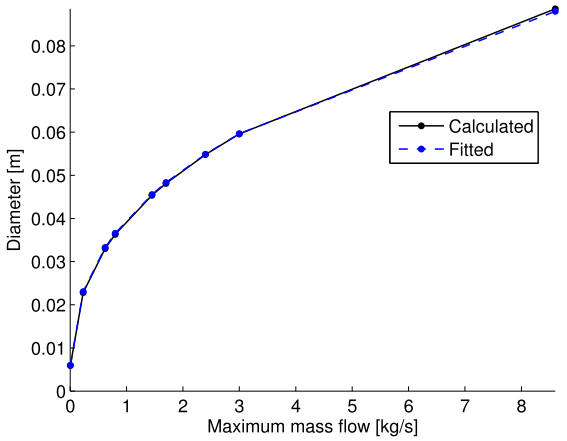

Fig. 4. Pipe diameter as a function of maximum mass flow: calculated assuming maximum pressure drop and using Eqs. (2) and (3), and fitted using Eq. (4).

2.2.2.2. Heat loss. In the present model, the supply and return lines were modelled as two separate pipes buried underground. Conduction heat transfer was found to be the dominating heat loss mechanism, with thickness and thermal conductivity of the insulation as the determining factors. Convection heat transfer from the water to the pipe surface as well as the conduction through the pipe wall were included first, however these were found to have negligible effect. This was also concluded in Ref. [20]. Convection heat transfer was additionally computationally heavy to calculate. The heat loss could therefore be calculated as:

$$\dot{Q}_{loss} = \frac{2L\pi\lambda_{ins}\left(T_{water} - T_{ground}\right)}{\ln\left(\frac{2s_{ins}+D}{D}\right)} \tag{5}$$

where λ_{ins} is the thermal conductivity, set to 0.022 W/(mK) [19], and s_{ins} is the insulation thickness. Values for s_{ins}, corresponding to the pipe diameter, were similarly found from Ref. [19]. The ground temperature T_{ground} was assumed to be constant (5 °C) in the calculations. A more complex heat loss model, including the effect of varying ground temperature and a temperature dependent thermal conductivity is discussed in Section 4.

As the supply and return lines are often placed together, heat can leak from the supply to the return line. This increases the heat losses in the supply line, yet reducing the overall losses as part of the heat lost from the supply line is transferred to the return line. The thermal interaction between the supply and return lines decreases with increasing distance between the pipes. In the present study, this distance was assumed to be large enough (> 20cm [21]), such that the thermal interaction between supply and return pipes could be neglected.

2.2.3. Heat supply plant

The heat supply plant ensures that heat at the desired supply temperature level and the required pressure difference and mass flow rate is delivered, depending on the outdoor temperature. The heat supply plant contains a circulation pump with a constant efficiency of 40%, and the pump is controlled by a PI-controller to achieve the required pressure lift. A pump model with an efficiency dependent on mass flow was tested, however this made the simulations slower, and the effect on the total pump energy use was small. An efficiency of 40% is somewhat lower than the average efficiency of new commercial pumps, but should correspond to an average efficiency of existing, older pumps. To be able to supply heat to the entire network, the PI-controller for the pump requires the signal of the lowest pressure difference in the system, corresponding to the building furthest away, as an input. The minimum pressure difference in the system was set to 70 kPa, as this is the value guaranteed by the local DH supplier in Trondheim. Customers located close to the central receive a much higher pressure difference than this, and this extra pressure is handled by the control valve.

2.3. Simulations

Three supply temperature levels were considered: 95, 65 and

55 °C. 95 °C represents the current practice, whereas 65 °C is considered as a potential future temperature level, considering the Norwegian legislation; and 55 °C was investigated as this represents an ultimate goal for the LTDH systems. For the highest temperature level, the supply temperature was outdoor temperature compensated according to the present practice of the local DH operator: assuming a supply temperature of 95 °C at outdoor temperatures of −20 °C and lower, and a temperature of 70 °C at +15 °C and higher, and a linear decrease in between the two limits. For 65 and 55 °C, constant supply temperatures were applied throughout the year.

To be able to calculate the mass flow set-point for each building, the desired return temperature level had to be defined. According to the local DH provider, existing networks in Denmark have supply/return temperature limits of approximately 90/45 °C and 50/25 °C. The required mass flow was calculated using these limits for return temperature, and assuming a linear relationship between them. A valve controlled the mass flow to achieve the desired return temperature, given the known heat demand and inlet temperature. As the controller is not perfect, the actual, regulated mass flow resulted in some deviations from the targeted values in the return temperature.

For the high-temperature case, a scenario assuming return temperatures 7 K lower than the given limits was additionally included in order to study how lower return temperature affects the circulation pump energy, and the heat losses. The different simulated scenarios are shown in Table 2.

Lower supply temperature will result in a lower temperature drop at the customer, and thereby a higher mass flow rate is needed to cover the heat demand. This will increase the pressure drop in the pipes beyond the allowable limit of 150 Pa/m and accordingly the pump power. Therefore, for the case with a supply temperature of 55 °C, a case assuming 50% bigger pipe diameters was simulated as well, yielding a total pump power similar to that of the 95 °C case.

Peak shaving is a relevant measure to reduce the required installed heat capacity and the demand for peak heating devices, which often operate with fossil fuels, having high operation costs and a negative environmental impact. In practice, this can be implemented by using thermal storage, such as hot water tanks, together with intelligent control systems to predict peak heating periods and to distribute the load over the preceding hours [10]. In our model, peak shaving was implemented in the input heat demand data for each building type such that heating demands exceeding 80% of the annual peak heating demand were distributed to five hours preceding the high-demand period. This measure had however hardly any impact on the total heat losses or the pump energy, and peak shaving was hence implemented only for the highest supply temperature case. No thermal losses from the thermal storages were accounted for, as the aim was only to estimate the potential savings while avoiding excessive computation times.

Table 2
The different simulated scenarios and their supply (T_{supply}) and return (T_{return}) temperatures.

Case	T_{supply} [°C]	T_{return} [°C]	Comments
95	95–70	47.5–35.0	–
65	65	32.5	–
55	55	27.5	–
55P	55	27.5	Pipe diameters 50% larger
LR	95–70	40.5–28.0	Lowered return temp. (by 7 °C)
PS	95–70	47.5–35.0	Peak shaving (max. demands reduced by 20%)

2.4. Energy mix and GHG emissions

An important aspect in shifting to lower distribution temperatures is the increased possibility for utilization of renewable and waste heat sources, and hence reduction in the GHG emissions related to DH. Although alternative heat sources were not included in the model at this stage, calculation of the GHG emissions was included, based on the actual energy mix applied by the local DH provider. The heat production is divided between the different sources, depending on the heat demand. For low demands, a large central boiler operating on municipal solid waste (MSW) is the only heat source. For higher heat demands, peak heating devices, such as heat pumps and biomass, electric and oil boilers, are added such that the least polluting sources are used first. The considered heat sources are given in Table 3. The table presents the operating limits of the different sources (minimum and maximum heat demand to employ the source), as well as the associated equivalent CO_2 emissions per kWh heat produced.

In the model it was assumed that the high-temperature (95–70 °C) case would have the same total energy mix over one year as the one from the local DH supplier. The capacity limits for each heat source were set so that this assumption was valid, and these limits were assumed also to the other supply temperature levels. Each source was assumed to be able to supply a constant, limited amount of heat. Hence, the difference in equivalent CO_2 emissions for the different scenarios was based on the differences in the heat demand as seen from the heat supply plant.

3. Results

Table 4 shows the results from a simulation over one year for the different scenarios given in Table 2. Included in Table 4 are results for the total and maximum heat delivered, heat losses, and pump energy and power demand; supply pressure and mass flow; as well as the global warming potential (GWP). Both the absolute value and the relative value as compared to the baseline case with 95–70 °C supply temperature are given.

Results of the most interest are the heat losses and the pump energy use (W). Fig. 5 presents these results for each case with respect to the total heat delivered (Q_{tot}), Q_{loss}/Q_{tot} and W/Q_{tot}, as an indication of the global energy efficiency. As the pump energy was generally an order of magnitude lower than the heat losses, W/Q_{tot} was multiplied by ten in the figure. In addition, the ratio between the total pump energy use and heat losses is included in Fig. 5.

For the 55 case, the relative heat losses are 31% lower (2.9%) than for the 95 case (4.2%). The heat losses are generally low, largely owing to the small size of the heat grid: the total length of the pipeline was only 3.55 km. The linear heat demand density for the area was 3.2 MWh/year per grid meter. Furthermore, the annual average supply temperature for the 95 case was relatively low, 76 °C, due to a relatively mild winter and a long period during the summer with a nearly constant supply temperature of 70 °C. The obtained heat loss per meter grid (trench) was 16 W for the 95 case, while normal values are 10–30 W/m for the somewhat higher supply temperatures usually applied. The heat losses were thereby realistic and the applied heat loss model could be considered reliable.

The relative pump energy use for the 55 case was 0.41%, which is 109% higher than for the 95 case (0.20%). The total pump energy use was the lowest, 0.31% of the total heat delivered, for the low return case. This was expectable, since the heat demand was the same, but temperature difference at the customers is higher, yielding a lower mass flow rate.

Fig. 6 shows the total pump energy use plotted over the total heat loss for the different cases. For the 55P case with 50% larger

Table 3
The energy mix considered, including the operating limits of the different sources (minimum and maximum heat demand to employ the source), and the equivalent CO_2 emissions per kWh heat produced. The maximum limit for the oil boiler was not known.

Heat source	Lower operation limit [kW]	Upper operation limit [kW]	Emissions [g CO_2-eqv./kWh]
Waste (MSW)	0	1671	11.2
Bio-boiler	1671	1805	19.8
Biogas	1805	1823	39.6
Heat pump	1823	1853	36.7
Electricity	1853	2133	110.0
LNG	2133	2173	243.0
LPG	2173	3072	274.0
Oil	3072	–	292.0

Table 4
Simulation results over one year for the different cases: The total annual heat delivered (Q_{tot}), heat losses (Q_{loss}) and pump energy (W); maximum heat delivered (P_{max}) and pump power ($\dot{W}_{max}$); maximum and average mass flow ($\dot{m}_{max}$ and $\dot{m}_{ave}$); maximum and average supply pressure ($p_{supply,max}$ and $p_{supply,ave}$); and the GWP as total CO_2 emission equivalents. The results are given as the total amount over a year, and as a percentage compared to the baseline case (95).

Case name/Variable	95		65		55		55P		LR		PS	
	Tot.	%	Tot.	%	Tot.	%	Tot.	%	Tot.	%	Tot.	%
Q_{tot} [GWh]	11.9	100	11.8	99.3	11.7	98.6	11.8	99.0	11.8	99.7	11.9	100
Q_{loss} [MWh]	494	100	414	83.6	342	69.2	381	76.8	450	90.8	494	100
W [MWh]	23.3	100	35.0	150	48.6	209	23.3	100	15.7	67.3	23.2	99.9
P_{max} [MW]	4.6	100	4.6	99.9	4.6	99.5	4.6	100	4.6	100	4.1	88.1
$\dot{W}_{max}$ [kW]	19.7	100	44.0	223	66.5	337	19.5	98.9	11.6	58.8	16.5	83.6
$\dot{m}_{max}$ [kg/s]	25.5	100	34.7	134	40.3	158	40.3	158	20.6	80.7	23.5	92.2
$\dot{m}_{ave}$ [kg/s]	8.9	100	10.7	120	12.4	139	12.4	140	7.2	80.3	8.9	100
$p_{supply,max}$ [bar]	4.1	100	6.1	149	7.6	187	2.9	72.2	3.2	79.7	3.8	93.5
$p_{supply,ave}$ [bar]	2.1	100	2.3	110	2.5	120	1.9	88.7	2.0	93.2	2.1	100
GWP [tons CO_2-eqv.]	432	100	423	98.0	418	96.8	421	97.5	428	99.2	432	100

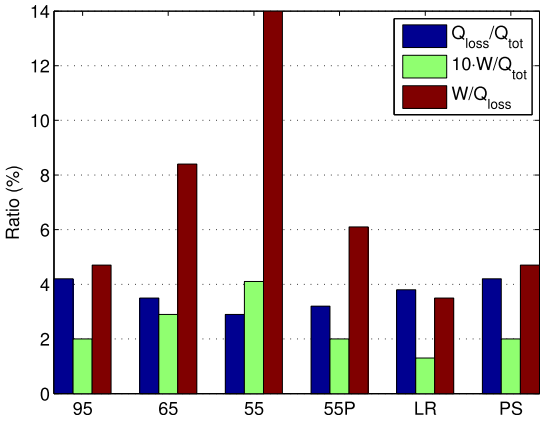

Fig. 5. The ratio between the total annual heat losses and the total heat delivered, the pump energy use and the total heat delivered multiplied by ten, as well as between the pump energy use and the heat losses.

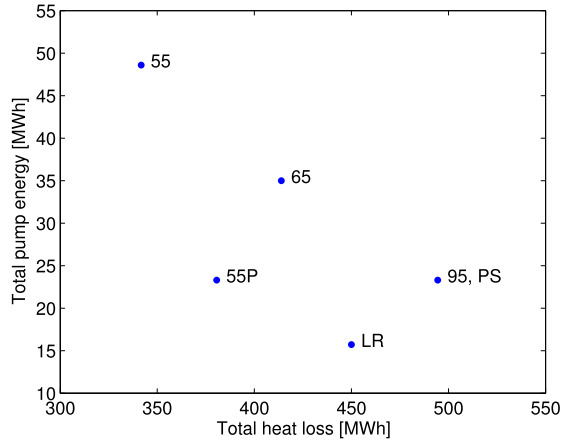

Fig. 6. Total pump energy use plotted over the total heat loss for the different cases.

pipe diameter, the total pump energy was almost identical with the 95 case, as intended. The heat loss is 23% lower for the 55P case compared to the 95 case. Based on Fig. 6, the 55P case appears as the most optimal solution with respect to heat losses and pump energy demand.

The peak shaving case is almost similar with the 95 case in terms of total heat losses and pump energy; the difference becomes only visible in the maximum heat delivered and maximum pump power (12 and 16% lower than the baseline case, respectively; see Table 4). Peak shaving measures are hence most important in enabling reduced installed capacity. The fact that the reduction in the total maximum heat delivered was lower than the 20% peak reduction applied for the individual buildings is probably because the peak demands of the different building types do not occur simultaneously. It is also worth mentioning that for the simulated year, the coldest day of the year was clearly colder than the rest of the year (see Fig. 2). This lead to a high peak heating demand with respect to the average demand, and lowered the effect of peak shaving. The utilization time for the year was 2206 h, and the load factor was 0.25, which is considered to be low [22]. To obtain a bigger impact, another peak shaving approach, or simply a lower threshold for the peak shaving, could be applied.

The low return case gave the lowest mass flow rate and total

pump energy, as expected. The reductions were quite large, around 20% reduction in both maximum and average mass flow rate and 33% in total pump energy with respect to the baseline case. Peak pumping power was 41% lower. Furthermore, the heat losses were reduced by 9% due to lower mass flow rates and return temperatures.

Fig. 7 presents the pressure lift as a function of mass flow rate at the heat supply plant. In Fig. 7, the coldest winter day is visible as a distinct peak in the mass flow rate vs. pressure lift for all other cases apart from peak shaving, which does not have this peak. The 55P case with bigger pipe diameters, shows more moderate increase in pressure lift with respect to the other cases, in accordance with Eq. (2). The low return case shows lowest mass flow rate and pressure lift, which is in line with the low pump energy use as discussed earlier.

Fig. 8 presents the mass flow rate as a function of ambient temperature for the different simulated scenarios. At ambient temperatures (T_{amb}) above approximately 18 °C, the mass flow rate is almost independent of T_{amb} and relatively similar for the different cases. This is most probably because at these temperature levels, the heating demand is primarily due to DHW preparation. At lower temperatures, strong dependency on T_{amb} and great variation between the simulated cases is present. At 5 °C ambient temperature for instance, the lowest mass flow rates, obtained for the LR case, are around 5 kg/s; while for 55 and 55P cases, mass flow rates up to 35 kg/s are observed.

4. Discussions

4.1. Heat losses

Lower heat losses is one of the primary motivations for shifting to LTDH. In the present study, the heat losses were 31% lower for the 55 case (constant supply temperature of 55 °C) as compared to the reference case with a supply temperature of 95–70 °C. In a similar simulation case study carried out for Graz, Austria [5], a reduction in heat losses of 29% was obtained comparing a reference scenario with a supply temperature of 120–75 °C to a LTDH scenario with a constant supply temperature of 58 °C. In another case study carried out for a network with low linear heat demand densities in Denmark, the heat losses were almost halved when comparing a baseline scenario (supply temperature 85 °C all year round) with a LTDH scenario (supply temperature 55 °C for normal conditions and optimal design to allow low return temperatures). Hence, the reduction in heat losses obtained in the present study appears reasonable.

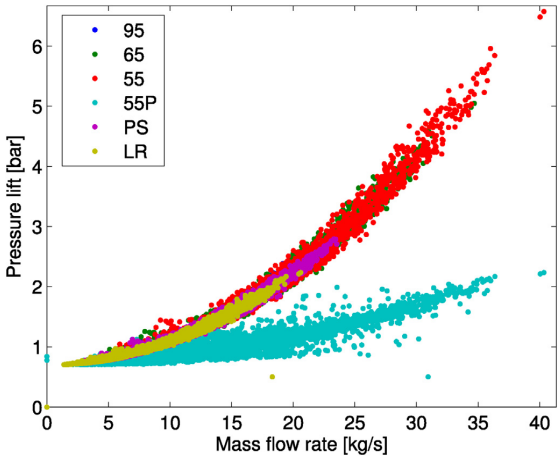

Fig. 7. Pressure lift required by the pump as a function of mass flow rate in the heat supply plant.

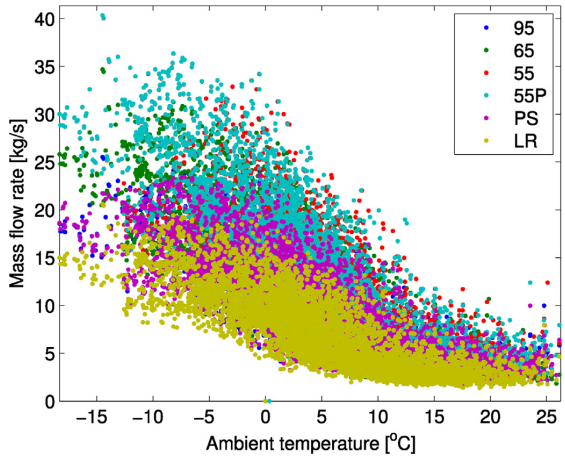

Fig. 8. Mass flow rate as a function of ambient temperature for the different simulated scenarios.

Overall, the heat losses were very low in the present study: 4% for the highest supply temperature case, and 3% for the lowest supply temperature case. The present DH system in Trondheim (covering the whole city) has heat losses of approximately 10–12%. This deviation can however be attributed to the particularly high linear heat demand density for the studied case; heat losses per meter trench were realistic when comparing to the existing network, as discussed in Section 3. The high linear heat demand density is probably partially due to the fact that subareas of several similar buildings were modelled as single large buildings, as explained in Section 2.2.1. The reduction in grid length resulting from this simplification will be taken into account in a further study.

Comparison of the applied heat loss model to a more complex model was also performed using a simple network with only two buildings and a heat supply plant providing water at 95-70 °C over a distance of 100 m. The more complex pipe models had ten pipe cells along the pipe; varying ground temperature over the year (sinusoidal variation by +4 K as in Ref. [20]; temperature dependent insulation conductivity according to [23]); and a radially sectioned insulation and surrounding ground layer (four layers each). For the insulation, both temperature and conductivity were varied from layer to layer; for the ground, only the temperature was varied, and for the conductivity, a constant value of 1.6 W/(mK) was assumed [20]. The uncertainty of soil conductivity is generally high – values between 0.5 and 2.5 W/(mK) have been reported, depending on the soil type and moisture content [20].

With the more advanced heat loss model, 9% lower total annual heat losses were obtained. From the studied parameters, variation in ground temperature hardly affected the results, while the insulation conductivity was of major importance. The level of complexity was however strongly increased, although the simulation time was hardly affected in the tested simple network. In a future model, a more complex heat loss model could be applied.

4.2. GHG emissions

The heating demand of the buildings in the network was identical for each simulated case. The reduction in the delivered heating – and in the GHG emissions – was hence solely due to reduction in the heat losses. The relative reduction in heat losses and emissions is however not similar for the different cases (see Table 4). In periods with high heating demand, when the heat demand is reduced due to the lower loss at lower supply temperatures, the heat sources to be removed are always the most polluting ones. Therefore, a stronger reduction in the GHG emissions with respect to the heat supply should be expected. For the PS case, the GHG emissions were not reduced despite a 12% lower peak demand compared to the 95 case. The reason for this is probably the low load factor as discussed earlier; most of the year the heat demand is identical for the PS and 95 cases. For all the other cases, the relative reductions in emissions are higher than the reductions in heat losses, and hence in the energy demand. The lowest GHG emissions were obtained for the 55 case, with 3% reduction in emissions as compared to the reference case. Obviously, the full potential of LTDH in terms of reduced GHG emissions is only seen when the heat supply is based on renewable and waste heat resources.

4.3. Pipe dimensions

According to [23], the DH network should be designed according to the maximum hydraulic load that can be withstood by the distribution pipeline (pressures of 1.2–1.5 times the nominal value). The duration of peak load, when the maximum pressures might occur, is marginal, and hence it is recommended to utilize the maximum pressure that can be withstood by the DH pipes in order to reduce pipe diameters and consequently decrease the heat losses in the network [23]. Based on the simulation results however, the 55P case appears as the most optimal solution with respect to both the heat losses and pump energy demand, as discussed in Section 3. Nevertheless, the pipe diameter, together with the insulation thickness and temperature levels, is a decisive factor in determining the heat losses and hence the cost-effectiveness of the DH system [24]. Alternative approaches for dimensioning the pipes, such as those suggested in Ref. [24], could be considered in further studies for finding the most optimal pipe diameters.

5. Conclusions

In this study, a heating network for a residential area in Trondheim, Norway, has been modelled using the dynamic simulation program Dymola in order to investigate the benefits of LTDH. Heat losses, pump energy use and GHG emissions were analyzed for six different scenarios, including three different supply temperature levels: 95-70 °C with outdoor temperature compensation, and constant supply temperatures of 65 and 55 °C. A scenario assuming bigger pipe diameters was also included for the 55 °C case. In addition, the effect of peak shaving and lower return temperature levels were studied for the highest supply temperature case.

The simulation results showed that reducing the supply temperature has a significant impact on the heat losses. By lowering the supply temperature to 55 °C, the heat losses could be reduced by approximately one third. The heat losses obtained were generally low: only 4% of the total delivered heat for the reference case supplying heat at 95–70 °C, owing to the high heat demand density of the network, and a mild year, yielding low average supply temperatures.

The total pump energy demand was doubled for the 55 °C supply temperature case as opposed to the reference case; however, the total pump energy was generally an order of magnitude lower than the heat losses. Hence, reducing the supply temperature has a positive overall environmental impact. With bigger pipe dimensions, the pump energy demand for the low-temperature case could be kept at the same level as in the high-temperature case, while the heat losses were still reduced significantly. Lowering the return temperature in the high-temperature case showed also to be very beneficial in reducing both pump work and heat losses. Peak shaving did not have any impact on the total heat losses or the pump power, but reduced the peak heating demand and the maximum pump power significantly. Furthermore, with lower heat losses resulting from lower supply and return temperatures, lower GHG emissions were obtained, as the use of peak heating devices based on fossil fuels or electricity could be reduced.

Future work will encompass including different renewable and waste heat sources as well as thermal storage into the model. Furthermore, an approach for calculating the total costs will be included, to be able to fully compare the different scenarios.

Acknowledgements

This work has been carried out as a part of the project Development of Smart Thermal Grids, supported by Statkraft Varme AS and the Research Council of Norway (RCN) under grant agreement number 245355. The authors would like to specifically thank Åmund Utne from Statkraft Varme AS for providing information regarding the DH network in Trondheim.

References

[1] Connolly D, Lund H, Mathiesen BV, Werner S, Möller B, Persson U, et al. Heat Roadmap Europe: combining district heating with heat savings to decarbonise the EU energy system. Energy Pol 2014;65:475–89.
[2] Lund H, Werner S, Wiltshire R, Svendsen S, Thorsen JE, Hvelplund F, et al. 4th Generation district heating (4GDH): integrating smart thermal grids into future sustainable energy systems. Energy 2014;68:1–11.
[3] Ommen T, Markussen WB, Elmegaard B. Lowering district heating temperatures – impact to system performance in current and future Danish energy scenarios. Energy 2016;94:273–91.
[4] Dalla Rosa A, Christensen JE. Low-energy district heating in energy-efficient building areas. Energy 2011;36(12):6890–9.
[5] Köfinger M, Basciotti D, Schmidt R, Meissner E, Doczekal C, Giovannini A. Low temperature district heating in Austria: energetic, ecologic and economic comparison of four case studies. Energy 2016;110:95–104.
[6] Olsen PK, Christiansen CH, Hofmeister M, Svendsen S, Thorsen J-E, Gudmundsson O, et al. Guidelines for Low-temperature District Heating, EUDP 2010-II: Full-scale Demonstration of Low-temperature District Heating in Existing Buildings. 2014.
[7] Direktoratet for Byggkvalitet. Byggteknisk forskrift (TEK 10): Veiledning om tekniske krav til byggverk. 2011.
[8] Giraud L, Baviére R, Vallée M, Paulus C. Presentation, validation and application of the districtheating modelica library. In: Proceedings of the 11th International Modelica Conference. Linköping University Electronic Press; 2015.
[9] Olsthoorn D, Haghighat F, Mirzaei PA. Integration of storage and renewable energy into district heating systems: a review of modelling and optimization. Sol Energy 2016;136:49–64.
[10] Basciotti D, Schmidt R. Peak reduction in district heating networks: a comparison study and practical considerations. In: The 14th International Symposium on District Heating and Cooling; 2014.
[11] Soons F, Torrens JI, Hensen J, Schrevel RD. A modelica based computational model for evaluating a renewable district heating system. In: 9th International Conference on System Simulation in Buildings; 2014.
[12] Kauko H. Heating and Cooling Demand of Buildings in Trondheim a Pre-study for Designing Local Low-temperature Thermal Grids, Project report for Development of Smart Thermal Grids (DSTG). 2015. RCN grant no 245355.
[13] Norge S. Kriterier for passivhus og lavenergibygninger - boligbygninger. 2013.
[14] Modelon, Dymola. 2015. URL, http://www.modelon.com/products/dymola/.
[15] TLK-Thermo, TIL Suite – simulates Thermal Systems. 2016. URL, https://www.tlk-thermo.com/index.php/en/software-products/til-suite.
[16] Li P, Nord N, Ertesvåg IS, Ge Z, Yang Z, Yang Y. Integrated multiscale simulation of combined heat and power based district heating system. Energy Convers Manag 2015;106:337–54.
[17] Frederiksen S, Werner S. District Heating and Cooling. Studentlitteratur AB; 2014.

[18] Incropera FP, Dewitt DP, Bergman TL, Lavine AS. Principles of Heat and Mass transfer. Wiley; 2013.
[19] LOGSTOR. URL, https://www.logstor.com/; 2016.
[20] Dalla Rosa A, Li H, Svendsen S. Method for optimal design of pipes for low-energy district heating, with focus on heat losses. Energy 2011;36(5):2407–18.
[21] Nielsen EKL. Lavtemperatur-varmenett. 2016.
[22] Tereshchenko T, Nord N. Implementation of CCPP for energy supply of future building stock. Appl Energy 2015;155:753–65.
[23] Christiansen C, Paulsen O, Bøhm B, Thorse J, Larsen CT, Jepsen B, et al. Udvikling og demonstration af lavenergi-fjernvarme til lavenergibyggeri, Hovedrapport og bilag. Taastrup, Denmark: Teknologisk Institut; 2009.
[24] Tol HI, Svendsen S. Improving the dimensioning of piping networks and network layouts in low-energy district heating systems connected to low-energy buildings: a case study in Roskilde, Denmark. Energy 2012;38(1):276–90.

Paper IV

H. Kauko, K. H. Kvalsvik, D. Rohde, N. Nord, and Å. Utne (2018). "Dynamic modeling of local district heating grids with prosumers: A case study for Norway." *Energy* 151, pp. 261–271. DOI: 10.1016/j.energy.2018.03.033.

Energy 151 (2018) 261–271

Contents lists available at ScienceDirect

Energy

journal homepage: www.elsevier.com/locate/energy

Dynamic modeling of local district heating grids with prosumers: A case study for Norway

Hanne Kauko [a, *], Karoline Husevåg Kvalsvik [a], Daniel Rohde [b], Natasa Nord [b], Åmund Utne [c]

[a] SINTEF Energy Research, Kolbjørn Hejes vei 1B, Trondheim, 7491, Norway
[b] Department of Energy and Process Engineering, Norwegian University of Science and Technology (NTNU), Kolbjørn Hejes vei 1B, Trondheim, 7491, Norway
[c] Statkraft Varme AS, Sluppenvegen 17 B, 7005, Trondheim, Norway

ARTICLE INFO

Article history:
Received 14 November 2017
Received in revised form
30 January 2018
Accepted 5 March 2018
Available online 7 March 2018

Keywords:
Low-temperature district heating
Thermal system modeling
Prosumers
Surplus heat
Energy planning

ABSTRACT

District heating (DH) will play an important role in the future fossil-free energy systems by enabling increased utilization of waste heat and renewable heat sources to cover buildings' heat demand. A prerequisite for this is a reduction in the distribution temperature and shift towards decentralized heat production. In this study, dynamic modeling has been applied to study the technical, energetic and environmental impacts of including prosumers – customers who both consume and produce heat – in a local low-temperature DH grid. Four different scenarios were studied for a planned building area in Trondheim, Norway: high- and low-temperature scenarios with the entire heat demand being covered by a heat central, and two low-temperature scenarios including heat supply from prosumers. A data center and two food retail stores were considered as the prosumers, each with different location and individual characteristics for the heat supply, allowing to study their impact on the water flow in different parts of the grid. The results show that utilizing local surplus heat is a significant measure to reduce the heat demand and the environmental impact of the DH grid. Decentralized heat supply additionally contributes to reduced heat losses, due to overall lower distances to transport the heat.

1. Introduction

District heating (DH) is an important technology in that it enables efficient and economical utilization of energy sources, that would otherwise be wasted, to cover buildings' heating demands [1]. DH will play an important role in the future fossil-free energy systems by enabling increased utilization of waste heat and renewable heat sources; however, a prerequisite for this is a reduction in the distribution temperatures and shift towards decentralized heat production [2–4]. With this, DH will allow reducing the load from the electric grid by utilizing DH for heating purposes instead of electricity wherever possible, hence promoting the utilization of electricity for other purposes where high-quality energy is needed, such as transport.

Reduced supply temperature level in DH provides a number of advantages. These include: (i) Reduction in the distribution heat losses [5–7]; (ii) Improved utilization of low-temperature waste heat sources from buildings and industry [3,8]; and (iii) Improved efficiency and production capacity for solar thermal and higher COP for heat pumps [9]. Highlighting the new era of district heating, the concept of 4th generation district heating (4GDH) has been introduced by Lund et al. [3]. 4GDH refers to low-temperature DH systems with waste heat utilization, integration of renewable heat and an ability to be an integrated part of smart energy systems, including thermal, electric and gas grids.

Conventionally, DH systems have been based on large, centralized combustion plants or utilization of industrial waste heat sources, characterized by high capacities and temperature levels. Potential for utilization of industrial waste heat sources is enormous, in particular in central Europe [10]. Such waste heat sources are however often placed outside cities and require high heat demand densities in order to justify the investments required for the heat distribution system. In Norway, heavy industries with high availability of surplus heat are often located in remote places in the coast due to availability of large hydro power resources and easy access by ships.

Potential surplus heat suppliers present in urban environments

* Corresponding author.
E-mail address: hanne.kauko@sintef.no (H. Kauko).

https://doi.org/10.1016/j.energy.2018.03.033
0360-5442/

are buildings with large chiller and refrigeration facilities, such as data centers, office buildings or food retail stores. Such buildings may have a demand for heat at low ambient temperatures and surplus heat available otherwise, and are thus referred to as heat prosumers. Urban waste heat recovery with prosumers is already practiced in for instance Stockholm under the Open District Heating Concept [11]. The impact of including prosumers in a DH grid has also been studied by the scientific community, considering the energy balance and environmental impact [8], as well as the technical challenges [12,13]. Brange et al. [8] studied the potential of prosumers for a building area in Sweden with a high number of prosumers, including e.g. supermarkets and an indoor ice skating rink, concluding that the prosumers could potentially cover the entire heating demand of the area. Electricity would however be needed to obtain the required temperature levels, either with heat pumps or direct electric heating, and the environmental impact of the DH system with prosumers hence depends on the source of the electricity. Lennermo et al. [12] and Brand et al. [13] have reported on problems with differential pressure in the DH network, resulting from decentralized heat supply by solar collectors at a lower temperature level, and rapidly varying heat demand. This calls for proper control strategies when introducing decentralized heat suppliers in DH systems.

Due to the high investment costs related to DH systems, there is a great interest in simulation and planning software to find the most optimal solutions regarding production and distribution of heat [14]. Such tools will become increasingly important with the increased complexity of 4GDH grids including decentralized heat production by prosumers, often in combination with thermal storage and an advanced control system. There are many software tools available for simulation of DH systems; a comprehensive overview has been given in Ref. [15]. For detailed physical modeling of DH systems, the dynamic simulation program Dymola using the object-oriented modeling language Modelica has been proven to be a flexible and efficient tool [6,14,16–18].

In a previous study [7], a component library for modeling local DH grids was created in Dymola in order to study and compare different scenarios with various supply temperature levels for the local DH grid. For the present study, the component library has been improved and extended to study the impact of including prosumers in a local low-temperature DH grid. Two types of prosumers were included, a data center and food retail stores, each with different, dynamic characteristics for the surplus heat delivery as well as different placement in the local DH grid. This enabled detailed investigation of the fluid flow in different parts of the grid during varying amounts of surplus heat delivery. The remaining heat demand was covered by a heat central, assumed to have the same energy mix as the DH supplier in Trondheim. The heating grid with prosumers was compared with two baseline cases, a high- and a low-temperature heating grid, in which the heat demand was entirely supplied by the heat central.

The objectives of this study are to (i) demonstrate dynamic modeling of a heating grid with prosumers; (ii) investigate the technical challenges related to inclusion of prosumers; and (iii) study the energetic and environmental benefits of surplus heat delivery.

2. Methodology

The methodology consisted of the following primary steps:

1. Collecting data for DH demand profiles for modern buildings representing different building categories, located in Trondheim (see Ref. [7]).
2. Upgrading the Dymola model for a local DH grid from the previous study [7], including new and improved components.
3. Simulating different scenarios for a local low-temperature grid with and without prosumers, and comparing the results to a reference, high-temperature scenario representing the current practice of the local DH provider.
4. Calculating the equivalent CO_2 emissions for the different simulated scenarios.

These phases are described in more detail in the following.

2.1. The building stock

The investigated building area was a new neighborhood, Brøset, which is planned to be built in Trondheim, Norway. The area included several different types of buildings, such as apartment blocks, nurseries, schools, nursing homes and commercial buildings, with a total heated area of 188,000 m^2 (excluding prosumers). The DH demand of the buildings was modelled entirely from the basis of real DH use data from existing buildings, with the building type and standard matching with the buildings to be built as well as possible. Apart from a few historical buildings, the applied DH demand data were retrieved solely from new buildings. The data included the total heating demand, i.e., both space heating and domestic hot water (DHW) preparation. From this data, DHW demand profiles were extracted by analyzing the average demand for summer months (June–August), when the space heating demand is minimal. The motivation to use existing data was to be able to model the simultaneity of peaks in heat demand throughout a day and the year as realistically as possible. For more detailed description of the modelled building area, see Ref. [7].

Apartment blocks constitute the largest share (75%) of the building mass at Brøset. In the previous work [7], the DH demand for all the apartment blocks was based on the DH demand profile of one existing building. As a result, the total DH demand profile for Brøset became unrealistically homogeneous. Hence, in the present study, three different demand profiles were used for the apartment blocks, yielding a more realistic compound profile, and an increase in the demand by 12%. The results from Ref. [7] will be compared with the present results throughout the paper.

The total annual DH demand for the area was 12 470 MWh, out of which 5640 MWh was for DHW heating and 6830 MWh for space heating. The linear heat demand density was 1.82 MWh/(m · year), corresponding to a total pipeline length of 6840 m.

2.2. Modeling approach

Dymola is a dynamic simulation software (DYnamic MOdeling LAboratory) [19], using the object-oriented modeling language Modelica. Object-oriented approach allows full re-usability, extensibility and adaptability of the created models. Furthermore, Modelica is an equation-based modeling language, meaning that it allows declaring relations among variables. Hence, the variables do not need to have explicit expressions; the Modelica code is transformed into efficient simulation code by Dymola using symbolic manipulation. An in-depth discussion of equation-based (acausal) modeling tools for energy system modeling and their advantages and disadvantages can be found in Refs. [18] and [20].

Previously, an in-house component library for modeling thermal grids has been created in Dymola. This component library is under constant development to reduce the simulation time and to enable various simulation case studies. The in-house component library includes models for primary components for transport of heat and fluid, such as sensors, valves, pumps and pipes. More complicated models were built from the primary components, e.g.

heat exchangers, twin-pipes surrounded by the ground, and customer substations. The modelled network included the building stock, prosumers, piping network, and a heat central delivering heat at the desired temperature level and the required pressure. These components are described in more detail below, and an outline of the local DH grid model in Dymola is shown in Fig. 1.

2.2.1. Number of transfer units (NTU) heat exchanger model

In an earlier version of the model [7], the heat exchanger was discretized into a number of individual cells along the length of the heat exchanger, each with a different average temperature. A high number of cells was required to obtain realistic return temperatures, increasing the computation time. For the present study, a heat exchanger model based on the NTU method was developed. In the NTU method, the heat flow in the heat exchanger is calculated from the state of the inlet streams using an analytical equation [21]:

$$Q_{flow} = \varepsilon \cdot C_{min} \cdot (T_{inlet,hot} - T_{inlet,cold}), \quad (1)$$

where ε is the effectiveness of the heat exchanger, that is, the ratio of the actual heat transfer rate to the maximum heat transfer rate. C_{min} is the minimum heat transfer rate:

$$C_{min} = min(C_{cold}, C_{hot}) = C_p \cdot min(C_p \dot{m}_{hot}, C_p \dot{m}_{cold}), \quad (2)$$

where C_p is the specific heat capacity of water and $\dot{m}_{hot}$ and $\dot{m}_{cold}$ are the mass flows on the hot and cold side of the heat exchanger, respectively. The effectiveness is a complex function of the number of transfer units (NTU) and the heat capacity rates on the hot and cold side [21]:

$$\varepsilon = f\left(NTU, \frac{C_{min}}{C_{max}}\right), \quad (3)$$

where C_{min}/C_{max} is equal to C_{cold}/C_{hot} or C_{hot}/C_{cold}, depending on the relative magnitudes of the hot and cold fluid heat capacity rates. NTU is a dimensionless parameter, defined as

$$NTU = \frac{UA}{C_{min}}, \quad (4)$$

where U is the average heat transfer coefficient and A the heat transfer area. Using the NTU approach, the simulation times were reduced by approximately 60% (from 8 to 3 h for the entire network) compared to the approach used in the previous study [7].

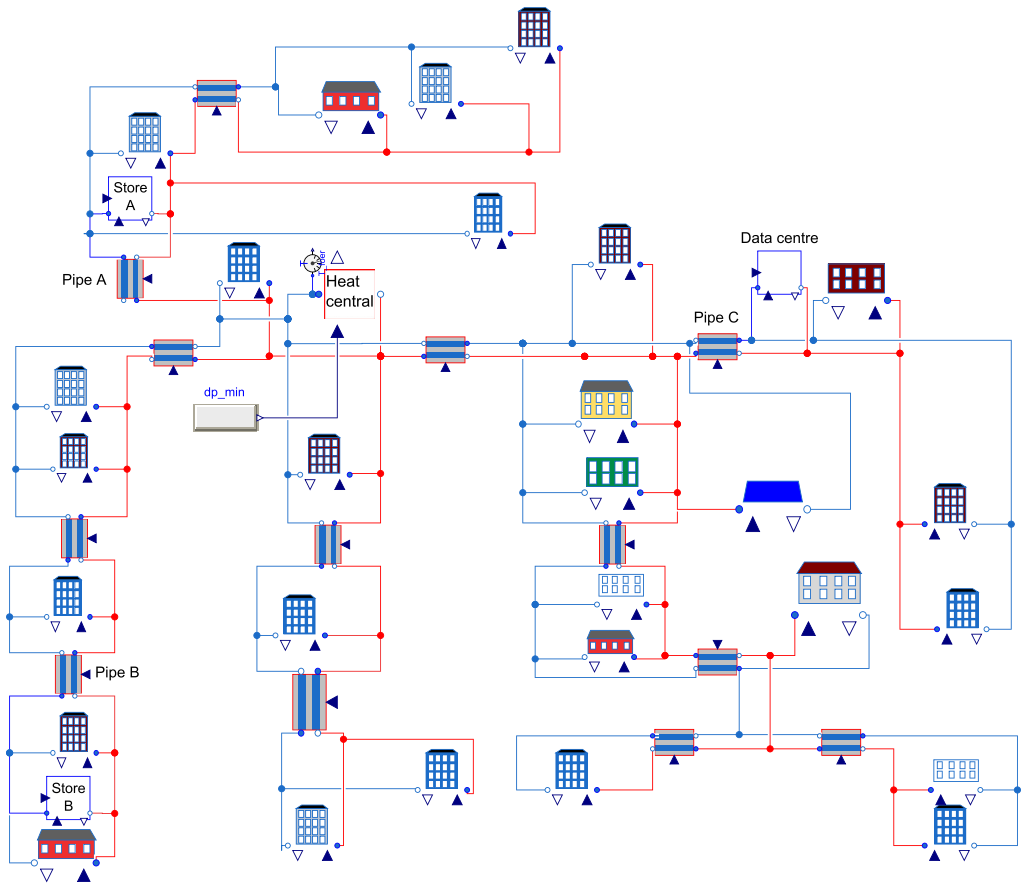

Fig. 1. The modeled building area in Dymola, including different building types, piping, prosumers (a data center and two food retail stores) and a heat central. The supply lines are denoted with red, and the return lines with blue. (For interpretation of the references to colour in this figure legend, the reader is referred to the Web version of this article.)

No heat losses were included in the heat exchanger model.

2.2.2. Twin pipe model

In the previous model [7], separate pipes without thermal interaction were used for the supply and return lines. For the present model, a twin pipe model was developed. In a twin pipe, the supply and return lines are enclosed in the same insulated pipe and hence thermally coupled with each other in addition to the ground. To model this effect without extensive computational efforts, the correlations developed by Ref. [22] were used. In this approach, the heat loss from each pipe is split into two: (i) heat loss from the entire pipe to the ground (symmetrical problem), q_s, based on the average temperature in the pipes [22]:

$$q_s = (T_s - T_0)2\pi\lambda_i h_s \tag{5}$$

and (ii) heat loss from the hot to the colder pipe (asymmetric problem), q_a, based on the temperature difference between the two pipes:

$$q_a = T_a \cdot 2\pi\lambda_i \cdot h_a. \tag{6}$$

T_s is the average temperature between the two pipes, $T_s = \frac{T_1+T_2}{2}$, related to the symmetrical problem (i); T_a is the temperature difference between the two pipes divided by two, $T_a = \frac{T_1-T_2}{2}$, related to the asymmetric problem (ii); and T_0 is the temperature on the ground surface. T_0 was therefore assumed to be equal to the ambient temperature, based on [23]. λ_i is the thermal conductivity of the insulation, and h_s and h_a are the heat transfer coefficients for the symmetric and asymmetric problem, respectively. The heat loss from the supply (1) and and return (2) pipes is calculated by superposition:

$$q_1 = q_s + q_a \tag{7}$$

$$q_2 = q_s - q_a. \tag{8}$$

The heat transfer coefficients h_s and h_a are complex functions of the pipe geometry, and the thermal conductivities of the ground and of the pipe. The parameter values applied in the simulations are given in Table 1. For the pipe insulation, insulation series 2 was assumed. The thermal conductivity of the ground varies between 0.5 and 2.5 W/(mK) depending on soil type and moisture [23]. In Trondheim there are different types of soils, with a large share of wet clay, corresponding to the highest thermal conductivity. A value of 1.8 W/(mK), somewhat above the average of the two extrema, was chosen for the present study.

The pipe diameters were selected assuming a maximum pressure drop of 150 Pa/m, as this is a normal design criteria used by the local DH suppliers. Based on the Darcy-Weissbach equation and Colebrook's expression for friction factor [25][p. 522], a relationship between maximum mass flow $\dot{m}_{max}$ and inner diameter D_i was derived in [7]:

$$D_i = 0.0379 \cdot \dot{m}_{max}^{0.37}. \tag{9}$$

Hence, for a given maximum mass flow in a pipe, the equation gives the pipe diameter at a pressure drop of 150 Pa/m. The calculated diameter was always rounded up to the nearest real diameter available from DH pipe suppliers [24].

2.2.3. Customer substation

For the building models, representing the customer substations, indirect connection with separate heat exchangers for DHW heating and space heating (SH) was applied. A schematic diagram of the model is shown in Fig. 2. Mass flow in the DHW/SH (secondary) loops was controlled by the DHW/SH demands, based on real DH use data as explained in section 2.1. Different input data was applied for different types of buildings (see Ref. [7] for more details). Mass flow on the primary side was controlled with valves, based on set-points for supply temperature on the secondary side.

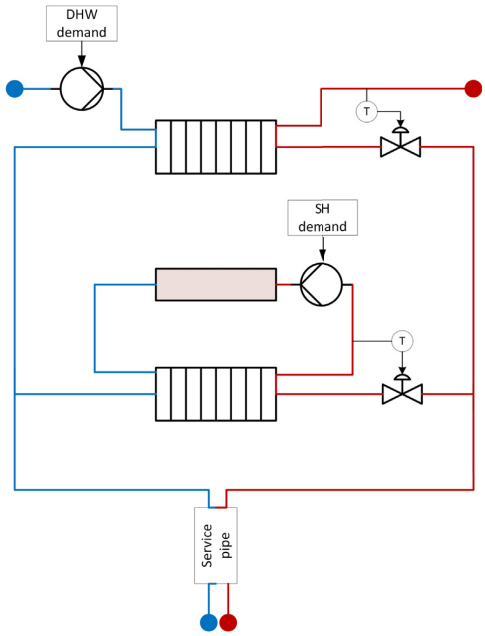

Fig. 2. Schematic diagram for the customer substation model.

Table 1
Parameter values applied in the simulations.

Parameter name	Symbol	Value	Comment
Ground thermal conductivity	λ_g	1.8 W/(mK)	Based on [23]
Insulation thermal conductivity	λ_i	0.024 W/(mK)	From Ref. [24]
DHW temperature set-point HT/LT	–	65/60 °C	–
Radiator temperature set-point (winter/summer)	–	60/40 °C	Outdoor compensated
DH supply temperature HT (winter/summer)	T_{supply}	115/75 °C	Outdoor compensated
DH supply temperature LT	T_{supply}	65 °C	Constant
DH return temperature HT (winter)	T_{return}	65 °C	Applied for dimensioning heat exchangers, see 2.2.3
DH return temperature LT (winter)	T_{return}	45 °C	Applied for dimensioning heat exchangers, see 2.2.3

For DHW heating, the desired supply temperature was 65 °C for the high-temperature (HT) simulations, and 60 °C for the low-temperature (LT) simulations. A temperature level of 8 °C was assumed for the incoming cold water. For SH, the supply temperature set-point for the radiators was outdoor compensated, with limits of 40/60 °C. The highest supply temperature was used from −20 °C and below, the lowest from 20 °C and above and a linear relationship between the two otherwise. Same limits were applied for HT and LT simulations.

As the heat demand was based on input data, heat loss from the buildings to the ambient was not included in the model. The radiator was set to exchange heat with a constant room temperature of 21 °C, and the mass flow in the SH loop was controlled by a pump to supply the required amount of heat, based on the SH demand. The radiator area was chosen based on the heated area of the building, and the maximum desired temperature difference in the radiator loop. The targeted return temperature was in the range 30–40 °C. The UA-value depended on the current radiator mass flow.

The UA-values for the DHW and SH heat exchangers were assumed constant and calculated separately for each building type. The values were based on the building's peak heating demand, and the logarithmic mean temperature difference for winter operation, based on the temperature limits given in Table 1. Two sets of UA-values were required for each building type; one for HT and one for LT simulations, as the supply- and return temperature limits were different for the two cases. On average, the UA-values for LT simulations were approximately 7.6 times larger than the UA-values for HT simulations for the SH heat exchangers, and 3.3 times larger for the DHW heat exchangers.

Every building connected to a DH grid has its own service pipe leading to only that building, as shown in Fig. 2. Therefore, all building models also included a twin pipe before and after the heat supply system. The length of the service pipe was estimated based on the building plan (see Ref. [7]).

As the interest in the present study lies in the potential of prosumers and low-temperature heat distribution from the perspective of the DH provider, the building heat distribution system was not a part of the model. However, the modelled building area is a new area to be built in Trondheim (see section 2.1), and the latest building standards will apply. It was thereby presumed that the buildings will have a heat distribution system that is suited for lower distribution temperatures, such as floor heating.

2.2.4. Heat central

The heat central ensures that the required supply temperature level and pressure lift is provided for the system at each moment. In an actual grid this central could represent the interface to the primary DH grid. The required pressure lift is determined by the building furthest away from the central, for which the transportation of water to the building has highest pressure drop. In addition, every customer substation has a pressure loss across its heat exchangers, and the local DH supplier in Trondheim guarantees a differential pressure of 70 kPa at the customers. Thus the heat supply plant model receives the pressure drop from the buildings furthest away as an input and applies a PI-controlled pump to keep the pressure drop at a minimum of 70 kPa for these customers. For buildings closer to the heat central, the pressure drop is naturally higher than 70 kPa. This excess pressure head is throttled by the valves in the substation, and is hence pure hydraulic loss. No maximum capacity limit was assumed for the heat central; it simply delivers the heat that is required by the local DH grid. Finding the required capacity was thus a part of the results rather than an input.

For the circulation pump, a constant efficiency of 50% was assumed, corresponding to the average efficiency of new commercial pumps. In reality, the pump efficiency is a function of the volume flow rate and pressure lift. Simulations with a pump with varying efficiency were tested in a previous study [7], however this gave no significant difference in total pump energy and resulted in a lower simulation speed.

2.2.5. Heat prosumers

For the present study, two types of heat prosumers were included, likely to be present in urban neighborhoods: data centers and food retail stores. For both of these, the surplus heat source is a cooling/refrigeration system, and the availability of surplus heat depends on the ambient temperature, while at low ambient temperatures there might be a demand for heat. The surplus heat capacity of the prosumers was hence defined as follows:

$$\dot{Q}_{pros} = \dot{Q}_{pros,0} \cdot (1 + k) \cdot \frac{T_{amb} - T_{inv}}{25 - T_{inv}}, \tag{10}$$

where T_{amb} is the ambient temperature (in °C); T_{inv} is a parameter, equal to the ambient temperature level below which the supplier has a demand for heat; $\dot{Q}_{pros,0}$ is the baseline capacity for the surplus heat, available at $T_{amb} = T_{inv}$; and k is a gain factor for summer operation. 25 °C was the highest measured outdoor temperature, hence the capacity at this temperature level is equal to $\dot{Q}_{pros,0} \cdot (1 + k)$. The surplus heat capacity will become negative, i.e., there will be a heat demand, at $T_{amb} < T_{inv}$.

In practice having the ability to supply and receive heat in the same model was accomplished by having two separate loops, each with its own heat exchanger (see Fig. 3): one for supplying heat, equipped with a pump to control the mass flow, and one for receiving heat, equipped with a valve. These loops are never active simultaneously, that is, the mass flow is zero in the loop that is not active. During periods of heat supply, i.e., when $T_{inv} < T_{amb}$, the water to be heated is taken from the return pipe and delivered in the supply pipe, as illustrated in Fig. 3. This type of connection, so-called R/S connection, has become the most common alternative for DH prosumers in Sweden, and has the largest potential according to [12]. During periods of heat demand, the flow is reversed; that is, water is taken from the supply pipe and delivered

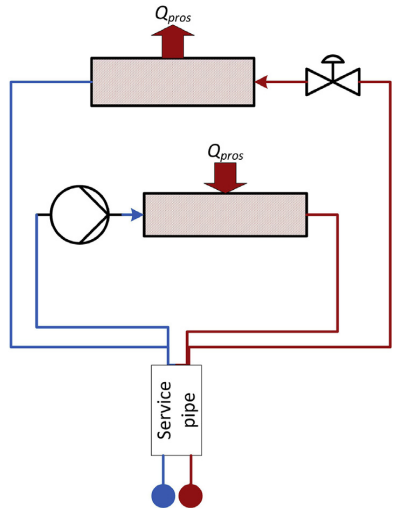

Fig. 3. Schematic diagram for the prosumer model.

in the return pipe, as in a normal customer substation. Based on the availability of the surplus heat, the mass flow in the pump was controlled such that the temperature supplied to the grid would be 65 °C. This heat delivery temperature corresponds to the temperature the Pionen data center delivers to the DH network in Stockholm [26]. Requiring a high enough supply temperature also enables to avoid the potential problems related to differential pressure [13]. Possible energy required for upgrading the heat was not considered in the model.

The values for T_{inv}, $\dot{Q}_{pros,0}$ and k applied in the simulations are given in Table 2. For the data center, lower values for T_{inv} and k were set with respect to the food retail store as it was assumed that data centers have surplus heat available all year round, and they are less affected by infiltration due to e.g. door openings, hence less dependent on the ambient temperature. In reality, free cooling is often applied in data centers in the wintertime, resulting in little surplus heat during these periods.

Two scenarios with different surplus heat capacities for the food retail stores and the data center were simulated, shown in Table 2. The heat capacities for the food retail store were chosen based on measurements from an existing store with surplus heat utilization [27]. The heat capacities for the data center were chosen keeping in mind the Pionen data center in Stockholm, which has a heat delivery of 600 kW during normal operation, with a floor area of 1100 m^2 [26]. For the present case, somewhat smaller capacities (200 and 400 kW) were chosen, as the simulated building area was rather small and having such a large data center would not have been realistic. Annual surplus heat profiles for the data center and the food retail store at the lower capacity level are shown in Fig. 4.

The network included two retail stores and one data center. To study the effect of heat delivery on different parts of the network, one of the retail stores (store A) was placed nearby the heat central, while the other one (store B) was placed next to the customer lying furthest away from the heat central (see Fig. 1).

In periods of high availability of surplus heat, the heat delivery and hence the mass flow from the prosumers might become so high that it exceeds the heat demand, and hence the mass flow available for supplying surplus heat in the grid. This problem called for a priority setting for when to receive heat from which prosumer, and the data center was given the first priority. In reality, the heat supplier with the first priority would be the one offering the lowest price. Pricing of surplus heat was not a part of the study, however the assumed priority setting in the model was equivalent to assuming a price ranking.

To apply the priority setting in practice, and to ensure that the heat supply from the prosumers never exceeded the demand, each prosumer was given a maximum allowed mass flow based on the mass flow available in the grid at each moment of time. The mass flow available is a function of the momentary heat demand and temperature lift in the heat central. The prosumer with the highest priority had access to maximum 95% of the mass flow in the grid, the one with second highest priority had access to 95% of the remaining mass flow and so on. The factor of 95% was included as an additional safety margin to avoid exceeding the demand. If a surplus heat supplier did not have enough mass flow available to do away with all its heat, the remaining heat was rejected to ambient.

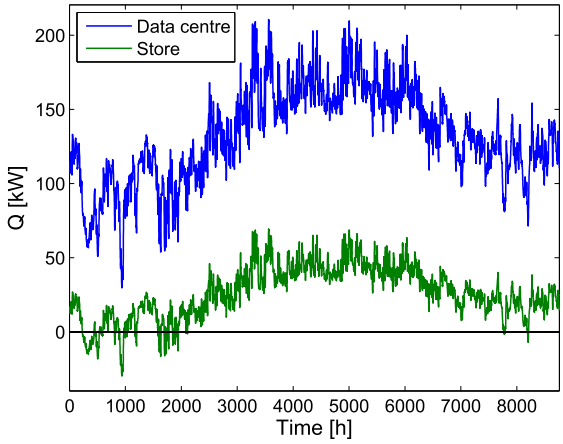

Fig. 4. Annual surplus heat profiles for the data center and the food retail store in the LTP1 scenario.

2.3. Simulations

Four different scenarios were simulated:

- High-temperature (HT): Supply temperature outdoor compensated. The highest temperature level (115 °C) is used from −20 °C and below, the lowest (75 °C) from 15 °C and above, and a linear relationship is applied between the two otherwise. The heat demand is covered by the heat central. This scenario represents the current practice for the main DH network in Trondheim.
- Low-temperature (LT): Constant supply temperature of 65 °C. The heat demand is covered by the heat central.
- Low-temperature with prosumers 1 (LTP1): Constant supply temperature of 65 °C. The heat demand is covered by the heat central and three distributed prosumers (one data center and two food retail stores) at a lower capacity level (see section 2.2.5 and Table 2).
- Low-temperature with prosumers 2 (LTP2): As LTP1, but with a higher capacity level for the three prosumers.

The return temperature limits for the HT and LT simulations were given in Table 1. In the previous study [7], different supply temperature levels were considered, however for the present study 65 °C was chosen as this represents the potential future temperature level, considering the Norwegian legislation.

2.4. Calculation of the CO_2 equivalent emissions

The GHG emissions for heating were calculated from the basis of the total annual simulated heat flow in the heat central. The DH supplier in Trondheim applies many different heat sources, and the same sources were assumed to be available for the heat central in

Table 2
Parameter values applied for the surplus heat providers in the two scenarios including prosumers, LTP1 and LTP2.

		$\dot{Q}_{pros,0}$ [kW]	T_{inv}[°C]	k
LTP1	Data center	200	−25	0.05
	Store	60	−5	0.15
LTP2	Data center	400	−25	0.05
	Store	100	−5	0.15

the present study. The GHG emissions for the different sources were found from Refs. [28] and [29]. It was assumed that each energy source has a fixed maximum capacity, and that the least polluting sources would be used first. The only exception is waste incineration, which the supplier is decreed to perform, and must thus always have the first priority. As the HT scenario represents the current operation strategy, it was assumed that the given energy mix – i.e., the relative share of the heat sources applied by the DH supplier – is valid for this scenario. Capacity limits for each energy source were thus calculated based on the HT scenario. The same capacity limits were applied for the other simulated scenarios. The energy required for the circulation pumps was also included in the calculations. For calculating the emissions for electricity, Nordic electricity mix was assumed [28]. For surplus heat delivery, zero emissions were assumed, as any energy needed for upgrading the heat was not considered.

3. Results

3.1. Overall comparison

Table 3 summarizes the results for total annual delivered heat by the heat central and the prosumers, as well as the total annual heat losses and pump work for the four simulated scenarios. For the LT scenario, the reduction in heat delivered by the heat central is only 1% with respect to the reference (HT) scenario, and this is solely due to the reduction in heat losses. For the LTP1 and LTP2 scenarios with surplus heat delivery, the reduction is 13 and 25%, respectively. The heat losses are reduced by 20% for the LT scenario, and by 22% for the LTP scenarios. The fact that the heat losses are lower for the LTP scenarios than for the LT scenario despite the same supply temperature is probably due to the distributed heat supply, yielding lower heat transportation distances.

The total pump work is increased by 61% for the LT scenario and 68% for the LTP scenarios; however, the pump work is an order of magnitude lower than the heat losses. The work delivered by the pumps at the surplus heat suppliers is included in the total pump work.

The relative heat losses are in general low; between 3.6 and 4.6%. The heat loss per meter grid (trench) was 10.2 W/m for the HT scenario, 8.2 W/m for the LT scenario and 8.0 W/m for the LTP scenarios. These are very similar to the values given by the pipe producer (7.2–8.7 W/m) [30]. The fact that the relative heat losses are low is thus due to the well-insulated twin pipes. The heat losses given here include only the losses in the pipelines; potential losses at the heat central or customer substations have not been taken into account.

Fig. 5 shows duration curves for the delivered heat for the different scenarios, with an insert showing the first 150 hours. As can ben seen from the figure, the difference in peak demand between the four scenarios is minimal, as the surplus heat supply is significant in the summertime, but low during the coldest periods.

In a previous study [7], the same building area was modelled at supply temperatures of 55, 65 and 95 °C, with more simplified models for e.g. pipes (single pipes), valves (controlling flow area rather than mass flow), and customer substations. The net demand in the present study is 1.4 GWh higher than in Ref. [7], which can be attributed to the different input data for apartment blocks (see section 2.1). The heat loss per meter grid line (trench) was 15.9 W/m for the previous simulation at 65 °C supply temperature, which is clearly higher than for the present LT scenario (8.2 W/m). This reduction in heat losses is obviously due to the application of twin

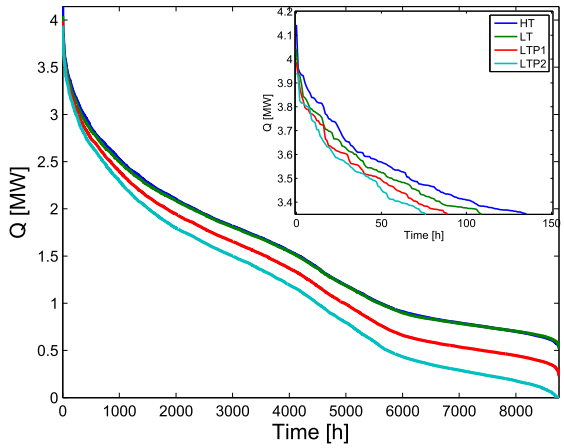

Fig. 5. Duration curves for heat delivered by the heat central for the different simulated scenarios. The insert displays the duration curves for the first 150 hours, showing the difference in the peak demand.

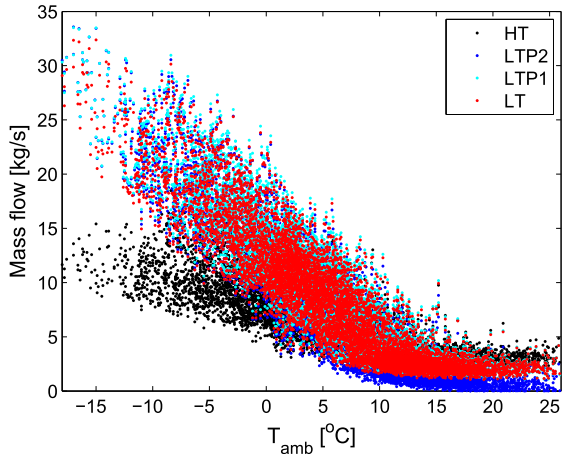

Fig. 6. Mass flow delivered by the heat central as a function of ambient temperature for the different simulated scenarios.

Table 3
Results for total annual heat delivered by the heat central (Q_{hc}) and the prosumers (Q_{pros}), as well as the total annual heat losses (Q_{loss}) and pump work (W_{pump}). In addition, total heat losses and pump work relative to the total delivered heat (Q_{del}) are given. Q_{del} includes heat from both the heat central and the prosumers.

Case	Q_{hc} [GWh]/(%)	Q_{pros} [GWh]	Q_{loss} [MWh]/(%)	W_{pump} [MWh]/(%)	$\frac{Q_{loss}}{Q_{del}}$ (%)	$\frac{W_{pump}}{Q_{del}}$ (%)
HT	13.4/100	0	609/100	13/100	4.56	0.10
LT	13.3/99	0	489/80	21/161	3.68	0.16
LTP1	11.7/87	1.63	477/78	22/168	3.59	0.16
LTP2	10.0/75	3.26	477/78	22/168	3.59	0.16

pipes.

Fig. 6 shows additionally the mass flow rate delivered by the heat central as a function of ambient temperature for the different scenarios. The mass flow rate is clearly higher for all the LT scenarios as compared to the HT scenario at ambient temperatures below 0–5 °C. At ambient temperatures above 10 °C, the mass flow is on average lower for the LT scenarios. This effect is pronounced for the LTP2 scenario owing to the fact that during summertime a large share of heat demand is covered by the prosumers.

In the summertime, the heat demand is dominated by the DHW demand. The fact that the mass flow rate is lower in the summertime for the LT scenarios with respect to the HT scenarios, is hence related to the size of the DHW heat exchangers and temperature difference in the heat exchangers. For HT, the temperature difference at the heat exchanger inlet on the primary side is in the summer time 10 °C. For LT scenarios, this temperature difference is 5 °C, but the heat exchanger area is 3.3 times higher (see section 2.2.3); thereby a lower mass flow is required to obtain the same heat flow rate.

3.2. Surplus heat delivery

Fig. 7 presents the share of the total heat demand covered by the prosumers and the heat central for the two scenarios including prosumers, LTP1 and LTP2. For the LTP1 scenario, the surplus heat delivery by the prosumers is between 40 and 50% during the summertime, and between 5 and 20% in the spring and autumn. For the LTP2 scenario, the contribution from the prosumers is up to 80–90% during summer, and considerable (10–30%) also during spring and autumn.

To investigate the effect of the surplus heat supply on the pipe mass flow, the mass flow in the twin pipes residing closest to the prosumers, (marked as Pipe A, B and C in Fig. 1) is plotted in Fig. 8 (a) and (b) for LTP1 and LTP2, respectively. In the summertime, the flow becomes negative for pipe C beside data center and to a larger degree also for pipe B beside store B, in particular in the LTP2 scenario. This indicates that the prosumer is in this period able to cover the heat demand for this part of the grid, and shows also that the model is able to handle bidirectional flow. For pipe B, the mass flow is approximately zero for most of the summer in the LTP1 scenario, which indicates that store B is able to cover the heating demand for the two buildings for this period. In the LTP2 scenario, with higher capacities, the data center is providing heat for the buildings beyond pipe C frequently also during winter, and in particular during autumn.

The fact that the flow in pipe A close to store A is positive all the time is because this store is located far away from the end of the branch. That is, beyond store A there are more buildings to supply heat for than in the case of store B, and additional heat delivery from the heat central is required to be able to cover the heat demand for these buildings.

Fig. 9 (a) shows additionally the heat delivered by the heat central and by the prosumers for a particular day in March with high surplus heat supply. Fig. 9 (b) shows the mass flow in pipes A, B and C for the same period. Fig. 9 (a) demonstrates that the heat delivery by the prosumers peaks around noon when T_{amb} is the highest, while the heat demand in the grid, reflected in the heat delivered by the heat central, peaks in the morning. From Fig. 9 (b) it can be seen that the mass flow profile in pipe A reflects very precisely the heat delivery by the heat central, while the mass flow profiles for pipes B and C are more affected by the heat supply from the prosumers, as could be expected.

3.3. CO_2 emissions

The reduction in CO_2 emissions is considered from two perspectives: (i) considering the heat delivery by heat central alone, in order to analyze how the local heat production affects the energy mix from the DH provider; and (ii) looking at the total heat delivery in the local grid, including the surplus heat supply. Table 4 shows the total equivalent CO_2 emissions for these two perspectives for the different scenarios, as well as the reduction in emissions relative to the HT scenario. The calculations for (i) includes the emissions from the heat delivery and the pump work by the heat central, and for (ii) the surplus heat (emission-free) and the pump work at the prosumers in addition. These two figures are obviously equal for the HT and LT scenarios where no prosumers are included. Furthermore, the total emissions are almost equal for the HT and LT scenarios, as the difference in the amount of heat delivered by the heat central is only 1% between these two scenarios. Hence the overall environmental impact of lowered distribution temperature alone is hardly noticeable, at least for a grid with low heat loss values as considered in this study.

For the scenarios including prosumers, a considerable reduction

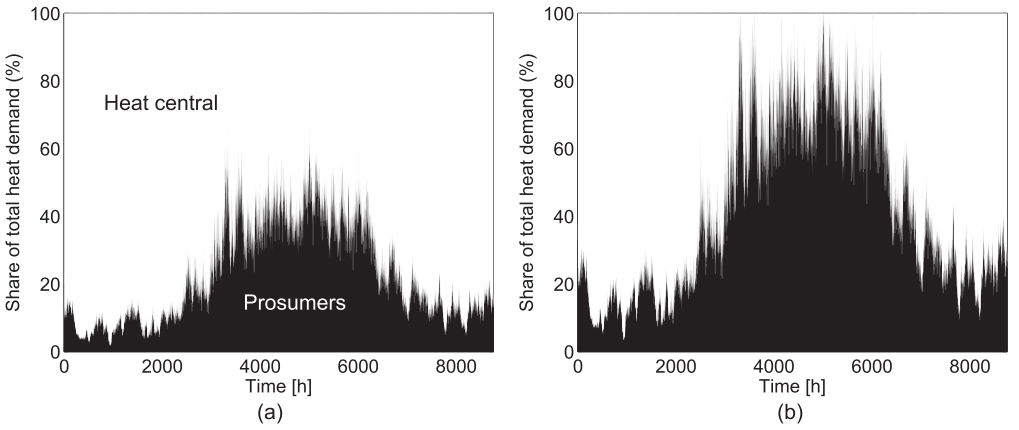

Fig. 7. The share of heat delivered by the prosumers and by the heat central with respect to the total heat demand: (a) LTP1 and (b) LTP2.

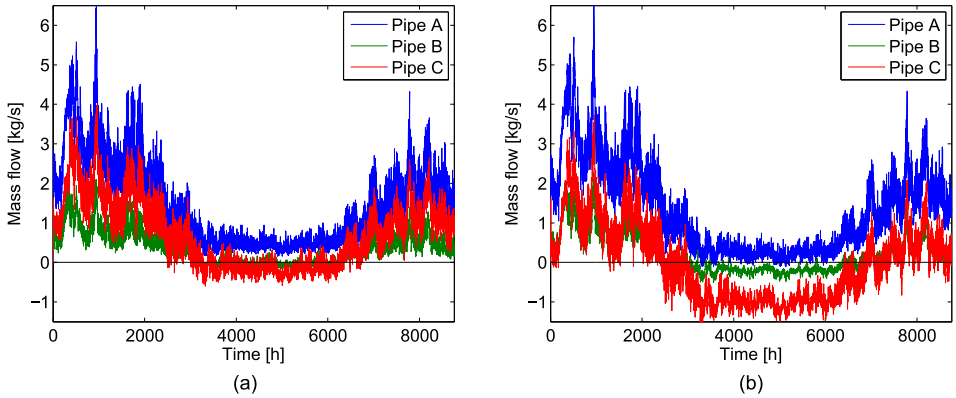

Fig. 8. Mass flows in the pipes nearby surplus heat suppliers: (a) LTP1 and (b) LTP2. For the location of the pipes, see Fig. 1.

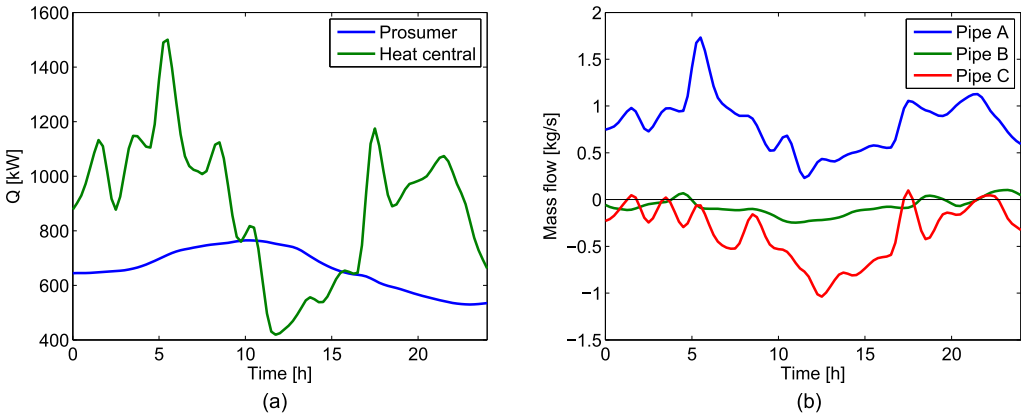

Fig. 9. (a) The total heat delivery by the prosumers and the heat central for the LTP2 scenario, considering a 24-h period in March and (b) the mass flow in pipes A, B and C for the same period.

Table 4
CO_2 equivalent emissions for the heat delivered by the heat central, and for the total heat delivery. The total heat delivery includes the surplus heat and the pump work at the prosumers. The total emissions per kWh produced heat is given, as well as the reduction in emissions relative to the HT scenario.

	Heat delivered by the heat central		Total delivered heat	
	[g/kWh]	Reduction in %	[g/kWh]	Reduction in %
HT	23.8	–	23.8	–
LT	23.6	1.1	23.6	1.1
LTP1	22.7	4.8	19.9	16.4
LTP2	22.4	5.9	17.0	28.9

in the emissions is obtained, in particular when considering the surplus heat delivery (reduction of 16/29% for the LTP1/LTP2 scenarios), but also when looking at the heat delivery by the heat central alone (5/6% for LTP1/LTP2). This is an important result, showing that local heat supply can contribute to reduction in the use of more polluting peak heating sources at the DH provider. This can be mainly attributed to the lowered demand for heat from the heat central, but also to some extent the lowered heat losses for the LTP scenarios (see section 3.1 and Table 3). The emissions considering the total delivered heat are lower, because they include the heat from prosumers and are thereby divided by a larger amount of heat than the emissions for heat delivered by the heat central alone.

Fig. 10 shows the distribution of the applied heat sources used in the four simulated scenarios, looking at the total heat delivery in the local grid. The results were obtained as explained in section 2.4; by assuming the energy mix for the HT scenario to be equal to the energy mix at the local DH supplier, and further assuming the same capacities for the heat sources for each simulated scenario. The distribution is practically the same for the HT and LT scenarios as the difference in the amount of heat delivered by the heat central is so small for these two scenarios. The LTP scenarios are clearly different from the HT and LT scenarios. Looking at Fig. 10, most obvious is the reduction in the total share of heat received from waste incineration: from 73 to 66/57% for LTP1/LTP2. Less visible in the figure is the relative reduction in the use of more polluting heat sources from the perspective of the heat central: 21/24% reduction for electricity, and 18/28% for the remaining heat sources, including biogas and liquefied petroleum gas (LPG). Furthermore, from the perspective of the heat central, the relative amount of heat from

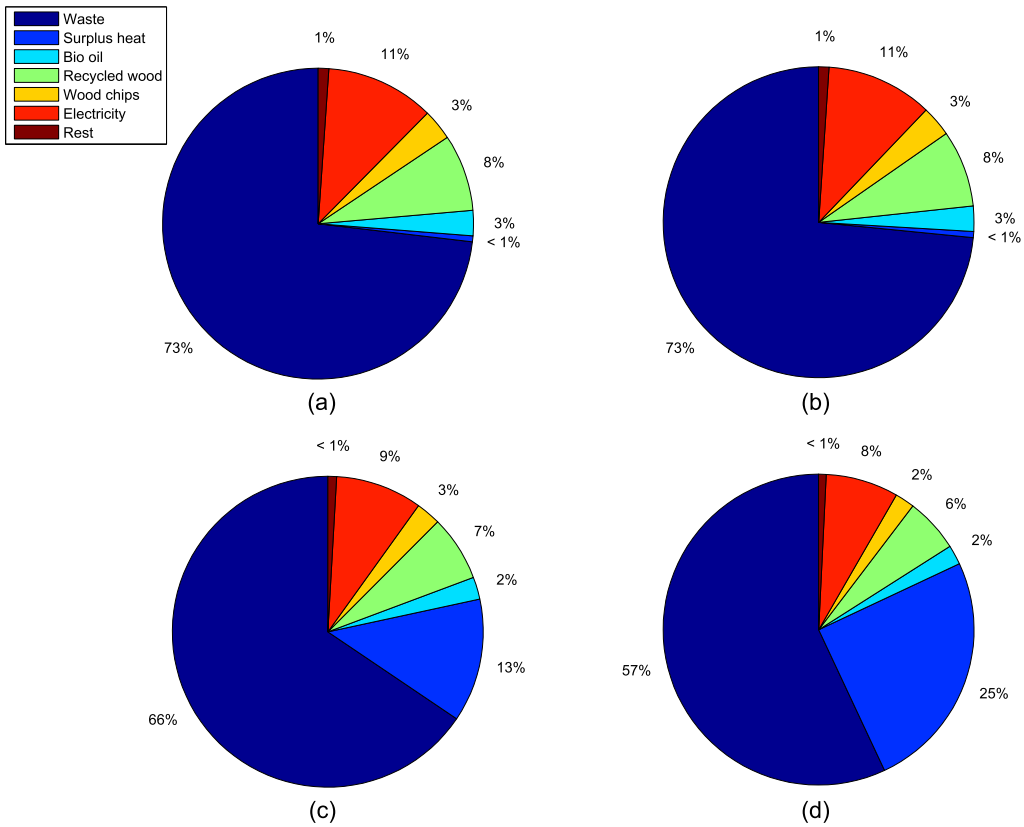

Fig. 10. The share of heat received from different heat sources for the different simulated scenarios: (a) HT, (b) LT, (c) LTP1, (d) LTP2. The "rest" includes LPG and biogas.

waste incineration was increased by 2–3%. It should be noted that the energy mix applied in the calculations is based on the DH system in Trondheim and the results are hence not directly transferable to other systems.

4. Discussions and conclusions

There is a high potential for utilization of local low-temperature surplus heat in small-scale DH grids. In the present simulation case study, considering a building area with two retail stores and a data center as the surplus heat suppliers, a reduction of up to 25% in the demand for delivered heat was obtained as compared to a high-temperature reference scenario. Regarding the environmental impact, a considerable reduction in CO_2 equivalent emissions was obtained when considering the total heat delivery, including the emission-free surplus heat supply. A clear reduction in the emissions was however obtained also when looking at the heat delivery by the heat central alone, showing that local heat supply can contribute to a reduction in the use of more polluting peak heating sources at the DH provider. The reduction in emissions can be mainly attributed to the lowered demand for delivered heat, but to some extent also to the lowered heat losses, resulting from overall lower heat transport distances in a DH grid including local, decentralized heat suppliers.

A problem with the type of prosumers considered in the present study, with surplus heat source being a refrigeration or cooling system, is that the availability of surplus heat is the highest during the summer. The reduction in the annual peak heating demand is hence minimal. Seasonal thermal energy storage could be introduced for extended utilization of the surplus heat, as suggested by Ref. [8]. Moreover, the heat supply from the prosumers peaks around noon, while the overall heat demand is the highest in the morning. Diurnal thermal storage could be applied to reduce the peak heating load in the heat central in the mornings, and hence to further reduce the environmental impact of the DH system. Diurnal thermal storage systems in the form of e.g. water tanks are generally easier to implement than seasonal thermal storage systems, and should be included in a further study.

In periods, the heat production by the prosumers may be sufficient to cover the entire heating demand for the grid segment it is located in. This induces flow reversals in the pipeline, which was handled well by the model. This was also demonstrated in a previous dynamic modeling study by Schweiger et al. [18]. The results from the present study hence further confirm that dynamic modeling suits well for simulating and analyzing small-scale DH grids with decentralized heat supply.

Another challenge associated with prosumers is that the differential pressure at the customers might drop, as suggested in Refs. [12,13]. This problem was not observed in the present study, probably owing to the fact that the prosumers were assumed to deliver heat at a constant, high (65 °C) temperature. In the previous studies by Brand and Lennermo et al. [12,13], heat supply from solar

collectors with varying, lower supply temperature was considered, yielding locally higher flow velocities and hence lower pressures. Nevertheless, in a grid with distributed heat suppliers, the location of the customer with lowest differential pressure will alter, depending on the location of the prosumers and their surplus heat delivery. In the present study, the required pressure lift at the heat central was determined by the building furthest away, however a more advanced control strategy would be needed in a grid including prosumers. This should be taken into account in a further study.

Losses not included in the present calculations are the heat losses in the heat exchangers, and the losses related to the production of heat. The latter is out of the scope of the present study, and the losses in the heat exchangers are considered to be minimal compared to the heat losses in the pipes.

Moreover, not considered in this study are the economic aspects related to low-temperature DH and utilization of local surplus heat. In many cases, surplus heat utilization may be beneficial from energetic and environmental point of view, but not profitable for the DH supplier. With the present supply temperature levels, upgrading the surplus heat is often necessary, which reduces the cost-efficiency. Introduction of 4th generation, low-temperature DH systems is hence crucial to increase the profitability of surplus heat delivery. It is also uncertain, which party should be responsible for the investment and operation costs of the required infrastructure, possibly including a heat pump for upgrading the heat. Furthermore, cost schemes for the surplus heat delivery are required, currently not existing in Norway. Finally, increase in investment costs due to e.g. larger heat exchangers needed at lower distribution temperatures should be taken into account.

To summarize; a possible future study should include diurnal thermal storage systems for extended utilization of surplus heat, take into account the energy required for upgrading the heat, and incorporate a more advanced control strategy to define the required pressure lift in a grid including prosumers. In addition, the economic aspects related to surplus heat delivery and reduction in the distribution temperature should be considered.

Acknowledgements

The authors greatly acknowledge support from the Research Council of Norway (RCN) under projects Development of Smart Thermal Grids (grant agreement (GA) number 245355), INTERACT (GA number 228656) and FME HighEFF (GA number 257632).

References

[1] Laajalehto T, Kuosa M, Mäkilä T, Lampinen M, Lahdelma R. Energy efficiency improvements utilising mass flow control and a ring topology in a district heating network. Appl Therm Eng 2014;69(1):86–95.
[2] Connolly D, Lund H, Mathiesen BV, Werner S, Möller B, Persson U, Boermans T, Trier D, Østergaard PA, Nielsen S. Heat Roadmap Europe: combining district heating with heat savings to decarbonise the EU energy system. Energy Pol 2014;65:475–89.
[3] Lund H, Werner S, Wiltshire R, Svendsen S, Thorsen JE, Hvelplund F, Mathiesen BV. 4th Generation District Heating (4GDH): integrating smart thermal grids into future sustainable energy systems. Energy 2014;68:1–11.
[4] Schmidt D, Kallert A, Blesl M, Svendsen S, Li H, Nord N, Sipilä K. Low temperature district heating for future energy systems. Energy Proced 2017;116:26–38.
[5] Dalla Rosa A, Christensen JE. Low-energy district heating in energy-efficient building areas. Energy 2011;36(12):6890–9.
[6] Köfinger M, Basciotti D, Schmidt R, Meissner E, Doczekal C, Giovannini A. Low temperature district heating in Austria: energetic, ecologic and economic comparison of four case studies. Energy 2016;110:95–104.
[7] Kauko H, Kvalsvik KH, Rohde D, Hafner A, Nord N. Dynamic modelling of local low-temperature heating grids: a case study for Norway. Energy 2017;139:289–97.
[8] Brange L, Englund J, Lauenburg P. Prosumers in district heating networks - A Swedish case study. Appl Energy 2016;164:492–500.
[9] Ommen T, Markussen WB, Elmegaard B. Lowering district heating temperatures - Impact to system performance in current and future Danish energy scenarios. Energy 2016;94:273–91.
[10] Persson U, Möller B, Werner S. Heat Roadmap Europe: identifying strategic heat synergy regions. Energy Pol 2014;74:663–81.
[11] Värme Fortum. Open district heating. 2017. https://www.opendistrictheating.com. accessed: 2017-10-12.
[12] Lennermo G, Lauenburg P, Brand L. Decentralised heat supply in district heating systems: implications of varying differential pressure. In: The 14th international symposium on DH and cooling, september 7th to september 9th, 2014, Stockholm, Sweden; 2014.
[13] Brand L, Calvén A, Englund J, Landersjö H, Lauenburg P. Smart district heating networks - A simulation study of prosumers impact on technical parameters in distribution networks. Appl Energy 2014;129:39–48.
[14] Giraud L, Baviére R, Vallée M, Paulus C. Presentation, validation and application of the districtheating modelica library. In: Proceedings of the 11th international Modelica conference. Linköping University Electronic Press; 2015.
[15] Olsthoorn D, Haghighat F, Mirzaei PA. Integration of storage and renewable energy into district heating systems: a review of modelling and optimization. Sol Energy 2016;136:49–64.
[16] Basciotti D, Schmidt R. Peak reduction in district heating networks: a comparison study and practical considerations. In: The 14th international symposium on district heating and cooling; 2014.
[17] Soons F, Torrens JI, Hensen J, Schrevel RD. A modelica based computational model for evaluating a renewable district heating system. In: 9th international conference on system simulation in buildings; 2014.
[18] Schweiger G, Larsson P-O, Magnusson F, Lauenburg P, Velut S. District heating and cooling systems - Framework for Modelica-based simulation and dynamic optimization. Energy 2017;137:566–78.
[19] Modelon. Dymola. 2017. http://www.modelon.com/products/dymola. accessed: 2017-10-12.
[20] Wetter M, Bonvini M, Nouidui TS. Equation-based languages - A new paradigm for building energy modeling, simulation and optimization. Energy Build 2016;117:290–300.
[21] Incropera FP, Dewitt DP, Bergman TL, Lavine AS. Principles of heat and mass transfer. Wiley; 2013. Ch. 11.
[22] Wallentén P. Steady-state heat loss from insulated pipes. Licentiate Thesis, Report TVBH-3017. Sweden: Dept. of Building Physics, Lund Institute of Technology; 1991.
[23] Dalla Rosa A, Li H, Svendsen S. Method for optimal design of pipes for low-energy district heating, with focus on heat losses. Energy 2011;36(5):2407–18.
[24] Logstor. 2017. https://www.logstor.com. accessed: 31.05.2017.
[25] Incropera FP, Dewitt DP, Bergman TL, Lavine AS. Principles of heat and mass transfer. Wiley; 2013.
[26] Fortum. Bahhof Pionen - Profitable recovery with open district heating. accessed: 12.10.2017. 2016. https://www.opendistrictheating.com/media/open-district-heating-bahnhof-pionen.pdf.
[27] Tønseth S. Drastic cut in electricity bill for supermarket. June 2014.
[28] Otterlei ET. Klimaregnskap for fjernvarme. Tech. rep. Norsk Fjernvarme; 2014.
[29] Gode J, Martinsson F, Hagberg L, Man A, Hglund J, Palm D. Miljöfaktaboken 2011: Estimated emission factors for fuels, electricity, heat and transport in Sweden. Tech. rep. Värmeforsk; 2011.
[30] Logstor. Dokumenterede lambdaværdier. 2016. https://www.logstor.com/media/1833/lambda-values_dk_p_dh.pdf. accessed: 2017-11-14.

Paper V

D. Rohde, T. Andresen, and N. Nord (2018). "Analysis of an integrated heating and cooling system for a building complex with focus on long–term thermal storage." *Applied Thermal Engineering* 145 (7), pp. 791–803. DOI: 10.1016/j.applthermaleng.2018.09.044.

Applied Thermal Engineering 145 (2018) 791–803

Contents lists available at ScienceDirect

Applied Thermal Engineering

journal homepage: www.elsevier.com/locate/apthermeng

Research Paper

Analysis of an integrated heating and cooling system for a building complex with focus on long–term thermal storage

Daniel Rohde[a,*], Trond Andresen[b], Natasa Nord[a]

[a] Norwegian University of Science and Technology, Kolbjørn Hejes vei 1A, 7491 Trondheim, Norway
[b] SINTEF Energy Research, Sem Sælands vei 11, 7034 Trondheim, Norway

HIGHLIGHTS

- Modelica is suitable for fast simulation of complex thermal energy systems.
- The heat balance of the long-term storage is important for long-term performance.
- More solar collectors or district heating import could enable sustainable operation.

ARTICLE INFO

Keywords:
Modelica
Heating and cooling system
Heat pumps
Borehole thermal energy storage

ABSTRACT

Modern building complexes have simultaneous heating and cooling demands. Therefore, integrated energy systems with heat pumps and long-term thermal storage are a promising solution. An integrated heating and cooling system for a building complex in Oslo, Norway was analyzed in this study. The main components of the system were heat pumps, solar thermal collectors, storage tanks, ice thermal energy storage, and borehole thermal energy storage. Dynamic simulation models were developed in Modelica with focus on the long-term thermal energy storage. One year measurement data was used to calibrate the system model and two COPs were defined to evaluate system performance. The simulation results showed that more heat had to be extracted from the long-term thermal storage during winter than could be injected during summer. This imbalance led to a decrease in ground temperature (3 °C after 5 years) and decreasing long-term performance of the system: both COPs decreased by 10% within five years. This performance decrease could be avoided by increasing the number of solar collectors from 140 to 830 or by importing more heat from the local district heating system. Both measures led to sustainable operation with a balanced long-term thermal storage.

1. Introduction

Buildings account for a large share of the world's energy use, with a share of around 40% in the European Union [1]. Nearly 55% of this energy is used for space heating, domestic hot water (DHW) heating, and space cooling [2]. Many efforts have been made to reduce the carbon emissions related to these thermal energy demands. Emissions can be reduced by decreasing the demands themselves, e.g. through better building envelopes and/or advanced control strategies, or by delivering the thermal energy at lower carbon costs, e.g. using more efficient energy systems and/or renewable energy sources.

District heating and cooling systems cover the heating and cooling demands of many buildings. The efficiency of such systems depends mainly on their energy sources and distribution losses. Much research is focused on 4th generation district heating (DH) and smart thermal grids [3]. On a smaller scale, micro-grids or integrated heating and cooling systems can be a promising solution, especially for new areas or major retrofitting projects [4,5]. Ground source heat pumps (GSHP) are an efficient technology to cover both heating and cooling demands, especially when they are combined with thermal energy storage [6]. Thermal storage is most effective when short and long-term storage are combined [7]. However, the annual heat balance of the long-term storage is an important aspect. For borehole thermal energy storages, the average temperature of the ground changes if the amounts of extracted and rejected heat differ. This ground temperature change will lead to reduced system efficiency after long-term operation as reported in [8–12]. GSHP systems for heating-dominated buildings are therefore often combined with solar thermal collectors to charge the long-term storage during summer to avoid a ground temperature decrease [13–15].

* Corresponding author.
E-mail address: daniel.rohde@ntnu.no (D. Rohde).

https://doi.org/10.1016/j.applthermaleng.2018.09.044
Received 6 April 2018; Received in revised form 22 July 2018; Accepted 8 September 2018
Available online 10 September 2018
1359-4311/

Nomenclature

Abbreviations

BTES	Borehole thermal energy storage
COP	Coefficient of performance
DH	District heating
DHW	Domestic hot water
GSHP	Ground source heat pump
HP	Heat pump
HX	Heat exchanger
ITES	Ice thermal energy storage
IHCS	Integrated heating and cooling system
NTU	Number of transfer units

Symbols

a_1	Linear heat loss coefficient [W/(m^2·K)]
a_2	Quadratic heat loss coefficient [W/(m^2·K^2)]
η	Efficiency (–)
ΔT	Temperature difference (K)
A	Area (m^2)
C	Heat capacity rate (W/K)
c_p	Specific heat capacity [J/(kg·K)]
ε	Heat exchanger effectiveness (–)
El	Electricity use (kWh)
FtP	Flow-to-power coefficient (W·s^2/m^6)
$\dot{m}$	Mass flow rate (kg/s)
Nu	Nusselt Number (–)
P	Power (W)
q	Exponent for calculation of heat transfer coefficient (–)
$\dot{Q}$	Heat flow rate (W)
R	Solar radiation per m^2 (W/m^2)
T	Temperature (K)
U	Heat transfer coefficient [W/(m^2·K)]
V	Volume (m^3)
$\dot{V}$	Volume flow rate (m^3/s)

Subscripts

amb	Ambient
cold	Cold side
col	Solar collector
cond	Condenser
const	Constant
evap	Evaporator
hot	Hot side
HP	Heat pump
in	Inlet
L	Lorentz
max	Maximum
meas	Measured
min	Minimum
nom	Nominal
opt	Optical
out	Outlet
pumps	Circulation pumps
r	Ratio
sec	Secondary

The inherent dynamics of thermal storage require dynamic simulation models for analysis. TRNSYS is a well-known commercial tool for dynamic simulations, which has been used for similar analyses in [16–19]. A common alternative is the open, object-oriented language Modelica, which has also been applied successfully for system analyses with thermal storage, see [20–23]. Modelica was chosen for this study because its high level of flexibility enables the development of specialized and fast simulation models.

A coefficient of performance (COP) is often used to evaluate system performance. However, many different COPs can be defined which makes it difficult to compare absolute values from different systems. Published COP values for system performance from systems similar to the one in this study were 3.3 (in heating period) [13], up to 3.4 [24], 3.8 [8], and 3.3–4.2 [17].

An integrated heating and cooling system (IHCS) for a small neighborhood in Oslo, Norway was described and analyzed in this study. Dynamic simulations were performed to analyze the system performance of the IHCS and all models were developed with the aim of a good trade-off between accuracy and simulation time. Focus was on the annual heat balance of the long-term thermal storage and its influence on the system performance. A new COP including this heat balance was defined.

This paper is structured as follows: the system description can be found in Section 2. In Section 3, the simulation models, the system control, and the sensitivity analysis are explained. Results from the simulations are presented in Section 4, followed by a discussion in Section 5 and concluding remarks in Section 6.

2. System description

2.1. The integrated heating and cooling system

An area of about 100 × 200 m in the Norwegian capital Oslo was renewed with several buildings and an integrated heating and cooling system (IHCS). Construction was completed in 2014 and the IHCS supplied a total floor area of 38,500 m^2. The supplied building types and their respective floor areas are shown in Table 1.

The IHCS delivered thermal energy for space heating, DHW heating, snow melting, space cooling, and product cooling. Snow melting was applied to the walkways between the buildings and product cooling was only delivered to the food court. A schematic of the IHCS is shown in Fig. 1.

The main components of the IHCS shown in Fig. 1 were heat pumps, heat exchangers, solar collectors, storage tanks, ice thermal energy storage (ITES), and borehole thermal energy storage (BTES). During heating season, the BTES and the surplus heat from space cooling and product cooling were used as heat sources on the evaporator side of the heat pumps. The condenser heat from the heat pumps was sent to space heating, DHW preheating, and snow melting. During cooling season, a lot of surplus heat was available from the cooling systems, which needed to be released on the condenser side of the heat pumps. In addition, the solar collectors also delivered heat and only a part of this heat was needed for space heating and DHW preheating. Therefore, heat was injected into the BTES during cooling season. The ITES was used to reduce space cooling peak demands during summer. The ITES was charged during the night and discharged during the day.

The IHCS was designed to deliver heat at 50–55 °C and was also connected to the city's DH system, which delivered heat at a

Table 1
Building floor area supplied by the IHCS.

Type	Offices	Shops	Hotels	Apartments	Food court	Event location	Total
Floor area (m^2)	15,000	6650	7600	3900	3500	1850	38,500

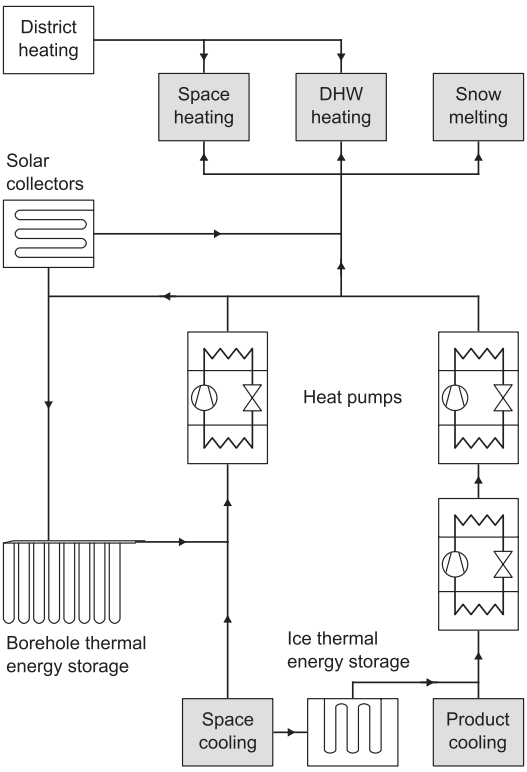

Fig. 1. Simplified overview of the integrated heating and cooling system.

temperature of 85–120 °C. This DH connection was used as backup (in case of system failure), for peak demand coverage, and as temperature lift for DHW heating, which had a supply temperature setpoint of 70 °C. A more detailed description of the IHCS can be found in [25], heat pump specifications are listed in Table 2.

2.2. Measurement data

The IHCS was equipped with a control and monitoring platform. Energy meters were installed to measure the delivered energy for heating and cooling in each connected building. However, no energy meters were installed to measure the energy exchange with the BTES or the performance of the solar collectors. Only the total electricity use of the system was measured, so the electricity use of single components was also not available. The amount of DH import was measured for each building.

Data from the building energy management system for the year 2015 was used in this study. The total heating demand was 3562 MWh and the total cooling demand was 1585 MWh. The values for each demand type as well as measured electricity use and DH import are shown in Fig. 2.

The on-site temperature was only measured by one sensor and solar radiation was not measured at all. Therefore, ambient temperature and solar radiation data from nearby weather stations were retrieved [26]. The on-site temperature was found to be around 5 °C higher than nearby measurements, which might be due to the location of the sensor or an offset error. Therefore, 5 °C were subtracted from the measured on-site temperature for the simulation input file. The input file also contained data for solar radiation from the nearest weather station. Other weather data like rain- and snowfall or wind speed were excluded from the analysis.

3. Methodology

The modelling approach that was chosen for this study is explained in this chapter. After some general information, the key component models are explained in detail, followed by a description of the system model and the system control. Afterwards, the sensitivity analysis is described.

The simulation models were developed using the open, object-oriented language Modelica [27]. Dymola was used as simulation environment and the standard solver DASSL was chosen with a tolerance of $1e^{-5}$. All models were developed with the aim to run parameter studies that require many model evaluations. Thus, low simulation time was an important requirement for the system model and a good trade-off between accuracy and simulation time was sought.

The library «Thermal», which is included in the «Modelica Standard Library» [28], was used as basis for the developed component models. However, many elements from the library were modified to increase simulation speed. All fluids were assumed incompressible and all fluid properties were assumed constant. The required fluid properties were calculated in Excel using the add-in CoolProp [29].

3.1. Component models

3.1.1. Heat exchanger model

All heat exchangers in the IHCS were counterflow plate heat exchangers. The heat flow rate from hot to cold fluid ($\dot{Q}$) was calculated with the effectiveness–NTU method [30]. The implemented relation for the effectiveness (ε) of a counterflow heat exchanger is shown in Eqs. (1)–(6). Measures were taken to avoid numerical instabilities at zero flow conditions and at $C_r = 1$, which both led to division by zero in some of the equations. The total heat transfer area (A) as well as nominal conditions for mass flow rate ($\dot{m}_{nom}$) and overall heat transfer coefficient (U_{nom}) were input parameters of the model.

$$C = \dot{m} \cdot c_p \tag{1}$$

$$C_{min/max} = \min/\max(C_{hot}, C_{cold}) \tag{2}$$

$$C_r = \frac{C_{min}}{C_{max}} \tag{3}$$

$$NTU = \frac{U \cdot A}{C_{min}} \tag{4}$$

$$\varepsilon = \frac{1-\exp[-NTU \cdot (1-C_r)]}{1-C_r \cdot \exp[-NTU \cdot (1-C_r)]} \tag{5}$$

$$\dot{Q} = \varepsilon \cdot C_{min} \cdot (T_{hot\_in} - T_{cold\_in}) \tag{6}$$

The overall heat transfer coefficient (U) in Eq. (4) was continuously

Table 2
Heat pump specifications.

	HP 1	HP 2	HP 3	HP 4 & 5
Type	WSA2802X	WSA1602X	WSA0701X	NXW0600X
Working fluid	R134a	R134a	R134a	R410a
Compressor	Screw (2)	Screw (2)	Screw	Scroll
Design data cooling (evap/cond)				
Temperatures	4.5 °C/48 °C	4.5 °C/48 °C	20 °C/55 °C	−8 °C/25 °C
Capacities	595/772 kW	334/436 kW	224/283 kW	87/110 kW
COP	4.36	4.27	4.80	4.78
Design data heating (evap/cond)				
Temperatures	0 °C/50 °C	0 °C/50 °C		
Capacities	473/652 kW	264/365 kW		
COP	3.64	3.61		

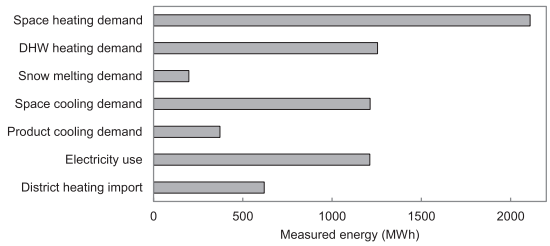

Fig. 2. Measured energy amounts for 2015.

calculated based on nominal and actual flow conditions according to [31], see Eq. (7).

$$U = U_{nom} \cdot \frac{(\dot{m}_{hot\_nom})^{-q} + (\dot{m}_{cold\_nom})^{-q}}{(\dot{m}_{hot})^{-q} + (\dot{m}_{cold})^{-q}} \quad (7)$$

Eq. (7) assumes similar heat transfer on both sides of the heat exchanger and negligible conduction resistance of the heat exchanger plates. The exponent q defines the influence of changes in mass flow rate on the heat transfer coefficient and lies in the order of 0.7 according to [31]. The Nusselt number for typical brazed plate heat exchanger configurations increases with $Re^{0.63}$ according to [32]. Therefore, q was set to 0.63.

3.1.2. Heat pump model

A heat pump consists of a closed thermodynamic cycle including two heat exchangers. These function as condenser and evaporator of the cycle's working fluid on the primary side. The heat sink and the heat source are connected to the condenser and the evaporator on the secondary side, respectively. The heat pump model used for this study was based on the theoretical Lorentz cycle. It is similar to the well-known Carnot cycle, but does not assume the heat source and sink to be isothermal. Instead, they have a finite heat capacity and thus change temperature during heat addition/extraction [33], which is the case for the fluid flows of the IHCS. Therefore, the Lorentz COP (COP_L) depended on both inlet and outlet temperatures on the secondary sides and required the calculation of the Lorentz temperature (T_L) for condenser and evaporator as shown in Eqs. (8) and (9). The COP_L was multiplied with a constant Lorentz efficiency (η_L) to calculate the heat pump's COP (COP_{HP}), see Eq. (10).

$$T_{L\_cond/evap} = \frac{T_{in\_sec\_cond/evap} - T_{out\_sec\_cond/evap}}{\ln\left(\frac{T_{in\_sec\_cond/evap}}{T_{out\_sec\_cond/evap}}\right)} \quad (8)$$

$$COP_L = \frac{T_{L\_evap}}{T_{L\_cond} - T_{L\_evap}} \quad (9)$$

$$COP_{HP} = COP_L \cdot \eta_L \quad (10)$$

$$\dot{Q}_{cond/evap} = \dot{m}_{sec\_cond/evap} \cdot c_p \cdot (T_{in\_sec\_cond/evap} - T_{out\_sec\_cond/evap}) \quad (11)$$

$$P_{HP} \cdot COP_{HP} = \dot{Q}_{evap} \quad (12)$$

$$P_{HP} + \dot{Q}_{evap} = \dot{Q}_{cond} \quad (13)$$

The Lorentz efficiency was an input parameter of the model and was chosen based on manufacturer specifications. The specifications included design data for different operating conditions, which allowed the calculation of η_L for each operating condition. Operating conditions that were not relevant were excluded and the average of the relevant values for η_L was used in this study. Values from 0.384 to 0.461 were obtained. This conforms well with the work of Østergaard and Andersen, where the Lorentz efficiency was also used as input parameter with values of 0.4 for small heat pumps and 0.5 for large heat pumps [34].

The mass flow rates ($\dot{m}_{sec\_cond/evap}$) and inlet temperatures ($T_{in\_sec\_cond/evap}$) on the secondary sides were calculated in the system model. One of the outlet temperatures on the secondary sides ($T_{out\_sec\_cond/evap}$) had to be set by an input signal to the heat pump model. The other outlet temperature and the required heat pump power (P_{HP}) could then be calculated. This approach was much faster and more stable than using P_{HP} as input signal and calculating both outlet temperatures in the model.

3.1.3. Borehole thermal energy storage model

A cross section model of the BTES was developed and several of these cross sections were connected in series to model the BTES. The three main parts of a BTES were included in the cross section model: a single U-tube pipe, the borehole with filling material, and the surrounding ground. A schematic and the simulation model are shown in Fig. 3.

The U-tube pipe segments in each cross section were modeled as fluid with uniform temperature. The borehole filling and the surrounding ground were modeled as thermal capacities. Thermal resistances were added to model two-dimensional heat transfer between the fluid in the pipe and the borehole wall according to the methodology published by Bauer et al. [35]. The thermal resistances were calculated based on Eqs. (16)–(21), (31), (33), and (42) in [35]. The thermal resistance between fluid and filling material depended on the fluid mass flow rate due to the convective resistance inside the pipe. As fluid properties were assumed constant, Eq. (14) was used to approximate the Nusselt number for the convective term of the thermal

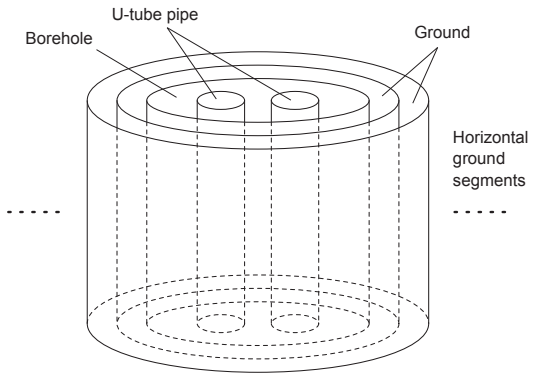

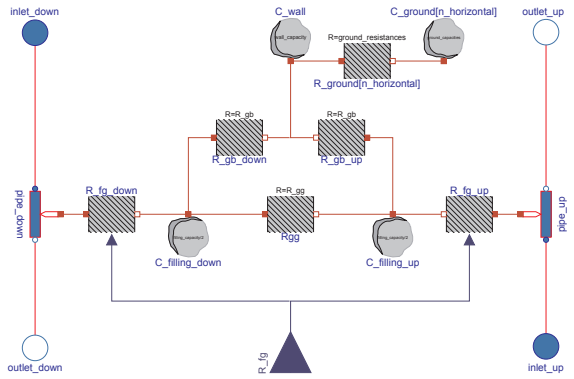

Fig. 3. BTES cross section model (left: schematic, right: simulation model).

resistance. The equation was based on the Nusselt correlation for turbulent pipe flow. Nu_{nom} was set to 160 and $\dot{m}_{nom}$ was set to 0.8 kg/s.

$$Nu = Nu_{nom} \cdot \left(\frac{\dot{m}}{\dot{m}_{nom}} \right)^{0.8} \quad (14)$$

The boreholes of the IHCS were filled with groundwater. Natural convection inside groundwater-filled boreholes may have a significant influence on the performance of the ground heat exchanger [36]. Nusselt correlations for this natural convection were published by Spitler et al. [37] and Holmberg et al. [38]. Holmberg et al. investigated a ground heat exchanger similar to the ones of the IHCS and found the Nusselt number to be 6.4 during heat injection and 3.68 during heat extraction. A constant Nusselt number of 5.0 was used for the system simulations.

One-dimensional, radial, heat transfer was modeled in the cylindrical ground shells. The capacities and heat transfer coefficients corresponded to the geometry of each shell element according to [39]. The conductivity of the ground at the location of the IHCS is about 2.75 with a standard deviation of 0.65 according to Ramstad et al. [40]. The pipe segments were connected from each cross section to the next, but no thermal connection was modeled between the thermal capacities of the cross sections. Nevertheless, the horizontal discretization of the ground was found to be more important than the vertical discretization. Therefore, the horizontal discretization was set to 30 and the vertical discretization was set to 4 as shown in Table 3.

The initial temperature of the ground had to be defined in the model. However, the temperature distribution was unknown, since the IHCS had been in operation before 2015. It was assumed that there was heat left to be extracted from previous charging of the BTES. A linear profile in radial direction was assumed for the initial temperature, ranging from 25 °C for borehole and pipe to 10 °C for the outmost ground capacity.

Arranging boreholes in a pattern and connecting them in series can increase the performance of a BTES, as described for example in [41]. The boreholes of the IHCS were drilled in a rectangular pattern with a rather large distance of eight meters and were connected in parallel. In the model, cylindrical shells were used and a diameter of nine meters was chosen to give a similar effective ground area between the boreholes. The assumed homogeneity of the ground led to identical temperatures for the outmost ground shell of all boreholes. Thus, no heat was transferred between boreholes in the model.

The BTES was used as seasonal thermal energy storage. However, the short-term response of the ground heat exchangers can also play an important role for system performance [42–44]. Beier et al. published experimental data for a 52–hour charging period of a grouted single U-tube borehole heat exchanger surrounded by wet sand [45]. The short-term response of the BTES model developed in this study was validated against this experimental data set. The experimental setup was imitated by changing the model specifications in Table 3 to the respective values of the experimental setup and using the measured inlet temperature and mass flow rate as simulation input. The simulated outlet temperature, the average wall temperature, and three average ground temperatures at different distances from the borehole were compared to the measured values from [45]. The developed model showed very good agreement with the measurement data as shown in Fig. 4.

3.1.4. Solar collector model

The installed collectors were flat plate solar collectors. The net heat flow rate for each collector ($\dot{Q}_{col}$) was calculated with Eq. (15), based on the widely used European Standard EN 12975-1:2006.

$$\dot{Q}_{col} = A_{col} \cdot [R \cdot \eta_{opt} - a_1 \cdot (T_{col} - T_{amb}) - a_2 \cdot (T_{col} - T_{amb})^2] \quad (15)$$

The solar radiation (R) was an input signal to the model and T_{col} was the average fluid temperature in the collector. For each installed collector, the effective area (A_{col}) was 1.9 m^2, the optical efficiency (η_{opt}) was 0.773, and the linear and quadratic heat loss coefficients (a_1 and a_2, respectively) were 3.676 W/(m^2·K) and 0.0143 W/(m^2·K^2). The fluid filling in each collector was 1.2 L.

Collectors in series were modeled individually with respective flow connections. The interaction of parallel collectors was neglected and distributing headers were not modeled. Herrero López et al. compared a simple collector model with a more detailed model and measurement data. They concluded that a simple model, like the one developed for this study, is well suited for system analysis [46].

3.1.5. Storage tank model

Storage tanks were modeled by dividing the fluid in the tanks into several horizontal layers. These layers were assumed to have a uniform temperature and the flow inside the tank was one-dimensional with the inlet and outlet of the tanks at the tank top and bottom (multi-node model as explained by Dumont et al. [47]). Internal heat exchange between the layers and heat transfer to the ambient were neglected.

The storage tank model for the solar collector loop was extended with an internal counterflow heat exchanger. The fluid in the heat exchanger was divided into the same number of layers as the storage tank with the same assumptions of uniform temperature and one-dimensional flow. The heat exchanger fluid was thermally connected to the tank fluid with a constant conductivity in each layer. The conductivity value was scaled based on the total effective area of the solar collectors. 100 W/K per m^2 of collector area was found to be a reasonable value. The volume of the solar storage tank and its internal heat exchanger were also scaled with a value of 15 and 1.5 dm^3 per m^2 of collector area, respectively.

3.1.6. Substation model

A substation model was developed, which represented the connection of the IHCS to the buildings. A heat exchanger transferred heat between the fluid loop of the IHCS and the building side. A fixed return temperature on the building side was assumed and pumps on each side were controlled to achieve the required heat flow rate. The heat flow rate was an input signal to the model. In the system model, these signals were based on the measured heating and cooling demands.

The IHCS was not designed to cover all heating demands. DH was used to cover peak demands for space heating and to lift the temperature of the DHW to the desired level. The amount of DH import was calculated based on the remaining heating demand.

The IHCS had separate heat exchangers for each building and demand type, which were connected to the heating and cooling loops in parallel. These parallel heat exchangers were modeled as one heat exchanger with the same total area and average heat transfer coefficient.

3.1.7. Ice thermal energy storage model

The ITES had a capacity of around 400 kWh. A nightly charging profile was created based on the nominal cooling capacity of the charging heat pump. Charging started at midnight with a constant cooling rate of 87 kW until the 400 kWh were reached. This charging profile was used as input signal for a substation model, which was

Table 3
BTES model specifications used for system simulations.

Parameter	Value	Unit	Parameter	Value	Unit
Borehole depth	300	m	Number of boreholes	62	–
Borehole diameter	0.14	m	Vertical discretization	4	–
Ground diameter	9	m	Horizontal discretization	30	–
Ground density	2600	kg/m^3	U-tube diameter	0.04	m
Ground heat capacity	850	J/(kg·K)	U-tube conductivity	0.42	W/(m·K)
Ground conductivity	2.75	W/(m·K)	Nusselt number inside borehole	5	–

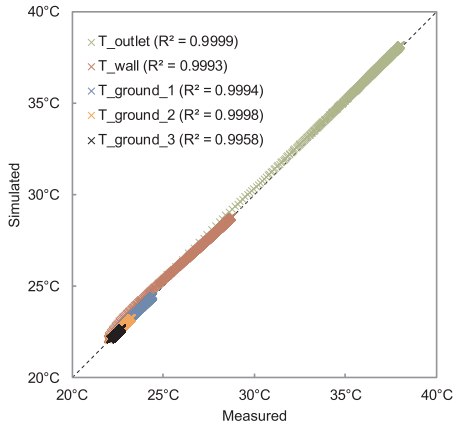

Fig. 4. BTES model validation against experimental data from [45].

connected to the low temperature loop of the IHCS and thus represented the charging of the ITES. A discharging profile with a maximum of 100 kW cooling rate was also created. The 400 kWh were distributed over seven hours (25 kW, 50 kW, 75 kW, 100 kW, 75 kW, 50 kW, and 25 kW) and the peak discharge hour was matched with the maximum space cooling demand each day. This profile was then deducted from the space cooling demand signal during cooling mode to represent the discharging of the ITES.

3.2. System model

The system model consisted of connected component models and a control system. All components and fluids were specified as close as possible to manufacturer specifications. Hourly values for all heating and cooling demands as well as ambient temperature and solar radiation were input data for the system model. Spline interpolation was used to create continuous signals between the hourly data points. The required CPU time for a one-year simulation was around 70 s with an Intel® Core™ i7-6700 K (4 GHz) and 64 GB RAM. The model is shown in Fig. 5.

HP1/2 in Fig. 5 represented two parallel heat pumps of the same type. These were modeled as one unit because their efficiencies were very similar. Pipes connecting the components of the IHCS were not modeled because specifications were not available. Distribution heat losses from the IHCS were thus not calculated. However, the losses from the distribution systems of the buildings were included in the measured demands.

The calculated electricity use of the system consisted of three parts: the electricity use of the heat pumps (El_{HPs}), the electricity use of the circulation pumps (El_{pumps}), and a constant term (El_{const}). El_{HPs} was calculated by integrating the simulated power of each heat pump (P_{HP}). The circulation pump models did not calculate pump power because pressure drops could not be calculated realistically due to missing pipe specifications. The relatively constant electricity use of all auxiliary systems was also unknown. Therefore, a system-level approach was chosen to calculate El_{pumps} and El_{const}. El_{pumps} was assumed proportional to the squared volume flow rate ($\dot{V}$) of the circulation pumps and was multiplied with a constant flow-to-power coefficient (FtP). FtP and El_{const} were found by calibrating the monthly calculated electricity use to the measured values with Eq. (16).

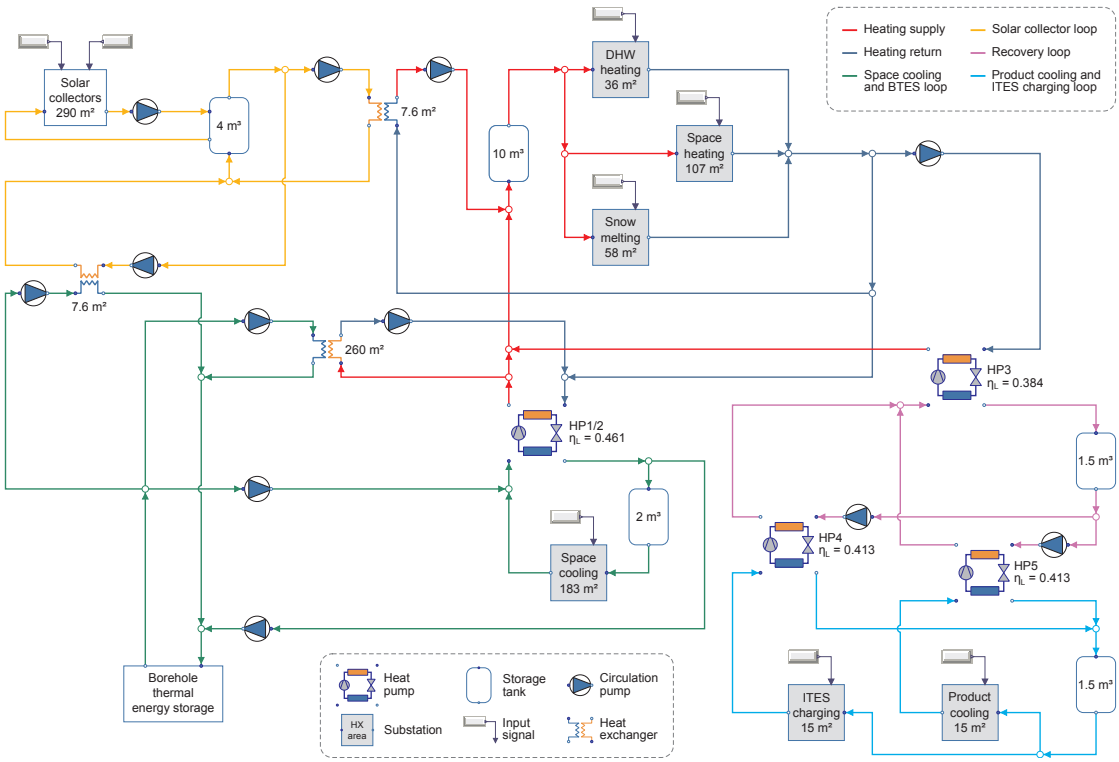

Fig. 5. System model with selected specifications.

$$\min \sum_{i=1}^{12} \left[El_{meas} - \left(El_{HPs} + FtP \cdot \sum_{El^{pumps}} \dot{V}^2_{pumps} + El_{const} \right) \right]^2, \; i = \text{month of the year} \quad (16)$$

Eq. (16) gave a value of $70.65e^6$ for FtP and a constant electricity use of 30.5 kW. The monthly values for electricity use after the calibration are shown in Fig. 6.

3.3. System control

The IHCS was equipped with a simple control system. The heat pumps received stepwise control signals to activate/deactivate their parallel circuits and compressor stages. These step signals were based on storage tank temperatures. The circulation pumps were controlled based on pressure difference setpoints or temperature setpoints. The storage tanks were only used as buffers.

In the system model, the heat pumps were controlled continuously since the individual compressor stages were not included in the heat pump model. The circulation pumps were controlled with PI-controllers based on temperature setpoints. The PI-controller outputs were limited to avoid unrealistically high mass flow rates.

The two operation modes of the IHCS, heating mode and cooling mode, are explained in the sections below. The real system required some downtime for a mode switch due to manual valve adjustments. Therefore, only one mode switch was performed between heating and cooling season. In the system model, this downtime was neglected and several mode switches were allowed. Models from the library «StateGraph», which is included in the «Modelica Standard Library» [28], were used to switch between modes based on the storage tank temperatures. A mode switch involved the activation/deactivation of the BTES circulation pumps, a change in heating supply temperature setpoint, and different control strategies for the solar collectors and the ITES.

3.3.1. Heating mode

In heating mode, the outlet temperature of HP1/2 on the condenser side was set to equal the heating supply temperature of 55 °C. The outlet temperature on the evaporator side of HP1/2 was controlled by the BTES pump with the space cooling supply temperature of 6 °C as setpoint. Rule-based control was applied for the solar collector loop. The solar storage tank could be used for heating supply and BTES charging. Heating supply was prioritized with a floating collector outlet temperature 10 °C above solar storage tank top temperature, similar to [48]. If the temperature in the solar storage tank was too low for heating supply, the BTES was charged. The ITES was not used in heating mode.

When the space cooling demand increased, less heat had to be extracted from the BTES. At some point, the BTES was not needed as heat source and the temperature in the cooling storage tank increased. When the average temperature in the cooling storage tank was higher than 10 °C, a mode switch was triggered to ensure that the space cooling demand could be covered.

3.3.2. Cooling mode

In cooling mode, the outlet temperature of HP1/2 on the evaporator side was set to equal the space cooling supply temperature of 6 °C. The outlet temperature on the condenser side of HP1/2 was controlled by the BTES pump with a reduced heating supply temperature of 51 °C as setpoint. The solar collectors were only used for BTES charging in cooling mode. The ITES was used to reduce space cooling peak demands and was charged by HP4 during the night.

When the heating demands increased, less heat was available to be injected into the BTES. At some point, the BTES was not needed as heat sink and the temperature in the heating storage tank decreased due to the increasing heat demands. When the average temperature in the heating storage tank was lower than 47 °C, a mode switch was triggered to ensure that the heating demands could be covered.

3.4. System performance and sensitivity analysis

Two COPs were defined to measure system performance: COP_{system} and $COP_{system+storage}$. These were evaluated at the end of each one-year simulation. COP_{system} was the ratio of the heating and cooling energy delivered by the IHCS to the electricity used by the IHCS as shown in Eq. (17). The amount of imported heat from the DH system was not included.

$$COP_{system} = \frac{\text{Heating delivered} + \text{Cooling delivered}}{\text{Electricity used}} \quad (17)$$

$COP_{system+storage}$ was similar to COP_{system} but included the annual heat balance of the BTES (heat injected – heat extracted) in the numerator as shown in Eq. (18). The heat balance was included because it affected long-term operation. $COP_{system+storage}$ thus gave a more holistic indication of system performance by penalizing unsustainable operation.

$$COP_{system+storage} = \frac{\text{Heating delivered} + \text{Cooling delivered} + \text{Heat balance BTES}}{\text{Electricity used}} \quad (18)$$

A sensitivity analysis was performed to evaluate the influence of selected input parameters on the system performance. Parameters were changed one at a time and the difference in COP compared to the base case scenario was calculated. A 20% change was chosen as standard value. However, some parameters were varied by a different percentage as shown in Table 4. The values for heating and cooling supply temperature were chosen to give a 20% change in the temperature difference in the heat exchanger of the space heating and space cooling substations. The values for the return temperatures in the substations were also chosen to change this temperature difference by 20%.

The number of solar collectors was changed during the sensitivity analysis. The number of serial collectors was set to five and the number of parallel collectors was changed. The storage tank with internal heat exchanger was scaled based on the total collector area as explained in Section 3.1.5. The area of the heat exchangers in the solar collector loop were also scaled to avoid bottlenecks. The maximum mass flow rate of the BTES pump was linearly scaled when the number of boreholes was changed.

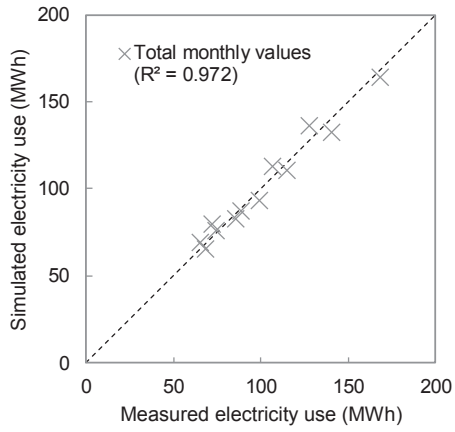

Fig. 6. Calibration of electricity use in system model.

Table 4
Parameter values used for sensitivity analysis.

Parameter	Unit	Lower value	Base case	Upper value	Change	Comment
Numerical discretization						
Factor storage tanks	–	0.8	1.0	1.2	20%	
Factor BTES	–	0.8	1.0	1.2	20%	
Uncertain inputs						
BTES: Nusselt number	–	3.5	5.0	6.5	30%	According to [38]
BTES: Initial temp. (near)	°C	22	25	28	12%	3 °C chosen instead of percentage
BTES: Initial temp. (far)	°C	7	10	13	30%	
BTES: Ground conductivity	W/(m·K)	2.10	2.75	3.40	24%	According to [40]
η_L HP1/2	–	0.410	0.461	0.512	11%	According to manufacturer specifications (all HPs changed at once)
η_L HP3	–	0.346	0.384	0.422	10%	
η_L HP4&5	–	0.339	0.413	0.487	18%	
Exponent q in HX	–	0.504	0.630	0.756	20%	Eq. (7)
Coefficient FtP	–	$56.52e^6$	$70.65e^6$	$84.78e^6$	20%	Eq. (16)
Assumptions						
Space heating return temp.	°C	37	40	43	8%	Secondary side changed to give 20% change in ΔT
Snow melting return temp.	°C	13	20	27	35%	
Space cooling return temp.	°C	13.2	15.0	16.8	12%	
Product cooling return temp.	°C	-5.2	-4.0	-2.8	30%	
Heating/cooling demands						
Demand factor all	–	0.8	1.0	1.2	20%	All demands multiplied
Demand factor heating	–	0.8	1.0	1.2	20%	Only heating demands
Demand factor cooling	–	0.8	1.0	1.2	20%	Only cooling demands
Control setpoints						
Mode switch ΔT	°C	3.2	4.0	4.8	20%	Heating/cooling mode
Heating supply temp.	°C	52	55	58	5%	Primary side changed to give 20% change in ΔT
Space cooling supply temp.	°C	4.2	6.0	7.8	30%	
System design						
Factor HX area	–	0.8	1.0	1.2	20%	All areas multiplied
Number of solar collectors	–	110	140	170	21%	
Number of boreholes	–	50	62	74	19%	

4. Results

The results from the system analysis are described in this chapter. First, the base case scenario results are analyzed and compared to the measurement data. Afterwards, the results from the sensitivity analysis are presented and solutions to avoid performance degradation are suggested.

4.1. Base case scenario

Daily values for the measured heating and cooling demands are shown in Fig. 7.

Space heating and cooling showed typical seasonal variations, while the DHW heating and product cooling depended on the users. Snow melting depended on temperature and precipitation and thus showed large daily variations. These demands were covered by the IHCS. Daily amounts of electricity and DH import used for this are shown in Fig. 8.

It can be seen from Figs. 7 and 8 that higher demands led to higher energy use. The main source of electricity use were the heat pumps, which had a share of 69% for the base case scenario. To recall, the electricity use of single components was not measured, so no reference value for this simulation result was available. The simulated daily values for electricity use and DH import showed good agreement with the measured values as shown in Fig. 8. However, large differences occurred at the beginning of the year during peak heating demands. For the real system, these peak demands led to high amounts of DH import (blue line) because the heat pumps were only able to cover a small share of these demands. In the simulated system, the heat pumps covered a larger share, which led to less simulated DH import (yellow line), but more electricity use (gray line vs. orange line). The heat pump models did not exceed the maximum power listed in the manufacturer specifications, so the overestimation of electricity use was most likely

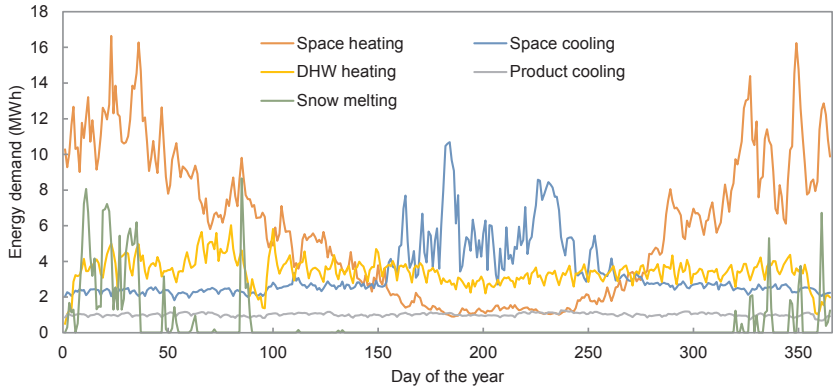

Fig. 7. Measured daily heating and cooling demands.

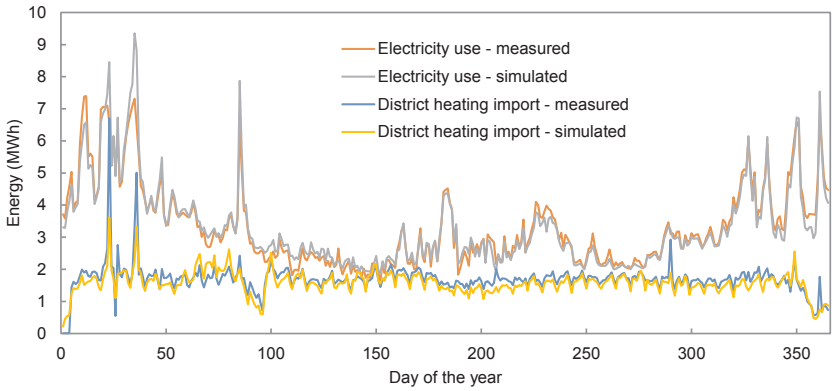

Fig. 8. Daily energy use of the integrated heating and cooling system.

due to the calculated pumping power. The BTES pumps accounted for 58% of the total pumping power for the base case scenario simulations, so a more detailed model of the BTES loop might improve these results.

Integral annual energy use values and R^2-values for hourly and daily results are shown in Table 5 for all the demands, DH import, and electricity use.

As explained in Section 2.2, measurements for the BTES and the solar collectors were unfortunately not available. The simulated daily heat balances for both components are shown in Fig. 9.

Fig. 9 clearly shows that the BTES was used as heat source during winter and as heat sink during summer, with a simulated annual heat balance of −469 MWh. The maximum heat flow rates were −856 kW during winter and 946 kW during summer. This corresponded to specific heat flow rates of −46 and 51 W/m of borehole, respectively. This is reasonable according to [49], where 50–80 W/m are listed as expected peak values.

The simulated amount of collected solar heat was 91 MWh, see Fig. 9. This corresponded to 2.6% of the total heating demands, which showed that the solar collectors played a minor role for the performance of the IHCS.

Monthly values for COP_{system} ranged from 3.3 to 4.2 for the base case scenario, with an annual average of 3.77. The annual average for $COP_{system+storage}$ was 3.38. These values were similar to the ones from other studies described in the introduction.

4.2. Sensitivity analysis

The results from the sensitivity analysis showed the relative change of each COP when a parameter value was increased or decreased, see Fig. 10.

The most important results from the sensitivity analysis are described below.

Increasing the numerical discretization had a negligible effect on the COPs. A reduction in discretization of the BTES led to a decrease of 0.5%, which shows that the base case scenario values were reasonable.

Some of the uncertain inputs influenced the COPs significantly. The heat pumps were the main electricity users, which is why their efficiency had a strong influence, especially on COP_{system}, see Fig. 10 (left). The initial temperature profile and the conductivity of the ground also showed strong influence on the COPs, while the Nusselt number for natural convection inside the borehole and the heat exchanger exponent q used in Eq. (7) were less important.

The return temperatures from the buildings' heating and cooling systems were assumed constant in this study. The influence of the assumed temperatures depended on the total amount of delivered energy, which is why the main demand (space heating) had the strongest influence on the COPs. In reality, the return temperatures can show larger variations than in this sensitivity study. Therefore, a more realistic calculation of the return temperatures could show larger influence on the system performance and should be included in future work. This is especially desirable for the space heating substation where the largest amount of heat was transferred.

The heating and cooling demands were based on the available measurements. The cooling demands were heat sources for the IHCS and the heating demands were heat sinks. Therefore, the difference between the total heating demand and the total cooling demand highly influenced the annual heat balance of the BTES. Changing all demands simultaneously thus altered the BTES balance less than changing only heating or cooling demands. This is why changing all demands showed less effect than changing only heating or cooling demands, especially for $COP_{system+storage}$.

The control setpoint for a mode switch had insignificant influence on the system performance due to the small number of mode switches during a year. The supply temperature setpoints changed the heat pump outlet temperatures and thus affected both the temperature lift of the heat pumps and the mass flow rates of the circulation pumps. Especially an increase in space cooling supply temperature showed strong influence on the COPs.

The system design parameters showed little effect on the COPs. Only a change in the number of boreholes changed the COPs by more than 1%. This change in COP was mainly due to the difference in required pumping power. The BTES outlet temperature changed slightly when the number of boreholes was changed, which in turn led to a small

Table 5
Comparison of measured and simulated values.

	Measured MWh	Simulated MWh	Difference MWh	R^2 hourly –	R^2 daily –
Space heating from IHCS	2096	2104	8	0.993	0.998
Space heating from DH	13	5	-8	0.454	0.812
Space cooling from IHCS	1213	1211	-2	0.928	0.997
DHW heating from IHCS	648	682	35	0.867	0.897
DHW heating from DH	607	572	-35	0.629	0.723
Product cooling from IHCS	372	372	0	0.972	1.000
Snow melting from IHCS	198	198	0	0.998	1.000
Electricity use IHCS	1212	1212	0	0.849	0.942

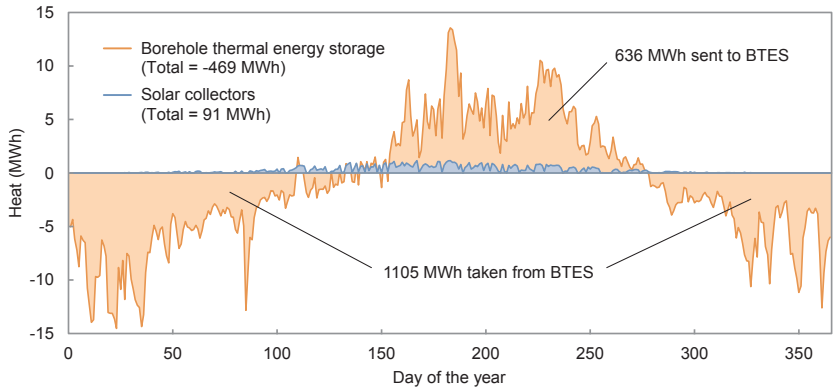

Fig. 9. Simulated daily heat balance for BTES and solar collectors.

change in the heat pump's COP. However, the annual heat balance of the BTES did not change significantly, since almost the same amounts of energy had to be injected/extracted each day.

4.3. Long-term operation analysis and system performance degradation

The simulated annual heat balance of the BTES was −469 MWh for the base case scenario due to the high heating demands and the insufficient solar charging, see Fig. 9. Two solutions to avoid a negative heat balance were analyzed in this study: the installation of more solar collectors and the increase of DH import for DHW heating.

4.3.1. Case I: More solar collectors

For this case, the number of solar collectors was increased until the annual heat balance of the BTES was close to zero. To achieve this balanced BTES, the number of collectors had to be increased from 140 to 830. This increased the simulated amount of collected solar heat from 91 MWh, as shown in Fig. 9, to 565 MWh. There is free roof area on some of the buildings, but installation possibilities and costs were not analyzed further.

4.3.2. Case II: More DH import

For this case, the mass flow from the IHCS to the DHW heating

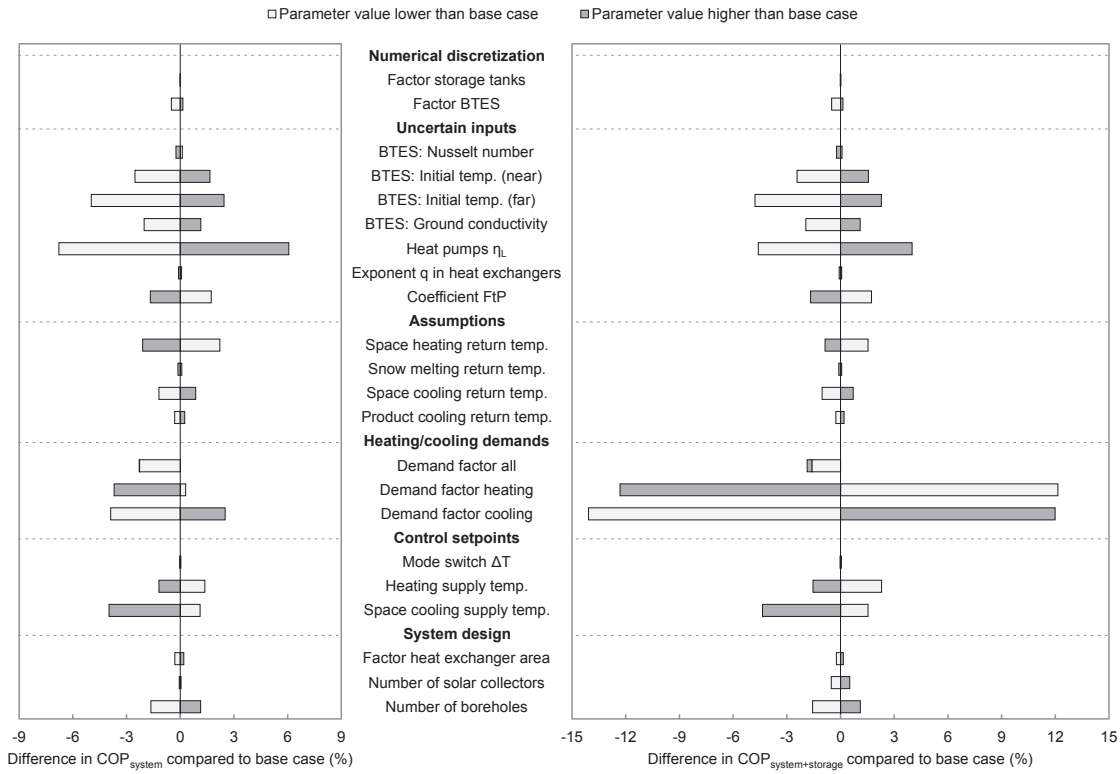

Fig. 10. Sensitivity analysis results.

substation was reduced to get a balanced BTES. This mass flow reduction led to an increased amount of DH import for DHW heating from 572 MWh, as shown in Table 5, to 1122 MWh. The mass flow was reduced by 55% during cooling mode and by 100% during heating mode. DHW heating was thus only covered by the IHCS during cooling mode, when excess heat was available. The simulated electricity use decreased from 1212 MWh, as shown in Table 5, to 1099 MWh for this case.

4.3.3. Long-term operation analysis

The COPs for the balanced cases and the unbalanced base case scenario for five-year operation are shown in Fig. 11. The input data for the year 2015 was repeated for this analysis.

The difference between the COPs in Fig. 11 is that $COP_{system+storage}$ (right) included the annual heat balance of the BTES, see Eqs. (17) and (18). This balance was close to zero for the balanced cases, which is why their values for both COPs were nearly identical. The COPs decreased slightly from the first year to the second, most likely due to the initial temperature profile in the BTES, and remained constant afterwards. The COPs for the base case scenario decreased from year to year and thus showed continuous plant degradation. This degradation was mainly due to the decreasing average ground temperature, which led to higher pumping power for the BTES pump for heat extraction during heating mode as shown in Fig. 12.

The BTES pump mass flow rate in cooling mode was much lower than in heating mode due to the larger temperature difference during heat injection. The long-term mass flow rate decrease during cooling mode was therefore insignificant.

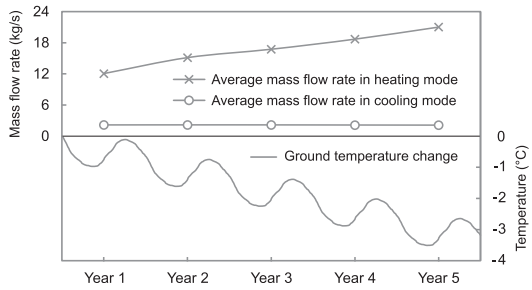

Fig. 12. Long-term operation of BTES pump.

5. Discussion

The aim of this study was a system level analysis of an existing IHCS with focus on the long-term thermal energy storage. Component models were therefore kept relatively simple and a validation on component level was out of scope. A flow coefficient was defined based on monthly electricity use, which led to a satisfactory correlation between simulated and measured system performance, see Fig. 8 and Table 5. However, the electricity use of the IHCS was overestimated during a peak heating period in the beginning of the year. Since the heat pump models did not exceed the maximum power listed in the manufacturer specifications, this overestimation was most likely due to the calculated pumping power. The BTES pumps accounted for a large share of the pumping power, so a more detailed model of the BTES loop could improve the reliability of the results. However, this was impeded by lacking measurements and specifications.

The sensitivity analysis was performed by changing one parameter at a time. A change of 20% was used for most parameters, but some exceptions were made. The efficiency of the heat pumps was varied within manufacturer specifications. For the supply and return temperatures, the temperature difference in the main heat exchanger was changed by 20% for a fair comparison. However, the return temperatures from the buildings' heating and cooling systems, which were assumed constant in this study, can vary much more in reality and thus show more influence on the system performance than in the sensitivity analysis. A more detailed calculation of the return temperatures would therefore be desirable.

Changing the heat exchanger area did not influence the system performance significantly. An area reduction of 20% reduced the COPs by less than 1%, see Fig. 10. This could either be due to the lumping of the parallel heat exchangers in the system model, as explained in Section 3.1.6, or an oversized design. Most heat exchangers were dimensioned with an average temperature difference of 2 °C, which led to relatively large heat exchanger areas. Confirming a possible oversizing by simulations with parallel units was outside the scope of this work.

Due to the cold climate in Norway, the building complex required more energy for heating than for cooling, see Fig. 2. The insufficient charging of the BTES during summer led to a simulated annual BTES heat balance of −469 MWh, see Fig. 9. Heat losses from components, pipes, and storages were neglected in this study. Including these losses would have led to a higher imbalance and thus to an even faster performance degradation than shown in Fig. 11.

The solar collectors were a minor component of the IHCS due to the small number of installed collectors. They showed little effect on the system performance in the sensitivity analysis due to the low base value, see Fig. 10. However, a significant increase in the number of collectors could lead to a balanced BTES and thus improve the long-term operation of the system, see Fig. 11. The calculation of installation costs and an economic evaluation were outside the scope of this work.

Another possibility to avoid performance degradation was increased DH import. This case was analyzed and showed favorable long-term operation of the IHCS with the defined COPs due to reduced electricity use, see Fig. 11. However, the increase in DH import exceeded the reduction in electricity use significantly and would thus most likely lead to increased operation costs. The calculation of operation costs with varying prices for electricity and DH was outside the scope of this work.

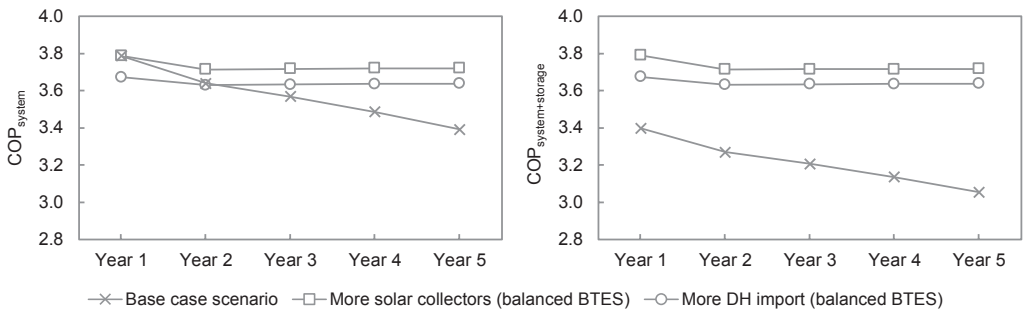

Fig. 11. COPs for long-term operation.

6. Conclusions

Dynamic simulations in Modelica were successfully applied to model an existing IHCS in Oslo, Norway. The simulation time for a one-year simulation was around 70 s despite the system's complexity. The short simulation time enables further analyses, e.g. parameter studies or dynamic optimization.

The system model was calibrated and a sensitivity analysis was performed. The results showed that the efficiency of the heat pumps and the annual heat balance of the BTES had strong influence on the system performance. The simulations showed a negative heat balance of the BTES (−469 MWh), which led to decreasing long-term performance. The $COP_{system+storage}$ was defined, which included this heat balance and thus gave a better indication of long-term performance even for a one-year simulation. This COP is therefore recommended to be used for one-year analyses of systems with long-term thermal storage.

Sustainable operation of the IHCS was possible by increasing the number of solar collectors from 140 to 830 or by importing more heat from the local DH system. However, the annual heat balance and system performance depended on the total heating and cooling demands, which may vary from year to year, as well as control setpoints, which were kept constant in this study. Future work could therefore include the analysis of more recent measurement data or improvement suggestions for the control strategy of the system. Model refinement, e.g. a more detailed calculation of the pumping power and/or the return temperatures from the building side, as well as an economic evaluation could also be included in future analyses.

Acknowledgements

The authors gratefully acknowledge the financial support from the Research Council of Norway, Norway for the project INTERACT (EnergiX program, grant agreement number 228656/E20) and FME HighEFF (grant agreement number 257632/E20).

References

[1] European Union, Directive 2010/31/EU of the European Parliament and of the Council of 19 May 2010 on the energy performance of buildings, Official J. Eur. Union, 2010, L 153, pp. 13–35.
[2] International Energy Agency, Heating and Cooling Technologies, in Transition to Sustainable Buildings: Strategies and Opportunities to 2050, International Energy Agency, 2013.
[3] H. Lund, et al., 4th Generation District Heating (4GDH): Integrating smart thermal grids into future sustainable energy systems, Energy 68 (2014) 1–11, https://doi.org/10.1016/j.energy.2014.02.089.
[4] Z.X. Jing, et al., Modelling and optimal operation of a small-scale integrated energy based district heating and cooling system, Energy 73 (2014) 399–415, https://doi.org/10.1016/j.energy.2014.06.030.
[5] C. Marguerite, et al., Simulation based multi-criteria evaluation of design scenarios for an industrial waste heat based micro district heating network supplying standard and low-energy buildings, Energy Procedia 116 (2017) 128–137, https://doi.org/10.1016/j.egypro.2017.05.061.
[6] N. Zhu, et al., Recent research and applications of ground source heat pump integrated with thermal energy storage systems: A review, Appl. Therm. Eng. 71 (1) (2014) 142–151, https://doi.org/10.1016/j.applthermaleng.2014.06.040.
[7] M. Lanahan, P. Tabares-Velasco, Seasonal thermal-energy storage: a critical review on BTES systems, modeling, and system design for higher system efficiency, Energies 10 (6) (2017) 743, https://doi.org/10.3390/en10060743.
[8] T. You, et al., A new solution for underground thermal imbalance of ground-coupled heat pump systems in cold regions: Heat compensation unit with thermosyphon, Appl. Therm. Eng. 64 (1) (2014) 283–292, https://doi.org/10.1016/j.applthermaleng.2013.12.010.
[9] P. Bayer, M. de Paly, M. Beck, Strategic optimization of borehole heat exchanger field for seasonal geothermal heating and cooling, Appl. Energy 136 (2014) 445–453, https://doi.org/10.1016/j.apenergy.2014.09.029.
[10] J. Luo, et al., Heating and cooling performance analysis of a ground source heat pump system in Southern Germany, Geothermics 53 (2015) 57–66, https://doi.org/10.1016/j.geothermics.2014.04.004.
[11] A. Capozza, A. Zarrella, M. De Carli, Long-term analysis of two GSHP systems using validated numerical models and proposals to optimize the operating parameters, Energy Build. 93 (2015) 50–64, https://doi.org/10.1016/j.enbuild.2015.02.005.
[12] Y. Nam, et al., Study on the performance of a ground source heat pump system assisted by solar thermal storage, Energies 8 (12) (2015) 12365, https://doi.org/10.3390/en81212365.
[13] Z. Han, et al., Numerical simulation of solar assisted ground-source heat pump heating system with latent heat energy storage in severely cold area, Appl. Therm. Eng. 28 (11) (2008) 1427–1436, https://doi.org/10.1016/j.applthermaleng.2007.09.013.
[14] X.Q. Zhai, et al., A review for the applications and integrated approaches of ground-coupled heat pump systems, Renew. Sustain. Energy Rev. 15 (6) (2011) 3133–3140, https://doi.org/10.1016/j.rser.2011.04.024.
[15] F.M. Rad, A.S. Fung, W.H. Leong, Feasibility of combined solar thermal and ground source heat pump systems in cold climate, Canada, Energy Build. 61 (2013) 224–232, https://doi.org/10.1016/j.enbuild.2013.02.036.
[16] A. Arteconi, et al., Experimental evaluation and dynamic simulation of a ground coupled heat pump for a commercial building, Int. J. Energy Res. 37 (15) (2013) 1971–1980, https://doi.org/10.1002/er.3059.
[17] H. Li, L. Sun, Y. Zhang, Performance investigation of a combined solar thermal heat pump heating system, Appl. Therm. Eng. 71 (1) (2014) 460–468, https://doi.org/10.1016/j.applthermaleng.2014.07.012.
[18] A. Carotenuto, R.D. Figaj, L. Vanoli, A novel solar-geothermal district heating, cooling and domestic hot water system: Dynamic simulation and energy-economic analysis, Energy 141 (2017) 2652–2669, https://doi.org/10.1016/j.energy.2017.08.084.
[19] S.H. Razavi, R. Ahmadi, A. Zahedi, Modeling, simulation and dynamic control of solar assisted ground source heat pump to provide heating load and DHW, Appl. Therm. Eng. 129 (2018) 127–144, https://doi.org/10.1016/j.applthermaleng.2017.10.003.
[20] R. Sangi, et al., Modeling and simulation of the heating circuit of a multi-functional building, Energy Build. 110 (2016) 13–22, https://doi.org/10.1016/j.enbuild.2015.10.027.
[21] A. Maccarini, et al., Energy saving potential of a two-pipe system for simultaneous heating and cooling of office buildings, Energy Build. 134 (2017) 234–247, https://doi.org/10.1016/j.enbuild.2016.10.051.
[22] M. Wetter, C. van Treeck, IEA EBC annex 60: new generation computing tools for building and community energy systems, Int. Energy Agency (2017).
[23] F. Liu, W. Zhu, J. Zhao, Model-based dynamic optimal control of a CO2 heat pump coupled with hot and cold thermal storages, Appl. Therm. Eng. 128 (2018) 1116–1125, https://doi.org/10.1016/j.applthermaleng.2017.09.098.
[24] E. Wang, et al., Performance prediction of a hybrid solar ground-source heat pump system, Energy Build. 47 (2012) 600–611, https://doi.org/10.1016/j.enbuild.2011.12.035.
[25] D. Rohde, et al. Documentation of an integrated thermal energy system for a building complex, in: 24th International Congress of Refrigeration, Yokohama, Japan, 2015.
[26] Norwegian Institute of Bioeconomy Research, Weather Data for Norway, Accessed May 2017; Available from: http://lmt.bioforsk.no/agrometbase/getweatherdata_new.php.
[27] Modelica Association Modelica® - A Unified Object-Oriented Language for Systems Modeling, Language Specification, 2017, Version 3.4.
[28] Modelica Association, Modelica Libraries, Accessed March 2018; Available from: https://www.modelica.org/libraries.
[29] I.H. Bell, et al., Pure and pseudo-pure fluid thermophysical property evaluation and the open-source thermophysical property library CoolProp, Ind. Eng. Chem. Res. 53 (6) (2014) 2498–2508, https://doi.org/10.1021/ie4033999.
[30] F.P. Incropera, et al., Heat exchangers, Fundamentals of Heat and Mass Transfer, John Wiley & Sons, 2007.
[31] L. Giraud, et al., Presentation, validation and application of the districtheating modelica library, in: 11th International Modelica Conference, Versailles, France, 2015. http://doi.org.10.3384/ecp1511879.
[32] J. Yang, A. Jacobi, W. Liu, Heat transfer correlations for single-phase flow in plate heat exchangers based on experimental data, Appl. Therm. Eng. 113 (2017) 1547–1557, https://doi.org/10.1016/j.applthermaleng.2016.10.147.
[33] H. Sofrata, Carnot and Lorenz cycles for dual absorption system, Wärme - und Stoffübertragung 28 (3) (1993) 107–116, https://doi.org/10.1007/BF01541106.
[34] P.A. Østergaard, A.N. Andersen, Booster heat pumps and central heat pumps in district heating, Appl. Energy 184 (2016) 1374–1388, https://doi.org/10.1016/j.apenergy.2016.02.144.
[35] D. Bauer, et al., Thermal resistance and capacity models for borehole heat exchangers, Int. J. Energy Res. 35 (4) (2011) 312–320, https://doi.org/10.1002/er.1689.
[36] J.D. Spitler, R. Grundmann, S. Javed, Calculation tool for effective borehole thermal resistance, in: 12th REHVA World Congress (CLIMA 2016), Aalborg, Denmark, 2016.
[37] J.D. Spitler, S. Javed, R.K. Ramstad, Natural convection in groundwater-filled boreholes used as ground heat exchangers, Appl. Energy 164 (2016) 352–365, https://doi.org/10.1016/j.apenergy.2015.11.041.
[38] H. Holmberg, et al., Numerical model for non-grouted borehole heat exchangers, Part 2 - evaluation, Geothermics 59 (2016) 134–144, https://doi.org/10.1016/j.geothermics.2014.11.002.
[39] P. Stephan, Fundamentals of heat transfer, VDI Heat Atlas, Springer, Berlin Heidelberg, 2010, pp. 15–30.
[40] R.K. Ramstad, et al., Thermal conductivity map of the Oslo region based on thermal diffusivity measurements of rock core samples, Bull. Eng. Geol. Environ. 74 (4) (2015) 1275–1286, https://doi.org/10.1007/s10064-014-0701-x.
[41] B. Sibbitt, et al., The performance of a high solar fraction seasonal storage district heating system – five years of operation, Energy Procedia 30 (2012) 856–865, https://doi.org/10.1016/j.egypro.2012.11.097.

[42] V. Partenay, et al., The influence of the borehole short-time response on ground source heat pump system efficiency, Energy Build. 43 (6) (2011) 1280–1287, https://doi.org/10.1016/j.enbuild.2011.01.009.
[43] F. Ruiz-Calvo, et al., Experimental validation of a short-term Borehole-to-Ground (B2G) dynamic model, Appl. Energy 140 (2015) 210–223, https://doi.org/10.1016/j.apenergy.2014.12.002.
[44] L. Xia, et al., Experimental investigation and control optimization of a ground source heat pump system, Appl. Therm. Eng. 127 (2017) 70–80, https://doi.org/10.1016/j.applthermaleng.2017.07.205.
[45] R.A. Beier, M.D. Smith, J.D. Spitler, Reference data sets for vertical borehole ground heat exchanger models and thermal response test analysis, Geothermics 40 (1) (2011) 79–85, https://doi.org/10.1016/j.geothermics.2010.12.007.
[46] S. Herrero López, et al., Dynamic modelling of a flat-plate solar collector for control purposes, in: 11th International Modelica Conference, Versailles, France, 2015. http://doi.org.10.3384/ecp15118419.
[47] O. Dumont, et al. Hot water tanks: How to select the optimal modelling approach?, in: 12th REHVA World Congress (CLIMA 2016), Aalborg, Denmark, 2016.
[48] F. Mosallat, et al., Modeling, simulation and control of flat panel solar collectors with thermal storage for heating and cooling applications, Procedia Comput. Sci. 19 (2013) 686–693, https://doi.org/10.1016/j.procs.2013.06.091.
[49] ASHRAE, Geothermal Energy, in: ASHRAE Handbook - Heating, Ventilating, and Air-Conditioning Applications (SI Edition), American Society of Heating, Refrigerating and Air-Conditioning Engineers, Inc, 2015.

Paper VI

D. Rohde, B. R. Knudsen, T. Andresen, and N. Nord (2019). "Dynamic optimization of control setpoints for an integrated heating and cooling system with thermal energy storages." *Submitted to Energy.*

Dynamic optimization of control setpoints for an integrated heating and cooling system with thermal energy storages

Daniel Rohde[a/b,*], Brage Rugstad Knudsen[b], Trond Andresen[b], Natasa Nord[a]

[a] Norwegian University of Science and Technology. Kolbjørn Hejes vei 1A, 7491 Trondheim, Norway

[b] SINTEF Energy Research. Sem Sælands vei 11, 7034 Trondheim, Norway

*Corresponding author. E-mail address: daniel.rohde@sintef.no (the author's affiliation was [a] during the work on this article, his current affiliation is [b])

Abstract

Energy systems for buildings and neighborhoods are expected to become more complex and flexible. Advanced control strategies are required to exploit the full potential of this flexibility and are especially important for systems with storages. In this study, the control of an integrated heating and cooling system for a building complex in Oslo, Norway, was analyzed. Focus was on the control setpoints for the main heat pumps, which had a total heating capacity of about 1 MW and were connected to thermal storage tanks. Previously developed simulation models of the system and its main components were made suitable for dynamic optimization with long time horizons. JModelica.org was used to find optimal control trajectories for the system with two different objectives. The first objective was to reduce the electricity use of the system and the second objective was to reduce the electricity costs of the system. The results showed that the electricity use of the system could be reduced by about 5 % for the analyzed year. The electricity costs could be reduced by about 5 to 11 % for the three analyzed winter months, depending on the variability of the electricity price and the size of the storage tanks.

Keywords: Heating and cooling system; Thermal energy storage operation; Heat pump; Optimization; JModelica.org

Nomenclature

Abbreviations

BAU	Business as usual
BTES	Borehole thermal energy storage
COP	Coefficient of performance
DH	District heating
DHW	Domestic hot water
GA	Genetic algorithm
HP	Heat pump
IHCS	Integrated heating and cooling system
ITES	Ice thermal energy storage
NLP	Nonlinear program
SC	Space cooling
SH	Space heating
SM	Snow melting
TES	Thermal energy storage

Symbols

e	Electricity price (NOK/MWh)
ε	Slack parameter (-)
$\dot{m}$	Mass flow rate (kg/s)
P	Power (W)
$\dot{Q}$	Heat flow rate (W)
t	Time (s)
T	Temperature (K)
v	Variability (-)
V	Volume (m^3)

Subscripts

Cond	Condenser
Evap	Evaporator
in	Inlet
L	Lorentz
out	Outlet
sec	Secondary

1 Introduction

Heating and cooling demands of buildings account for a large share of the world's energy use (European Union 2010, International Energy Agency 2013). The development of new buildings and integrated energy systems aims at reducing the environmental impact of these energy demands. Such future systems are expected to be more complex and flexible due to the inclusion of fluctuating energy sources (Lund, Werner et al. 2014) and thermal energy storage (TES) (Alva, Lin et al. 2018). Simulation and optimization are key methods for the analysis of these complex systems and their operation (Jorissen, Reynders et al. 2018, Schweiger, Heimrath et al. 2018). In particular, optimized control is essential to unlock the full potential of TES (Lu, Wang et al. 2015, Ooka and Ikeda 2015). However, TES increases the optimization problem complexity, especially when short- and long-term thermal storage are combined (Ikeda, Choi et al. 2017, Renaldi and Friedrich 2017).

Several studies on the optimization of TES operation can be found. Liu et al. optimized the charging of a hot and a cold storage tank with a dual-mode transcritical CO_2 heat pump using Dymola and a genetic algorithm (GA) (Liu, Zhu et al. 2018). Talebi et al. optimized a hybrid community district heating system with TES using TRNSYS and GenOpt (Talebi, Haghighat et al. 2019). Kamal et al. optimized TES control in buildings using EnergyPlus and a GA (Kamal, Moloney et al. 2019). Urbanucci et al. optimized a cogeneration system with TES using mixed integer linear programming and a GA (Urbanucci, D'Ettorre et al. 2019). Li et al. optimized the thermal management for industrial waste heat recovery with TES using a biogeography-based optimization algorithm (Li, Wang et al. 2019). All of these studies used derivative-free optimization algorithms, which are not the best choice for the optimization of TES system operation (Kuang, Zhang et al. 2018). On the contrary, Knudsen et al. have optimized TES operation for surplus-heat exchange in industry clusters using JModelica.org (Knudsen, Kauko et al. 2019). JModelica.org is an open-source optimization platform based on Modelica and uses a gradient-based optimization algorithm to solve a nonlinear programming (NLP) problem (Magnusson and Åkesson 2015).

In a previous study, an integrated heating and cooling system (IHCS) with TES for a small neighborhood in Oslo, Norway has been analyzed by means of dynamic simulations with Modelica models (Rohde, Andresen et al. 2018). It was shown that the control setpoints influenced the system performance. Therefore, the aim of this study was to optimize these setpoints with two main objectives. The first objective was to analyze the potential reduction of the system's electricity use with the currently installed components. The second objective was to analyze if the installation of larger storage tanks could lead to a reduction of the system's electricity costs. To this end, dynamic optimizations with JModelica.org were performed similar to the ones presented by Knudsen et al. However, the optimization models in this study contained both short- and long-term TES and a heat pump model. This increased the optimization problem complexity due to the different time-scales of the storages and the part load operation of the heat pump. In addition, relatively long time horizons were necessary to avoid

suboptimal usage of the long-term storage during optimization. This increased the optimization problem size significantly. The resulting NLP sizes in this study were therefore larger than the reported sizes in other studies using JModelica.org, e.g. (Belkhir, Cabo et al. 2015, Holmqvist and Magnusson 2016, Barsali, Giglioli et al. 2017, Cao, Acevedo et al. 2017, Sellberg, Nolin et al. 2018, Audino, Campanyà et al. 2019).

The remainder of this paper is structured as follows: a short description of the IHCS and brief results from the previous study are given in Section 2. In Section 3, the optimization approach is described in detail. Results from the optimizations are presented in Section 4, followed by a discussion in Section 5 and concluding remarks in Section 6.

2 Case study

2.1 System description

The IHCS was located in the Norwegian capital Oslo and delivered thermal energy for space heating (SH), domestic hot water (DHW) heating, snow melting (SM), space cooling (SC), and product cooling to several different building types. Snow melting was applied to the walkways between the buildings and product cooling was delivered to a food court. A simplified schematic of the IHCS is shown in Figure 1.

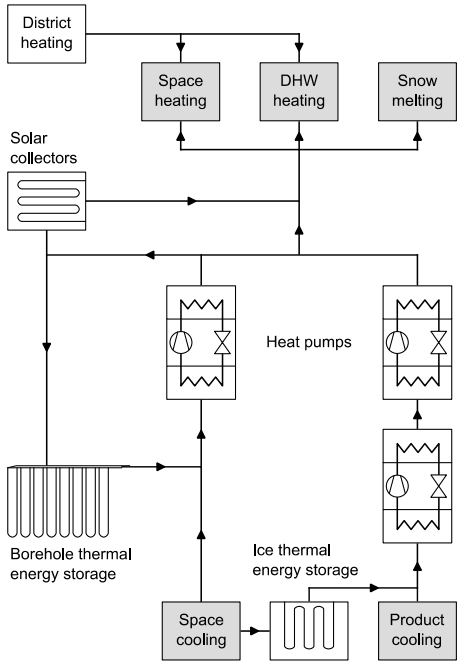

Figure 1. Simplified schematic of the integrated heating and cooling system

The main components of the IHCS were heat pumps (HPs), heat exchangers, solar collectors, storage tanks, ice thermal energy storage (ITES), and borehole thermal energy storage (BTES). The BTES was used as heat source during heating season and as heat sink during cooling season. The IHCS was designed to deliver heat at 50-55°C and was also connected to the city's district heating (DH) system, which delivered heat at a temperature of 85-120°C. A more detailed description of the IHCS can be found in (Rohde, Bantle et al. 2015) and (Rohde, Andresen et al. 2018).

The IHCS was equipped with a control and monitoring platform. Energy meters were installed to measure the delivered energy for heating and cooling in each connected building. Hourly values of these demands were retrieved and used as input data for all the simulations and optimizations. Aggregated daily demand data for the year 2015 are shown in Figure 2.

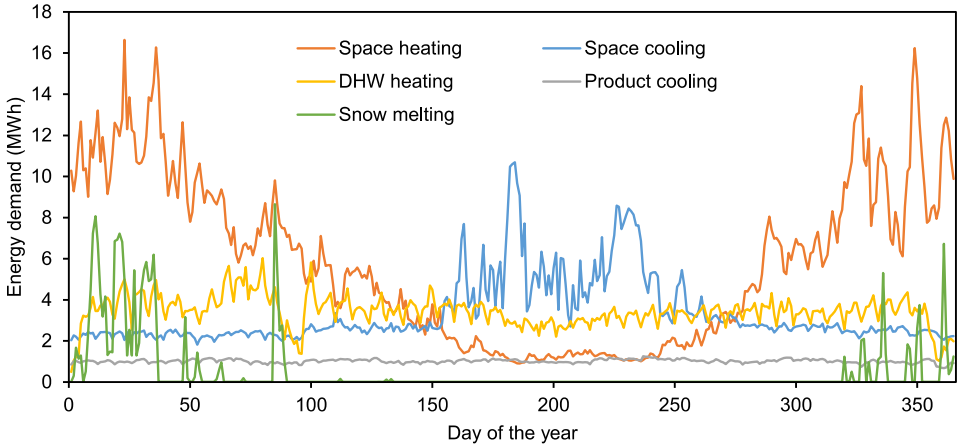

Figure 2. Measured daily heating and cooling demands in 2015

2.2 Results from the previous study

The IHCS was analyzed in a previous study by means of dynamic simulations (Rohde, Andresen et al. 2018). Modelica models were developed for the main components with focus on a good trade-off between accuracy and simulation time. The system model was calibrated with one-year measurement data and the results showed good agreement between simulated and measured values for electricity use and DH import.

The simulation results showed that more heat was extracted from the BTES during winter than was injected during summer. This can be seen in Figure 3, which shows the daily heat balances for the BTES and the solar collectors. This was shown to reduce the system's long-term performance.

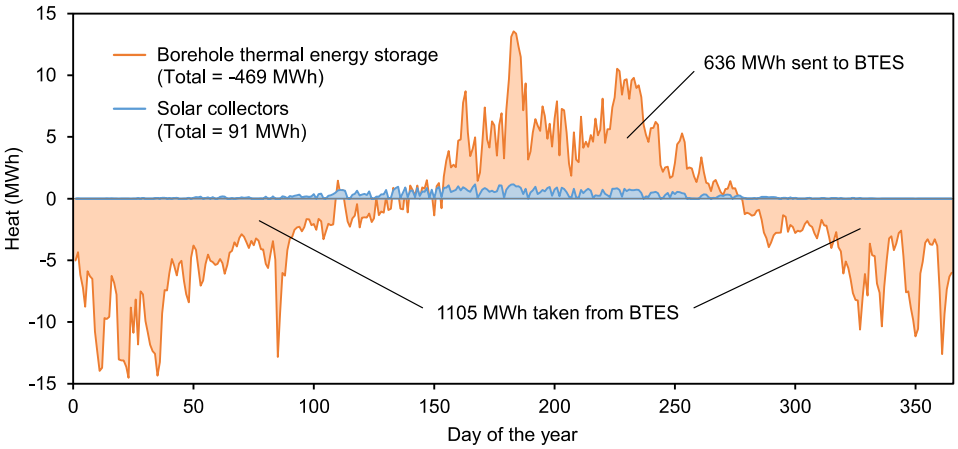

Figure 3. Simulated daily heat balance for BTES and solar collectors

A sensitivity study was performed and the results showed that the supply temperature setpoints for heating, T_{supply_heat}, and space cooling, T_{supply_cold}, were important for the system performance. These setpoints were used for the control of the main heat pumps as well as the BTES circulation pumps, which were responsible for 62% and 5% of the total electricity use, respectively. The IHCS had two operation modes: heating mode and cooling mode. T_{supply_heat} was set to 55 °C during heating mode and 51 °C during cooling mode. T_{supply_cold} was set to 6 °C during both operation modes. This control approach is called business as usual (BAU) throughout this paper.

3 Methodology

The IHCS was modeled in Modelica and simulated with Dymola as described in the previous section. The aim of this study was to optimize the operation of the IHCS, in particular the setpoint temperatures for heating and cooling supply, T_{supply_heat} and T_{supply_cold}, respectively. To this end, dynamic optimizations were performed with JModelica.org. The resulting setpoints from the optimizations were implemented into the system simulations in Dymola. The workflow of the entire analysis is shown in Figure 4.

	1. Simulation with BAU setpoints	2. Optimization of setpoints	3. Simulation with opt. setpoints
Model	Full system model	Seasonal submodels	Full system model
Environment	Dymola	JModelica.org	Dymola
Task	Simulation	Optimization	Simulation
Result	Electricity use/costs for BAU case	Optimized setpoints	Electricity use/costs with opt.-based control

Figure 4. Workflow of the analysis applying both simulation and optimization

All elements of the optimization procedure (Part 2 in Figure 4) are explained in detail in the next subsections. First, the optimization platform JModelica.org is described in Section 3.1. The development of seasonal models, which were suitable for numerical optimization, is described in Section 3.2. Finally, in Section 3.3, the control variables, constraints, and objective functions of the optimization problems are explained.

3.1 Optimization platform

JModelica.org is an open-source platform for simulation and optimization of complex dynamic systems (Magnusson and Åkesson 2015). JModelica.org is based on the modeling language Modelica and the Functional Mock-up Interface standard which enables coupling to different software packages. It uses the language extension Optimica, which enables high-level formulation of optimization problems (Åkesson 2008). All the optimizations in this work were performed with JModelica.org version 2.2 via 64-bit Python scripting. The main steps of the optimization procedure are described in this section and are shown in Figure 5.

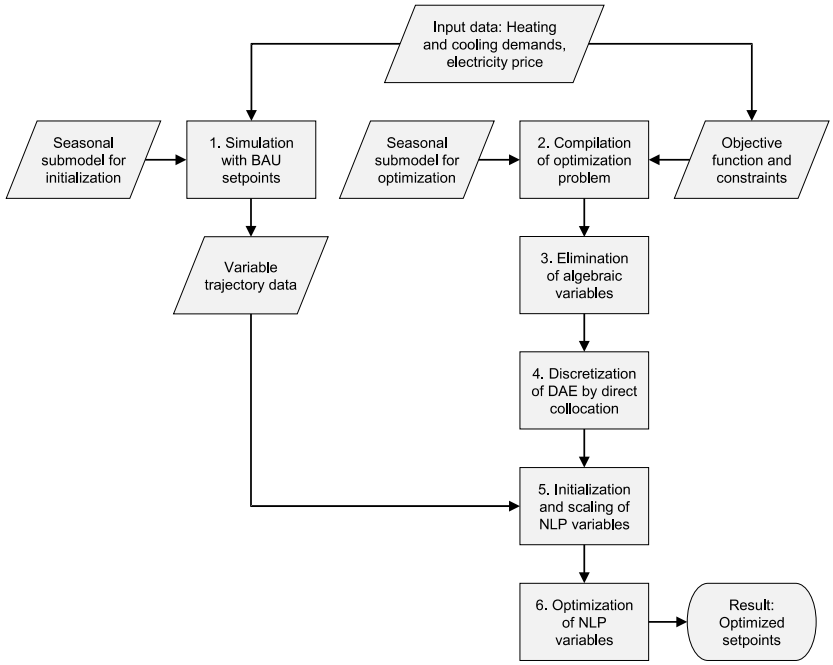

Figure 5. Main steps of optimization procedure with JModelica.org via Python scripting

Step 1: An initial simulation was required to obtain variable trajectory data for initialization and scaling of the NLP variables in Step 5, see Figure 5. To this end, the Modelica model for initialization was compiled into a Functional Mock-Up Unit and simulated using the CVode solver from the SUNDIALS suite (Hindmarsh, Brown et al. 2005), which is included in JModelica.org.

Step 2: The Modelica model for optimization and the problem formulation (Optimica code) were compiled and transferred to the CasADi interface of JModelica.org. CasADi was used for the computation of derivatives using algorithmic differentiation (Andersson, Gillis et al. 2018).

Step 3: Symbolic elimination based on block-triangular ordering was applied to reduce the number of algebraic variables as explained in (Magnusson and Åkesson 2018). This step was found to be crucial for successful converge as it significantly reduced the size of the resulting NLP.

Step 4: Code for orthogonal collocation on finite elements (Biegler 2010) is included in JModelica.org and was used to transform the infinite-dimensional dynamic optimization problem into a finite-dimensional NLP. The number of collocation elements and the number of collocation points in each element has a strong influence on the size of the resulting NLP. Initial testing with a prediction horizon of one-week was performed to compare the resulting setpoint temperatures with two different collocation configurations. The fine discretization had an element length of 15 min and two collocation points per element. The coarse discretization had an element length of 30 min and one collocation point per element. Applying the coarse discretization led to a reduction of the NLP variables from $598 \cdot 10^3$ to $178 \cdot 10^3$ and a reduction of the solution time from 103.2 s to 30.4 s for the one-week prediction horizon. However, the average absolute difference between the optimized setpoints for the fine and coarse discretization was less than 0.1 K, which was regarded as insignificant. Therefore, the coarse collocation discretization was used for all the optimization cases in this study.

Step 5: Variable trajectory data obtained during the initial simulation (Step 1) was used for automatic initialization and scaling of the NLP variables.

Step 6: The resulting NLP was solved using version 3.12.4 of the primal-dual interior-point solver IPOPT (Wächter and Biegler 2006) with linear solver MA57 from HSL (HSL 2018). All optimizations were performed with an Intel® Core™ i7-6700K processor (4GHz) and 64 GB RAM.

3.2 Optimization models

Initial testing showed that the complexity of the full system model developed in (Rohde, Andresen et al. 2018) impeded its applicability for dynamic optimization. To enable optimization of the system model over relevant prediction horizons, seasonal models were developed as a means of reducing model complexity. This section describes the reduction of the full system model and its decomposition into seasonal models.

3.2.1 Reduction of the full system model

The full system model could not be used for dynamic optimization due to the large number of components and their interconnections as mentioned above. Therefore, certain parts of the system had

to be removed to reduce the complexity and the size of the resulting NLP. The full system model and the removed parts (covered with gray) are shown in Figure 6.

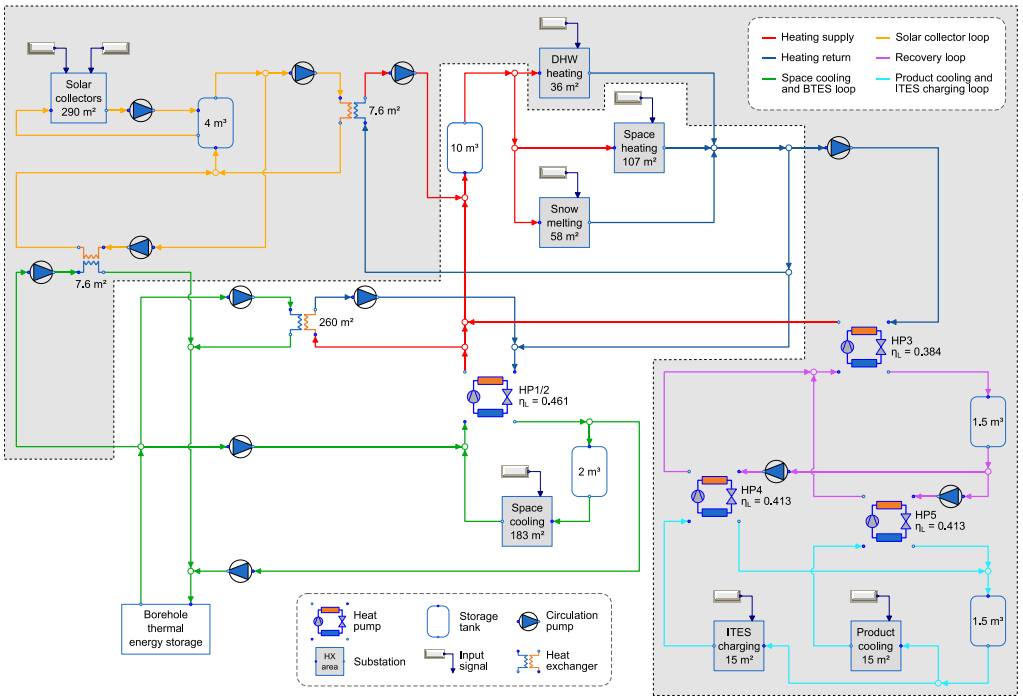

Figure 6. Full system model for simulation (gray part not used for optimization)

It can be seen in Figure 6 that the solar collector loop, the DHW heating substation, the product cooling and ITES charging loop, and the recovery loop were removed. The solar collector loop was removed because it played a minor role for the system performance, see Figure 3. The DHW heating substation, the product cooling, and the ITES charging loop were removed because the recovered heat from HP3 was similar to the delivered heat in the DHW heating substation (620 MWh and 682 MWh, respectively). Removing these parts therefore caused insignificant mismatch in the total heat balance. The simulated electricity use of the removed parts accounted for 18% of the total electricity use in the previous study, which showed that the key components of the system were kept. For clarity, the reduced system model is shown in Figure 7.

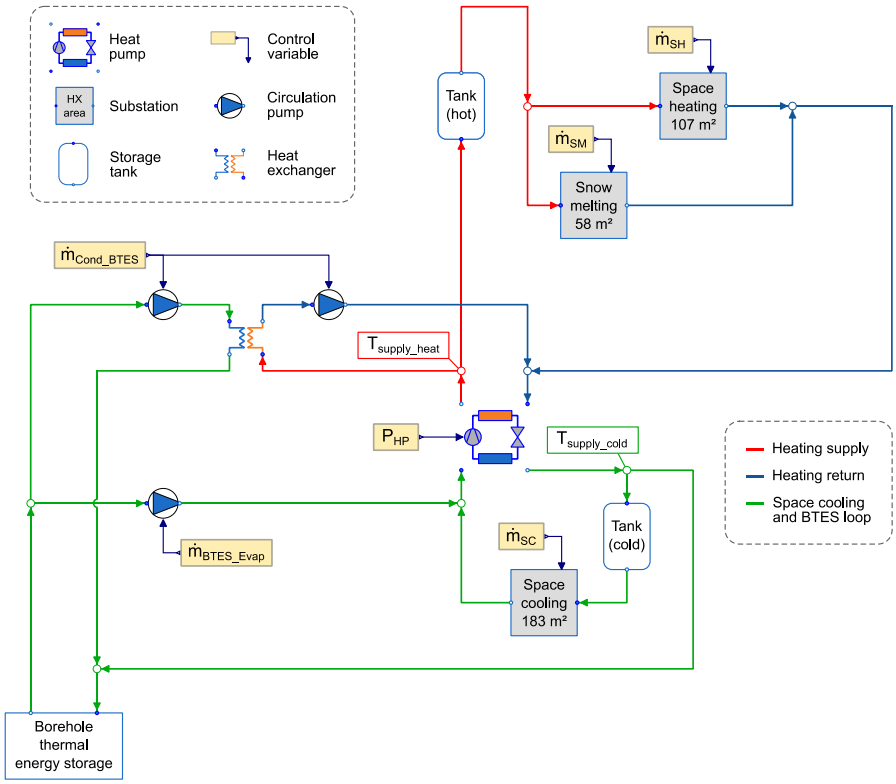

Figure 7. Reduced system model for optimization

3.2.2 Modifications of the component models

The component models described in (Rohde, Andresen et al. 2018) were developed for stable and fast dynamic simulations. However, due to the different numerical use of the model equations during simulation and optimization, some modifications were required to make all the component models suitable for optimization. These modifications are described in this section. To recall, the simulation models are shown in Figure 6 while the optimization model is shown in Figure 7.

The substation model for simulation, see Figure 6, received a demanded heat flow rate as input signal, which was based on the corresponding demand type. This input signal was used to control the mass flow rate of the circulation pumps within the substation model. Initial testing showed that the implemented PI-controller model led to convergence issues. Therefore, a different approach was chosen for the optimization model. The mass flow rate of the circulation pumps was used as input signal, see the yellow boxes in Figure 7, and the required heat flow rate was formulated as a constraint in the optimization problem, see Section 3.3.

Similar to the substation model, a new approach was also chosen for the HP model. The HP model for simulation received one of the outlet temperatures on the secondary side as input signal (not

shown in Figure 6). The HP model for optimization received the heat pump power (P_{HP}) as input signal, see the yellow box in Figure 7. Initial testing showed that this modification increased the convergence rate significantly.

The calculation of the Lorentz temperature in the heat pump model in (Rohde, Andresen et al. 2018) impeded successful convergence and was therefore approximated in the optimization model as:

$$T_{L\_cond/evap} = \frac{T_{in\_sec\_cond/evap} + T_{out\_sec\_cond/evap}}{2} \quad (1)$$

The difference in Lorentz temperature due to this modification was less than 0.1 K for all relevant operating conditions, which was regarded as insignificant.

The numerical discretization of the BTES and the storage tanks had strong influence on the number of NLP variables. A one-week test optimization was performed to compare the resulting setpoint temperatures with high and low discretization values. The horizontal and vertical discretization of the BTES was set to 30 and 4 for the high discretization case and 10 and 2 for the low discretization case, respectively. The discretization of the heating and cooling tanks was set to 15 and 5 for the high discretization case and 5 and 2 for the low discretization case, respectively. Reducing the discretization led to a reduction of the NLP variables from $178 \cdot 10^3$ to $53 \cdot 10^3$ and a reduction of the solution time from 30.4 s to 2.8 s. However, the average absolute difference between the optimized setpoints for the high and low discretization case was less than 0.1 K, which was regarded as insignificant. Therefore, the low discretization values were used for all the optimizations in this study.

3.2.3 Seasonal models

Some parts of the IHCS were only used during certain periods of the year, because the heating and cooling demands varied from season to season, see Figure 2. Optimizing unused parts would unnecessarily increase the optimization problem size. Therefore, three seasonal models were created based on the reduced system model shown in Figure 7 and the unused parts of each model were removed.

For the winter model, the BTES charging heat exchanger and respective circulation pumps could be removed because no heat was sent to the BTES during winter, see Figure 3. For the transition model used for spring and fall season, the snow melting substation could be removed since there was no snow melting demand, see Figure 2. For the summer model, the snow melting substation and the BTES discharging pump could be removed because there was no snow melting demand and no heat was taken from the BTES during summer, see Figures 2 and 3. The three seasonal models are listed in Table 1 together with the unused parts.

Table 1. Seasonal models used for optimization

Seasonal model	Unused parts
Winter	BTES charging heat exchanger and pumps
Transition	Snow melting substation
Summer	Snow melting substation and BTES discharging pump

Two versions of each seasonal model were required: one for the initial simulation and one for the optimization, see Figure 5. In the initialization models, the component models for simulation were used. The component models for optimization, explained in the Section 3.2.2, were used during the optimizations.

3.3 Optimal control problem formulation

The seasonal models described in the previous section were used to find optimal heating and cooling supply temperature setpoints for simulations with the full system model as shown in Figure 4. The optimization problems for the different models were formulated as continuous-time optimal control problems. The control variables, constraints, and objective functions of the optimization problems are explained in the following subsections.

3.3.1 Control variables

The control variables in the optimal-control problems were the heat pump power, P_{HP}, and the mass flow rates for the circulation pumps. These are marked yellow in Figure 7 and are written as a vector:

$$\mathbf{u}(t) := \left[P_{HP}(t), \dot{m}_{SH}(t), \dot{m}_{SM}(t), \dot{m}_{SC}(t), \dot{m}_{BTES\_Evap}(t), \dot{m}_{Cond\_BTES}(t)\right]' \tag{2}$$

The temperatures T_{supply_heat} and T_{supply_cold} were not included in the vector $\mathbf{u}(t)$. This was due to the fact that the optimization models did not contain PI-controllers, as explained in Section 3.2.2, and thus could not receive a setpoint temperature. The temperatures T_{supply_heat} and T_{supply_cold} depended on the control variables and were calculated during the optimizations. The resulting values were then used as input for the new simulations (Part 3 in Figure 4).

3.3.2 Constraints

Lower and upper bounds were defined for the control variables based on their operational limits, yielding the following linear inequality constraints:

$$0 \leq P_{HP}(t) \leq 300\ \text{kW} \tag{3}$$

$$0 \leq \dot{m}_i(t) \leq \dot{m}_{i\_max}, \qquad i \in \{SH, SM, SC, BTES\_Evap, Cond\_BTES\} \tag{4}$$

To ensure practically feasible operation, the supply temperatures for heating and cooling were constrained by:

$$T_{supply\_heat}(t) \leq 65\ ℃ \tag{5}$$

$$T_{supply\_cold}(t) \geq -5\ ℃ \tag{6}$$

Constraints were also added to ensure that the correct amount of energy was delivered from the IHCS to the connected buildings. Enforcing this demand satisfaction as an equality constraint led to convergence issues. Therefore, the following upper and lower bounds were defined for the heat flow rates in the substations based on the heating and cooling demands:

$$\dot{Q}_{i\_delivered}(t) \geq \dot{Q}_{i\_demanded}(t), \qquad i \in \{SH, SM, SC\} \tag{7}$$

$$\dot{Q}_{i\_delivered}(t) \leq \varepsilon \cdot \dot{Q}_{i\_demanded}(t), \qquad i \in \{SH, SM, SC\} \tag{8}$$

This formulation improved the numerical performance. The parameter ε was set to 1.005 so that only a small slack in energy supply was allowed.

3.3.3 Definition of the objective function for reduction of electricity use

The calculated electricity use of the system consisted of three parts: the electricity use of the heat pumps, the electricity use of the circulation pumps, and a constant term from auxiliary systems (Rohde, Andresen et al. 2018). The first aim of this study was to analyze how much this electricity use could be reduced. Therefore, the following objective function was defined in order to minimize total electricity use:

$$\min_{\mathbf{u}(t)} \int_{t_{start}}^{t_{final}} \left(P_{HP}(t) + \sum_{i} P_{i\_pump}(t) \right) dt, \qquad i \in \{SH, SM, SC, BTES\_Evap, Cond\_BTES\} \tag{9}$$

Note that the constant term of the electricity use had no influence on the optimal solution and was therefore removed from the objective function. The year was divided into seasonal periods and each period was optimized separately with the corresponding values for the period's beginning (t_{start}) and end (t_{final}). The length of each season and the resulting NLP problem size of the respective optimization are shown in Table 2.

Table 2. Optimization periods and problem size

Days	Seasonal model	Number of finite elements	Number of NLP variables	Number of NLP Constraints
1 – 95	Winter	4562	$7.2 \cdot 10^5$	$7.8 \cdot 10^5$
96 – 155	Transition	2883	$4.2 \cdot 10^5$	$4.6 \cdot 10^5$
156 – 260	Summer	5043	$6.7 \cdot 10^5$	$7.3 \cdot 10^5$
261 – 290	Transition	1443	$2.0 \cdot 10^5$	$2.2 \cdot 10^5$
291 – 365	Winter	3602	$5.7 \cdot 10^5$	$6.2 \cdot 10^5$

The initial state of the BTES and storage tank models for each season were chosen based on the result of the previous season.

3.3.4 Definition of the objective function for reduction of electricity costs

The second aim of this study was to analyze if the electricity costs of the system could be reduced with improved control setpoints. In Norway, electricity prices are much higher during winter than during summer due to the market based electricity price model and the high amount of electricity used for space heating. The first three months of the year accounted for 44% of the total electricity costs for the simulated year. Therefore, these three months were chosen for the cost-reduction analysis to limit the number of required optimization runs. This way, all the optimizations could be performed with the winter model. The following objective function, including the time-varying electricity price e(t), was defined in order to minimize electricity costs:

$$\min_{\mathbf{u}(t)} \int_{t_{start}}^{t_{final}} e(t) \cdot \left(P_{HP}(t) + \sum_{i} P_{i\_pump}(t) \right) dt, \qquad i \in \{SH, SM, SC, BTES\_Evap\} \tag{10}$$

The electricity spot prices for the location of the IHCS for the first three months of the previous four years are shown in Figure 8. At the time of writing, the exchange rate from Norwegian Krone to Euro is 1 NOK = 0.1026 EUR (XE Corporation 2019). Note that the prices in Figure 8 are market spot prices. Customers also have to pay electricity grid prices and additional fees, which were not considered in this study.

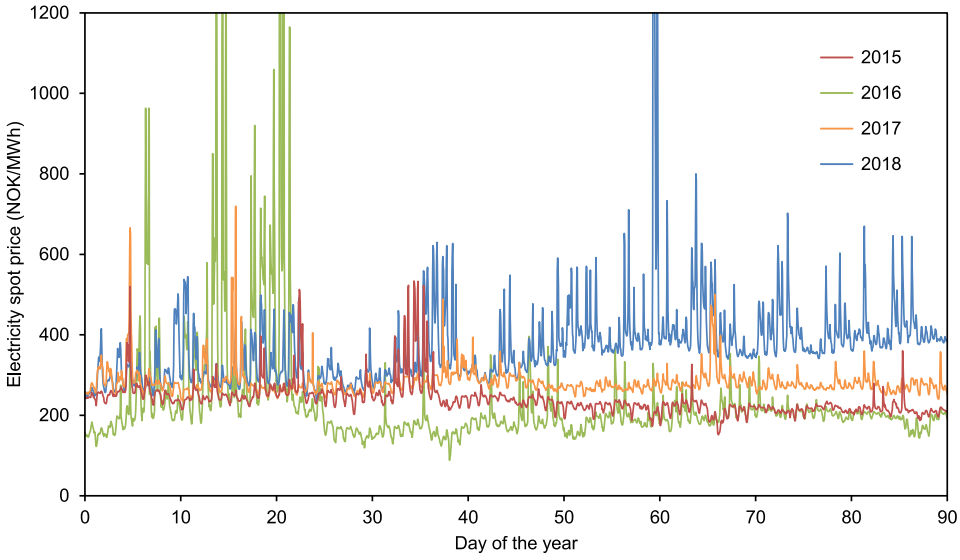

Figure 8. Hourly electricity spot prices for Oslo (Nord Pool AS 2019). Peak values omitted for better readability (max value = 2454 NOK/MWh).

It can be seen from Figure 8 that the electricity price showed relatively little variation in 2015. Therefore, additional price signals were defined with different fluctuations to analyze the influence of the variability of the electricity price, v, on the cost saving potential. The price signals were based on the average price of the first three months of 2015 (239 NOK/MWh) and the original price signal ($e_{Oslo2015}$). Values of 0, 1, 2, and 3 were chosen for v and the price signals were calculated as follows:

$$e_v(t) = 239 + v \cdot (e_{Oslo2015}(t) - 239) \tag{11}$$

The four resulting price signals were used for the optimizations and are shown in Figure 9.

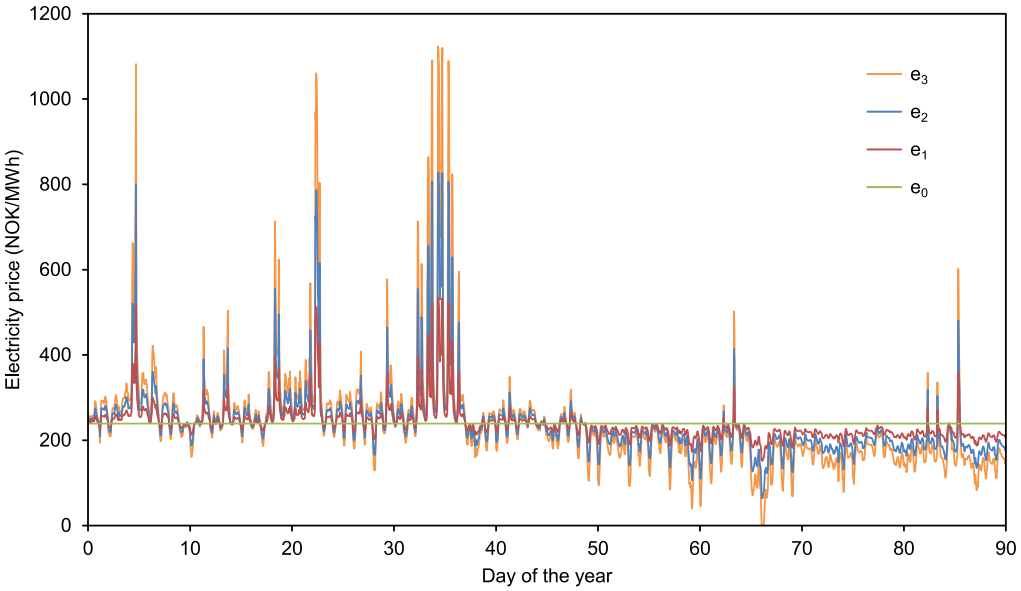

Figure 9. Electricity prices used for the optimizations ($e_1 = e_{Oslo2015}$)

This approach, similar to the one presented in (Fischer, Lindberg et al. 2016), was chosen instead of using electricity prices from other years to maintain the correlation between the electricity price and the climate conditions. Note that this correlation is not kept for v = 0, which corresponds to a constant and thus unrealistic electricity price.

The storage tanks of the IHCS were relatively small and only used as buffer to even out the supply temperatures of the heating and cooling loop. Storage tanks are a relatively cheap component, so the installation of larger tanks may be considered as a realistic retrofitting option. To investigate the effect of larger storage tanks on the cost saving potential, three different tank size combinations were chosen: the installed 10 m^3 and 2 m^3 for the heating and cooling tank, respectively, as well as 100 m^3 and 500 m^3 for both tanks.

The four different price signals and the three different tank size combinations led to the twelve optimization cases listed in Table 3.

Table 3. Case IDs of optimizations for electricity cost reduction

		Electricity price signal			
Heating tank volume (m^3)	**Cooling tank volume (m^3)**	e_0	e_1	e_2	e_3
10	2	10-2_e_0	10-2_e_1	10-2_e_2	10-2_e_3
100	100	100-100_e_0	100-100_e_1	100-100_e_2	100-100_e_3
500	500	500-500_e_0	500-500_e_1	500-500_e_2	500-500_e_3

All the cases listed in Table 3 were optimized separately with the winter model. According to the prediction horizon of three months, t_{start} and t_{final} were set to 0 and $7.776 \cdot 10^6$ in the objective function, Equation 10, respectively. Optimal operation over this prediction horizon would lead to emptied short term storages at t_{final}, i.e. the average temperature ($T_{average}$) in the hot storage tank would be as low as possible and the average temperature in the cold storage tank would be as high as possible. This would lead to an unfair comparison, especially when different tank sizes were compared. Therefore, the following constraints were added for these twelve optimizations to avoid this effect and thus ensure a fair comparison:

$$\text{Heating\_tank\_}T_{average}(t_{final}) \geq \text{Heating\_tank\_}T_{average}(t_{start}) \tag{12}$$

$$\text{Cooling\_tank\_}T_{average}(t_{final}) \leq \text{Cooling\_tank\_}T_{average}(t_{start}) \tag{13}$$

4 Results

In this section, the results from the simulations and the optimizations are presented. First, the results leading to reduced electricity use of the system are shown. For these results, the five optimizations listed in Table 2 were performed, which included all the seasonal models and an analyzed period of one year. Afterwards, the results leading to reduced electricity costs of the system are presented. For these, the twelve optimizations listed in Table 3 were performed with the winter model and an analyzed period of three months. Note that perfect prediction of the heating and cooling demands as well as the electricity price was assumed for all the simulations and optimizations.

4.1 Reduction of annual electricity use with optimization-based control

The optimized values for the control variables leading to minimized electricity use are presented in this section. The optimal heat pump power P_{HP} is shown in Figure 10, the optimal mass flow rates for the substation circulation pumps are shown in Figure 11, and the optimal mass flow rates for the BTES circulation pumps are shown in Figure 12.

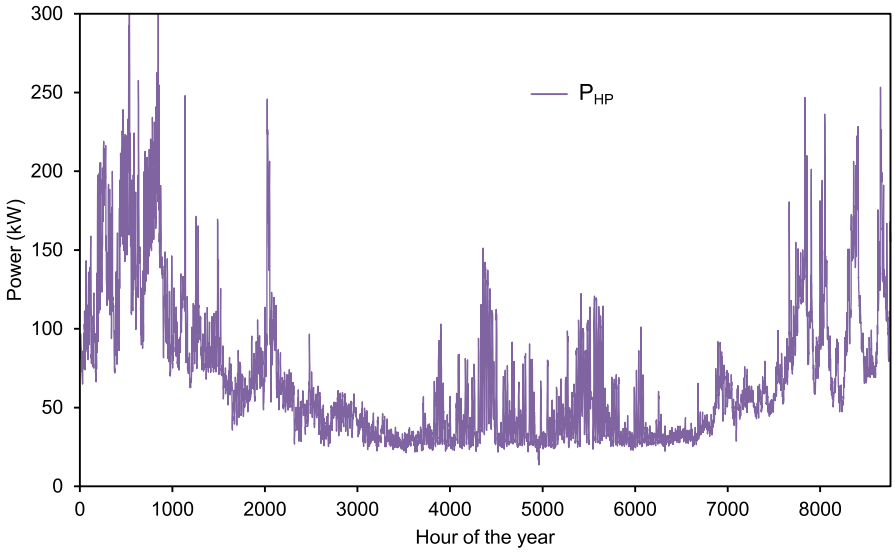

Figure 10. Optimized heat pump power

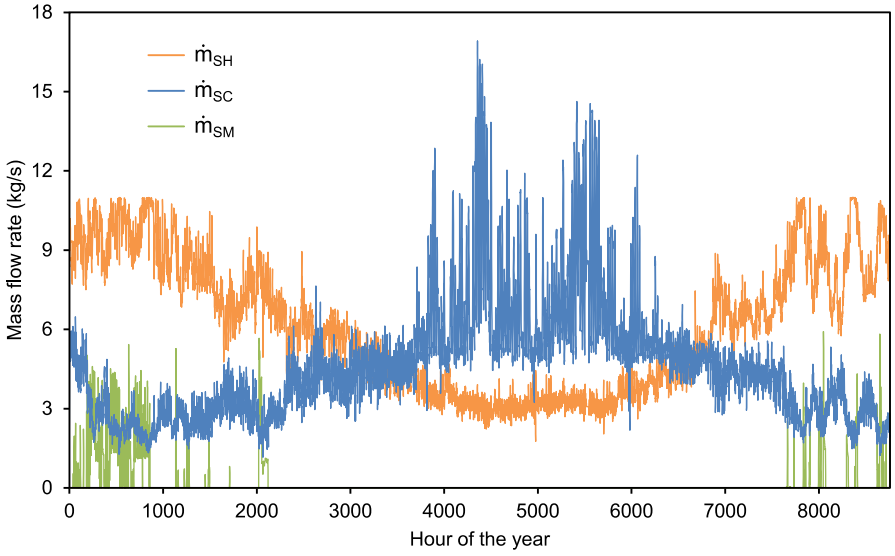

Figure 11. Optimized mass flow rates for the substation circulation pumps

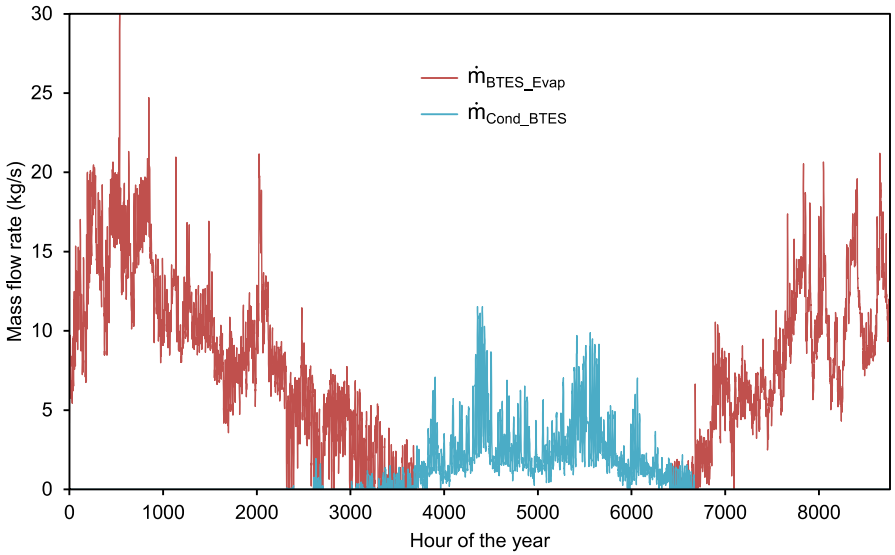

Figure 12. Optimized mass flow rates for the BTES circulation pumps

A validation was performed to confirm that the energy demand constraints, Equations 7 and 8, were not violated during the optimizations. To this end, a one-year simulation with the reduced system model shown in Figure 7 was performed. The optimized values for the control variables were used as input and the resulting heat flow rates in the substations' heat exchangers were compared to the demanded heat flow rates. Daily values for demanded and delivered energy are shown in Figure 13.

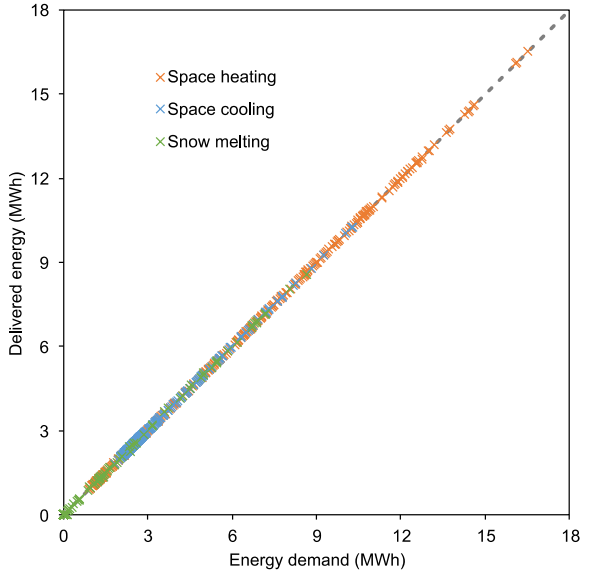

Figure 13. Daily values of demanded and delivered energy for the substations of the IHCS

It can be seen from Figure 13 that there was no mismatch between the demanded and the delivered energy. Slight deviations were observed on hourly basis. This was due to the slack formulation in Equation 8 and the fact that the constraints were only enforced at the collocation points and not during the entire width of the collocation element. However, the R^2-values for all three demand types were above 0.99 on hourly basis, showing that the deviations were insignificant.

The optimized values for heating and cooling supply temperature are shown in Figure 14 and Figure 15, respectively. The former setpoints from the previous study, used during Part 1 in Figure 4, are also shown for comparison.

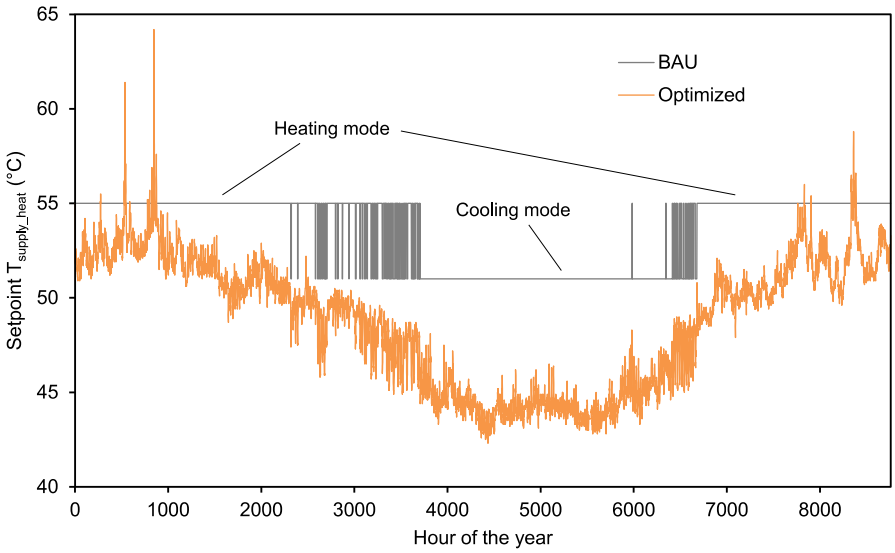

Figure 14. Heating supply temperature setpoint

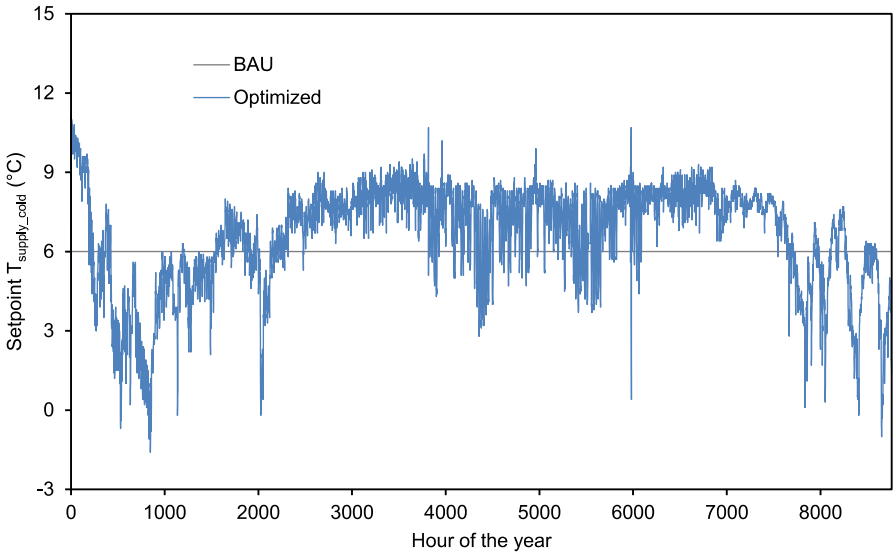

Figure 15. Cooling supply temperature setpoint

The optimized values for T_{supply_heat} and T_{supply_cold} were implemented into the full system model, where they were used as replacement for the mode-based setpoints of the BAU case (Part 3 in Figure 4). The resulting energy amounts for the simulated year are shown in Figure 16.

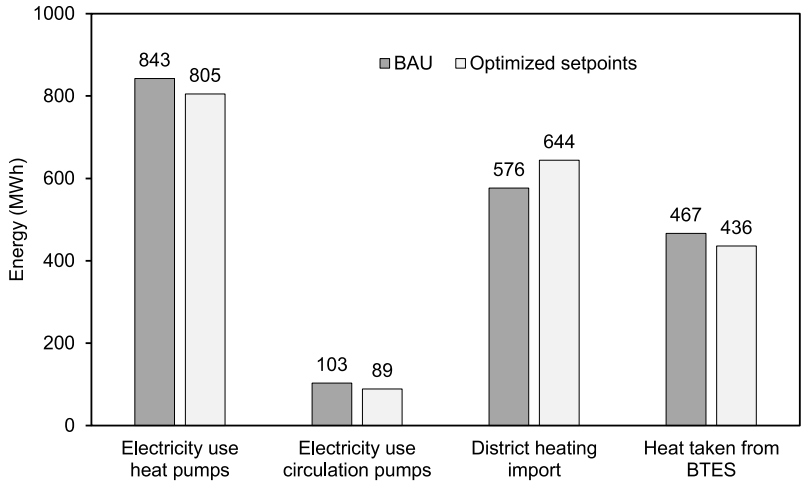

Figure 16. Total simulated energy amounts for 2015

It can be seen from Figure 16 that the electricity use for the heat pumps and the circulation pumps decreased by 5 and 14 %, respectively, with the optimized setpoints compared to the BAU case. Due to the circulation pump's low share of electricity use, this corresponded to a minor total reduction of electricity use. The amount of heat imported from DH increased by 12 % for the simulated year. The amount of heat taken from the long-term storage decreased by 7 %.

4.2 Reduction of electricity costs during winter with optimization-based control

Selected result values from the optimizations leading to minimized electricity costs are shown in this section. February 14th and February 3rd were days with very different variations in electricity spot price. The price signals for these two days are shown in Figures 17 and 18, respectively.

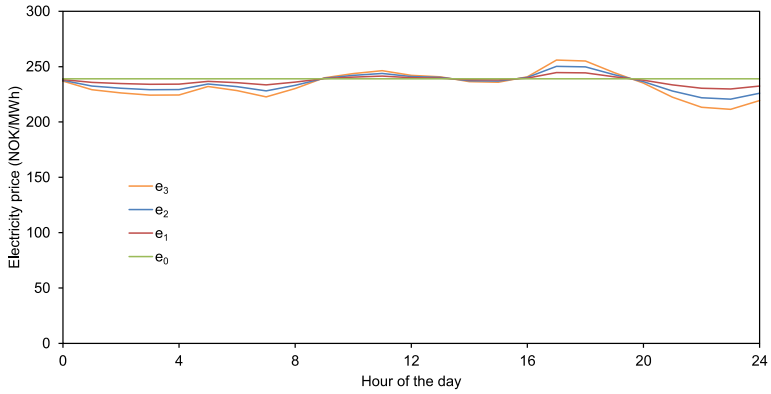

Figure 17. Electricity prices for February 14th ($e_1 = e_{Oslo2015}$)

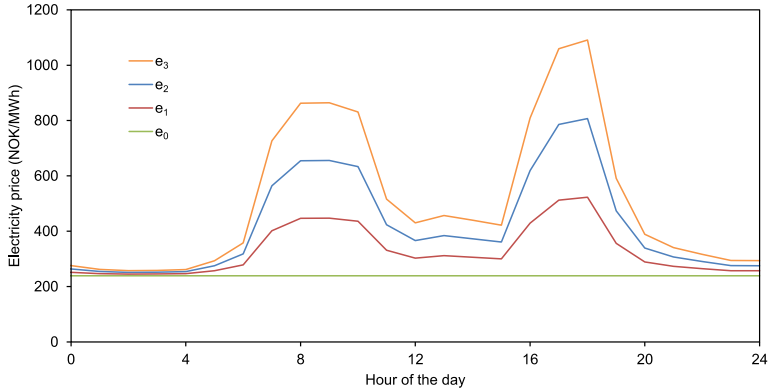

Figure 18. Electricity prices for February 3rd ($e_1 = e_{Oslo2015}$)

It can be seen from Figure 17 that the electricity price was almost constant on February 14th. On the contrary, the electricity price varied significantly on February 3rd as shown in Figure 18. Peak hours were in the morning and afternoon, which is typical for Norway (Clauß, Stinner et al. 2019). Detailed results for the optimal heat pump power and temperature setpoints are presented for these two days for selected cases from Table 3. The results for February 14th for the cases with the original electricity price and different tank size combinations are shown in Figure 19.

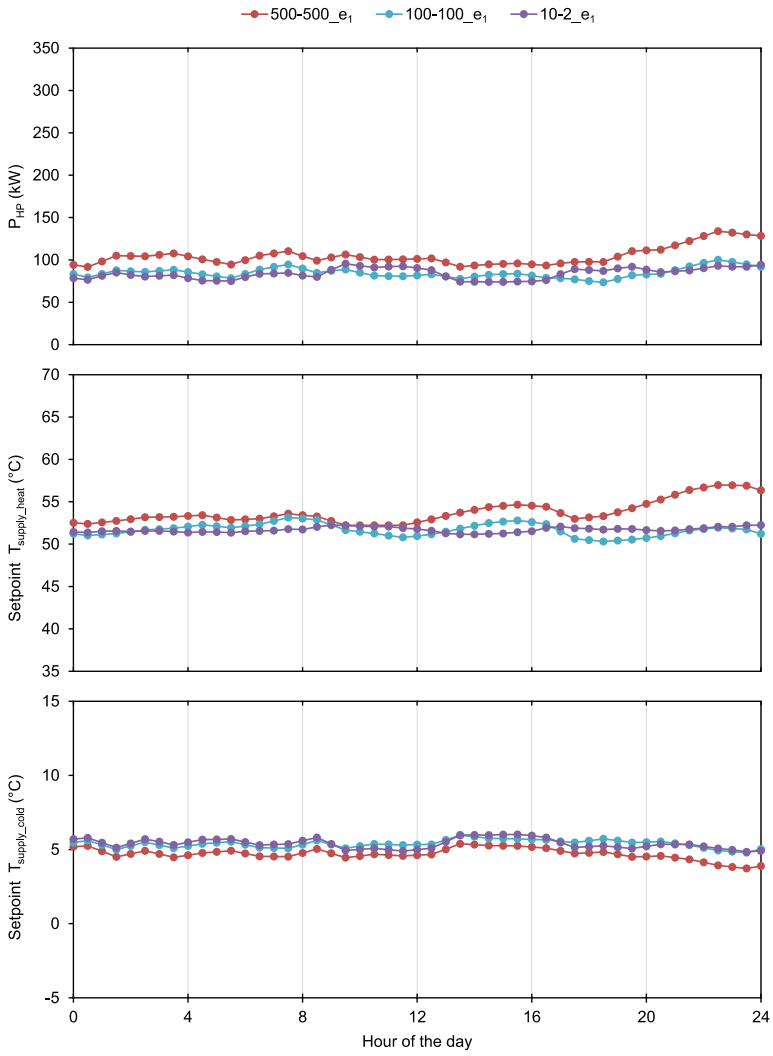

Figure 19. Optimization results for February 14th with different tank size combinations

It can be seen from Figure 19 that the different tank size combinations yielded very similar results for February 14th. This was expected due to the relatively constant electricity price during that day. The results for February 3rd for the same cases are shown in Figure 20.

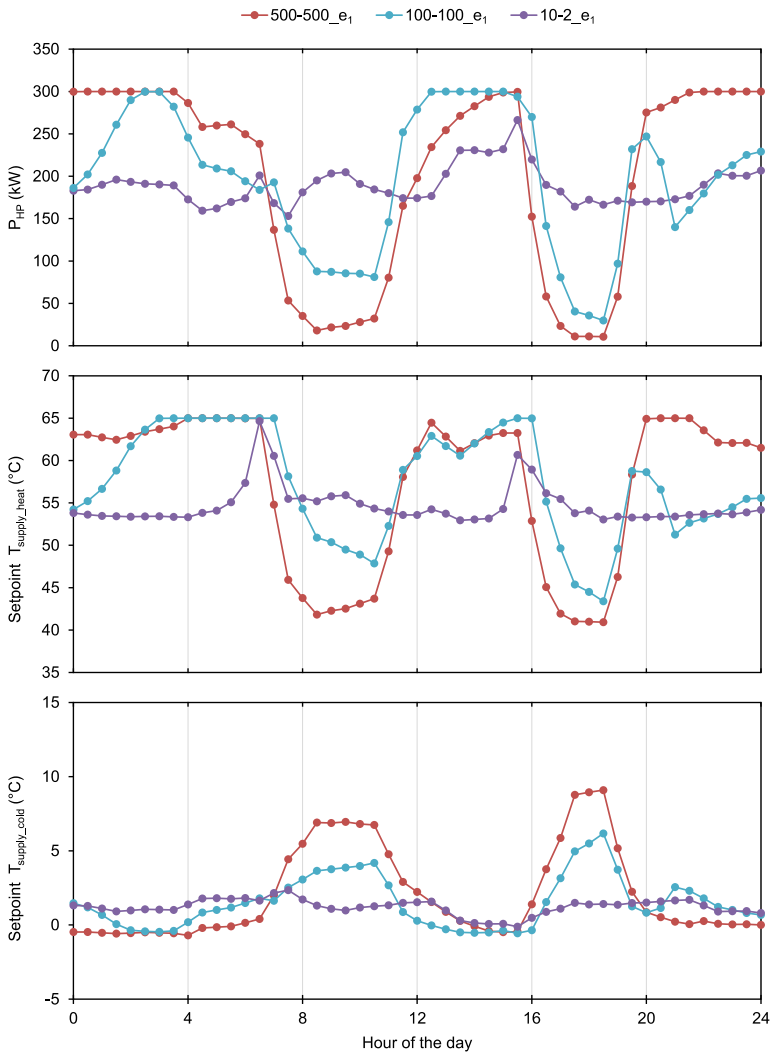

Figure 20. Optimization results for February 3rd with different tank size combinations

It can be seen from Figure 20 that the optimal control trajectories for February 3rd depended highly on the size of the storage tanks. Larger tanks led to larger variations, due to the possibility to shift electricity use from peak hours (with high prices) to off-peak hours (with low prices) and thus decrease the total electricity costs.

Figure 20 clearly shows that the installed tanks (Case 10-2_e_1) were too small to take advantage of the electricity price variations. The heat pump power only varied between 150 kW and 270 kW for this case and the temperatures setpoints were relatively constant as well, expect for two short peaks of T_{supply_heat}. For Case 100-100_e_1, the heat pump power varied across nearly the entire allowed range from 0 to 300 kW. It was higher during off-peak hours to charge the storage tanks, corresponding to high values for T_{supply_heat} and low values for T_{supply_cold}. On the contrary, the heat pump power was low during

peak hours and the energy demands of the buildings were to a large extent covered by discharging the tanks. For Case 500-500_e_1, this effect was even more pronounced, leading to the largest variations in the optimal values for T_{supply_heat} and T_{supply_cold}.

The results for February 3rd for the cases with the largest tanks and different variability of the electricity price are shown in Figure 21.

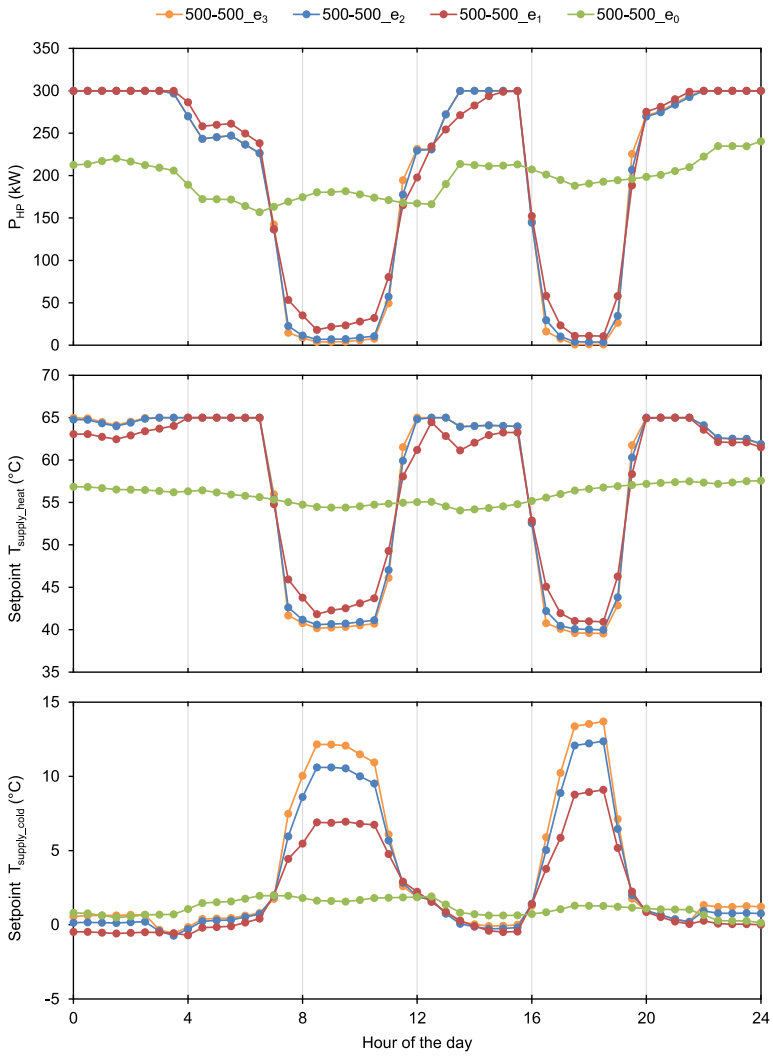

Figure 21. Optimization results for February 3rd with different electricity price variability ($e_1 = e_{Oslo2015}$)

It can be seen from Figure 21 that there were large differences between the results with a constant electricity price, Case 500-500_e_0, and the cases with price variations. Although the costs were optimized for all the cases, the constant price led to a minimization of the total electricity use for Case 500-500_e_0 (i.e. Equation 9 and 10 yielded equal results). The control of the heat pump and the

circulation pumps were therefore optimized depending on the energy demands of the buildings. For the other three cases, the electricity use was significantly higher during off-peak hours. The cases with different variability showed very similar results for February 3rd. The optimal control trajectories became slightly more pronounced for larger values of variability, but only T_{supply_cold} showed significant differences. This showed that even larger tanks would be required to take advantage of the variations during that day. However, other days showed larger differences between these cases.

The optimized setpoints were implemented into the full system model and a simulation for the first three months was performed for all the cases listed in Table 3. The simulated total electricity costs for this period are shown in Figure 22. The simulated costs with BAU control were included to show the potential savings. All the results are shown relative to the BAU case, because the different price signals led to different costs for the BAU case.

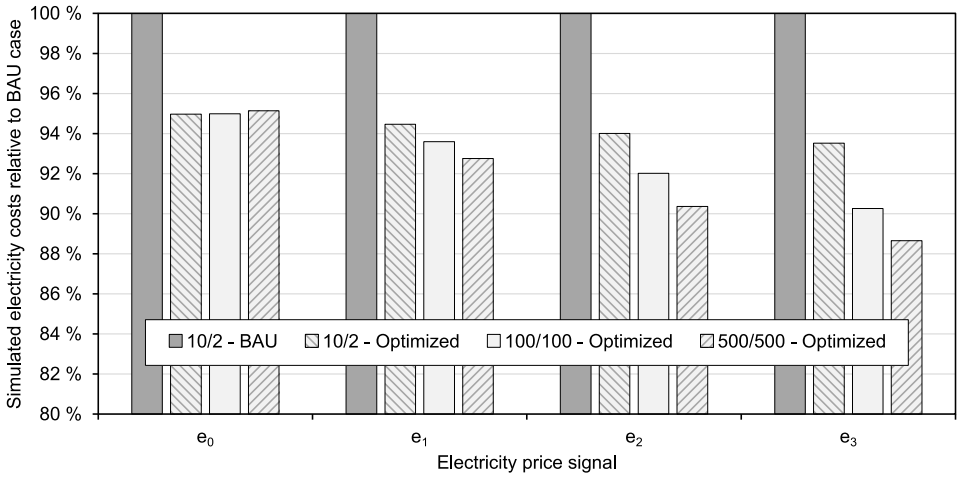

Figure 22. Simulated electricity costs for the first three months relative to the BAU case ($e_1 = e_{Oslo2015}$)

It can be seen from Figure 22 that all the optimized cases led to lower electricity costs compared to the BAU case. The relative savings were in the range of 5 to 11 %. The relative savings increased with larger variability of the electricity price signal. Larger tanks also led increased relative savings, except for the cases with constant electricity price (e_0).

5 Discussion

In this section, general matters regarding the applied methodology are discussed first. Afterwards, the reduction of electricity use and electricity costs are discussed in detail.

All the optimizations were performed with reduced system models. Minor components, responsible for 18% of the annual electricity use, were removed from the full system model to avoid convergence issues of the NLP solver. In addition, the year was divided into five seasons and each

season was optimized separately. From this point of view, the results can be seen as a lower bound, since the control of the removed parts were not optimized. This means that potential improvements were disregarded and a one-year optimization of the full system model would be desirable. However, numerical optimization is significantly more challenging than simulation for this type of integrated systems and the complexity of the full system model impeded a one-year optimization. The authors find it worth noting that JModelica.org version 2.0 was used initially, which only supported 32-bit Python. The memory usage of a 32-bit Python process is limited to about 2 GB, which was insufficient for the optimizations in this study and led to frequent memory allocation errors. JModelica.org version 2.2 was released in March 2018 and was the first version to support 64-bit Python. The upgrade to version 2.2 was crucial for this study and the same results could therefore not have been produced before March 2018.

The input data for the whole year were used as input in this study. The optimizations were thus performed with perfect prediction. From this point of view, the results can be seen as an upper bound, since perfect prediction is not a realistic scenario. The energy demands of buildings and the electricity price in Norway both depend on ambient conditions. In practice, the uncertainty of the weather forecast thus makes detailed optimizations over a long prediction horizon obsolete. Shorter periods are therefore chosen in practical applications such as Model Predictive Control (Jorissen, Boydens et al. 2019). An advantage of shorter prediction horizons are that more detailed models can be optimized. A disadvantage is that the use of long-term storages needs special attention. For a short prediction horizon, the optimization of a long-term storage is fundamentally difficult. Unsustainable usage may result unless a sufficiently high cost is put in the objective function or constraints are imposed. The implementation of such measures was outside the scope of this study and long prediction horizons were chosen to ensure optimal operation of the BTES.

The simulated electricity use of the IHCS was reduced by improving the control setpoints T_{supply_heat} and T_{supply_cold}. The coefficient of performance (COP) of the heat pump model was calculated based on a constant Lorentz efficiency, see (Rohde, Andresen et al. 2018). Thus, the COP depended on the temperature lift of the heat pump, which varied significantly with the optimized setpoint trajectories. Part-load operation was therefore included in the model, but depended only on the temperature levels and not on the heat flow rates. The optimized setpoints led to reduced electricity use of the heat pumps and the circulation pumps as shown in Figure 16. However, the electricity used by the heat pumps was converted to useful heat and thus partly covered the heating demands of the buildings. Reducing this electricity use thus led to more heat being imported from DH. The increase in DH import depended on the amount of heat taken from the BTES. Too high heat extraction from the BTES can lead to unsustainable operation as shown in the previous study (Rohde, Andresen et al. 2018). However, importing heat from DH is more expensive in the short run. An economic analysis is therefore required to find the optimal operation strategy that balances short- and long-term cost considerations. In general,

DH is an essential technology for decarbonization, so its use should be preferred over electricity use (Connolly, Lund et al. 2014). Charging the BTES with low-grade heat, e.g. the DH return line, could be an interesting option to investigate in future work.

The electricity costs shown in Figure 22 were calculated by multiplying the electricity use of the system by the local electricity spot price. However, this is only a part of the actual costs that large customers have to pay in Norway. The electricity grid in Norway is stressed significantly more during the winter than during the rest of the year due to the high use of electricity for space heating. Therefore, the electricity grid prices include additional costs to consider the electricity grid stress. For business customers, this may induce peak-load tariffs and charging for their peak electricity use of each calendar month. This was not taken into account in this study as the measurement data showed that the peak use of the IHCS was almost the same for all the winter months. This cost was therefore assumed fixed and not included in the optimizations. The 25 % taxes that have to be paid were also neglected because they did not affect the relative savings.

The relative savings shown in Figure 22 were obtained by comparing three-month simulations with different tank size combinations and different temperature control setpoints. Larger tanks were shown to lead to reduced electricity costs. However, the difference between the BAU case (10/2 - BAU) and the case with the currently installed tanks and optimized setpoints (10/2 - Optimized) was larger than the difference between the cases with different tank sizes and optimized setpoints (10/2 – Optimized vs. 500/500 - Optimized). This means that the optimized control led to higher relative savings than the installation of larger tanks. However, these savings only included the electricity costs and not the costs for DH import. Since the DH import increased for the cases with the optimized setpoints compared to the BAU case, an economic analysis including the calculation of the total operating costs is required to decide if larger storage tanks should be installed. The costs for the advanced control system should be taken into account in such an analysis since the installation of larger tanks would not lead to savings with the current control strategy.

6 Conclusions

The simulated performance of an integrated heating and cooling system with thermal energy storages was analyzed in this study. Dynamic optimizations were applied to find optimal control trajectories for operation leading to reduced electricity use and reduced electricity costs. The results showed that the electricity use of the system could be reduced by about 5 %. However, this led to increased import of heat from the district heating grid. Possible savings therefore depended on the electricity and district heating prices.

The installation of larger storage tanks was shown to decrease electricity costs when the optimized control setpoints were implemented. However, the savings depended on the variability of the

electricity price and could only be achieved with a more advanced control system than the one currently implemented. During the analyzed period, the variability of the electricity price was too low to make the installation of larger storage tanks seem profitable in practice. Higher peak load tariffs and/or an increased variability of the electricity price might change this conclusion in the near future. Further work should therefore include more detailed optimization models and more advanced cost calculations.

Acknowledgments

The authors gratefully acknowledge the financial support from the Research Council of Norway for the projects INTERACT (grant agreement number 228656/E20), FME HighEFF (grant agreement number 257632/E20), and LTTG+ (grant agreement number 280994/E20).

References

G. Alva, Y. Lin and G. Fang (2018). "An overview of thermal energy storage systems." Energy 144: 341-378. DOI: https://doi.org/10.1016/j.energy.2017.12.037.

J.A.E. Andersson, J. Gillis, G. Horn, J.B. Rawlings and M. Diehl (2018). "CasADi: a software framework for nonlinear optimization and optimal control." Mathematical Programming Computation. DOI: https://doi.org/10.1007/s12532-018-0139-4.

F. Audino, G. Campanyà, M. Pérez-Moya, A. Espuña and M. Graells (2019). "Systematic optimization approach for the efficient management of the photo-Fenton treatment process." Science of The Total Environment 646: 902-913. DOI: https://doi.org/10.1016/j.scitotenv.2018.07.057.

S. Barsali, R. Giglioli, G. Lutzemberger, D. Poli and G. Valenti (2017). "Optimised operation of storage systems integrated with MV photovoltaic plants, considering the impact on the battery lifetime." Journal of Energy Storage 12: 178-185. DOI: https://doi.org/10.1016/j.est.2017.05.003.

F. Belkhir, D.K. Cabo, F. Feigner and G. Frey (2015). "Optimal Startup Control of a Steam Power Plant Using the JModelica Platform." IFAC-PapersOnLine 48(1): 204-209. DOI: https://doi.org/10.1016/j.ifacol.2015.05.050.

L.T. Biegler (2010). Simultaneous Methods for Dynamic Optimization. Nonlinear Programming, MOS-SIAM Series on Optimization**:** 287-324.

Y. Cao, D. Acevedo, Z.K. Nagy and C.D. Laird (2017). "Real-time feasible multi-objective optimization based nonlinear model predictive control of particle size and shape in a batch crystallization process." Control Engineering Practice 69: 1-8. DOI: https://doi.org/10.1016/j.conengprac.2017.08.008.

J. Clauß, S. Stinner, I. Sartori and L. Georges (2019). "Predictive rule-based control to activate the energy flexibility of Norwegian residential buildings: Case of an air-source heat pump and direct electric heating." Applied Energy 237: 500-518. DOI: https://doi.org/10.1016/j.apenergy.2018.12.074.

D. Connolly, H. Lund, B.V. Mathiesen, S. Werner, B. Möller, U. Persson, T. Boermans, D. Trier, P.A. Østergaard and S. Nielsen (2014). "Heat Roadmap Europe: Combining district heating with heat savings to decarbonise the EU energy system." Energy Policy 65: 475-489. DOI: https://doi.org/10.1016/j.enpol.2013.10.035.

European Union (2010). "Directive 2010/31/EU of the European Parliament and of the Council of 19 May 2010 on the energy performance of buildings." Official Journal of the European Union L 153: 13–35.

D. Fischer, K.B. Lindberg, H. Madani and C. Wittwer (2016). "Impact of PV and variable prices on optimal system sizing for heat pumps and thermal storage." Energy and Buildings 128: 723-733. DOI: https://doi.org/10.1016/j.enbuild.2016.07.008.

A.C. Hindmarsh, P.N. Brown, K.E. Grant, S.L. Lee, R. Serban, D.E. Shumaker and C.S. Woodward (2005). "SUNDIALS: Suite of nonlinear and differential/algebraic equation solvers." ACM Transactions on Mathematical Software 31(3): 363-396. DOI: https://doi.org/10.1145/1089014.1089020.

A. Holmqvist and F. Magnusson (2016). "Open-loop optimal control of batch chromatographic separation processes using direct collocation." Journal of Process Control 46: 55-74. DOI: https://doi.org/10.1016/j.jprocont.2016.08.002.

HSL (2018). "A collection of Fortran codes for large scale scientific computation." From http://www.hsl.rl.ac.uk (accessed 03/2018).

S. Ikeda, W. Choi and R. Ooka (2017). "Optimization method for multiple heat source operation including ground source heat pump considering dynamic variation in ground temperature." Applied Energy 193: 466-478. DOI: https://doi.org/10.1016/j.apenergy.2017.02.047.

International Energy Agency (2013). Heating and Cooling Technologies. Transition to Sustainable Buildings: Strategies and Opportunities to 2050, International Energy Agency.

F. Jorissen, W. Boydens and L. Helsen (2019). "TACO, an automated toolchain for model predictive control of building systems: implementation and verification." Journal of Building Performance Simulation 12(2): 180-192. DOI: https://doi.org/10.1080/19401493.2018.1498537.

F. Jorissen, G. Reynders, R. Baetens, D. Picard, D. Saelens and L. Helsen (2018). "Implementation and verification of the IDEAS building energy simulation library." Journal of Building Performance Simulation 11(6): 669-688. DOI: https://doi.org/10.1080/19401493.2018.1428361.

R. Kamal, F. Moloney, C. Wickramaratne, A. Narasimhan and D.Y. Goswami (2019). "Strategic control and cost optimization of thermal energy storage in buildings using EnergyPlus." Applied Energy 246: 77-90. DOI: https://doi.org/10.1016/j.apenergy.2019.04.017.

B.R. Knudsen, H. Kauko and T. Andresen (2019). "An Optimal-Control Scheme for Coordinated Surplus-Heat Exchange in Industry Clusters." Energies 12(10): 1877. DOI: https://doi.org/10.3390/en12101877.

J. Kuang, C. Zhang, F. Li and B. Sun (2018). "Dynamic Optimization of Combined Cooling, Heating, and Power Systems with Energy Storage Units." Energies 11(9): 2288. DOI: https://doi.org/10.3390/en11092288.

D. Li, J. Wang, Y. Ding, H. Yao and Y. Huang (2019). "Dynamic thermal management for industrial waste heat recovery based on phase change material thermal storage." Applied Energy 236: 1168-1182. DOI: https://doi.org/10.1016/j.apenergy.2018.12.040.

F. Liu, W. Zhu and J. Zhao (2018). "Model-based dynamic optimal control of a CO2 heat pump coupled with hot and cold thermal storages." Applied Thermal Engineering 128: 1116-1125. DOI: https://doi.org/10.1016/j.applthermaleng.2017.09.098.

Y. Lu, S. Wang, Y. Sun and C. Yan (2015). "Optimal scheduling of buildings with energy generation and thermal energy storage under dynamic electricity pricing using mixed-integer nonlinear programming." Applied Energy 147: 49-58. DOI: https://doi.org/10.1016/j.apenergy.2015.02.060.

H. Lund, S. Werner, R. Wiltshire, S. Svendsen, J.E. Thorsen, F. Hvelplund and B.V. Mathiesen (2014). "4th Generation District Heating (4GDH): Integrating smart thermal grids into future sustainable energy systems." Energy 68: 1-11. DOI: https://doi.org/10.1016/j.energy.2014.02.089.

F. Magnusson and J. Åkesson (2015). "Dynamic Optimization in JModelica.org." Processes 3(2): 471. DOI: https://doi.org/10.3390/pr3020471.

F. Magnusson and J. Åkesson (2018). "Symbolic elimination in dynamic optimization based on block-triangular ordering." Optimization Methods and Software 33(1): 92-119. DOI: https://doi.org/10.1080/10556788.2016.1270944.

Nord Pool AS (2019). "Historical Market Data." From https://www.nordpoolgroup.com/historical-market-data/ (accessed 01/2019).

R. Ooka and S. Ikeda (2015). "A review on optimization techniques for active thermal energy storage control." Energy and Buildings 106: 225-233. DOI: https://doi.org/10.1016/j.enbuild.2015.07.031.

R. Renaldi and D. Friedrich (2017). "Multiple time grids in operational optimisation of energy systems with short- and long-term thermal energy storage." Energy 133: 784-795. DOI: https://doi.org/10.1016/j.energy.2017.05.120.

D. Rohde, T. Andresen and N. Nord (2018). "Analysis of an integrated heating and cooling system for a building complex with focus on long–term thermal storage." Applied Thermal Engineering 145: 791-803. DOI: https://doi.org/10.1016/j.applthermaleng.2018.09.044.

D. Rohde, M. Bantle, T. Andresen and N. Nord (2015). Documentation of an Integrated Thermal Energy System for a Building Complex. 24th International Congress of Refrigeration, Yokohama, Japan.

G. Schweiger, R. Heimrath, B. Falay, K. O'Donovan, P. Nageler, R. Pertschy, G. Engel, W. Streicher and I. Leusbrock (2018). "District energy systems: Modelling paradigms and general-purpose tools." Energy 164: 1326-1340. DOI: https://doi.org/10.1016/j.energy.2018.08.193.

A. Sellberg, M. Nolin, A. Löfgren, N. Andersson and B. Nilsson (2018). "Multi-flowrate Optimization of the Loading Phase of a Preparative Chromatographic Separation." Computer Aided Chemical Engineering 43: 1619-1624. DOI: https://doi.org/10.1016/B978-0-444-64235-6.50282-5.

B. Talebi, F. Haghighat, P. Tuohy and P.A. Mirzaei (2019). "Optimization of a hybrid community district heating system integrated with thermal energy storage system." Journal of Energy Storage 23: 128-137. DOI: https://doi.org/10.1016/j.est.2019.03.006.

L. Urbanucci, F. D'Ettorre and D. Testi (2019). "A Comprehensive Methodology for the Integrated Optimal Sizing and Operation of Cogeneration Systems with Thermal Energy Storage." Energies 12(5): 875. DOI: https://doi.org/10.3390/en12050875.

A. Wächter and L.T. Biegler (2006). "On the implementation of an interior-point filter line-search algorithm for large-scale nonlinear programming." Mathematical Programming 106(1): 25-57. DOI: https://doi.org/10.1007/s10107-004-0559-y.

XE Corporation (2019). "Currency Converter." From https://www.xe.com/currencyconverter/convert/?From=NOK&To=EUR (accessed 07.02.2019).

J. Åkesson (2008). Optimica - An Extension of Modelica Supporting Dynamic Optimization. 6th International Modelica Conference, Bielefeld, Germany.

ISBN 978-82-326-4022-5 (printed version)
ISBN 978-82-326-4023-2 (electronic version)
ISSN 1503-8181

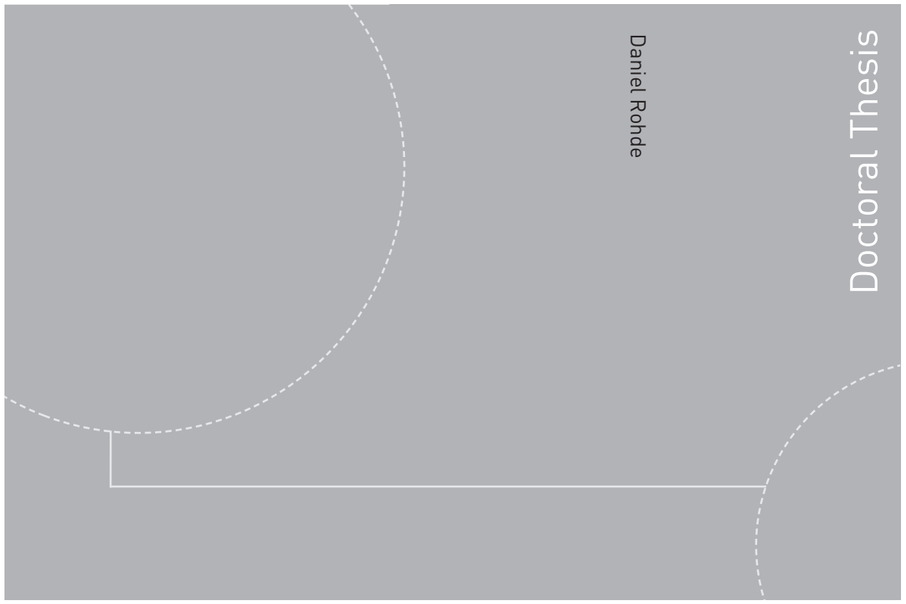

Doctoral theses at NTNU, 2019:213

Daniel Rohde

Dynamic simulation of future integrated energy systems

NTNU
Norwegian University of
Science and Technology
Faculty of Engineering
Department of Energy and Process Engineering

NTNU
Norwegian University of
Science and Technology

Doctoral theses at NTNU, 2019:213

NTNU

NTNU
Norwegian University of
Science and Technology